



HAL
open science

Design, synthesis and biological evaluation of novel selective inhibitors of Focal Adhesion Kinase (FAK) with potential anti-tumor activity

Bo Li

► **To cite this version:**

Bo Li. Design, synthesis and biological evaluation of novel selective inhibitors of Focal Adhesion Kinase (FAK) with potential anti-tumor activity. Medicinal Chemistry. Université Paris Cité, 2019. English. NNT: 2019UNIP5060 . tel-03860631

HAL Id: tel-03860631

<https://theses.hal.science/tel-03860631v1>

Submitted on 18 Nov 2022

HAL is a multi-disciplinary open access archive for the deposit and dissemination of scientific research documents, whether they are published or not. The documents may come from teaching and research institutions in France or abroad, or from public or private research centers.

L'archive ouverte pluridisciplinaire **HAL**, est destinée au dépôt et à la diffusion de documents scientifiques de niveau recherche, publiés ou non, émanant des établissements d'enseignement et de recherche français ou étrangers, des laboratoires publics ou privés.

Université de Paris

ÉD563 : Médicament, Toxicologie, Chimie, Imageries

Laboratoire de Chimie et Biochimie Pharmacologiques et Toxicologiques

CNRS UMR 8601

Thèse

Par **BO LI**

**Design, Synthesis and Biological Evaluation of Novel
Selective Inhibitors of Focal Adhesion Kinase (FAK) with
Potential Anti-tumor Activity**

Spécialité : **Pharmacochimie**

Dirigée par Dr Huixiong CHEN et Pr Mélanie ETHEVE-QUELQUEJEU

Mercredi 20 Novembre 2019

Composition du jury :

Rapporteurs

Mme. Delphine JOSEPH

Professeur des Universités – Université Paris-sud

Mme. Sandrine PIGUEL

Maître de conférences - Institut Curie

Examineur

M. Charles TRUILLET

Chercheur - CEA

Mme. Christiane GARBAY

Professeur Emérite – Université de Paris

Mme. Mélanie ETHEVE-QUELQUEJEU

Professeur des Universités – Université de Paris

M. Huixiong CHEN

Maître de conférences – Université de Paris



ACKNOWLEDGEMENTS

I would like to express my sincere gratitude to all the people who have supported me professionally and personally in my journey to this PhD.

First and foremost I would like to pay my sincere thanks to my PhD supervisors, Dr Huixiong CHEN and Prof Mélanie ETHEVE-QUELQUEJEU. I thank Dr Huixiong CHEN for helping me to apply for the scholarship and giving me the chance to work on this project. He cultivated my working ability independently, which is a useful quality in my future career. I am grateful to Prof Mélanie ETHEVE-QUELQUEJEU, who welcomed me into her team. Her rigorous and meticulous spirits in science have deeply influenced me. In addition, her encouragement and support have always kept me to move forward.

Next, I would like to thank Prof Delphine JOSEPH and Dr Sandrine PIGUEL for agreeing to be the reporters of my thesis. I thank Dr Charles TRUILLET for being the jury of my defence and examining the manuscript. I would like to express my profound gratitude to Pr Christiane GARBAY for her help during the preparation of this thesis and truly appreciate her willingness to be the jury.

I also would like to express my gratitude to all the collaborators: Mr Daniel LIETHA, who cultured and resolved the crystal structures of our inhibitors in complex with FAK kinase domain; Mr John DAWSON and Mr Yongliang LI, who contributed a lot of time on the biological evaluation in cells. I also would like to thank Mrs Céline TOMKIEWICZ-RAULAE, who gave me the training of biological experiments and performed many *in vitro* evaluations of our compounds. In addition, I want to say thanks to Mr Cédric CARADEUC and Mr Gildas BERTHO, who gave a lot of help with NMR spectroscopy, and Mr Patrice GERARDO, who did the analyse of HR-MS for me.

I am grateful to all my current and ex lab members in the team of Pr Melanie ETHEVE-QUELQUEJEU. I am especially grateful to Dr Laura INNAZZO and Dr Emmanuelle BRAUD for the discussion of chemistry, for the help in dealing with ‘tous les merdes’ in

France. Without their help, life here would not be like this. I also want to express my sincere thanks to Colette, who is so kind and gives me a lot of encouragement. I would like to thank Said, Camélia, Flavie, and Karolina for their help and supports. Additionally, I want to thank all my interns, including Imene, Huafen, Alexandre, and Manel.

Next, I would like to say thanks to my friends, Tuan and Xiaowei. They are always standing on my side, accompanying me and sharing every good and bad moment in the PhD journey. I wish them all the best to reach the end of their PhD journey next year. I would like to express my thanks to Qier for her suggestions and help in this year, also for every anecdote and funny story she shared, which bring me a lot of joy when I work in front of the computer.

Most importantly, I am deeply indebted to my loving parents and sister, who have always shown faith in every decision of my life. Without their love and support, I would not be the person I am today.

At last, I would like to express my gratitude to the Chinese Scholarship Council for the financial supporting during my study in France.

Table of content

Abbreviations	7
General introduction	9
1. Cancer: A burden all of the world	9
2. Current treatments for cancers	10
Summary.....	13
Chapter I. Protein kinase and targeted small molecular inhibitors	15
1. Protein kinases	15
1.1. Protein Kinase structure	15
1.2. Protein kinase targeted small molecules	17
1.2.1. Type I inhibitor.....	19
1.2.2. Type II inhibitor	22
1.2.3. Allosteric inhibitors (type III and type IV).....	24
1.3. Covalent kinase inhibitors	27
1.3.1. Binding mode of covalent inhibitors	28
1.3.2. The covalently modified residues	29
1.3.3. Electrophilic groups for the covalent inhibitor	34
2. Focal adhesion kinase (FAK)	36
2.1 Structure and function of FAK.....	36
2.2 FAK signalling pathway and biological functions	39
2.4 FAK inhibitors	42
3. Previous work in the laboratory	53

4. Objectives	53
Chapter II. Development of covalent inhibitors of FAK	55
Part 1. Improvement of synthesis and characterization of the first covalent inhibitor of FAK	56
1. Introduction.....	56
2. Sequences alignment.....	57
3. Synthesis of the desired inhibitors	59
3.1. Synthesis of inhibitors with a squaramide linker	59
3.2. Synthesis of inhibitors with a triazole linker.....	65
4. Characterization of irreversible inhibition	68
4.1. <i>In vitro</i> evaluation of the enzymatic activity.....	68
4.2. Inhibition of FAK autophosphorylation in SCC cells	73
4.3. X-Ray crystallography	74
5. Conclusion	75
Part 2. Design, synthesis and biological evaluation of new irreversible and reversible covalent inhibitors	77
1. Design of new irreversible covalent inhibitors	77
2. Synthesis of irreversible inhibitors modified on the part A.....	78
3. Synthesis of irreversible inhibitor modified on the part B	84
4. Design of reversible covalent inhibitors	87
4.1. Concept of reversible covalent inhibitor	87
4.2. Design of reversible covalent inhibitors	89
5. Synthesis of reversible covalent inhibitors	89
6. Biological evaluation	91

6.1. <i>In vitro</i> enzymatic activity	91
6.2. In cell evaluation.....	94
6.3. Kinase selectivity profiling.....	102
7. Conclusion and perspective	102
Part 3. Synthesis of imidazopyrimidine precursors for the development of bicyclic covalent inhibitor.	105
1. Introduction.....	105
2. Synthesis of imidazopyrimidine-based covalent inhibitor	106
3. X-Ray crystallography	112
4. Conclusion and perspective	113
Chapter III. Study of microwave-assisted synthesis of 2,5-disubstituted pyrimidine derivatives	115
1. Introduction.....	115
1.1. The Pd-catalysed C-N coupling reaction	116
1.2. Microwave in organic reaction	118
2. Optimization of coupling conditions.....	119
3. Expanding the scope of substrates	121
3.1. The substrate scope of amines.	121
3.2. The substrate scope of 5-bromo-2-substituted pyrimidines	124
3.2.1. Preparation of substrates	125
3.2.2. C-N coupling reaction of various 5-bromo-2-substituted pyrimidine	127
4. Conclusion	130
Chapter IV. Synthesis of fluorescent covalent binding tools of FAK	131
1. Introduction.....	131

1.1. Fluorescence and nitrobenzoxadiazole (NBD) fluorophore.	133
2. Synthesis of Fluorescent compounds	135
2.1. Synthesis of compounds with a fluorophore connected to pyrimidine through an amino group.....	135
2.2. Synthesis of compounds with a fluorophore connected to pyrimidine through an aliphatic linker	139
3. Fluorescence properties and biological evaluation	140
3.1. Absorption and fluorescence spectra.	140
3.2. In vitro enzymatic activity.....	141
4. Conclusion and perspective	142
General conclusion	143
EXPERIMENTAL PART	147
References	251
Publication	279

Abbreviations

5-FU	Fluorouracil
ABL	Abelson
ADP	Adenosine diphosphate
AKT	RAC serine/threonine-protein kinase
ALK	Anaplastic lymphoma kinase
ALK1/2	Activin receptor-like kinase 1/2
Alloc	Allyloxycarbonyl
ATP	Adenosine triphosphate
BCR	Breakpoint cluster region protein
BINAP	2,2'-Bis(diphenylphosphino)-1,1'-binaphthyl
Boc	<i>tert</i> -Butyloxycarbonyl
B-Raf	Serine/threonine-protein kinase B-Raf
BTK	Bruton's tyrosine kinase
CAR-T cells	Chimeric antigen receptor T cells
CDK	Cyclin-dependent kinase
CML	Chronic myelogenous leukaemia
COX-1/2	Cyclooxygenase-1/2
CSA	(1S)-(+)-10-Camphorsulfonic acid
DCM	Dichloromethane
DcpS	Scavenger mRNA-decapping enzyme
DFG	Asp-Phe-Gly
DIPEA	<i>N,N</i> -Diisopropylethylamine
DMF	<i>N,N</i> -Dimethylformamide
DNA	Deoxyribonucleic acid
EC₅₀	Half maximal effective concentration
EDCI	1-Ethyl-3-(3-dimethylaminopropyl)carbodiimide
EGFR	Epidermal growth factor receptor
ERK	Extracellular signal-regulated kinase
Etk	BMX non-receptor tyrosine kinase
FAK	Focal adhesion kinase
FAT	Focal adhesion targeting region
FERM	Four-point-one, ezrin, radixin, moesin domain
FGFR	Fibroblast growth factor receptor
Flt (VEGFR)	Vascular endothelial growth factor receptor 1
Fmoc	Fluorenylmethyloxycarbonyl
FRNK	FAK-related-non-kinase domain
Grb	Growth factor receptor-bound protein
GSH	Glutathione
HER2 (erbB2)	Human epidermal growth factor receptor 2

HM	Hydrophobic motif
HOBT	Hydroxybenzotriazole
HRB	Hinge region binding
IC₅₀	Half maximal inhibitory concentration
IGF-1R	Insulin-like growth factor 1 receptor
IR	Insulin receptor
mAbs	Monoclonal antibodies
MAPK	Mitogen-activated protein kinase
MEK-1/2	Mitogen-activated protein kinase kinase 1/2
MTT	3-(4,5-Dimethylthiazol-2-yl)-2,5-diphenyltetrazolium bromide
NBD	7-Nitrobenz-2-oxa-1,3-diazol-4-yl
NES	Nuclear export sequence
NLS	Nuclear localization sequence
PBS	Phosphate-buffered saline
PD-1	Programmed cell death protein 1
Pd₂dba₃	Tris(dibenzylideneacetone)dipalladium (0)
PDGFR	Platelet-derived growth factor receptor
PDL-1/2	Programmed death-ligand 1/2
PH domain	Pleckstrin homology domain
PK/PD	Pharmacokinetic/Pharmacodynamic
pKa	Acid dissociation constant
PTSA	<i>p</i> -Toluenesulfonic acid
PYK2	Proline-rich tyrosine kinase 2
RNA	Ribonucleic acid
RSK2	Ribosomal protein S6 kinase alpha 2
SCC	Squamous cell carcinoma
S_NAr	Nucleophilic aromatic substitution
SPhos	2-Dicyclohexylphosphino-2',6'-dimethoxybiphenyl
SRPK	Serine-arginine protein kinase
TLC	Thin layer chromatography
TFA	Trifluoroacetic acid
THF	Tetrahydrofuran
Tregs	Regulatory T cells
VEGFR	Vascular endothelial growth factor receptor
XantPhos	4,5-Bis(diphenylphosphino)-9,9-dimethylxanthene
Xphos	2-Dicyclohexylphosphino-2',4',6'-triisopropylbiphenyl

General introduction

1. Cancer: A burden all of the world

Cancer, also called malignant tumour, is a group of diseases involving uncontrolled malignant cell growth which has the potential to invade or transfer to other parts of the body. Cancer is the second cause of death across the world behind cardiovascular diseases and the single most important block to increasing life expectancy in the 21st century. In accordance with the statistics of WHO, approximately 14 million cases were diagnosed in 2012, and 8 million lives were deprived by the cancer-related diseases.¹ This number has significantly climbed during recent years.² The latest statistics for the most common cancer (excluding non-melanoma skin cancer) in 2018 all over the world was provided by World Cancer Research Fund. There were around 18 million cancer cases diagnosed in 2018, of 9.5 million cases were in man and 8.5 million in women. This trend will continue and it is predicted that in 2040 the number of cases will reach 29.5 million (**Figure1**).³

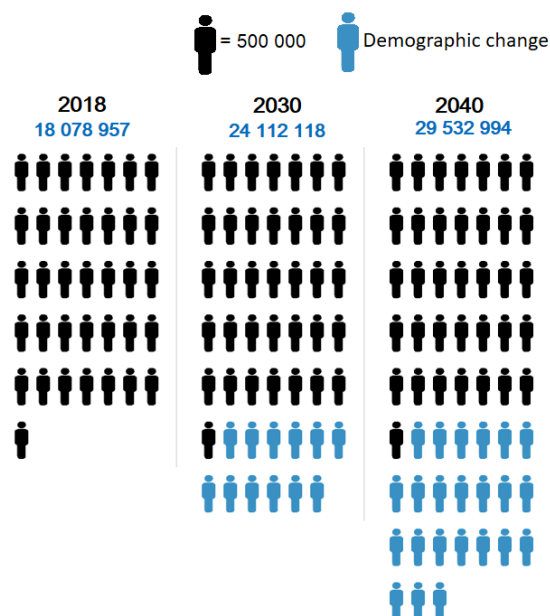


Figure 1: Estimated number of incident cases from 2018 to 2040, all cancers, both sexes, all ages.³

2. Current treatments for cancers

Cancer is historically conceived as a cell-autonomous disease driven by the activation of (proto)oncogenes or the inactivation of onco-suppressor genes. Since cancer severely threatens human health, a lot of endeavours have been made to conquer this problem. After the diagnosis, different treatments may be given separately, successively or in association to the patient, which depend on the type of cancer and how advanced it is. These treatments in terms of technical approaches are essential including surgery, radiation therapy, chemotherapy and immunotherapy. Targeted therapy and hormone therapy can be considered as sub-classes of chemotherapy and immunotherapy.

Surgery

Surgery is a procedure used to remove solid tumours from the body. This is an effective and valuable treatment for non-metastatic solid tumours, such as breast cancer, colorectal cancer, pancreatic cancer, etc. However, generally, surgery is not sufficient. In most conditions, surgery is considered as primary treatment and it is also combined with other treatments to control the progress of cancer. Moreover, for most types of cancer, biopsy is the main way for the diagnosis. During a surgical biopsy, the suspicious tissues are removed in order to find the origins of the tumour through anatomopathological analyses, which allow improving treatments.

Radiotherapy

Radiotherapy, also called radiation therapy, uses ionizing radiation, usually X-ray in order to treat cancer cells and shrink tumours. Only the solid and local cancers could be treated with radiotherapy. Ionizing radiation could damage the DNA of cancerous tissues. Radiotherapy is usually used as adjuvant therapy after surgery to prevent tumour recurrence and is generally accompanied by chemotherapy.

Chemotherapy

Chemotherapy is the way to eradicate cancer cells by use of chemical drugs. Cancer chemotherapy history began in the 1940s after the 2nd world war with the use of nitrogen mustards and folic acid antagonist drugs. Chemotherapy was developed on the observation that cancer cells grow more rapidly than normal cells. Chemotherapy is the most important component of cancer treatment for patients. This treatment is available to both solid tumours and non-solid cancers, such as leukaemia.

Chemotherapeutic agents display their anticancer activities by various mechanisms and have some specificity. For instance, paclitaxel is widely used for the treatment of several types of cancer. It kills cancer cells by promoting polymerization of tubulin dimers to form microtubules and preventing depolymerisation.⁴ 5-Fluorouracil (5-FU) is an antimetabolite drug. It takes effect by misincorporation of fluoronucleotides into RNA and DNA and inhibition of the nucleotide synthetic enzyme thymidylate synthase.⁵

However, despite their success, conventional chemotherapies were limited due to non-sufficient specificity for tumour cells over normal cells resulting in insufficient drug concentrations in tumours or toxic effects on normal cells. In order to decrease the systemic toxicity and to prevent the appearance of drug-resistant tumour cells, several strategies have been proposed. These include alternative formulations e.g., liposomes, resistance modulation e.g., PSC833, antidotes/toxicity modifiers e.g., ICRF-187.⁶ Finally targeted therapies have gained importance due to their specificity towards cancer cells while sparing toxicity to off-target cells.

Hormone therapy

Hormone therapies are chemotherapeutic agents which allow to slow or stop the growth of cancer that dependent on hormones. Generally, hormone therapy is used to treat prostate and breast cancers along with other treatments. Androgen suppression therapy is used for men with prostate cancer. Estrogen deprivation therapy is used for women with estrogen

receptor-positive breast cancer.

Targeted therapy

Targeted therapy includes several types of agents. In a first time, chemotherapeutic drugs were conjugated to agents able to recognize specific markers of certain tumour cells. This was possible with the progressive understanding of cancer biology. Various targeted drugs and monoclonal antibodies have been discovered and marketed. Now there are many treatments that use targeted drugs or antibodies alone which target specific genes or proteins in cancer cells that help them grow, divide and spread in cancer. Thus, the targeted therapy is the most effective treatment for most types of cancers and it's also the basis of precision treatment. Protein kinases involved in cell growth and sometimes mutated or overexpressed in different cancer types constitute important targets. Imatinib was designed for targeting the fusion protein tyrosine kinase *bcr-abl*, caused by the Philadelphia chromosome abnormality which is specific in chronic myeloid leukaemia (CML). Imatinib is the first small molecule that was used in the targeted therapy of the chronic myeloid leukaemia (CML). It binds to the active site of *bcr-abl* kinase and locked it in a self-inhibited conformation.⁷ Hence, the effect of imatinib on normal cells is less than that on cancer cells. Antibodies are also largely developed since they can be expressed under a humanized form. Thus monoclonal antibodies, (mAbs) working mainly by attaching to and blocking antigens on cancer cells are designed. For example, trastuzumab (Herceptin ®) is an antibody against the HER2 protein, which inhibits its activity in cellular growth. The approach with mAbs refers to targeted therapy and immunotherapy.

Immunotherapy

Immunotherapy is constituted by the ways to help the body's immune system to fight cancer, either by helping the immune system to attack the cancer cells directly or by stimulating the immune response against cancer cells. The immunotherapy has been well

developed with specific monoclonal antibodies and has been approved to treat numerous types of cancer. There are several ways to help the immune system act against cancer development, such as adoptive cell transfer and monoclonal antibody mark, vaccination and immune checkpoint inhibition.

In this field, it was recently shown that immune checkpoint proteins such as Programmed death 1 (PD-1)/ programmed cell death 1 ligand (PDL-1) constitute very good targets. PD-1 protein, which is on the surface of T cells, regulates the immune response of T cell by binding with programmed cell death 1 ligand (PD-L1) or programmed cell death 2 ligand (PD-L2). Many cancer cells can express PD-L1 which inactivates T cells and protects cancer cells from the attacking of T cells.⁸ The anti-PD-1 monoclonal antibody, such as Nivolumab (Opdivo ®), that selectively block the interaction of PD-1 receptor with its ligands PD-L1 and PD-L2,⁹ can treat inoperable or metastatic melanoma, squamous non-small cell lung cancer.

Summary

The anti-cancer treatments are always on the rise, particularly with targeted approaches and in the field of immunotherapy. A variety of efforts are also underway to propose new anti-cancer therapies. For instance, in the field of gene therapy, the CAR T-cell therapy is very promising and expected to receive several approvals in the near future.¹⁰

It must be noted that important progress in terms of diagnosis allows treating patients earlier and with more appropriate targeted therapies depending on the type and stage of cancers. However, at this time, people with cancer generally receive several types of treatment, often combined to prevent cancer growth and invasion. Due to the complexity and variety of cancer, and even in spite that there are existing a great number of treatment strategies, it's still hard to cure cancers. Hence, there is still a strong demand to develop new drugs against cancers.

So this thesis will describe an approach for targeting the focal adhesion kinase (FAK), due to its role in oncogenic signalling pathways and immune response when it is over-

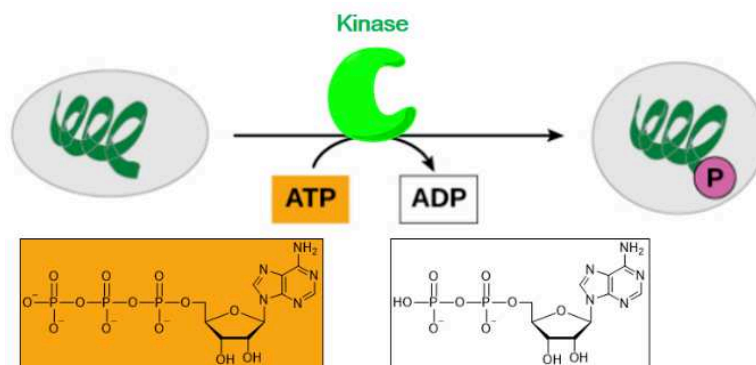
expressed.

In chapter 1, a review on the protein kinase structure and different types of small molecular inhibitors will be described. The structure of focal adhesion kinase (FAK) and the progress of FAK targeted inhibitors are also presented. Next chapters will describe the design, synthesis and properties of our new small molecular inhibitors of FAK. In chapter 3, a microwave-assisted palladium-catalyzed amination of 5-bromopyrimidine study will be presented. The last chapter is dedicated to the synthesis of fluorescent compounds for the FAK imaging study.

Chapter I. Protein kinase and targeted small molecular inhibitors

1. Protein kinases

Kinases are enzymes that catalyze the transfer of the terminal phosphate group of ATP in two steps to a substrate giving phospho-substrate and releasing ADP (**Scheme 1**). The substrate of kinases varies from small molecules to various types of compounds, such as oligonucleotides, lipids, carbohydrates, proteins and receptors. Hence, kinases are classified into broad groups by their substrate: protein kinases, lipid kinases, carbohydrate kinases and others. Protein kinase is the largest group and constitutes 2% of human genes.¹¹ The phosphorylation process of protein kinase mediates most signal transductions and regulates various cellular activities in eukaryotes.¹² By modification of substrate activity, protein kinases are involved in many cellular processes such as metabolism, transcription, cell cycle progression, cytoskeletal rearrangement and cell movement, apoptosis, and differentiation.¹¹



Scheme 1: Kinase phosphorylation process.

1.1. Protein Kinase structure

Thanks to the unfolding of the human genome, 518 protein kinases have been identified, which consist of 1.7% of human genes. These 518 protein kinases are classified into 9 groups, 90 families and 145 subfamilies by sequence comparison.^{11,13} Though their primary sequence

is various, almost all protein kinases share a highly similar 3D structure, especially in the catalytic active domain.

The 3D structure of a protein kinase consists of an N-terminal and a C-terminal domain connected by a hinge region (**Figure 2**). At the N-terminus, residues are mostly folded to β -sheets and usually only one α -helix structure exists, which is termed C-helix. The C-terminal domain contains mostly α -helices with a small number of sheets. The ATP molecule binds in a cleft formed between the two lobes of the protein kinase. Residues in the ATP binding pocket are highly conserved. The adenine of ATP was anchored to the hinge region through hydrogen bonds. The residue just before the hinge region is called gatekeeper residue, whose side-chain forms hydrophobic interaction with ATP. Around the ATP binding pocket, all the kinases conserve two flexible loops, a glycine-rich loop (called P-loop) and an activation loop (called A-loop). The glycine-rich loop is also termed as the phosphate-binding loop because phosphates of ATP form magnesium-mediated hydrogen bonds to this region. The activation loop controls the access of the substrate to the active site and can be characterized by a conserved amino acid sequence Asp-Phe-Gly (DFG).^{12,13}

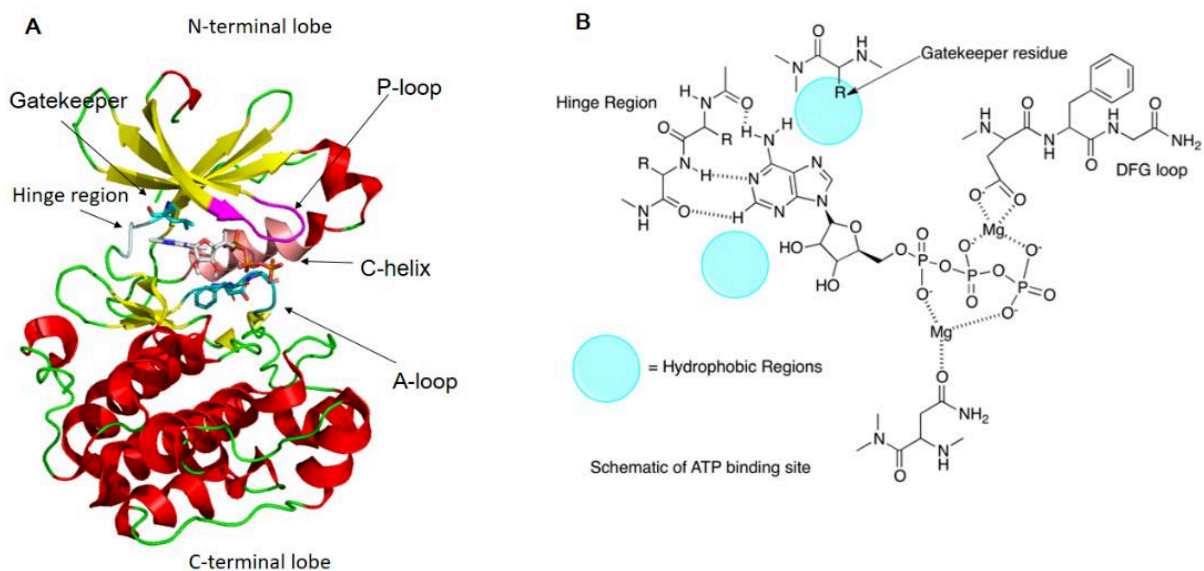
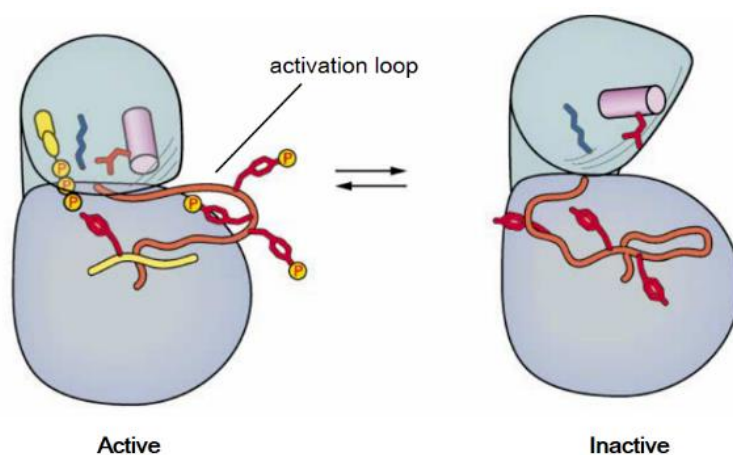


Figure 2: (A) The 3D structure of protein kinase PDK1 with ATP (PDB: 4RRV); (B) Schematic representation of the ATP binding site.

Protein kinases exist in active and inactive conformations (**Scheme 2**).¹⁴ When the kinase is active, its activation loop is phosphorylated and adopts an open and extended conformation offering a space for the substrate. The peptide substrate binds into the platform provided by the activation loop in front of the nucleotide binding pocket of ATP. Asp-Phe-Gly residues (DFG motif) are highly conserved in the activation loop. The Asp residue of the DFG motif is required for the recognition of the ATP nucleotide through a divalent Mg^{2+} cation and the DFG motif adopts a conserved spatial conformation among the majority of kinases. Therefore, the active conformation is also called “DFG-in conformation”, while in an inactive state of kinase, the activation loop changes conformation and destroys the platform for the substrate and ATP binding. For many kinases, the conformational changes involve crankshaft-like motions in the N-lobe of the activation loop resulting in the appropriate orientation of the DFG motif within the active site.¹⁵ Hence, the inactive conformation is also called DFG-out conformation.



Scheme 2: The kinase active and inactive conformations.¹⁴

1.2. Protein kinase targeted small molecules

For the last 30 years, kinases have been intensively investigated and emerged as important therapeutic targets for the treatment of numerous diseases such as cancers, inflammatory diseases,¹⁶ central nervous system disorders,¹⁷ cardiovascular diseases,¹⁸ and complications of diabetes.¹⁹ FDA approved the first kinase inhibitor Imatinib (**Figure 3**) in 2001 for the treatment of chronic myeloid leukemia (CML), which was a milestone for the

kinase inhibitor design. Until the year of 2019, 48 kinase inhibitors have been approved by the FDA.²⁰

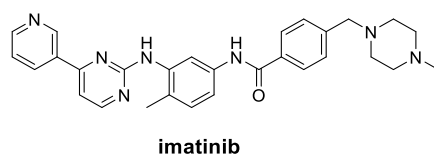


Figure 3: Chemical structure of Imatinib.

Among the 48 approved inhibitors, 45 small molecules interact directly with the kinase domain.²⁰ These inhibitors usually target the ATP binding site of the kinases, resulting in a decrease of enzyme activity. In light of the binding mode, kinase inhibitors can be divided into two categories: reversible inhibitors and irreversible inhibitors. The former categories can be further classified into 4 types on the basis of binding pocket: 1) type I inhibitor that occupies the ATP binding site; 2) type II inhibitor that occupies the ATP binding site and an adjacent hydrophobic pocket formed by activation loop; 3) type III inhibitor that binds to an allosteric site near the active site; 4) type IV inhibitor that occupies a pocket far away from the active site (**Figure 4**).

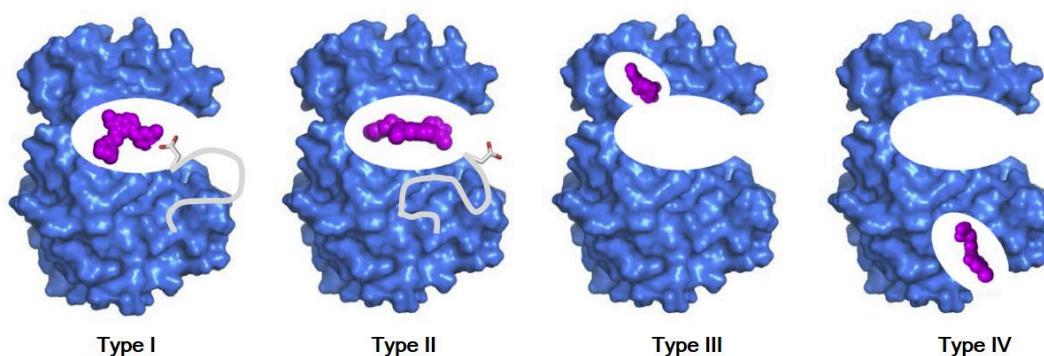


Figure 4: Four types of reversible binding mode, the activation loop was shown in grey, the DFG-motif in Type I (active conformation) and Type II (Inactive conformation) was shown in grey and red sticks.²¹

1.2.1. Type I inhibitor

Definition

A type I inhibitor is a small molecule that competes with ATP for binding to the active site of kinases. Most kinase inhibitors discovered belong to the type I. The predominance of type I inhibitors in the discovery is a consequence of the fact that the design of inhibitors was made to mimic the structure of ATP and used highly activated recombinant kinase catalytic domain in biochemical screening.²² Due to the similarity of the ATP pocket, type I inhibitors can often inhibit several kinases at the same time leading to a loss of selectivity. For example, the natural product Staurosporine (**Figure 5**) is a type I inhibitor, found by the screening of protein kinase C (PKC) inhibitors. This compound has excellent inhibitory activity against PKC with an IC_{50} value of 2.7 nM.²³ Unfortunately, Staurosporine doesn't have any selectivity and inhibits nearly over 90% kinase.²⁴ This promiscuous inhibitory activity prevented the development of kinase inhibitor until selective epidermal growth factor receptor (EGFR) inhibitors were reported.

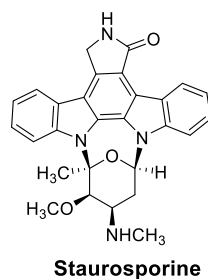
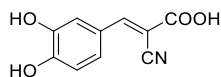


Figure 5: Chemical structure of Staurosporine.

Search for selectivity

The possibility to selectively inhibit tyrosine kinase activity with synthetic small molecules was demonstrated by the discovery of “tyrphostins” (**Figure 6**), which were found to effectively block the autophosphorylation of EGF receptor, but not the homologous insulin receptor kinases.²⁵



example of tyrphostins

Figure 6: Chemical structure of tyrphostin.

In 2003, the FDA approved the first targeted EGFR inhibitor Gefitinib (**Figure 7**) for the treatment of non-small cell lung cancer.²⁶ An *in vitro* kinase inhibition profile showed that Gefitinib inhibits EGFR at least 100-fold more potently than other tyrosine kinases, including erbB2, KDR and Flt-1. Additionally, Gefitinib didn't inhibit the activity of the serine/threonine kinase Raf, MEK-1 and ERK-2.²⁷ The crystallographic structure of the complex of Gefitinib with wild type EGFR unambiguously elucidated the binding mode of type I inhibitor. As shown in **Figure 7**, the quinazoline is oriented with the 1-N in the back of the ATP-binding pockets, where it forms hydrogen bonds with the hinge region residue Met793. In addition, the 3-chloro-4-fluoro aniline substituent extends into the hydrophobic pocket behind the ATP-binding cleft. The 6-propylmorpholino group exposures to the solvent.²⁸

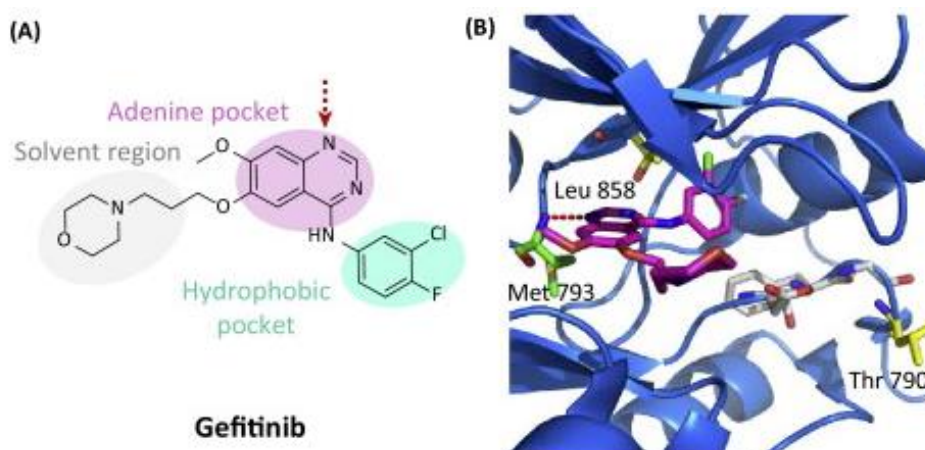


Figure 7: Chemical structure of Gefitinib and crystal complex with EGFR.²¹

With the deep understanding of kinase structure, selective type I inhibitors could be designed by exploiting the subtle differences of residues in the active site^{29,30} and by elaborately tailoring the molecular structure to complement the kinase pocket geometry³¹

and form hydrogen bonds with the pocket residues. For instance, during the design of selective p38 α mitogen-activated protein kinase (MAPK) inhibitors, two differences of residues between p38 α MAPK and other kinases were found to improve the selectivity.³² The first one is that p38 α MAPK has a small gatekeeper residue (Thr106) (**Figure 8**). However, among most of the protein kinases, it's a bulky residue serving as the gatekeeper, such as methionine, leucine or phenylalanine. The presence of a small gatekeeper residue creates a hydrophobic “back pocket” in the active site.³³ Therefore, an additional aromatic ring was introduced to the hinge region binding moiety for the exploitation of the small gatekeeper region.³⁴ The second residual difference is that in p38 α MAPK a glycine (Gly110) is directly adjacent to the linker residue (Met109), which only exists in 9.2% of all kinases (**Figure 8**).³² The glycine can undergo a so-called glycine flip causing a position change between the glycine carbonyl oxygen and the glycine NH group, which resulted in forming two hydrogen bonds with a carbonyl oxygen atom in the inhibitors.³² By taking advantage of above-mentioned features, researchers successfully discovered very selective type I inhibitors of p38 α MAPK, such as Skepinone-L (**Figure 8**).³⁴

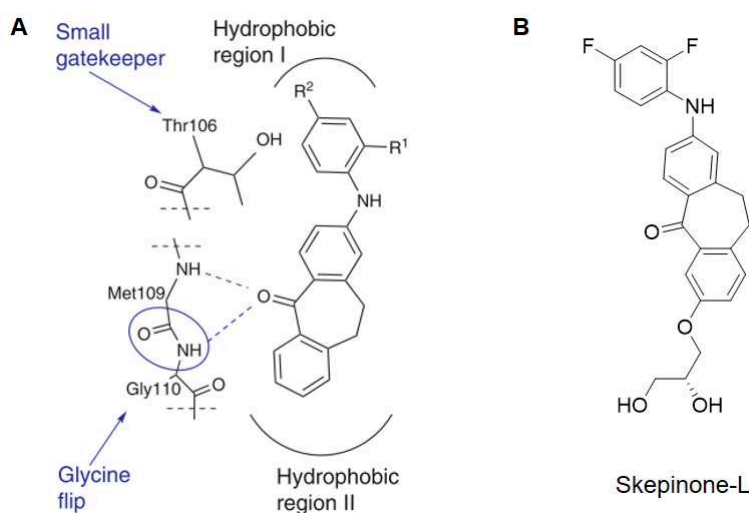


Figure 8: (A) Binding mode of selective p38 α MAPK inhibitor; (B) Chemical structure of Skepinone-L.³⁴

1.2.2. Type II inhibitor

Definition and discovery

Type II inhibitors are small molecules that recognize the inactive conformation of the kinase domain and occupy the active site and an adjacent hydrophobic pocket created by a unique conformation of the activation loop (DFG-out). The DFG-out conformation is not universal for kinases and has been observed by crystallography only in 48 kinases among the 518 kinases.³⁵

In addition, as a consequence of the flexibility of the activation loop which constitutes of 20~30 residues in length, the allosteric pocket is not conserved among kinases. This provides a new opportunity for selective inhibition.

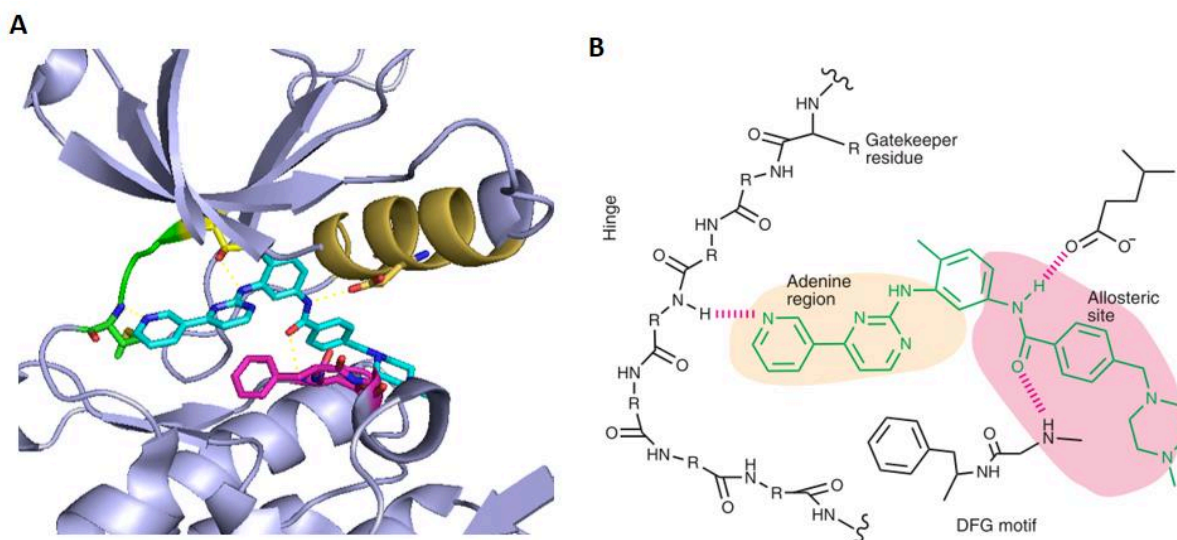


Figure 9: (A) Crystal structure of Imatinib and *Abl* kinase complex. The hinge region is highlighted in green, gatekeeper residue in yellow and DFG-motif in purple (PDB: 1IEP),³⁶ (B) Schematic representation of Imatinib binding site. The hydrogen bonds between the inhibitor and kinase are represented with dash lines.²²

At the beginning, the discovery of type II inhibitors was serendipitous, such as Imatinib and Sorafenib (**Figure 10**). Imatinib was the first type II inhibitor, and its binding mode to kinase *Abl* was elucidated by crystallography.³⁶ The crystal structure (PDB: 1IEP) demonstrated that the inhibitor takes an outstretched conformation rather than a U-shape

conformation required for the type I binding mode in the complex with protein *Abl*. As shown in **Figure 9**, the pyridine ring of Imatinib inserts into the hinge region and forms a hydrogen bond with Met318. A hydrophobic *para*-substituted benzamide region extends to the allosteric pocket created by the DFG motif.

Rational design of type II inhibitor

The good selectivity of type II inhibitors has attracted researchers to put more efforts into the screening and design of such inhibitors. Until 2018, 7 type II inhibitors have applied in the clinic³⁷ and several dozen are under clinical trials. Since the first generation of type II inhibitors was serendipitously discovered, a pharmacophore-based rational design strategy was proposed.²²

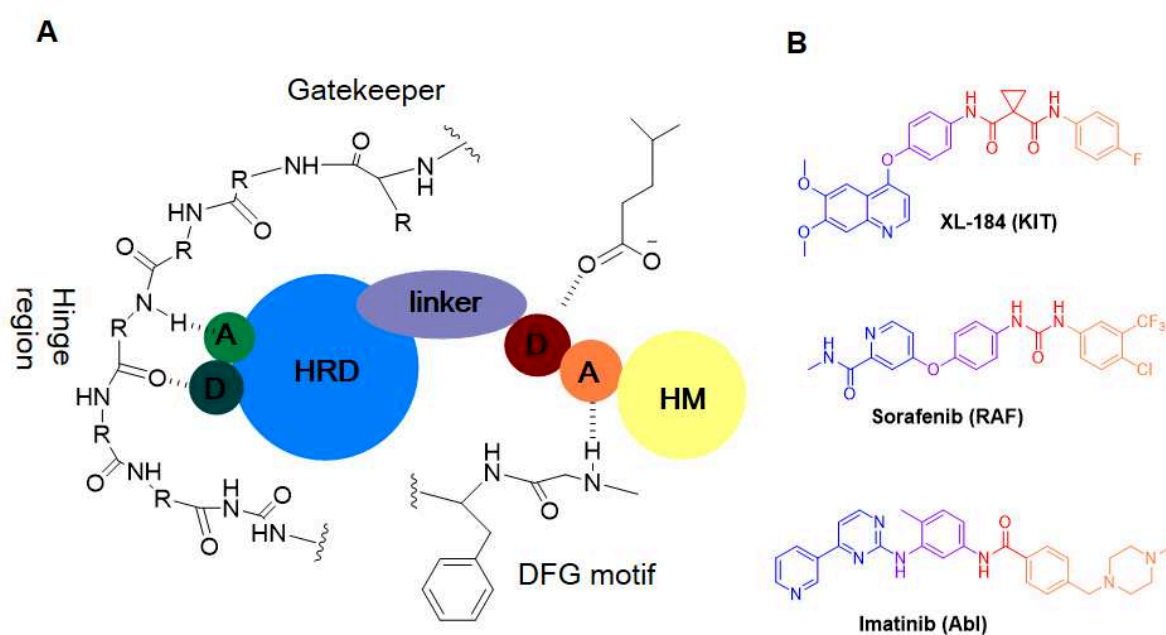


Figure 10: (A) A general pharmacophore model for the rational design of type II inhibitors. A, hydrogen bond acceptor; D, hydrogen bond donor; HRB, hinge region binding; HM, hydrophobic motif;²² (B) Some examples of known type II kinase inhibitors.

As shown in **Figure 10**, the pharmacophore of type II inhibitors consists of four parts.^{22,35}

A hinge region binding moiety. Usually, a heterocyclic structure serves as the hinge region

binding moiety. Like type I inhibitors, the heterocycle can be decorated with appropriate substituents to fit the geometry of the active site.

A linker segment. A linker segment is responsible for traverse of the gatekeeper region. Therefore, the linker part can adopt a flexible aliphatic chain or rigid aromatic ring depending on the structures of gatekeeper and adjacent residues.

A hydrogen bonding moiety. The hydrogen bonding moiety is necessary for type II inhibitors. It's usually an amide or urea structure, which forms several hydrogen bonds with the C-helix and DFG motif. The location of hydrogen bonding moiety plays an important role in tuning the kinase selectivity.

A hydrophobic moiety. The hydrophobic moiety usually is a rigid aromatic ring, which is introduced to occupy the allosteric pocket created by the DFG-out flip. Sometimes, the aromatic ring can be decorated with nitrogen-containing substituents to adjust the water solubility.

A number of type II inhibitors can be mapped by the above-mentioned pharmacophore.³⁵ Thus, the pharmacophore guided approach provided a good strategy to design new type II inhibitors.

1.2.3. Allosteric inhibitors (type III and type IV)

Definition

Allosteric inhibitors are defined as molecules that bind to an allosteric pocket with neither occupation of the ATP binding pocket nor interaction with the hinge region. Allosteric inhibitors include type III inhibitors and type IV inhibitors. Type III inhibitors bind in an adjacent pocket of the active site, whereas this pocket does not overlap with the ATP binding site. Type IV inhibitors bind to an allosteric site that is distant from the ATP binding pocket (**Figure 11**).³⁸ Generally, allosteric inhibitors have a strong preference for their targeted kinase because the allosteric pocket is distinct in each kinase.

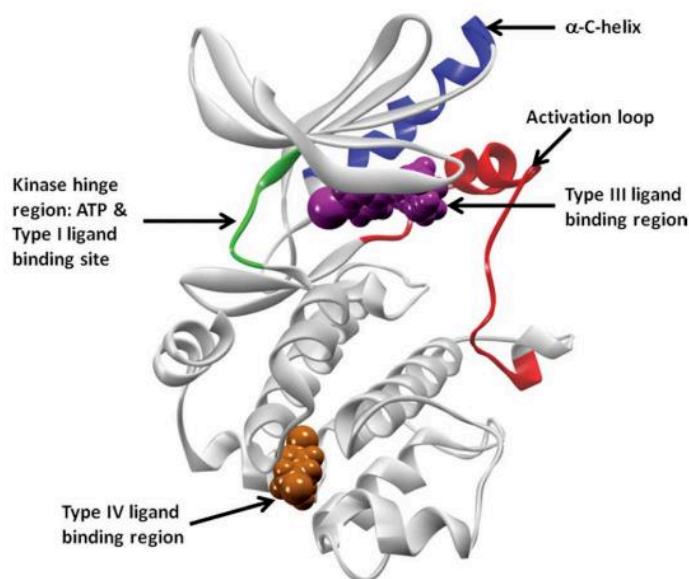


Figure 11: Binding site of type III and type IV inhibitor in kinase.³⁹

Most of the allosteric kinase inhibitors were discovered by serendipity. There is no real rational strategy to design allosteric inhibitors except for deliberately designed screening. Owing to the high selectivity, a massive effort has been made to identify allosteric inhibitors, some of which have completed the clinical trials and entered the market (**Figure 12**).

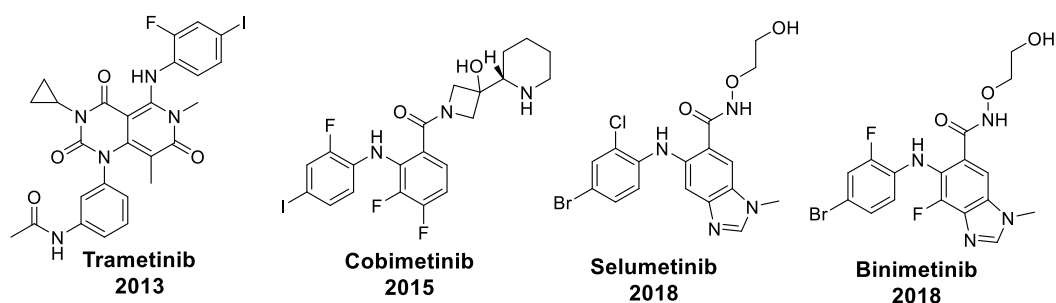


Figure 12: Examples of allosteric inhibitors approved by FDA

Trametinib was the first type III inhibitor of MEK 1/2 that received approval from FDA in 2013 for the treatment of patients with either B-Raf V600E or V600K mutated metastatic melanoma.⁴⁰ Trametinib has a high selectivity. It was shown on *in vitro* test to have no obvious inhibition on a panel of 98 kinases at 10 μ M, while it strongly inhibited the activity of MEK1/2 with a value of IC_{50} from 0.92 nM ~ 3.4 nM.⁴¹ Though there is no crystal structure of Trametinib with MEK, mutually exclusive binding study with PD0325901,

which bound in an adjacent pocket of the active site confirmed by X-ray crystallography (**Figure 13**),⁴² showed that Trametinib had the same binding mode as PD0325901.⁴³

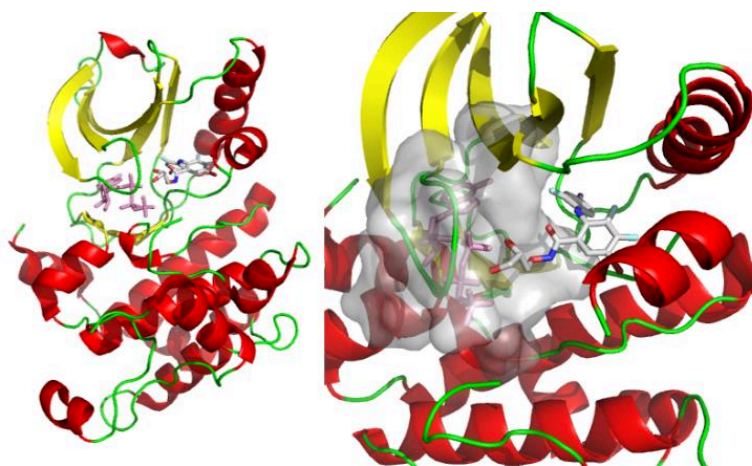


Figure 13: Complex of MEK with ATP (pink) and type II ligand (silver) (PDB: 1S9J).⁴²

GNF2 (**Figure 14**), discovered by phenotypic screening, is a well-identified type IV inhibitor of *Bcl-Abl*.⁴⁴ In spite of the lack of *in vitro* inhibition of Abl kinase, GNF2 resulted in the inhibition of *Bcr-Abl* autophosphorylation, inhibition of cell proliferation, and increase of apoptosis on Ba/F3.p210 cells. Through the molecular docking studies, the binding site of GNF2 was presumed at the myristoyl pocket located in the C lobe of the kinase. Thus, the mutation in the myristoyl pocket of *bcr-abl* gave the Ba/F3 cells resistance to GNF2 while this mutation had little impact on the ATP competitive inhibitor Imatinib, which supported the allosteric inhibition of GNF2.⁴⁴ In 2010, the binding mode of GNF2 to *Abl* was confirmed by X-ray crystallography.⁴⁵ The overall *Abl* kinase structure of complexed to GNF2 was similar to that of the complex of myristic acid, and binding position of GNF2 was overlapped with that of myristic acid in the complex of *Abl*/imatinib/myristate (**Figure 14**).

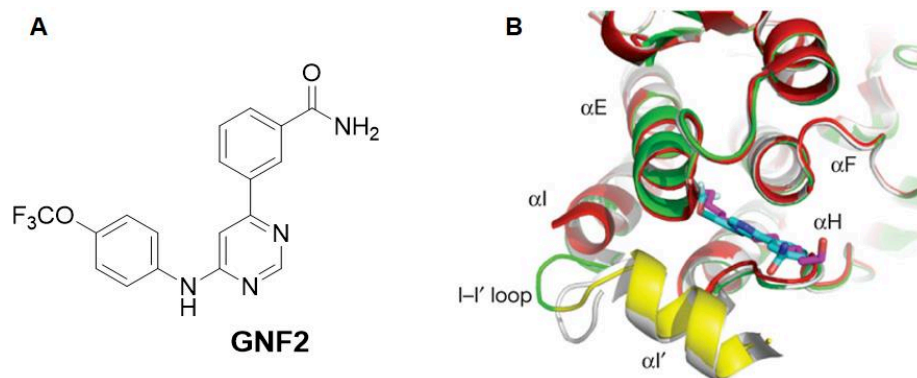
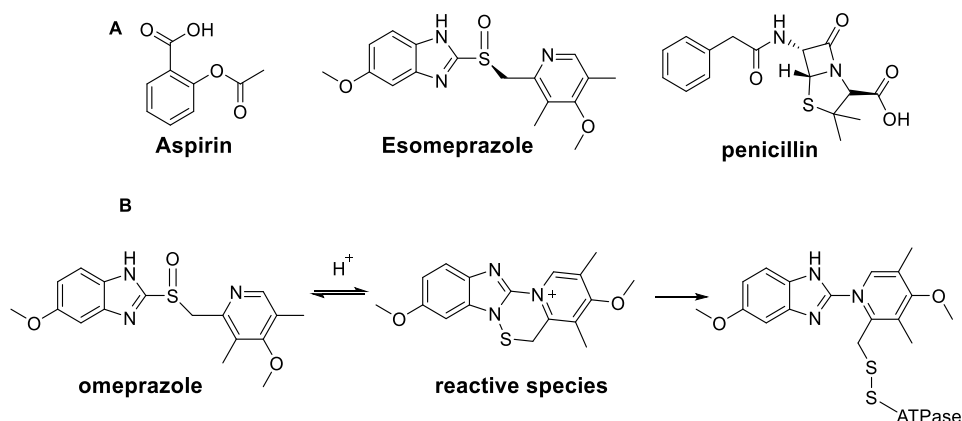


Figure 14: (A) Chemical structure of GNF2, (B) Superposition of the crystal complex *Abl*/imitinib/myristate (white), crystal complex *Abl*/imitinib/GNF-2 (green and yellow) and crystal complex *Abl*/imitinib (red). GNF-2 is coloured in cyan and myristic acid in magenta.⁴⁵

1.3. Covalent kinase inhibitors

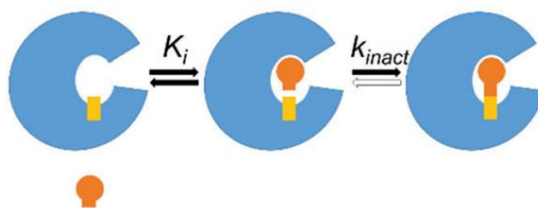
The interactions between inhibitor and kinase are usually due to hydrogen bonds, salt bridges or Van der Waals interactions. The other trend for the design of kinase inhibitors is covalent inhibitor which binds to enzyme irreversibly through a covalent bond. The covalent binding to the enzymes or receptors was not very well considered in drug design for a long time due to the fear of potential toxicity caused by non-specific modifications of proteins, nucleic acids, and other key biomolecules.⁴⁶ However, covalent drugs already exist on the market (**Scheme 3A**) and some of them became blockbusters, such as the esomeprazole (an *S* isomer of omeprazole). These covalent inhibitors are usually derivatives of natural products and their covalent binding mode was elucidated later. For example, Aspirin exerts its pharmacological effects through irreversible acetylation of a serine residue in the active site of cyclooxygenase 2. Omeprazole, a proton pump inhibitor for the treatment of gastric ulcers, translates into the reactive species under the acidic condition in the stomach and binds to the ATPase by forming a disulfide bridge (**Scheme 3B**). The success of these predecessors of covalent inhibitors has paved the way for the design of covalent kinase inhibitors. The new generation of covalent inhibitors is designed by addition of an electrophilic functional group with low reactivity to a highly selective reversible motif. The innovative inhibitors are termed as targeted covalent inhibitors (TCI), which obtain the most attention for the treatment of cancers.



Scheme 3: (A) Examples of covalent inhibitor and (B) covalent binding mode of omeprazole.

1.3.1. Binding mode of covalent inhibitors

In general, covalent inhibitors take effect through a two-step binding mode (**Scheme 4**). Firstly, the inhibitors form a reversible complex with the enzyme. This step is driven by the affinity of inhibitors to the enzyme. Then in the second step, the electrophile in the inhibitor attacks the targeted residue in the enzyme forming a covalent liaison.⁴⁷ Due to the covalent bond, the inhibitors tightly bind to the targeted proteins and can't be replaced by the natural substrate or cofactors of the targets. Therefore, the covalent inhibitors have an increased target potency.



Scheme 4: Cartoon showing the binding of a covalent inhibitor to a target binding pocket.⁴⁷

For reversible inhibitors, the potency is usually described by the inhibitory binding constant (K_i) or IC_{50} . On account of the covalent binding, IC_{50} values for covalent inhibitors are time-dependent, so that it's difficult to compare IC_{50} values of covalent inhibitors. Based on the two-step binding mode of covalent inhibitor, it's more suitable to interpret the potency of covalent inhibitors in terms of k_{inact} / K_i besides IC_{50} . K_i corresponds to the affinity of

initial non-covalent binding and k_{inact} is the kinetic rate constant for the formation of the covalent bond between protein and inhibitor.⁴⁸

1.3.2. The covalently modified residues

Recently a lot of efforts have been put to discover new covalent inhibitors because of their advantages. The properties of targeted residue play a pivotal role in the development of selective covalent inhibitors. The successful covalent modifications of cysteine, lysine, tyrosine, serine, and threonine residues have been reported.

a) Cysteine

Cysteine is the most exploited residue in the targeted covalent inhibitor design in spite of the fact that cysteine exists rarely in proteins with a low prevalence of 1.9%.⁴⁹ The thiol group of cysteine is a moderate nucleophile with a typical pKa of 8.5.⁵⁰ Owing to the big size and the high energy of lone pairs in sulfur, the thiol group is readily deprotonated resulting in the formation of highly nucleophilic thiolate form. Therefore, all the six approved covalent kinase inhibitor drugs targeted non-conserved cysteine.²⁰

The cysteine is not conserved in the kinase and is amenable to covalent modification in at least 200 kinases. The distribution of cysteine in the vicinity of ATP pocket is classified into five groups according to the relative positions (**Figure 15**).^{51,52}

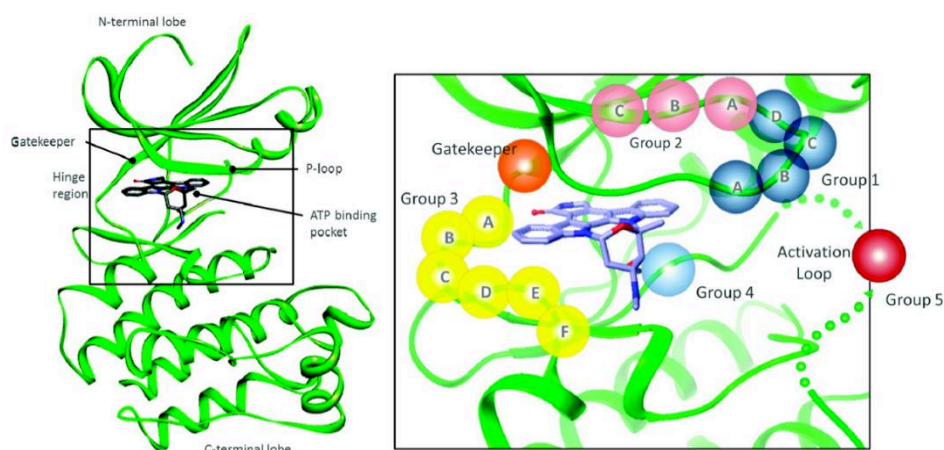


Figure 15: Distribution of cysteine in the vicinity of the ATP pocket. The sphere indicates the location of cysteines that are in principle accessible for covalent modification.⁵¹

The group 1 shown in the dark blue sphere is located in the glycine-rich loop, which anchors the phosphate of ATP. There are 16 kinases containing a cysteine at this position.⁵³

The pink sphere represents the group 2 which is on the roof of the ATP binding pockets. There are 11 kinases which dropped into the group 2 region.

The group 3 represented with the yellow sphere is located on the hinge region and front pocket. The third group covers more than 100 kinases.⁵³ The cysteine in group 3 receives by far the most attention.

The group 4 highlighted with the light blue sphere is near the DFG-motif. The cysteine on this special position is limited in 48 human kinases.⁵³

The group 5 shown in dark red sphere represents the cysteine on the activation loop. There are 8 kinases containing a cysteine on the activation loop. Nevertheless, it is hard to target the cysteine of group 5 because of the flexibility of A-loop.⁵¹

Afatinib is one of the FDA-approved covalent kinase inhibitors targeting the epidermal growth factor receptor (EGFR).²¹ The gatekeeper residue mutation (T790M) confers EGFR resistance against the ATP competitive inhibitors. The irreversible inhibitor afatinib can form a covalent ligation with the residue Cys797 and effectively overcome the drug resistance induced by gatekeeper mutation. The anilinoquinazoline core of afatinib enters into the ATP binding pocket and has a conserved hydrogen bond with the hinge region. The substituted acrylamide induces the formation of a covalent bond with Cys797 (**Figure 16**).⁵⁴

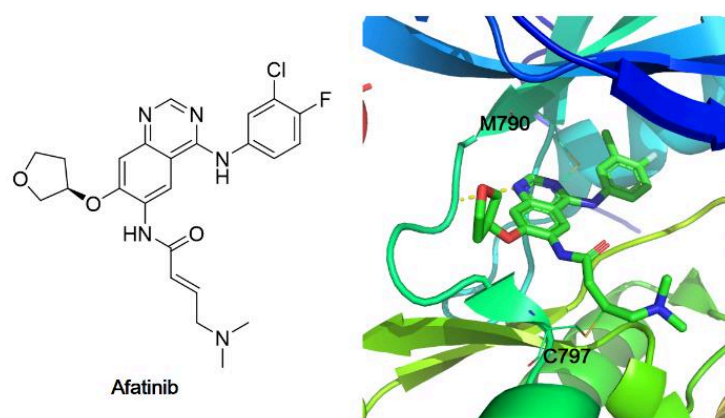


Figure 16: Chemical structure of afatinib and co-crystal structure of afatinib and mutant T790M of EGFR (PDB: 4G5P)

b) Lysine

The covalent modification of lysine has been exploited when the kinase didn't have a suitable cysteine around the ATP pocket.⁵⁵ Lysine exists more abundantly than cysteine in the structure of kinases. The covalent modification of lysine is more challenging in comparison with cysteine. The typical pK_a of lysine is 10.4.⁵⁰ Therefore, under the physiological condition where the pK_a is 7.4, most surface lysine residues are protonated and are not nucleophilic. The buried lysine residues are usually in the neutral form because of the less access of solvent and perturbation in pK_a .⁵⁶ According to the hard-soft-acid-base concept, the ϵ -amino in lysine is a harder nucleophile⁵⁷ in comparison with the thiol in the cysteine or glutathione (GSH), and thus should react more readily with harder electrophiles, such as aldehyde.⁵⁸ It provides the possibility of selective modification of lysine. The intrinsic reactivity of lysine towards various electrophiles was determined by Dahal *et al.*⁵⁹ It was reported that lysine is more reactive than GSH towards vinyl sulfones, while the commonly used acrylamide electrophiles are prone to react with cysteine.

CDKs are crucial protein kinases in the regulation of the eukaryotic cell cycle and in transcription. Irreversible inhibition of CDK2 with a small molecule NU6300 (**Figure 17**) was reported by Anscombe *et al.*⁶⁰ This covalent inhibitor of CDK2 entered ATP pocket and bonded to the hinge region by the purine ring. The vinyl sulfone group formed a covalent bond with Lys89, which was confirmed by the X-Ray crystallography.

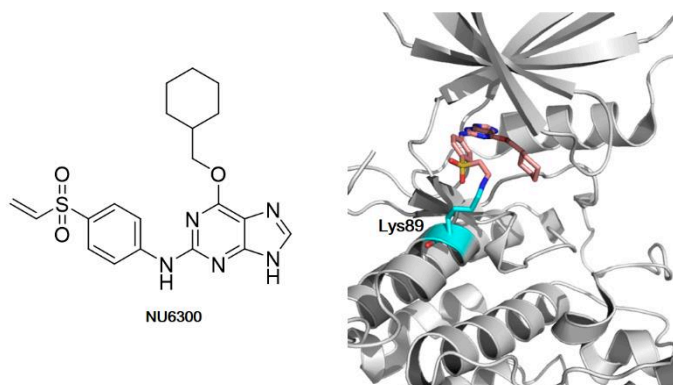


Figure 17: Structure of NU6300 and binding mode of NU6300 with CDK2.⁶⁰

c) Tyrosine

The modification of neutral tyrosine is challenging due to its relatively low intrinsic nucleophilicity. The pK_a value of tyrosine is 9.7 which is lower than that of protonated lysine.⁵⁰ However, it is worth to be noticed that the pK_a value of tyrosine can be profoundly perturbed in the enzyme active site environment. In the bacterial ketosteroid isomerase, the pK_a of Tyr57 was perturbed by around 4 units to 6.3.⁶¹ The lowered pK_a is favourable for the formation of phenoxy anion, which is a high reactive nucleophile. Sulfonyl fluorides are usually used to label tyrosine in the proteome. Whereas sulfonyl fluoride is reactive enough to modify lysine and tyrosine, the preference to tyrosine is observed when the tyrosine is proximal to basic amino acid residues.⁶²

Rational design of tyrosine targeted covalent inhibitor was reported by Gray's group.⁶³ The lead compound alectinib, which is an anaplastic lymphoma kinase (ALK) inhibitor, exhibited strong inhibitory activity toward the SR-protein kinase SRPK1 with an IC_{50} value of 11 nM. The X-ray structure of a complex of alectinib with SRPK1 showed that Tyr227 in the front region of ATP binding site might be covalently modified by the installation of an electrophilic warhead to the lead compound (**Figure 18**). The 4-morpholinopiperidine moiety was replaced by a meta-substituted phenyl ring bearing a sulfonyl fluoride substituent. This modification in the SRPKIN conferred selectivity towards SRPK1 over ALK with IC_{50} values of 36 nM and 195 nM respectively. The covalent binding mode of this compound was also supported by washout experiments and further confirmed by MS.⁶³

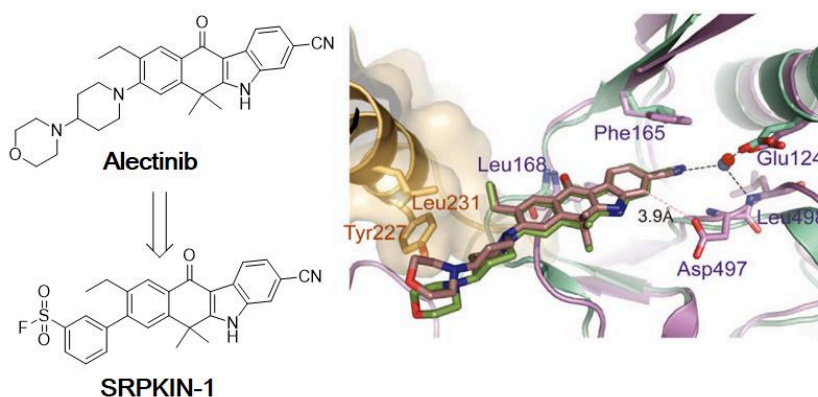
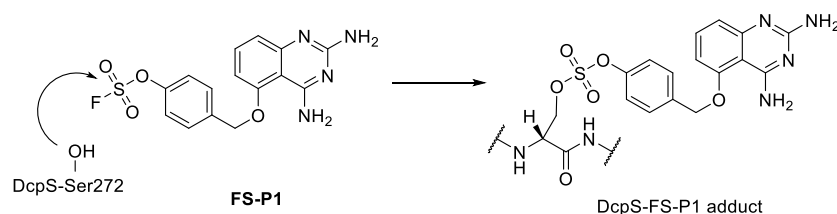


Figure 18: Chemical structure of Alectinib and SRPKIN-1 (left), the binding mode of Alectinib in SRPK (purple) and overlap of Alectinib in ALK (green).⁶³

d) Serine and threonine

Serine and threonine have a side-chain containing hydroxyl group which can be covalently modified. When serine or threonine is located at the catalytic site of proteases and other hydrolase enzymes, the side chain hydroxyl group is extensively activated due to the perturbation of pK_a by surrounding residues.⁶⁴ However, the non-catalytic serine and threonine are less nucleophilic owing to the intrinsic low activity and acidity (typical pK_a 13). In spite of the low reactivity, the mechanism study found that in cyclooxygenase the non-catalytic serine Ser530 was acetylated by aspirin.⁶⁵ Recently, researchers from Pfizer reported a pioneering work,⁶⁶ in which a non-catalytic serine (Ser272) in the mRNA decapping scavenger enzyme (DcpS) was covalently targeted using fluorosulfate electrophilic warhead (**FS-P1**, **Scheme 5**). The authors emphasized that the covalent modification of serine might be attributed to the appropriate orientation of ligand and pK_a perturbation of serine induced by the nearby basic residues. Therefore, targeting serine or threonine provides an opportunity to develop next-generation of covalent modulators.



Scheme 5: Covalent binding of serine and fluorosulfate.⁶⁶

1.3.3. Electrophilic groups for the covalent inhibitor

The reactivity of electrophile is correlated with the kinetic process of covalent bond formation. On the other hand, it's also responsible for off-target labelling. Therefore, most electrophiles used in the covalent inhibitors have modest reactivity, such as the Michael acceptor acrylamide.

In recent years, in order to reduce the risks concerning promiscuous covalent binding, Taunton's laboratory developed chemically tuned electrophiles that could form a reversible covalent bond with non-catalytic cysteine.^{67,68} Installation of a nitrile group to electron-deficient olefins increased the olefins' reactivity, but paradoxically eliminated the formation of irreversible adducts. Shindo and colleagues⁶⁹ reported electrophile such as chlorofluoroacetamide which also exhibited a reversible covalent modification of kinase cysteine. They demonstrated that the covalent adduct of chlorofluoroacetamide and cysteine was stable in solvent-sequestered ATP-binding pocket of EGFR, while under aqueous conditions it was hydrolyzed to free thiol and hydrated glyxamide.⁶⁹

During the development of covalent inhibitors, the scope of electrophile groups is well studied and expanded, including acrylamide, fumaric acid ester, propiolonitrile, α -halomethyl amide/ester/ketone, α -cyanoacrylamide, aldehyde, isothiocyanate, vinyl sulfone, sulfonyl fluoride, aryl fluorosulfate etc.⁷⁰ The common warheads used in the drug design and their binding mode were summarized in the **Table 1**.

Table 1: covalent warheads for targeted amino acid labelling of kinase and their binding mode

Chemical structure	Targeted residues	Kinetic properties	Binding mode
	Cys	Irreversible covalent	
	Cys	Irreversible covalent	
X=Cl, Br			
	Cys	Irreversible covalent	
	Cys	Irreversible covalent, Metabolically limited reactivity	
	Cys	Reversible covalent	
	Lys Tyr	Irreversible covalent	
	Lys Cys His	Irreversible covalent	

2. Focal adhesion kinase (FAK)

The focal adhesion kinase (FAK) was initially identified using homology-based cDNA cloning approach in 1992.⁷¹ It's a cytoplasmic 125-kDa non-receptor protein tyrosine kinase. FAK and proline-rich tyrosine kinase 2 (PYK2) constitute the FAK family of tyrosine kinase, and they share a 65% similarity in sequence.⁷² FAK is ubiquitously expressed in most tissues and cells throughout the human body, while the expression of PYK2 is conserved in the brain tissues.⁷²

2.1 Structure and function of FAK

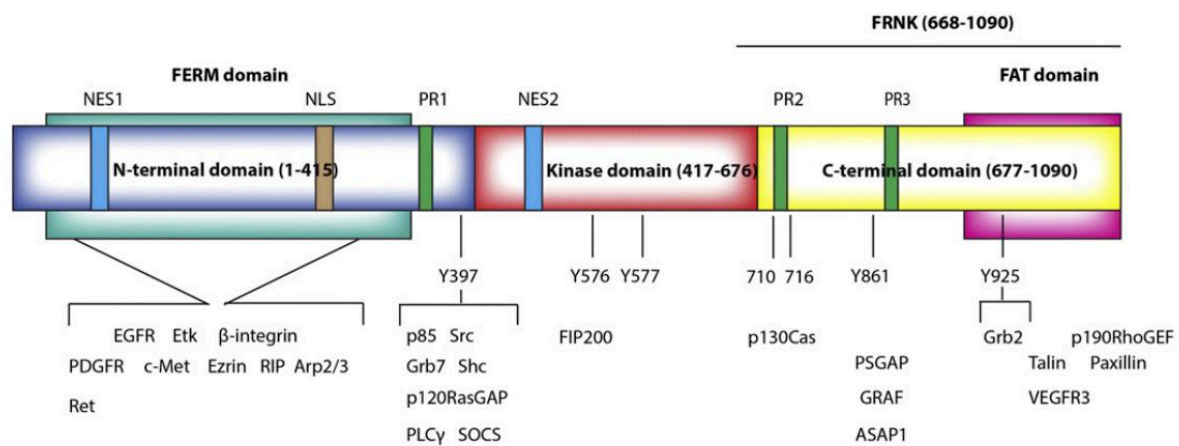


Figure 19: Schematic representation of FAK.⁷³

The FAK protein comprises three major domains: a central kinase domain, flanked by an N-terminal domain and a C-terminal non-catalytic domain (**Figure 19**).

a) N-terminal domain

The large N-terminal domain in FAK is composed of 415 amino acids and contains the FERM (four-point-one, ezrin, radixin, moesin) domain, a nuclear export sequence 1 (NES1) and nuclear localization sequence (NLS). The FERM domain plays a pivotal role in the regulation of the FAK kinase activity and is involved in protein-protein interactions as a

scaffold for the signal transduction. For example, the tyrosine kinase Etk mediates the cell migration in response to the stimuli of extracellular proteins, while the activation process of Etk is dependent on an interaction between the PH domain of Etk and FERM domain of FAK.⁷⁴ The nuclear function of FAK also associates with the FERM domain as it regulates the subcellular localization of FAK.⁷⁵

b) C-terminal domain

The C-terminal domain of FAK is composed of 414 amino acids and contains two proline-rich regions (PR2 and PR3) and a focal adhesion targeting region (FAT).⁷⁶ The FAT domain shares a similar four-helix bundle structure among FAK and other adhesion proteins, such as vinculin, Cas, and α -catenin. The FAT sequence is essential for the localization of FAK to the adhesion complexes and required for FAK signalling.⁷⁶ The non-catalytic domain in C-terminal of FAK, termed FRNK (FAK-related-non-kinase) serves as a negative regulator of kinase activity and is expressed independently in certain cells. It has been demonstrated that forced overexpression of FRNK inhibits cell spreading, cell migration and growth-factor-mediated signals to MAP kinase.⁷⁶

c) Kinase domain

The central kinase domain in FAK (residue 417- 676) is structurally similar to the other receptor and non-receptor tyrosine kinases with a small N-lobe and a big C-lobe connected with the hinge region (**Figure 20A**). The N-lobe consists of four β -sheets and an α C-helix. Residues from Gly429 to Gly434 constitute the glycine-rich-loop (GXGXXG) also called a P-loop, which forms Mg^{2+} -mediated interaction with the phosphates of ATP. The C-lobe comprises several α -helix and two important loops for the kinase catalytic function. Residues from His544 to Asn551 consist of the catalytic loop (C-loop) and residues from Gly563 to Ser568 are part of the activation loop (A-loop). The FAK kinase is autoinhibited by the interaction with the FERM domain. The activation process requires a displacement of the FERM domain. Superposition of the active kinase domain on the structure of the

autoinhibited kinase showed that the α C-helix adopts the same position (“ α C-helix in” conformation) in these two states, while the activation loop in the inactive conformation extends to the FERM domain and blocks the entrance of ATP to the catalytic region (**Figure 20B**).⁷⁷

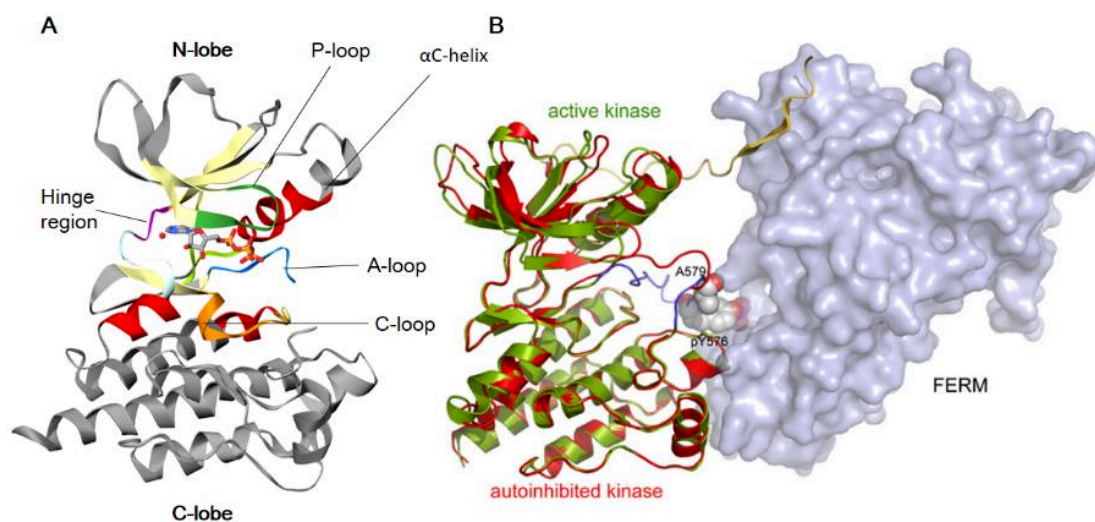


Figure 20: (A) crystal complex of FAK with ATP, (B) superposition of active FAK kinase (green) and autoinhibited kinase (red) by FERM.⁷⁷

The active site of FAK

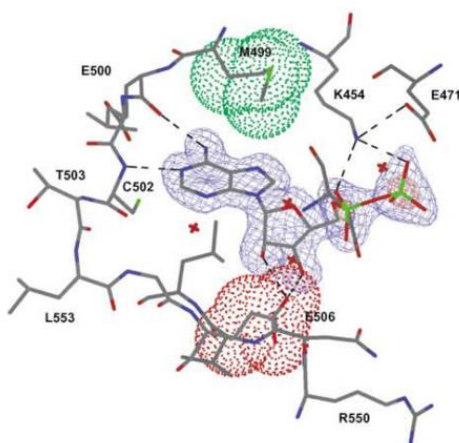


Figure 21: binding mode of ATP to FAK kinase.⁷⁸

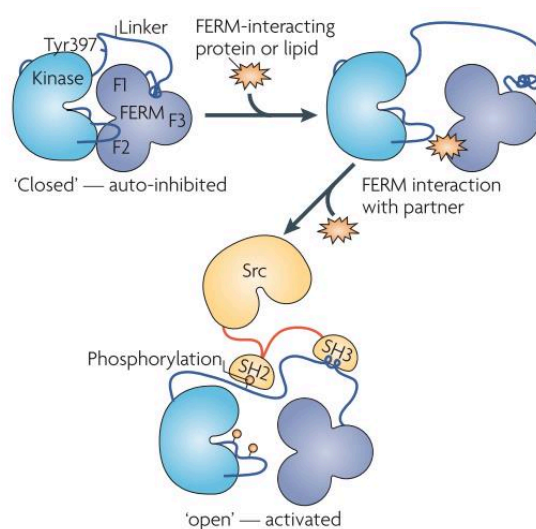
Nowakowski *et al*⁷⁸ solved the crystal structure of FAK kinase domain in 2002 and revealed the binding mode of ATP to FAK. The ATP binding site of FAK is shown in **Figure**

21. The N1 nitrogen and the amino group of the adenine ring bind to the main chain of Cys502 and Glu500, respectively. The 2'-, 3'- hydroxyl group of the ribose bond to the side chain of residue Glu506 through two hydrogen bonds. The phosphates of ATP are stabilized by interaction with residue Lys454 and Glu471. Moreover, around residue Met499, this region forms a hydrophobic pocket in FAK kinase.

2.2 FAK signalling pathway and biological functions

a) The activation process of FAK

FAK is a pivotal protein in the integrin signalling. The stimuli of extracellular matrix to integrins assembles FAK localized to focal adhesion. Then the auto-inhibitory interaction of the kinase domain and FERM domain is disrupted to release FAK into activated conformation. In this conformation autophosphorylation of Tyr397 reveals the binding site for SH2 domain of Src. The Src protein is activated by binding to FAK and then it conversely phosphorylates residues Tyr576 and Tyr577 in the activation loop of FAK. The mutually activated FAK/Src complex triggers a cascade of phosphorylation events and protein-protein interactions to activate several signalling pathways (**Scheme 6**).^{76,79}



Scheme 6: Activation process of FAK.⁸⁰

b) Biological functions of FAK

FAK kinase plays an important role in regulating cell motility, invasion, and cell survival.^{73,76,81,82,83} Deregulation of FAK also participates in the development of cancers. Enhanced expression of FAK protein has been observed in a number of cancers, including breast⁸⁴, colon⁸⁵, thyroid⁸⁶, prostate⁸⁷, lung⁸⁸, stomach⁸⁹ and ovary.⁹⁰ As shown in **Table 2**, it was observed that advanced cancer cells exhibited higher-level expression of FAK protein compared with benign tumours and normal tissues.⁹¹

Table 2: FAK expression in tumours

Tissue	Normal	benign	Pre-invasive	Invasive	metastatic	ref
Breast	+/-			+++	++++	92
Colon	+	-	+++	+++	+++	92
Thyroid	+/-	+		+/+	++++	93
Prostate	+/-	+		+	+++	87
Liver	-			+++		92
Brain	-	-	+	-	+++++	94

The expression of FAK promotes the survival of cancer cells. The first clue of the relationship between FAK and cell survival was demonstrated in 1996 that expression of active FAK could suppress anoikis of MDCK cells.⁹⁵ It was also demonstrated that the function of tumour suppressor protein p53 which induces apoptosis and cell cycle arrest was disturbed due to interaction of FAK and p53.⁹⁶ The nuclear FAK also promotes p53 ubiquitination and degradation.⁹⁷ In addition, inhibition of FAK in tumour cells promotes apoptosis and loss of adhesion.^{98,99}

Studies have demonstrated that FAK is an important regulator of cell migration¹⁰⁰ which was required for the invasion and metastasis of cancer cells. FAK integrates several

signalling responses that control focal-adhesion assembly and disassembly. Phosphorylation of FAK recruits a number of signalling and structural proteins promoting the assembly of focal adhesion, such as Src, Cas and paxillin. On the other hand, FAK also recruits extracellular signal-regulated kinase 2 (ERK2) and calpain-2 to focal adhesion and promotes calpain-2-mediated cleavage of focal adhesion.^{101,102}

FAK functions also related to the angiogenesis and lymphangiogenesis based on the observations that FAK-knock-out mice displayed embryonic lethal phenotype with defects of vasculogenesis.¹⁰³ In addition, it was demonstrated that inhibition of FAK expression resulted in reduced VEGF expression through FAK-Grb2-MAPK signalling pathway and caused small avascular tumours in mice.¹⁰⁴

Another interesting point is that recent studies indicated that FAK might be a crucial driver of immune escape and inhibition of FAK might have a synergetic effect with immunotherapy. Regulatory T cells (Tregs) could dull the anti-tumour immune response of immune-base therapy which aimed at activation of CD8+ T cell. A study in squamous cell carcinoma cells showed that nuclear FAK regulates chemokine/cytokine and ligand-receptor networks to recruit Tregs in the tumour microenvironment, which resulted in the inhibition of antigen-primed cytotoxic CD8+ T cell activity, and promoted immunological tolerance and permitted tumour growth. Furthermore, this study also demonstrated inhibition of FAK activity with small molecule could promote immune-mediated tumour regression.¹⁰⁵ Another study performed in human pancreatic ductal adenocarcinoma (PDAC) showed that FAK was highly activated in human PDAC and correlated with the immunosuppressive tumour environment. Treatment with FAK inhibitor increased the response of KPC mouse to T cell immunotherapy and PD-1 antagonists.¹⁰⁶ These findings indicate that FAK signalling may play a significant role in tumour immunity. Therefore, immunotherapy treatment in combination with FAK kinase inhibition may provide promising therapeutic opportunities.

2.4 FAK inhibitors

Because of the importance of FAK functions in cancer, many efforts have been made for the development of FAK inhibitors. Here, the inhibitors of FAK both under development and in preclinical studies are summarized according to the classification of kinase inhibitors.

2.4.1. Type I FAK inhibitors

Type I inhibitors of FAK have been extensively studied. Up to now, there are 7 type I inhibitors of FAK under clinical trials. In structure, type I inhibitors of FAK conserve a multi-substituted heterocycle scaffold, such as pyrimidine, pyridine, etc. Herein, the represented type I inhibitors of FAK are introduced according to the heterocyclic scaffold.

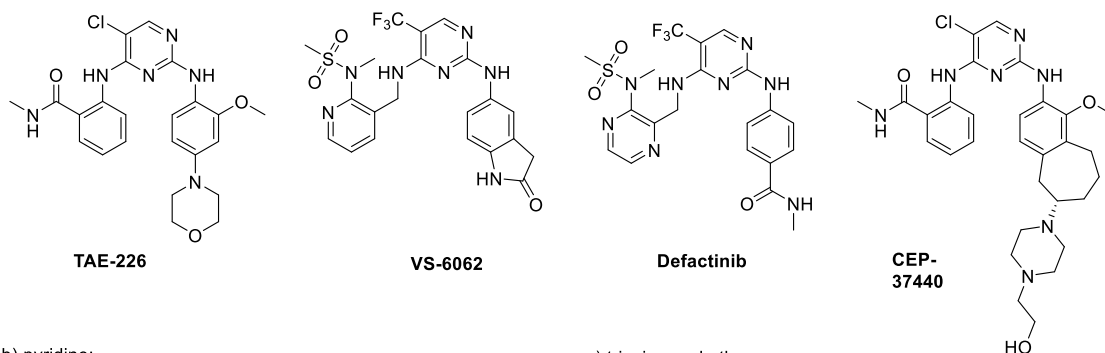
a. pyrimidine, pyridine, and triazine based inhibitors.

Pyrimidine-based inhibitors

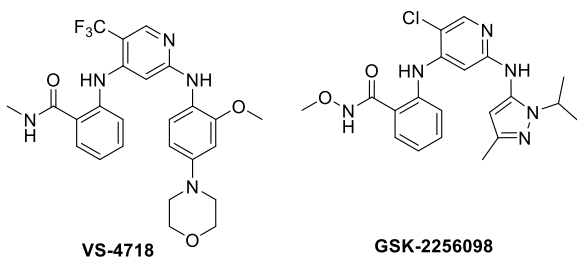
The 2,4-diaminopyrimidines (**Figure 22**) constitute the most reported FAK inhibitors, and this kind of scaffold delivered several clinical candidates, such as VS-6062,¹⁰⁷ Defactinib,¹⁰⁸ and CEP-37440.^{109,110}

TAE-226 (**Figure 22**), developed by Novartis is a dual inhibitor of FAK and IGF-IR proteins. It exhibited strong inhibitory activity against FAK and IGF-IR *in vitro* with an IC₅₀ value of 5.5 nM and 160 nM and reduced autophosphorylation of FAK and IGF-IR in glioma cells U87-MG and U251.¹¹¹ In addition, TAE-226 retarded the cell growth of a battery of glioma cell lines accompanied by flat, enlarged morphology and multiple nuclei in single cell.¹¹¹ TAE-226 also affected cell cycle distribution and induced apoptosis in glioma cell lines with mutant p53, such as U251, LN18, and LN229, whereas the cell line with wt-p53 U87-MG was less sensitive to TAE-226.¹¹¹ However, TAE-226 was stopped at the preclinical study due to the inhibition of insulin receptor kinase with an IC₅₀ value of 26 nM.¹¹¹

a) pyrimidine:



b) pyridine:



c) triazine and others

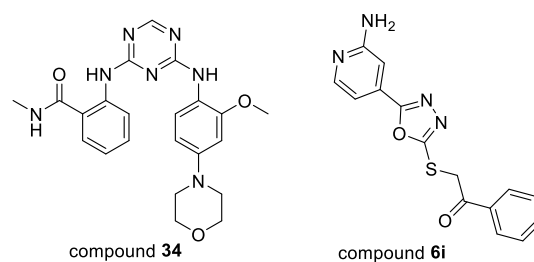


Figure 22: Chemical structures of some FAK inhibitors.

Several groups^{109,112,113,114} synthesized analogues of TAE-226, among which the modification is concentrated on the replacement of morpholine moiety. One of the analogues CEP-37440 (**Figure 22**) developed by Teva pharmaceuticals is a dual inhibitor of FAK and ALK with IC_{50} values of 2.0 nM and 3.1 nM, respectively.¹⁰⁹ CEP-37440 displayed inhibitory activity against insulin receptor with IC_{50} value of 65 nM, whereas it strongly inhibited the autophosphorylation of ALK (IC_{50} = 22 nM) and FAK (IC_{50} = 80 nM) in cell rather than insulin receptor (IC_{50} = 2000 nM).¹⁰⁹ Moreover, CEP-37440 was able to inhibit proliferation of a part of inflammatory breast cancer cell lines at low concentration (< 1 μ M), such as FC-IBC02, SUM190, and KPL4, but not affecting the proliferation of normal breast epithelial cells.¹¹⁰

VS-6062 (**Figure 22**) is also an ATP-competitive inhibitor of FAK, which selectively inhibited the enzymatic activity of FAK with an IC_{50} value of 1.5 nM *in vitro* and inhibited autophosphorylation of FAK with an IC_{50} value of 5 nM in cells.¹⁰⁷ Kinase selectivity profile showed that VS-6062 had a good kinase selectivity on a panel of 42 kinases, and the concentration for half inhibition of IGF-IR was over 500 nM.¹⁰⁷ The good selectivity results

from a helical conformation of “DFG motif” induced by VS-6062. The methane sulfonamide moiety of VS-6062 forms a hydrogen bond with backbone NH of Asp564, and the pyridinyl of VS-6062 has a hydrophobic interaction with the side chain of Leu567 (**Figure 23**).¹⁰⁷ The results of a phase I clinical trial showed that VS-6062 was a potent CYP3A inhibitor, which may cause toxicity in the situation of co-administration with other drugs.¹¹⁵

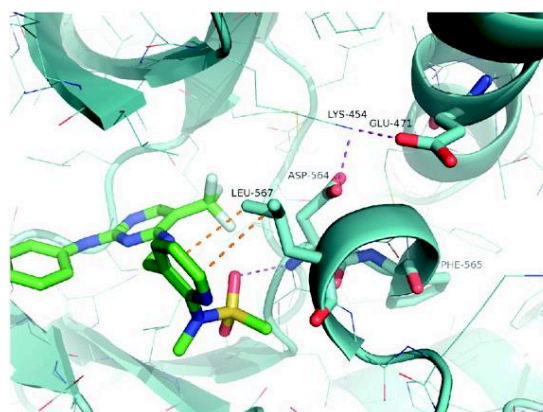


Figure 23: Binding mode of VS-6062 in the active site of FAK.

The analogue of VS-6062, Defactinib (**Figure 22**), is the second generation of FAK inhibitor, which has weak inhibitory activity against CYP3A and a more favourable PK/PD profile.¹⁰⁸ VS-6063 could increase the sensitivity of drug-resistant cancer cells to chemotherapy. VS-6063 in combination with paclitaxel significantly decreased proliferation and increased apoptosis in taxane-resistant ovarian carcinoma cell lines.¹¹⁶ Docetaxel in combination with VS-6063 caused a great decrease in the viability of docetaxel-resistant metastatic castration-sensitive prostate cancer cells.¹¹⁷ The enhanced inhibitory effects were also observed in squamous cell lung carcinoma when VS-6063 combined with AKT inhibitors.¹¹⁸ Moreover, several phase I clinical trials in patients with advanced solid tumours indicated that VS-6063 has an acceptable safety profile and mild adverse events.^{108,119} Now VS-6063 is under phase II clinical study.

Pyridine-based inhibitors

VS-4718 and GSK-2256098 (**Figure 22**) are pyrimidine-based FAK inhibitors. VS-4718 was an analogue of TAE-226. It displayed inhibitory activity against FAK with an IC₅₀ value of 1.5 nM *in vitro* and about 0.1 μM for inhibition of FAK Tyr397 phosphorylation in breast carcinoma cells.¹²⁰ Kinase selectivity profile showed that VS-4718 only inhibited the activity of FAK and Flt3 greater than 50% at 0.1 μM concentration, whereas VS-4718 didn't show obvious inhibition against IGF-IR and IR at 0.1 μM concentration.¹²⁰ VS-4718 selectively blocked FAK and p130Cas phosphorylation and triggered cell apoptosis in a cell suspension culture. In contrast, the proliferation or survival of cell was not affected in attached culture.¹²⁰

The small molecule GSK-2256098 (**Figure 22**) developed by GlaxoSmithKline inhibited the FAK activity by blocking the phosphorylation of Tyr397. GSK-2256098 showed strong preferential inhibition of FAK with an IC₅₀ value of 0.4 nM,¹²¹ which is 1000-fold less than that of Pyk2.¹²² GSK-2256098 inhibited cell growth, decreased cell motility in anchorage-independent conditions.¹²² Up to now, three phase I clinical trials of GSK-2256098 have been completed. The Phase I clinical trial (NCT 01138033) in the treatment of patients with advanced solid tumours, showed that the adverse events included light grades of nausea, diarrhea, vomiting and decreased appetite.¹²³

Triazine-based inhibitors and others

In 2013, our team¹²⁴ synthesized a family of diarylamino-1,3,5-triazine derivatives as FAK inhibitors. The most potent compound **34** (**Figure 24**) has a similar effect to TAE-226 on inhibition of cell viability of human umbilical vein endothelial cells (HUVEC) with IC₅₀ values of 1.5 μM and 1.0 μM, respectively. However, *in vitro* enzymatic activity of compound **34** was nearly 45-fold weaker than that of TAE-226. The cocrystal structure of compound **34** and FAK was resolved and revealed that the 1,3,5-triazine derivative **34** bound to the hinge region in a similar conformation of TAE 226. The loss of enzymatic activity of compound **34** might be attributed to the fact that interaction between 5-chlorine of TAE-226

and Met499 was lost in our thiazine derivative.

The group of Zhu reported the study of different five-member heterocyclic ring derivatives as cellular-active anticancer agents and FAK inhibitors, such as 1,3,4-thiadiazole,^{125,126} 1,3,4-oxadiazole,^{127,128} 1,2,4-triazole,¹²⁹ and imidazole.¹³⁰ A 1,3,4-oxadiazol derivative **6i** (**Figure 22**) exhibited the most potent antitumour activity against MCF-7 breast cancer line and A431 epidermoid carcinoma cell line with IC₅₀ values of 140 nM and 10 nM, respectively. Its inhibitory enzymatic activity of FAK kinase gave IC₅₀ value of 20 nM.¹²⁷ Unfortunately, no further study of this compound was reported.

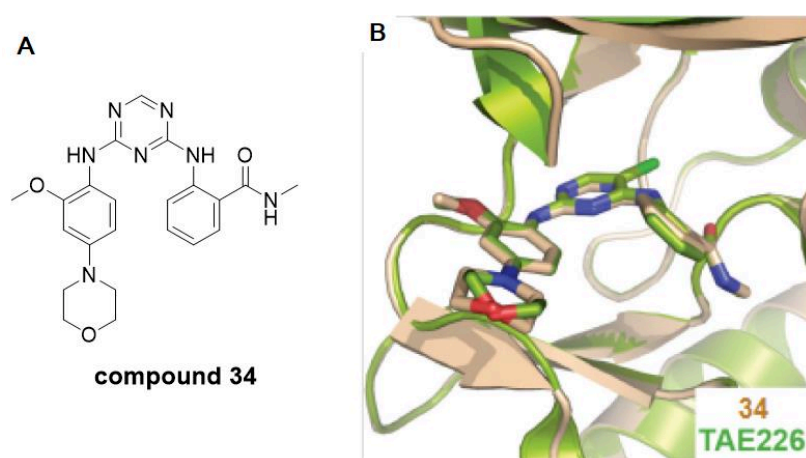


Figure 24: (A) Structure of compound **34**, (B) Superposition of the structures of **34** and TAE-226 bound to FAK.

b. fused heterocycles-based inhibitors

Choi *et al*^{131,132} elucidated the discovery of a series of 7*H*-pyrrolo[2,3-*d*]pyrimidines as FAK inhibitors. Through extensively structural modification study, compound **32** (**Figure 25**) was obtained as a potent FAK inhibitor with an IC₅₀ value of 4 nM.¹³² It was demonstrated that the integrity of pyrrolo-pyrimidine was important to the inhibition of FAK because the reduction or expansion of the five-member ring caused a loss of activity.¹³¹ In addition, the existence of an extended carboxyl group on the pyridinyl ring significantly improved the anti-FAK enzymatic activity.¹³² Molecular docking showed that the carboxyl group formed a salt bridge with K454 (**Figure 26**)

Herinrich *et al*¹³⁴ reported a fragment-based discovery of highly substituted 7-azaindole as FAK inhibitors. Compound **37** (**Figure 25**) was the most potent inhibitor of FAK among all the 7-azaindole derivatives. An electron-withdrawing substituent at position 5 of the 7-azaindole core could improve the binding affinity, and introduction of a CF₃ group improved the inhibitory activity against FAK and selectivity. The substituent at position 4 pointed to the DFG-motif of FAK. The substituents, like benzamide or sulphonamide which provide a hydrogen bond acceptor, were beneficial to improve the activity. The substituents at position 2 played a significant role in kinase selectivity. The best kinase selectivity was obtained when 4-F-phenyl group was introduced.¹³⁴ Compound **37** strongly inhibited enzymatic activity of FAK *in vitro* (IC₅₀ = 37 nM) and Tyr397 phosphorylation of FAK in HT-29 cells (IC₅₀ = 2.015 μM). Kinase selectivity profiling showed that only 1 kinase (IGF-IR) was inhibited with higher potency than FAK among 120 tested kinases.¹³⁴

The dihydropyrrolopyrimidine derivative, CT-707 (**Figure 25**), is a multi-kinase inhibitor targeting FAK, ALK, and Pyk2, with significant inhibitory effect on FAK (IC₅₀ value of 1.6 nM). *In vitro*, CT-707 displayed an effect on cancer cell growth and cell detachment. *In vivo*, CT-707 exhibited inhibition of tumour growth and metastasis in T47D, Karpas299 and 4T1 xenograft models. Combination of CT-707 with the MET inhibitor Cabozantinib showed synergistic anti-tumour effects against HCC *in vitro* and *in vivo*.¹³⁵ Now a phase I clinical study of CT-707 is initialling.

A series of imidazo[1,2-a][1,3,5]triazines were synthesized as FAK inhibitors by our group¹³⁶. The most potent compound **19a** (**Figure 25**) inhibited the FAK enzymatic activity with an IC₅₀ value of 50 nM. Kinase selectivity assay of compound **19a** on a panel of 30 kinases showed that compound **19a** rather specifically inhibited FAK kinase. The further biological evaluation showed that compound **19a** could block the Tyr397 phosphorylation of FAK in the tested cell lines, such as U-87MG, HCT-116, MDA-MB-231 and PC-3, and this compound also inhibited cell proliferation by arresting cell cycle at G2/M phase in U87-MG and HCT-116 cells.¹³⁶

2.4.2. Type II FAK inhibitors

Researchers from the Merck Serono Research group disclosed the structure of a type II inhibitor (compound **13**, Figure 27) which was discovered by high throughput screening.¹³⁷ Compound **13** displayed submicromolar inhibitory potency against FAK ($IC_{50} = 266$ nM). The crystal structure of FAK in complex with compound **13** revealed that the activation loop adopted a DFG-out conformation and the 5-*tert*-butyl-2-*p*-tolyl-pyrazole ring of **13** is buried into a hydrophobic pocket induced by a conformational change of activation loop. In addition, the authors conducted replacement of purine ring of compound **13** with the fragments containing smaller molecular weight and heteroatom content which were identified as a good hinge region-binder in a surface plasmon resonance binding assay, but the new analogues unexpectedly showed significantly decrease in binding affinity to FAK.

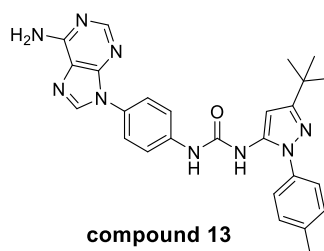


Figure 27: Structure of compound **13**

2.4.3. Allosteric FAK inhibitors

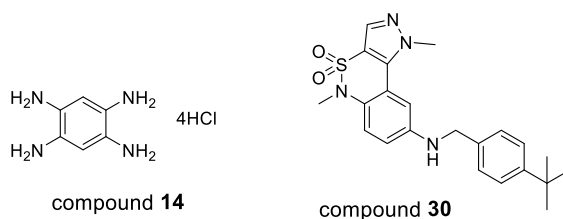


Figure 28: Chemical structures of allosteric inhibitors of FAK.

In 2008 Golubovskaya *et al*¹³⁸ reported a small molecule named **14** (Figure 28) as FAK inhibitor. The authors screened a compound library containing 1 400 000 molecules with computer modelling and obtained 35 compounds that could bind to the pocket of FAK

containing Tyr397 with satisfied scores of binding energy. Then these 35 compounds were tested for the effect on cell viability by MTT assay on 6 cancer cell lines, including BT474, T47D, MCF-7 breast cancer, HT29 colon cancer, C8161 melanoma and A549 lung cancer cell lines. Compound **14** among the 35 lead compounds exhibited the best inhibition of cell viability in all the tested cancer cell lines. Compound **14** blocked the Tyr397 phosphorylation in a dose- and time-dependent manner in BT474 breast cancer cells. Although compound **14** failed to induce apoptosis at 50 – 100 μM , it effectively caused cell detachment and inhibited cell adhesion. In addition, compound **14** could effectively cause breast tumour regression in mouse models.

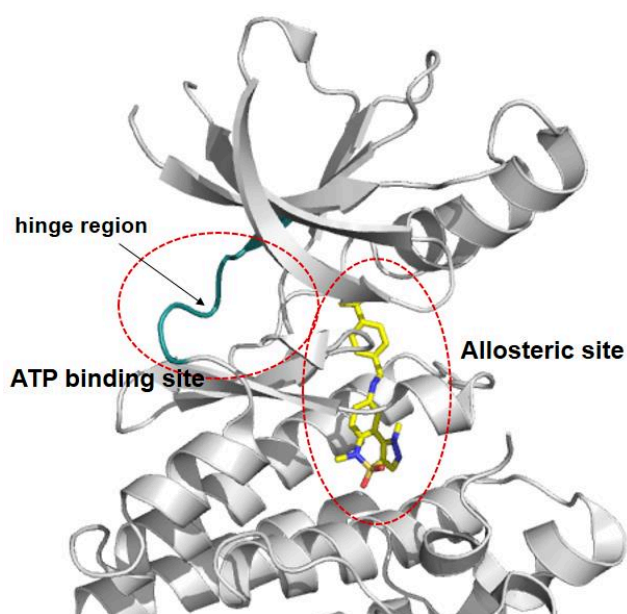


Figure 29: Co-crystal structure of compound **30** with FAK (PDB: 4I4F).

The researchers from Takeda Pharmaceutical Company reported tricyclic sulfonamides as type III inhibitors of FAK.^{139,140} A cellular-active allosteric inhibitor of FAK exemplified compound **30** (**Figure 28**) was reported in 2013.¹³⁹ Compound **30** exhibited time-dependent inhibitory activity against FAK ($\text{IC}_{50} = 2.2 \mu\text{M}$, pre-incubation 5 min; $\text{IC}_{50} = 0.64 \mu\text{M}$, pre-incubation 60 min) with 0.5 μM ATP in the testing system and significantly reduced FAK phosphorylation with an IC_{50} value of 7.1 μM .¹³⁹ Kinase selective profiles suggested that compound **30** was a specific FAK allosteric inhibitor with an IC_{50} value over 10 μM against a panel of kinases including Pyk2, Scr, HER2, Akt1, Aurora B, MEK1 and p38 α . The X-ray

crystal structure of compound **30** in complex with FAK kinase (**Figure 29**) showed that compound **30** bound to an allosteric site. The structure-activity relationship analysis demonstrated that the methyl group at 1-position of pyrazole ring is embedded in a hydrophobic pocket and prevents the pyrazolo[4,3-c][2,1]benzothiazine core from entering the ATP binding site.

2.4.4. Inhibitors targeting FAK-protein interactions

The tyrosine kinase FAK plays its biological roles in cells through both kinase-dependent and independent ways. Vascular endothelial growth factor receptor 3 (VEGFR3) is a tyrosine receptor kinase, which is involved in lymphangiogenesis, angiogenesis and tumourigenesis. In tumour cells, VEGFR3 binds to the FAT domain in C-terminal of FAK and promotes cell survival. Small drug-like molecules that interfere in the protein-protein interaction of FAK were reported as well.

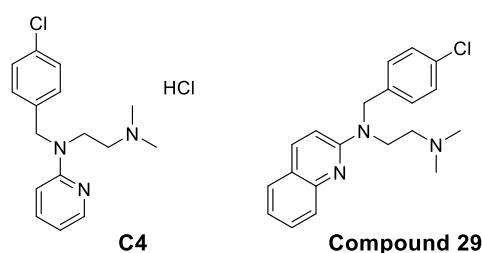


Figure 30: Chemical structure of compounds **C4** and **29**.

In 2009, Kurenova *et al*¹⁴¹ identified a small molecule chloropyramine hydrochloride (**C4**, **Figure 30**) through screening *in silico* as an inhibitor of FAK-VEGFR3 interaction. Compound **C4** bound to a pocket in FAT domain containing residue His1025, which was a key residue for FAK-VEGFR3 interaction. Subsequent studies confirmed that **C4** interrupted the colocalisation of FAK-VEGFR3 complex and disrupted FAK and VEGFR3 binding in breast cancer cells. **C4** caused apoptosis and reduced viability of breast cancer cells that expressed VEGFR3. In addition, **C4** could inhibit the tumour growth in xenograft mouse models with VEGFR3 high-expressed breast cancer.

In 2014, Gogate¹⁴² reported an analogue of **C4**, compound **29** (**Figure 30**) which was a more potent inhibitor of FAK-VEGFR3 interaction. Kinase selectivity screening on a panel of 10 kinases, which are related to FAK or VEGFR3 proteins or in FAK downstream signalling cascades showed that none of the tested kinases was inhibited over 50% at the concentration of 1 μ M. The cellular assay showed that compound **29** was specifically cytotoxic to pancreatic cancer lines, Panc-1-luc and MiaPacCA-2-luc which expressed a high level of FAK and VEGFR3 proteins.

3. Previous work in the laboratory

Our laboratory has put numerous endeavours on development of FAK inhibitors and synthetic methodology study for constructing new heterocyclic scaffold. The ATP-competitive inhibitors with scaffold of 1,3,5-triazine, 1,2,4-triazine, or imidazo[1,2-a][1,3,5]triazine^{136,124,143} were investigated. On the other hand, Expédite Yen Pon (thesis 2013 – 2016) put her efforts on the development of ATP-noncompetitive inhibitors, such as type II inhibitors and covalent inhibitors.^{144,145}

The initial work of the development of covalent inhibitors was dedicated to exploring suitable linkers and electrophiles. Several potential covalent inhibitors with three types of linkers including aliphatic chain, triazole, and squaramide were synthesized in modest yields. The preliminary biological evaluations showed that the compounds bearing squaramide linker and triazole linker displayed strong inhibitory activity against FAK.

4. Objectives

As mentioned in chapter 1, FAK is emerging as a promising therapeutic target, because it is over-expressed in many types of solid and non-solid tumours, whereas no inhibitors of FAK is on the market except those in clinical trials. On the other hand, the novel role of FAK in the regulation of cancer stem cell functions and immunology still need to be clarified and explored in the future. For these reasons, it is still necessary to develop selective and potent inhibitors of FAK.

Based on the encouraging results obtained in our team, the primary objective of my thesis focused on the development of covalent inhibitors of FAK. For this work, a) The first step was to improve the synthesis of diaminopyrimidine based covalent inhibitors and prepare the corresponding reversible inhibitor without the electrophilic warhead in order to perform the biochemical characterization of the covalent inhibitor of FAK. b) The second step was to design and synthesize new irreversible and reversible covalent inhibitors in order

to improve the selectivity and bioavailability.

The second objective was to optimize the synthetic route of 2,5-disubstituted pyrimidines which are important scaffolds for developing type II inhibitors of FAK. Despite the simple structural features of these scaffolds, the substitution at 5 position of pyrimidine encountered major setbacks due to the low reactivity at the 5 position of the pyrimidine ring. Therefore, it was necessary to develop a concise approach for the synthesis of these compounds with large functional group compatibility and in good yield.

The last objective of my thesis was the synthesis of fluorescent probes of FAK as tools for the visualization of FAK in cells, which could benefit the study of FAK signalling cascades.

Chapter II. Development of covalent inhibitors of FAK

The objective of this chapter is to develop targeted covalent inhibitors of FAK. As described in chapter I, FAK kinase is a very promising therapeutic target and a lot of efforts have been made to discover highly selective FAK inhibitors. Though there have been some inhibitors in the clinical research, all these compounds compete with ATP and show a reversible inhibition against FAK. The targeted covalent inhibitors have many advantages over the reversible inhibitors such as increased efficiency, better selectivity, lower risk of drug resistance derived from active site mutation and prolonged duration of inhibition. Up to our work, it was a blank field to covalently inhibit the FAK activity. This chapter of my work dedicates to the discovery of highly selective targeted covalent inhibitors of FAK.

This chapter consists of three parts: 1. Improvement of synthesis and characterization of the first covalent inhibitor of FAK; 2. Design, synthesis and biological evaluation of new irreversible and reversible covalent inhibitors; 3. Synthesis of imidazopyrimidine precursors for the development of bicyclic covalent inhibitors.

Part 1. Improvement of synthesis and characterization of the first covalent inhibitor of FAK

1. Introduction

Based on the preliminary results obtained in our laboratory, my first work consisted of improvement of chemistry involved in the synthesis of covalent inhibitors, the chemical and biochemical characterization. The work in this part was published in the journal of ACS Chemical Biology, 2018, 13(8), 2067-2073.¹⁴⁵

In the FAK kinase domain, there exist Cys427 and Cys502 two cysteines in proximity to ATP pocket, which belong to the group 1 and group 3 respectively according to the cysteine classification mentioned in chapter I. Cys502 is located in the hinge region. Cys427 is on the top of the ATP pocket close to the glycine rich-loop (**Figure 31**). This region is exposed to the solvent resulting in a decrease of pKa of Cys427,¹⁴⁶ which means Cys427 is more reactive than Cys502.

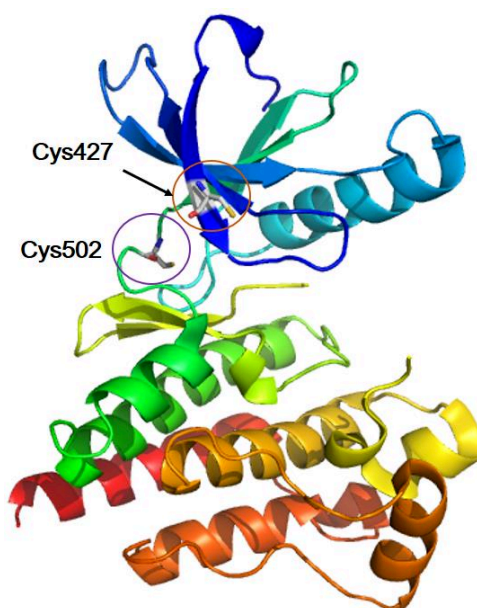


Figure 31: Location of cys427 and cys502.

The design of covalent inhibitor was based on a cocrystal structure of FAK and type I inhibitor TAE-226. The distance between TAE-226 and Cys427 is around 8.3 Å so that an electrophile warhead could be delivered to the vicinity of Cys427 by a linker with adapted length positioned on the diarylamino-pyrimidine scaffold (**Figure 32**).

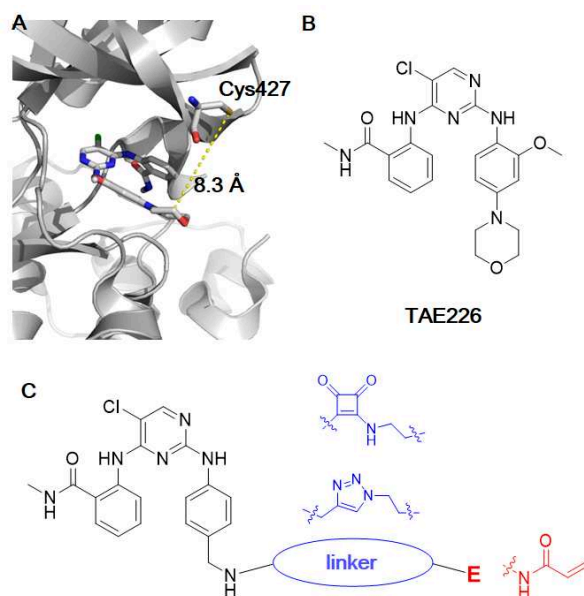


Figure 32: (A) cocrystal structure of TAE-226 and FAK enzymatic site, yellow dash line represents the distance between Cys427 and inhibitor. (B) Chemical structure of TAE-226. (C) The general structure of designed covalent inhibitors, represented linkers and electrophilic group are shown.

In the first part, we performed a kinome-wide sequence cysteine alignment, optimization of the synthetic route to obtain enough amount of compounds for biological evaluation, characterization of irreversible inhibition by biochemical experiments and crystallographic data.

2. Sequences alignment

For the covalent inhibitor design, the targeted nucleophilic residue should be non-conserved in human kinases, which could increase the selectivity of the covalent inhibitor. Hence, a kinome wide kinase sequence alignment was important.

Kinase-Ligand Interaction Fingerprints and Structures database¹⁴⁷ (KLIFS, <http://klifs.vu-compmedchem.nl/index.php>), developed at the division of medicinal

chemistry in VU University Amsterdam, is a database that revolves around the protein structure of catalytic kinase domains and the way that kinase inhibitors can interact with them. This database collected 4616 PDB entries which include 295 kinases of 98 families. A sequence search by binding pocket composition was realized in this database.

Cys427 in FAK is the second residue preceding the glycine-rich loop. In the search parameters, we set this position as cysteine and limited the searching range to the wild type sequence. The results showed that only 5 kinases possess a cysteine at this position including FAK, activin receptor-like kinase 1 (ALK1), activin receptor-like kinase 2 (ALK2), pancreatic eukaryotic initiation factor-2 α kinase (PEK) and serine/threonine-protein kinase RIO1 (RIOK1) (**Figure 33**).

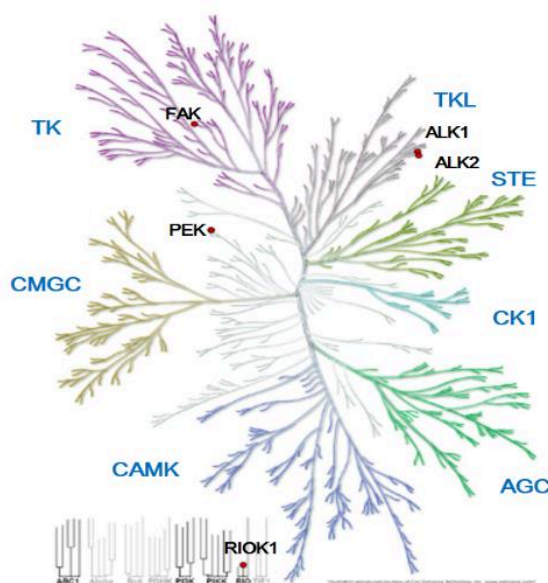


Figure 33: Distribution of kinases that possess a cysteine at the same position of Cys427 in FAK.

Subsequently, the protein sequences of these 5 kinases and other 15 kinases such as Pyk2, ABL1, IGFR1, HER2, IR, EGFR, SRC, FGFR1, ALK, VEGFR, PDGFR α , BTK, C-KIT, B-Raf and AKT2 were aligned using EMBL-EBI web service tool Clustal Omega.¹⁴⁸ The multiple sequence alignment results (**Figure 34**) were in accordance with the searching results in KLIFS. PEK, RIO1, ALK1, and ALK2 were the only kinases that have a cysteine at the same position as FAK. Therefore, Cys427 is non-conserved in human kinases. Covalently targeting Cys427 of FAK might provide improved selectivity to pyrimidine based

FAK inhibitors.

FAK	3BZ3:A	PDBID	CHAIN	SEQUENCE/	[424]	GRCIGEGQFGDVHQGIYM	[490]	ENPVWIIMELCTLGELRSFLQVRKY
PEK	4X7J:A	PDBID	CHAIN	SEQUENCE/	[595]	IQCLGRGGFGVVFEAKNK	[663]	KVYLYIQMLCRKENLKDWMNGRCT
RIO1	40TP:A	PDBID	CHAIN	SEQUENCE/	[182]	NGCLSTGKEANVYHASTA	[285]	PAPLLKNVQ-----
ALK1	3MY0:A	PDBID	CHAIN	SEQUENCE/	[204]	VECVGKGRYGEVWRGLWH	[269]	STQLWLIITHYHEHGSLYDFLQRQTL
ALK2	300M:A	PDBID	CHAIN	SEQUENCE/	[210]	LECVGKGRYGEVWRGSWQ	[275]	STQLWLIITHYHEMGSLYDYLQLTTL
ATK2	3D0E:A	PDBID	CHAIN	SEQUENCE/	[154]	LKLLGKGTFGKVILVREK	[221]	HDRLCFVMEYANGGELFFHLSRERV
B-Raf	1UWH:A	PDBID	CHAIN	SEQUENCE/	[458]	GQRIGSGSFGTVYKGGKWH	[520]	APQLATVITQWCEGSSLYHHLHITET
EGFR	5U8L:A	PDBID	CHAIN	SEQUENCE/	[714]	IKVLGSGAFGTVYKGLWI	[782]	TSTVQLIMQLMPFGCLLDYVREHKD
HER2	3PP0:A	PDBID	CHAIN	SEQUENCE/	[722]	VKVLGSGAFGTVYKGTWT	[790]	TSTVQLVITQLMPYGCCLLDHVRENRG
Pyk2	4H1J:A	PDBID	CHAIN	SEQUENCE/	[427]	NRILGEGFFGEVYEGVYT	[494]	EEPTWIMELYPYGELGHYLERNKN
BTK	5KUP:A	PDBID	CHAIN	SEQUENCE/	[404]	LKELGTGQFGVVYKGVWR	[466]	QRPFIITTEYMANGCLLNLYREMRH
ABL1	5H9:A	PDBID	CHAIN	SEQUENCE/	[244]	KHKLGSGGQYGEVYEGVWK	[307]	EPPFYIITTEFMTYGNLLDYLRECNR
SRC	2H8H:A	PDBID	CHAIN	SEQUENCE/	[269]	EVKLGQGCFFGEVWMGTWN	[330]	EEPIYIVTEYMSKGSLLDFLKGETG
FGFR1	5B7V:A	PDBID	CHAIN	SEQUENCE/	[480]	GKPLGEGAFGQVVLAEAT	[553]	DGPLYVIVEYASKGNLREYLQARRP
VEGFR	1VR2:A	PDBID	CHAIN	SEQUENCE/	[836]	GKPLGRGAFGQVIEADAI	[908]	GGPLMVIIEFCFKGNLSTYLRSKRN
C-Kit	1T46:A	PDBID	CHAIN	SEQUENCE/	[591]	GKTLGAGAFGKVEATAY	[662]	GGPTLVITEYCCYGDLLNFLRRKRD
PDGFRa	5K5X:A	PDBID	CHAIN	SEQUENCE/	[595]	GRVLGSGAFGKVVVEGTAY	[666]	SGPIYITTEYCFYGDLVNVLHKNRD
ALK	4Z55:A	PDBID	CHAIN	SEQUENCE/	[1118]	IRGLGHGAFGEVYEGQVS	[1188]	SLPRFILLMAGGDLKSFLRETRP
TR	1TRK:A	PDBID	CHAIN	SEQUENCE/	[998]	LRRLGQGSFGMVYEGNAR	[1068]	GQPTLVVIELMAHGDLKSYLRSLRP
IGFR1	1K3A:A	PDBID	CHAIN	SEQUENCE/	[971]	SRELGQGSFGMVYEGVAK	[1041]	GQPTLVVIELMTRGDLKSYLRSLRP

Figure 34: Sequences alignment of 20 kinases. Position of Cys427 was highlighted in yellow colour, the position of gatekeeper residue was highlighted in cyan.

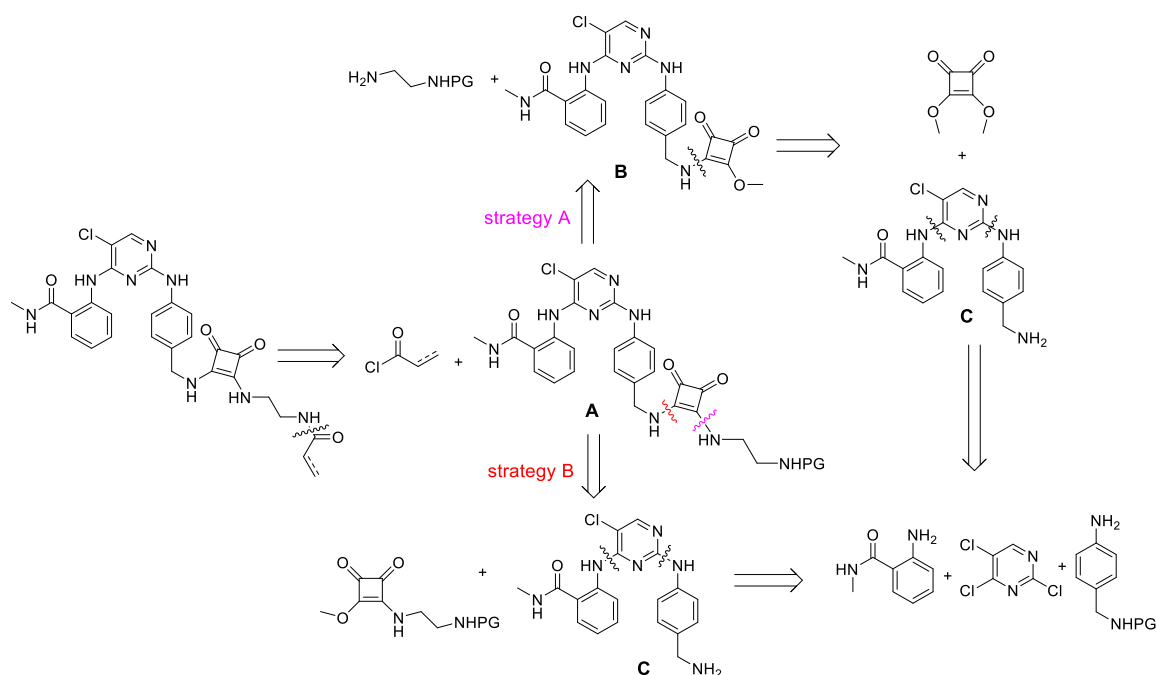
3. Synthesis of the desired inhibitors

3.1. Synthesis of inhibitors with a squaramide linker

1) Retrosynthetic analysis

The retrosynthesis for the desired molecules is shown in **Scheme 7**. To obtain the intermediate **A**, there are two strategies to introduce the squaramide moiety. In strategy **A**, squarate is directly introduced to the diaminopyrimidine **C** followed by condensation with the aliphatic amine. In strategy **B**, the intermediate **A** is synthesized from fragment **C** and a squaramide monoester which is prepared beforehand from squarate and amine. The diaminopyrimidine **C** can be prepared from 2,4,5-trichloropyrimidine and substituted arylamines.

In previous work, the desired compound was obtained only in small quantities with a very low yield (6.8%). In addition, it's also difficult to get this compound in sufficient purity for further study. To progress the development of covalent inhibitors of FAK, the two strategies were both attempted, and the conditions of key steps were optimized to ensure that the desired compounds could be obtained in good yield and purity.



Scheme 7: Retrosynthetic analysis

2) Reactivity of 2,4,5-trichloropyrimidine

2,4,5-trichloropyrimidine is an important starting material for the synthesis of disubstituted pyrimidines, which constitute a large part of kinase inhibitors, such as those of FAK,¹⁰⁹ ALK,¹⁴⁹ and EGFR,¹⁵⁰ etc. The reactivity of each halide in the pyrimidine follows the general order C4(6) > C2 >> C5. This order was observed in the functionalization of 2,4,5-trichloropyrimidines including nucleophilic aromatic substitution reaction (S_NAr),¹⁵¹ palladium-catalyzed Suzuki,¹⁵² and Stille¹⁵³ coupling reactions.

The 4-chlorine in 2,4,5-trichloropyrimidine can be region-selectively substituted by amines in the presence of 1 equivalent of the base to consume produced hydrochloric acid in modest to high yield depending on the nucleophilicity of the amine.¹⁵¹ This preference for position 4 is attributable to the Meisenheimer intermediate where the *para* nitrogen to the tetrahedral carbon in the ring can bear the negative charge better than the *ortho* nitrogen (**Figure 35**).¹⁵⁴ In addition, the chlorine on 5-position increases the electron-deficiency of position 4 through an induced effect.

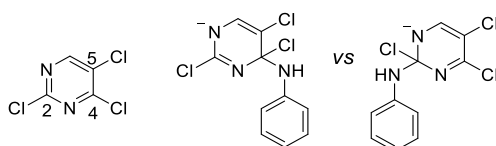
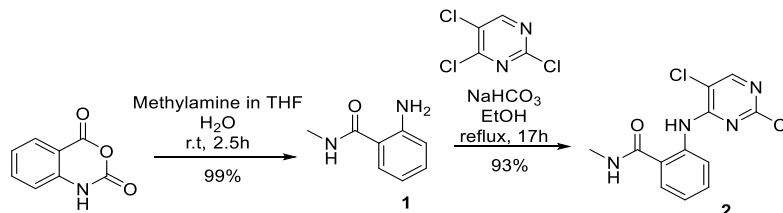


Figure 35: Meisenheimer intermediates

The chlorine at position 2 can be substituted by nucleophile under harsh conditions, like heating over 100 °C overnight¹⁴⁹ or palladium-catalyzed coupling.¹⁵⁵ In general, the yield of this step is moderate.

3) Synthesis of diarylamino pyrimidine

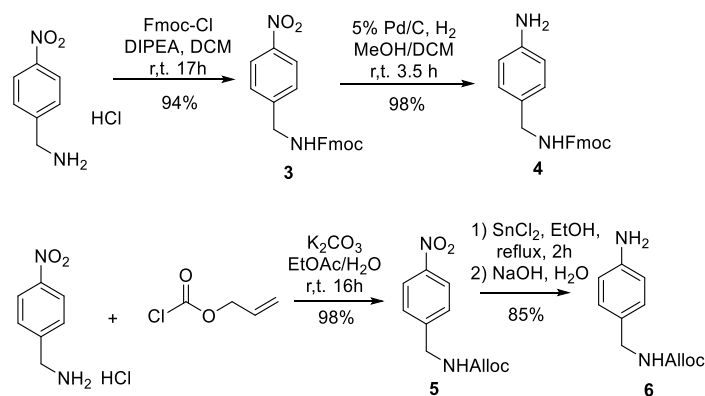
Arylamine **1** was synthesized in excellent yield from commercial available isatoic anhydride and methylamine.¹⁵⁵ Then compound **1** was refluxed in ethanol with commercial starting material 2,4,5-trichloropyrimidine in the presence of NaHCO₃ affording monosubstituted pyrimidine **2** in 93% yield (**Scheme 8**).¹⁵⁰



Scheme 8: synthesis of compound **2**.

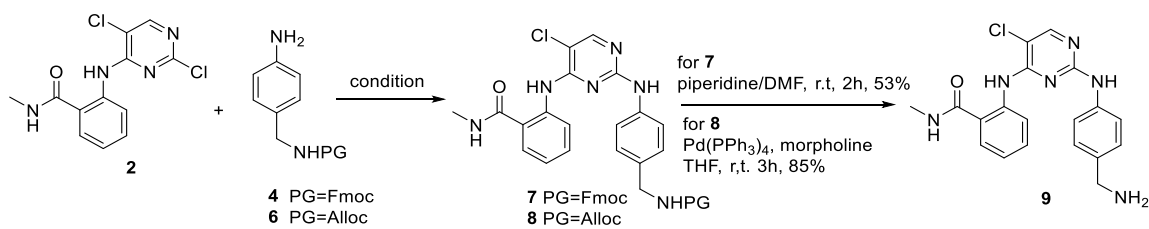
Two (4-aminobenzyl) carbamates (**4** and **6**) were synthesized in the process of optimizing the synthetic conditions for substitution of the chlorine at the position 2 of pyrimidine. Starting from 4-aminobenzylamine and Fmoc chloride, compound **4** was obtained only in 10% yield accompanied by the di-protected product. In order to optimize the yield, this compound was prepared in two steps from 4-nitrobenzylamine. The Fmoc protection of the amine was done in a classical condition giving intermediate **3** in 94% yield,¹⁵⁶ then the nitro group was reduced to an amino group by catalytic hydrogenation using 5% Pd/C in good yield (**Scheme 9**). Allyl (4-aminobenzyl) carbamate **6** was prepared

through two steps as well. The reaction of 4-nitro benzylamine and allyl chloroformate gave compound **5** in 98% yield.¹⁵⁷ Reduction of the nitro group was easily completed after reflux for 2 h in ethanol with SnCl₂ as reductant without damage to the double bond of the Alloc-protecting group (**Scheme 9**).¹⁵⁸



Scheme 9: synthesis of (4-aminobenzyl) carbamates

To substitute the 2-chlorine on the pyrimidine ring of compound **2**, aniline **4** was first used to optimize the reaction conditions (**Scheme 10**). With ethanol or isopropanol as the solvent, the reactants were refluxed for 20 h in the presence of HCl, but only traces of the desired product were generated. When n-butanol was used as the solvent, which has a boiling point at 118 °C, we isolated product **7** in 38% yield with 0.1 eq of HCl and in 52% yield with 1.0 eq of HCl, respectively. Camphorsulfonic acid (CSA) was then tested as a replacement for HCl, but there was no improvement in the yield. The poor solubility of compound **7** in organic solvent caused difficulties in purification. After removal of protecting group Fmoc in solution of 20% piperidine in DMF, compound **9** was obtained in 53% yield. To circumvent above-mentioned troubles, aniline **6** was prepared and reacted with compound **2** affording intermediate **8** in 44% yield, which has better solubility in organic solvents. Deprotection of **8** was performed under smooth conditions with Pd(PPh₃)₄ and morpholine in THF giving **9** in 85% yield.¹⁵⁹



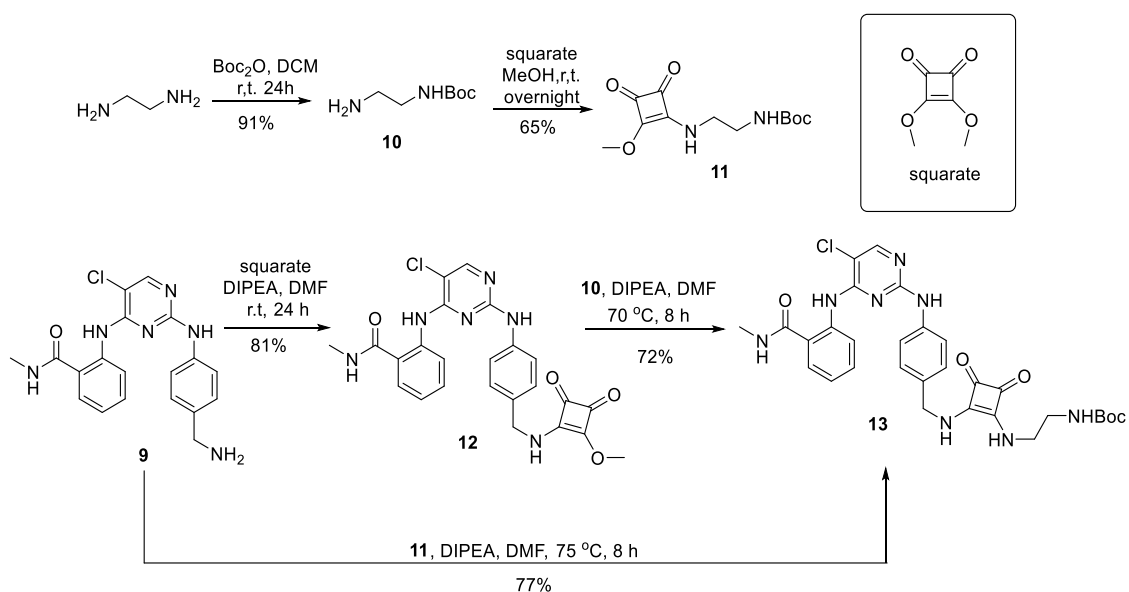
Aniline	Product	Condition	yield
4	7	0.4 eq HCl, EtOH, reflux, 20h	trace
4	7	0.4 eq HCl, i-PrOH, reflux, 20h	trace
4	7	0.1 eq HCl, n-BuOH, reflux, 20h	38%
4	7	1.0 eq HCl, n-BuOH, reflux, 20h	52%
4	7	0.1 eq CSA, n-BuOH, reflux, 20h	45%
4	7	0.5 eq CSA, n-BuOH, reflux, 20h	35%
6	8	1.0 eq HCl, n-BuOH, reflux, 20h	44%

Scheme 10: Synthesis of diarylaminopyrimidine **9**.

4) Incorporation of squaramide linker

In order to prepare compound **13**, strategy A and strategy B described in the retrosynthetic analysis (**Scheme 7**) were both employed. Excess of ethylenediamine was treated with Boc_2O in DCM at room temperature giving the mono-amino group protected product **10**. Condensation of dialkoxysquarate and excess aliphatic amine usually generates symmetrical squaramide in high yield under mild basic conditions at room temperature, while the mono-substitution could be controlled by adding only one equivalent amine in the system.¹⁶⁰ Condensation of amine **10** with a slight excess of dimethoxysquarate in methanol gave mono-squaramide **11** in 65% yield. In strategy A, amine **9** reacted with dimethoxysquarate firstly giving compound **12** in 81% followed by condensation with linker **10** in the presence of 1 equivalent of DIPEA under conditions of heating at 70 °C for 8 h delivering compound **13** in 72% yield. In this synthetic strategy, the intermediate **12** had very poor solubility causing difficulties in the purification and loss of products. In strategy B, compound **13** was obtained in 77% yield by heating the mixture of compound **9** and mono-

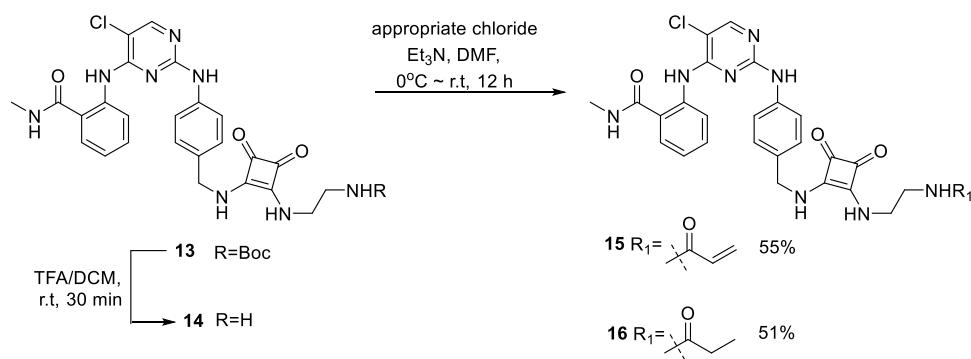
squaramide **11** with DIPEA in DMF at around 75 °C for 8 h. In comparison with strategy A, the synthetic route of strategy B is more convenient and easier for purification.



Scheme 11: Synthesis of compound **13**.

5) Incorporation of electrophilic groups

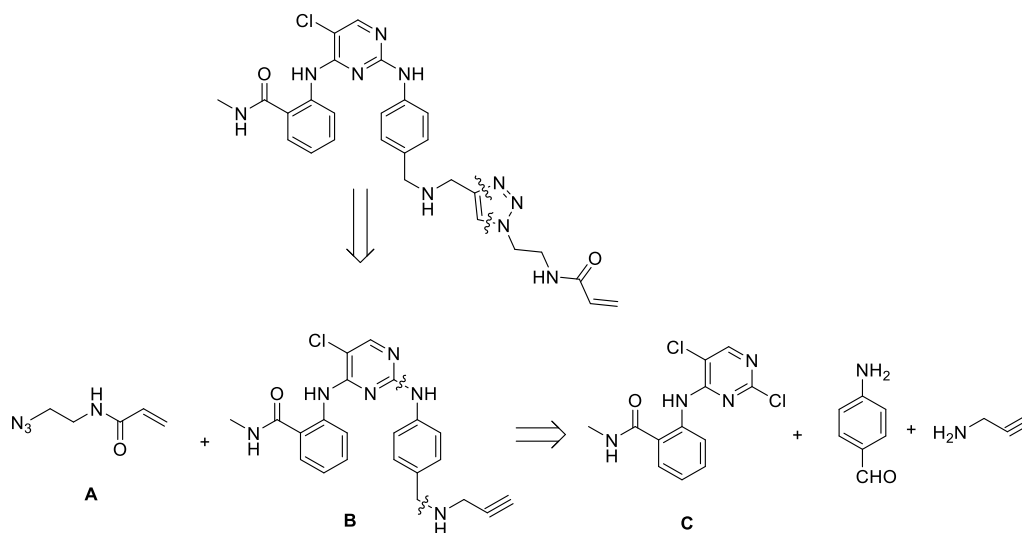
The Boc group in compound **13** was removed by treatment with TFA at room temperature for 30 min. After removing the solvent, the crude product **14** was directly acylated by acryloyl chloride or propionyl chloride to give the desired covalent inhibitor **15** or the corresponding non-covalent inhibitor **16** in yield of 49% and 51% for two steps, respectively (**Scheme 12**).



Scheme 12: Synthesis of compounds **15** and **16**.

3.2. Synthesis of inhibitors with a triazole linker.

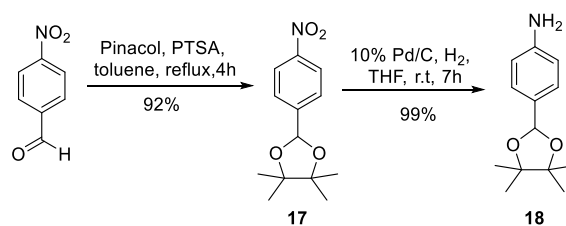
1) Retrosynthetic analysis



Scheme 13: retrosynthetic analysis

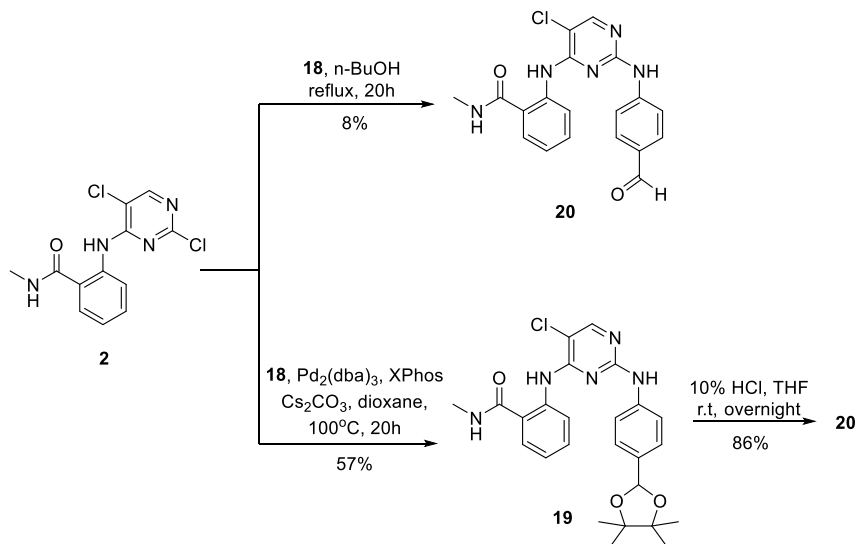
As shown in the retrosynthetic pathway (**Scheme 13**), the inhibitor with triazole linker could be coupled from an azide (fragment **A**) and an alkyne (fragment **B**) via copper-catalyzed Huisgen cycloaddition. The azide part **A** could be prepared from 2-bromoethylamine through substitution and acylation reaction. The alkynyl group in fragment **B** could be introduced through a reductive amination reaction of aldehyde and propynylamine. The 2,4-diarylamino-pyrimidine scaffold could be prepared from fragment **C** and arylamine by S_NAr reaction or palladium-catalyzed C-N coupling reaction.

2) Preparation of alkyne fragment B



Scheme 14: synthesis of arylamine **18**.

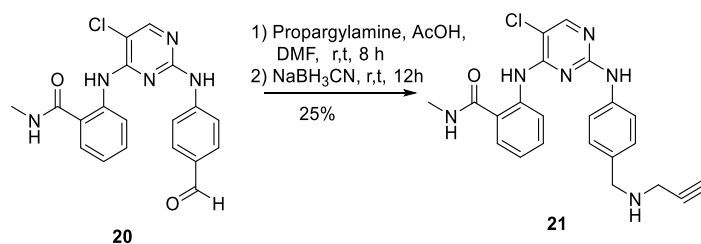
4-Nitrobenzaldehyde and pinacol with *p*-toluenesulfonic acid (PTSA) were refluxed in toluene for 4 h giving acetal **17** in 92% yield.¹⁶¹ Then the reduction of the nitro group by catalytic hydrogenation gave aniline **18** in 99% yield (**Scheme 14**).



Scheme 15: Synthesis of diarylamino pyrimidine **20**.

To substitute the chlorine atom at position 2 of compound **2**, we initially attempted the conditions used before. The compound **2** and **18** refluxed in butanol with HCl gave no product, and the aniline **18** was degraded. Without adding acid to the reaction system, deprotected compound **20** was isolated in a low yield (8%). Given the instability of acetal **18** to acid, we tried to add one equivalent base to consume the produced HCl, but the substitution reaction didn't proceed.

Hence, we attempted the palladium-catalyzed C-N coupling reaction to prepare compound **19**. This compound was obtained in 57% yield with Pd_2dba_3 as catalyst and XPhos as ligand. Afterwards, the aldehyde group was recovered with Firstenberge's protocol¹⁶² using 10% of HCl solution in THF affording compound **20** in 86% yield (**Scheme 15**).

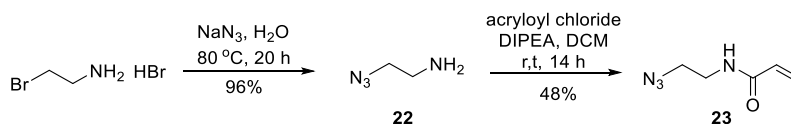


Scheme 16: Synthesis of Compound **21**.

The alkyne **21** was obtained through a reductive amination reaction (**Scheme 16**).¹⁶³ Aldehyde **20** reacted with the propargylamine in DMF at room temperature. A drop of acetic acid as catalyst was added to generate an iminium intermediate, which was then reduced by NaBH₃CN.

3) Synthesis of azide part A.

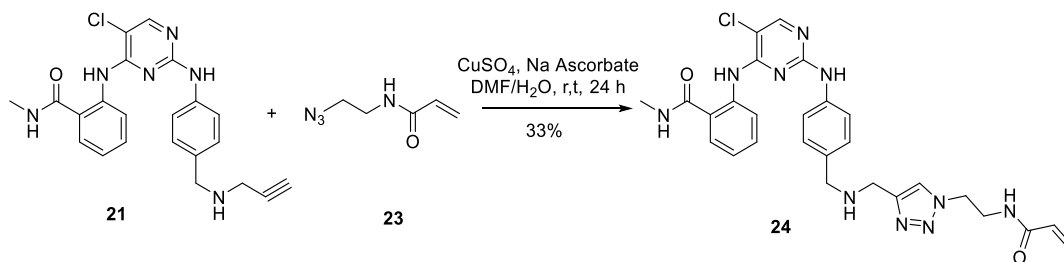
Compound **22** was prepared in 96% yield using the method described by Bandyopadhyay¹⁶⁴ from 2-bromo ethylamine and sodium azide. Then an acylation of **22** by acryloyl chloride gave the functionalized azide **23** in 48% yield (**Scheme 17**).



Scheme 17: Synthesis of azide **23**.

4) Synthesis of the 1,2,3-triazole linker

The 1,2,3-triazole linker could be formed by copper (I)-catalyzed alkyne-azide cycloaddition.¹⁶⁵ Alkyne **21** and azide **23** were coupled with catalysts of CuSO₄ and sodium ascorbate to generate the desired compound **24** in modest yield (**Scheme 18**). The low yield of **24** could be attributed to poor solubility of diarylaminopyrimidino alkyne **21** in the reaction system.



Scheme 18: Synthesis of compound **24**.

In this part, we have optimized the synthetic route to obtain the potential covalent inhibitors of FAK and synthesized two squaramide containing inhibitors (**15**, **16**, **Scheme 12**) and a triazole containing inhibitor **24**. Next, we evaluated the *in vitro* enzymatic activity and performed biochemical characterization to confirm the formation of the covalent bond between the kinase and inhibitor.

4. Characterization of irreversible inhibition

The biological evaluation and characterization of irreversible inhibitors of FAK were carried out by our collaborators. The enzymatic evaluation was done by C. Tomkiewicz-Raulet in University Paris Descartes, INSERM UMR-S 1124. The FAK-phosphorylation assay in cells and washout experiments were completed by J. Dawson in Edinburgh cancer research UK centre, University of Edinburgh. X-ray crystallography was carried out by D. Lietha in the Spanish National Cancer Research Center in Madrid, Spain.

4.1. *In vitro* evaluation of the enzymatic activity

In order to evaluate the *in vitro* inhibitory activity of FAK, we used ADP-Glo™ kinase assay.¹⁶⁶ The ADP-Glo kinase assay is a luminescent ADP detection assay that measures kinase activity by quantifying the amount of ADP produced during a kinase reaction.

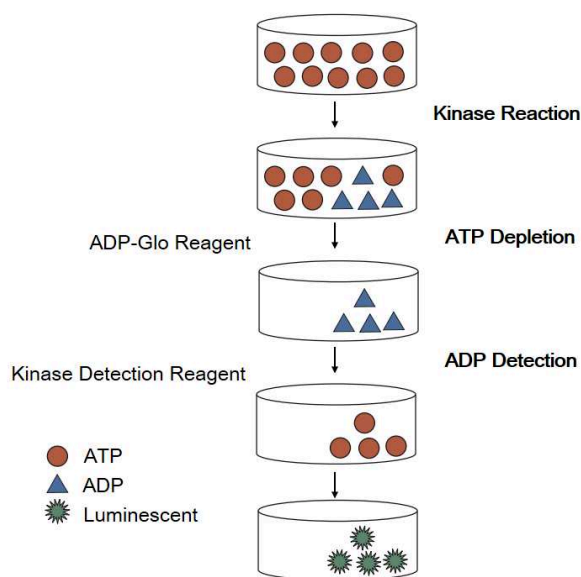


Figure 36: Principle of the ADP-Glo kinase assay.

The principle of ADP-Glo kinase assay is a two-step process (**Figure 36**). In the first step, the kinase reaction is stopped by addition of ADP-Glo reagent, and the remaining ATP is depleted. The second step is the addition of kinase detection reagent to convert the ADP to ATP and allows the new synthesized ATP to be measured using a luciferase/luciferin reaction. The light generated correlates to the amount of ADP produced in the kinase assay, which indicates the kinase activity.

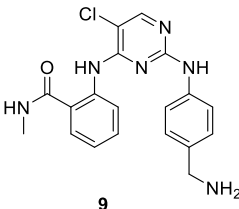
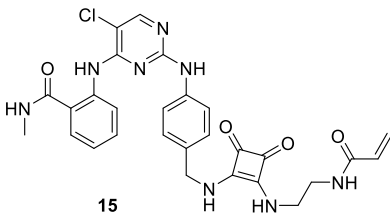
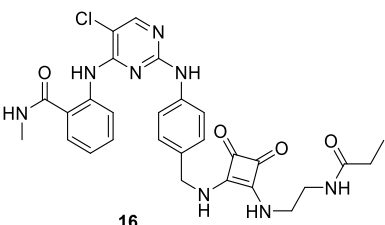
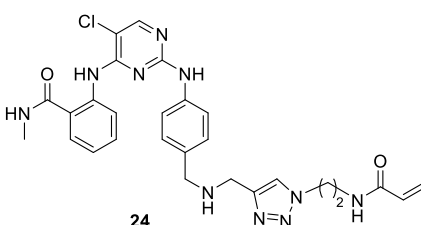
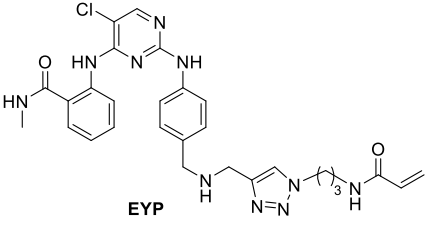
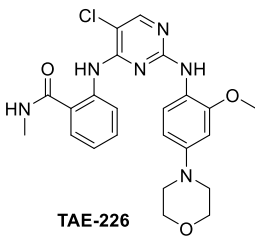
1) Inhibition of FAK enzymatic activity

The newly synthesized compounds **15**, **16** and **24**, intermediate **9**, compound **EYP** (synthesized before in our laboratory, for the structure of **EYP** see **Table 3**), and TAE-226 as control were evaluated for their inhibitory activity against FAK. The results given as IC_{50} values are shown in **Table 3**.

The intermediate **9** ($IC_{50} = 26$ nM) was less potent than TAE-226 ($IC_{50} = 5.8$ nM), whereas the reversible inhibitor **16** showed equivalent inhibition of FAK as TAE-226 with IC_{50} values of 4.7 nM and 5.8 nM, respectively. However, the compounds bearing an electrophile (**15**, **24** and **EYP**) showed improved inhibitory activity against FAK. Indeed, in comparison with TAE-226, compound **15** showed 10-fold improved potency against FAK with an IC_{50} value of 0.6 nM, while compound **16** and **EYP** inhibited the activity of FAK

with IC₅₀ values of 2.3 nM and 1.2 nM, respectively.

Table 3: *In vitro* evaluation of FAK inhibition

Compound	IC ₅₀ (nM)	Compound	IC ₅₀ (nM)
	26±2.2		0.6±0.04
	4.7±0.5		2.3±0.3
	1.2±0.1		5.8±0.6

2) The effect of exposure time on the enzymatic activity

Owing to the two-step binding mode, the covalent inhibitors should show increased inhibitory potency over exposure time. Therefore, the enzymatic activity was tested at 30 min, 1 h and 2 h for the kinase reaction at 3 concentrations (0.01 nM, 1.0 nM, and 100 nM) of inhibitors **15**, **16**, **24** and **EYP**. As shown in **Figure 37**, all these 4 compounds have a dose-dependent inhibitory effect on FAK. The kinase activity declined at a higher tested concentration of inhibitors. In addition, compound **15** showed time-dependent inhibition of

FAK (**Figure 37A**). The enzymatic activity was reduced as the incubation time prolonged from 30 min to 2 h. However, this time-dependent inhibition was not observed for other compounds (**Figure 37B, C, and D**). From these results, we could conclude that only compound **15** exhibited covalent inhibition properties.

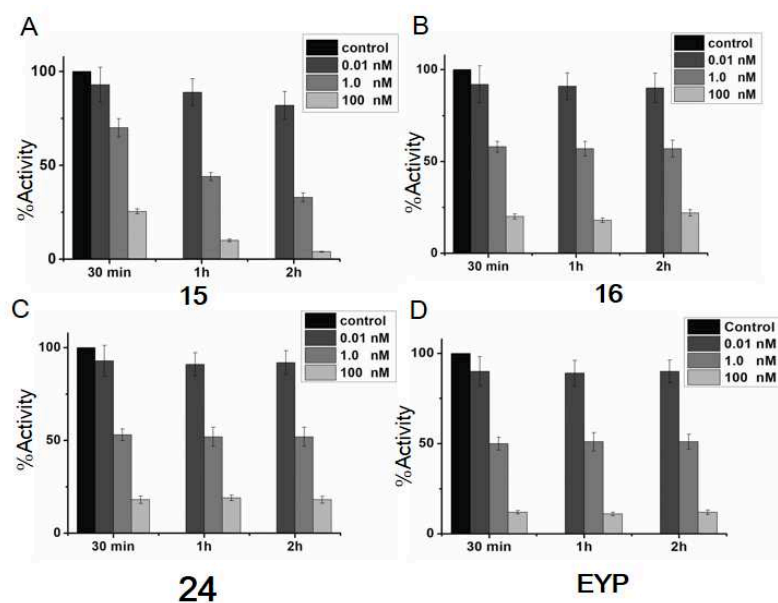


Figure 37: Remaining enzymatic activity after the treatment of inhibitors **15**, **16**, **24** and **EYP** at different concentrations and reaction times.

3) Effect of ATP concentration on the inhibition of FAK

The inhibitory effect of covalent inhibitor usually is not affected by the concentration of ATP in the testing system since they are not competitive with ATP. Therefore, the ability of compounds **15** and **16** to inhibit FAK was evaluated in the presence of 1 μM , 10 μM , 50 μM and 100 μM ATP, respectively.

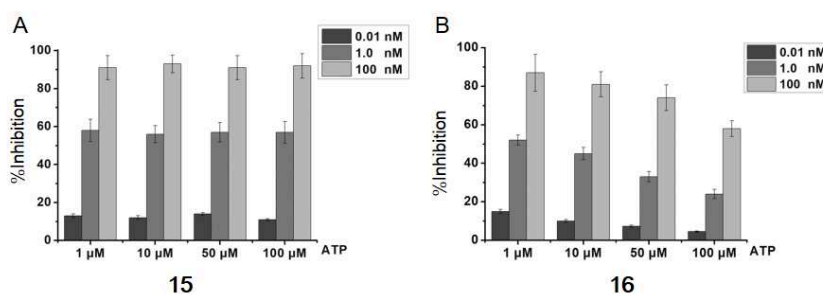


Figure 38: Inhibition of the enzymatic activity of FAK by compounds **15** and **16** at different concentrations of ATP.

The results showed that the FAK activity remains inhibited by compound **15** with the concentrations of ATP rising from 1 μM to 100 μM . In contrast, the inhibition of FAK declined in the presence of a high concentration of ATP for reversible inhibitor **16** (**Figure 38**). The *in vitro* enzymatic inhibition results are in accordance with the fact that compound **15** could irreversibly inhibit the activity of FAK.

4) Kinase selectivity of compound **15**

The kinase selectivity profiling was performed by Eurofins Scientific. The compound **15** was assayed on a panel of 9 kinases at a concentration of 1 μM . The results (**Table 4**) showed that at this concentration compound **15** inhibited several oncogenes related kinases and receptors, such as Src, c-kit, EGFR, IGF1-R, IRR, PDGF-R α , and Pyk2, whereas HER2 was not inhibited by compound **15** at all. It is worth noting that compound **15** at a concentration of 1 μM only showed 21% inhibition of insulin receptor (IR), which was strongly inhibited by TAE-226 ($\text{IC}_{50} = 260 \text{ nM}$).¹¹¹

Table 4: Kinase selectivity of compound **15** on a panel of 9 kinases.

Kinase	Inhibition at 1 μM
FAK	100%
Src	87%
c-kit	70%
EGFR	88%
HER2/ErbB2	0%
IGF1-R	95%
IRR	96%
PDGF-R α	98%
Pyk2	100%
IR	21%

4.2. Inhibition of FAK autophosphorylation in SCC cells

FAK was overexpressed in squamous cell carcinoma (SCC) cells and involved in the immunosuppressive microenvironment.⁹⁷ The inhibition of FAK autophosphorylation in SCC cells was evaluated with compound **15** and a reversible inhibitor VS-4718 as control. As shown in **Figure 39a** and **Figure 39b**, VS-4718 and compound **15** could effectively block the autophosphorylation of FAK on Tyr397, and the autophosphorylation was significantly inhibited even at the concentration as low as 0.1 nM for compound **15**. Next, we studied the reversibility of the FAK autophosphorylation by washout experiments. In this assay, inhibitors were washed out after incubation for 48 h with SCC cells, and fresh medium was added. It was observed that the cancer cells treated with VS-4718 recovered the phosphorylation on Tyr397 (**Figure 39c**), while the phosphorylation was still blocked for the cells treated by compound **15** (**Figure 39d**). It could be concluded that compound **15** produced an irreversible inhibition of FAK phosphorylation in SCC cells.

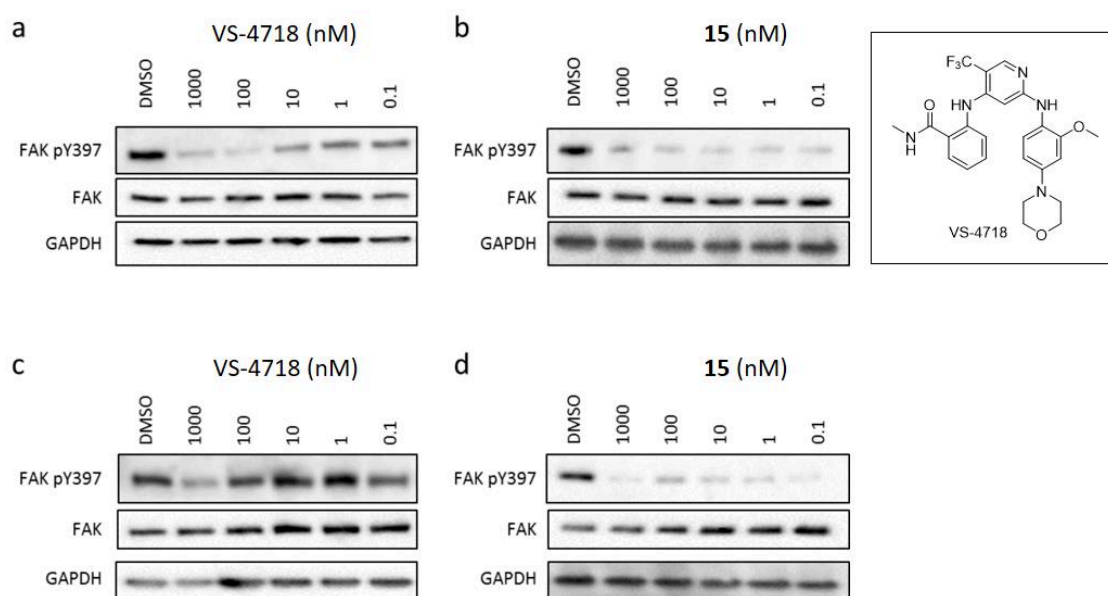


Figure 39: FAK autophosphorylation in SCC cells. a, SCC cells treated by VS-4718; b, SCC cells treated by compound **15**; c, After washout of inhibitor VS-4718; d, After washout of inhibitor **15**.

4.3. X-Ray crystallography

Compounds **15**, **16** and **24** were crystallized with FAK kinase domain in the group of D. Lietha.

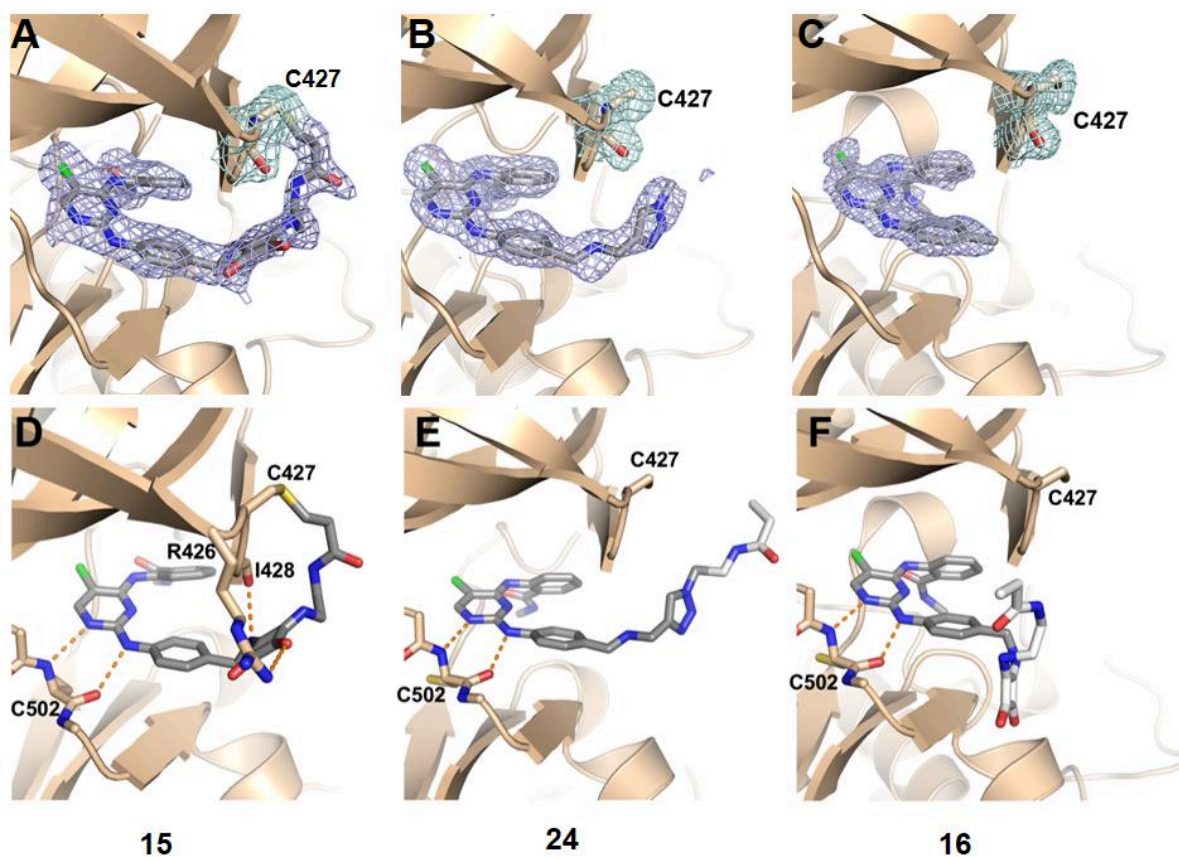


Figure 40: Crystal structures of the FAK kinase domain in complex with inhibitors **15** (A and D) (PDB ID: 6GCR), **24** (B and E) (PDB ID: 6GCX) and **16** (C and F) (PDB ID: 6GCW). (A-C) 2F_o-F_c electron density countered at 1 σ is shown for the compounds (blue mesh) and Cys427 (cyan mesh), which are shown in stick representation. The disordered region of compounds are omitted; (D-E) The binding mode of compounds **15**, **24** and **16** to the active site of FAK are shown. Compounds are shown in grey for ordered regions and in white for disordered regions. Key hydrogen bonds between the compounds and FAK are shown as orange dashed lines.

From the crystal complex (**Figure 40**), it shows that the diarylaminopyrimidine moiety entered the active site of FAK and formed two hydrogen bonds with Cys502 in the hinge region. In the crystal complex of compound **15** and FAK, there is a consecutive electron density from compound **15** to Cys427 (**Figure 40A**) and a covalent bond between the acrylamide electrophile and Cys427 is observed (**Figure 40D**). The carbonyl group in

squaramide formed a hydrogen bond with the side chain of Arg426. This hydrogen bond is important to maintain the orientation of the linker part and to well place the electrophilic group toward the vicinity of Cys427 (**Figure 40D**), and facilitate the formation of the covalent bond. In contrast, compound **24** didn't form covalent interaction with Cys427 due to an unsuitable orientation of the electrophilic group (**Figure 40E**). Therefore, the covalent interaction was formed only when the electrophile was positioned stably near the targeted cysteine. Compound **16** without the electrophilic warhead bound to the hinge region through pyrimidine scaffold, whereas the linker moiety exposed to the solvent (**Figure 40F**).

5. Conclusion

In this part, we have developed a feasible synthetic route for the preparation of diarylaminopyrimidine scaffold for covalent inhibitors in a good yield. Then, we established the biochemical characterization of the first covalent irreversible inhibitor of FAK.¹⁴⁵ Finally, we successfully obtained a crystal complex of FAK kinase domain and compound **15**, which revealed the inhibitor's binding mode in the ATP binding site and confirmed the covalent linkage between the targeted Cys427 of FAK and the electrophilic group of the inhibitor. In addition, the cocrystal structures underlined the importance of squaramide linker to satisfy the structural requirements for the formation of the covalent bond.

Part 2. Design, synthesis and biological evaluation of new irreversible and reversible covalent inhibitors

This part is devoted to the synthesis of new pyrimidine-based irreversible and reversible inhibitors for improvement of kinase selectivity and decrease of off-target toxicity. Our compounds were tested for their inhibitory activity against FAK *in vitro* and anticancer activity in cells. The effect on cell growth, cell cycle, apoptosis, cellular morphology and cell migration were evaluated.

1. Design of new irreversible covalent inhibitors

The diaminopyrimidine moiety in covalent inhibitors of FAK is responsible for binding into the ATP pocket. Due to the two-step binding process of covalent inhibitors, the binding affinity and selectivity of the first step directly affect the overall biochemical and cellular potency.¹⁶⁷ In order to improve the kinase selectivity, new irreversible inhibitors were designed.

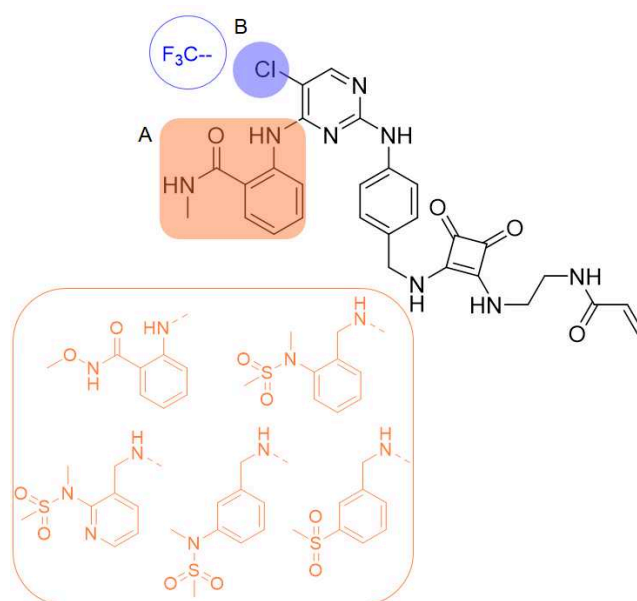
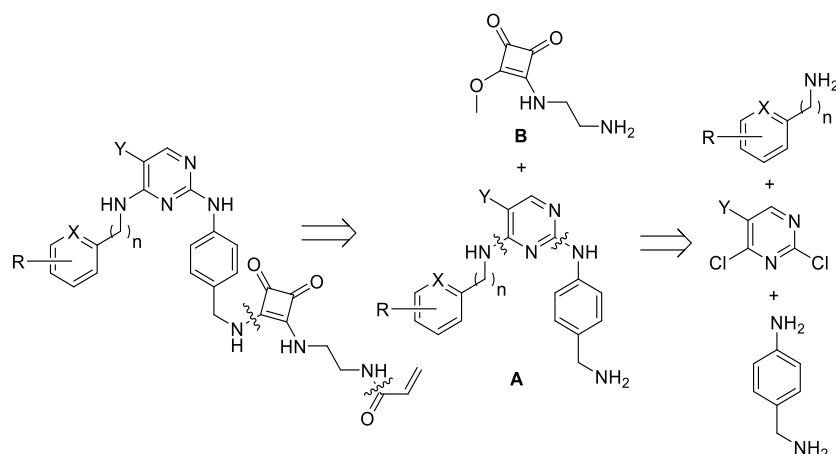


Figure 41: Structures of new potentially irreversible covalent inhibitors.

The modification was carried out from two aspects. As shown in **Figure 41**, the substituent at position 4 of pyrimidine (part A) was replaced by *N*-methoxybenzamide, aryl-*N*-methylmethanesulfonamides or arylmethylsulfonyl. In addition, to increase the hydrophobic interaction with gatekeeper residue a trifluoromethyl group was introduced to replace the chlorine (part B).

2. Synthesis of irreversible inhibitors modified on the part A

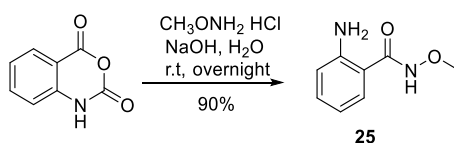
1) Retrosynthetic pathway



Scheme 19: Retrosynthetic pathway

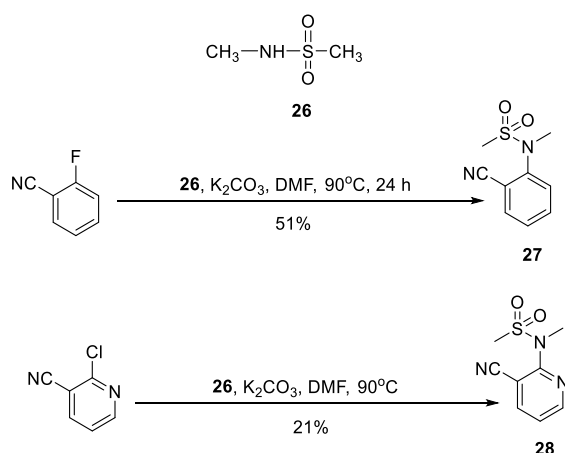
The strategy described in Part 1 was applied to synthesize the new compounds. The irreversible covalent inhibitors could be prepared from a squaramate linker **B** and a substituted pyrimidine moiety **A**. The moiety **A** was synthesized by 2 steps substitution of 2,4-dichloro-5-substituted pyrimidine with appropriate amines.

2) Synthesis of amine synthons



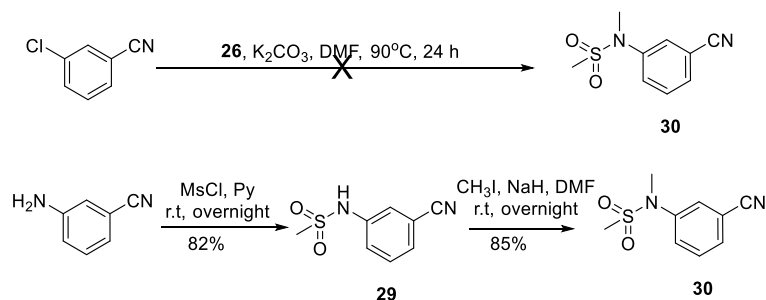
Scheme 20: Synthesis of compound **25**.

The 2-amino-*N*-methoxybenzamide **25** was prepared using Cheng's method.¹⁶⁸ *O*-methylhydroxylamine hydrochloride was neutralized in water by 2 M NaOH solution in an ice bath. Then isatoic anhydride was added in portion. Stirring for one night at room temperature provided the desired product **25** in 90% yield after purification (**Scheme 20**).



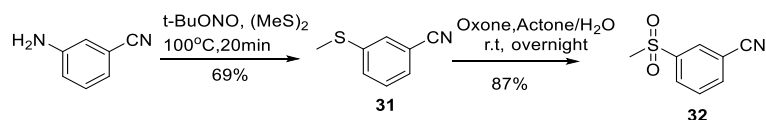
Scheme 21: Synthesis of compounds **27** and **28**.

To synthesize compounds **27** and **28**, *N*-methylmethanesulfonamide **26** was prepared according to a described method in a patent.¹⁶⁹ Methane sulfonyl chloride was slowly dropped to an ice-cooled solution of methylamine in water. Then the mixture was stirred at room temperature overnight to generate **26** in 77% yield. The reaction of **26** and 2-fluorobenzonitrile in DMF in the presence of K_2CO_3 generated compound **27** in 51% yield.¹⁷⁰ Using the same conditions, compound **28** was obtained in 21% yield from 2-chloronicotinonitrile.



Scheme 22: Synthesis of compound **30**.

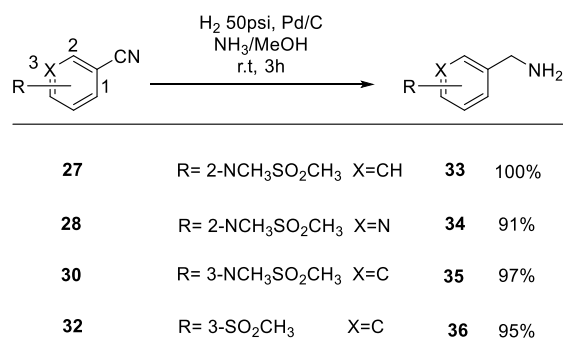
The reaction between 3-chlorobenzonitrile and **26** didn't happen using the previous protocol as shown in **Scheme 22**. Therefore, we tried to synthesize the desired compound **30** from 3-aminobenzonitrile. Sulfonylation of 3-aminobenzonitrile yielded sulfonamide **29** in 82% yield. Then *N*-methylation of **29** with methyl iodide and sodium hydride gave **30** in 85% yield.



Scheme 23: Synthesis of compound **32**.

To introduce a sulfone group at the *meta*-position of benzonitrile, we used a reported method¹⁷¹ starting from 3-aminobenzonitrile. The reaction of arylamine with *tert*-butyl nitrite produced an aromatic radical. Then it attacked the dimethyl disulfide which used as the solvent to give sulfide **31**. The oxidation of sulfide **31** with Oxone (2KHSO₅·KHSO₄·K₂SO₄) generated sulfone **32** in 87% yield (**Scheme 23**).

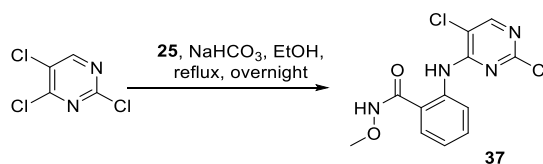
The nitrile group could be reduced to an amine by a reducing agent or transition metal.¹⁷² To obtain the desired benzylamines, we used 10% Pd/C under 50 Psi hydrogen and ammonia solution (7 M in methanol) as solvent to suppress the formation of by-products. Under these conditions, four nitrile compounds were reduced to the corresponding primary amines (**33** – **36**) in excellent yield (**Scheme 24**).



Scheme 24: Reduction of nitrile compounds

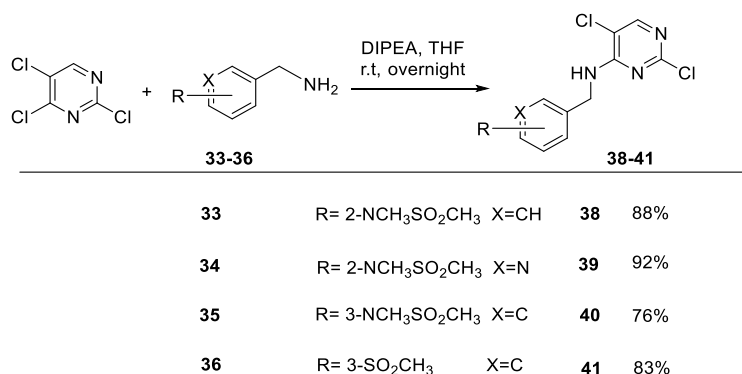
3) Synthesis of 4-amino-2,5-dichloropyrimidines.

As shown in **Scheme 25**, compound **37** was prepared from 2,4,5-trichloropyrimidine and compound **25** in the presence of NaHCO₃ in ethanol under the condition of reflux overnight in 77% yield.



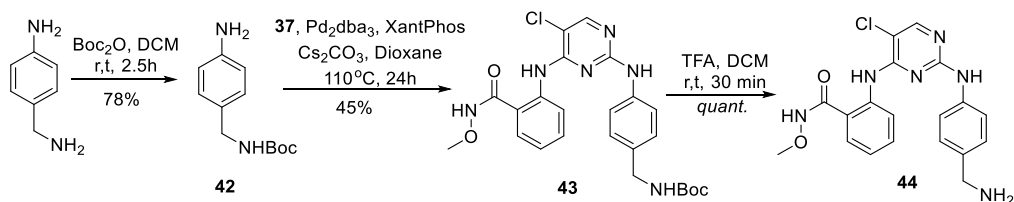
Scheme 25: Synthesis of compound **37**.

For the synthesis of compounds **38 – 41**, the mixture of appropriate arylmethanamine (**33 – 36**) and 2,4,5-trichloropyrimidine in THF in the presence of DIPEA was stirred overnight at room temperature. Compounds **38 – 41** were obtained with a yield of 76% - 92% (**Scheme 26**).



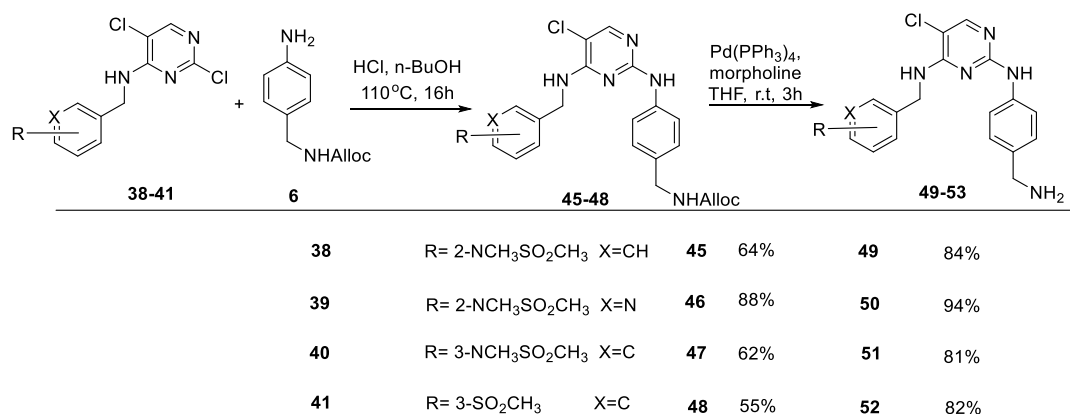
Scheme 26: Synthesis of compounds **38 – 41**.

4) Synthesis of 2,4-diaryl-amino-5-chloropyrimidines



Scheme 27: Synthesis of compound **44**.

To obtain diarylamino-pyrimidine **43**, the S_NAr reaction between **37** and arylamine **6** under acidic conditions was attempted, but the benzamide moiety of compound **37** was degraded. Therefore, the palladium-catalyzed C-N coupling reaction was employed. We prepared arylamine **42** from 4-aminobenzylamine and Boc_2O ,¹⁷³ and then the coupling reaction of compound **37** and **42** catalyzed by Pd_2dba_3 and XantPhos generated the desired compound **43** in 45% yield. Subsequently, the protecting group was removed quantitatively with TFA giving compound **44** (Scheme 27).

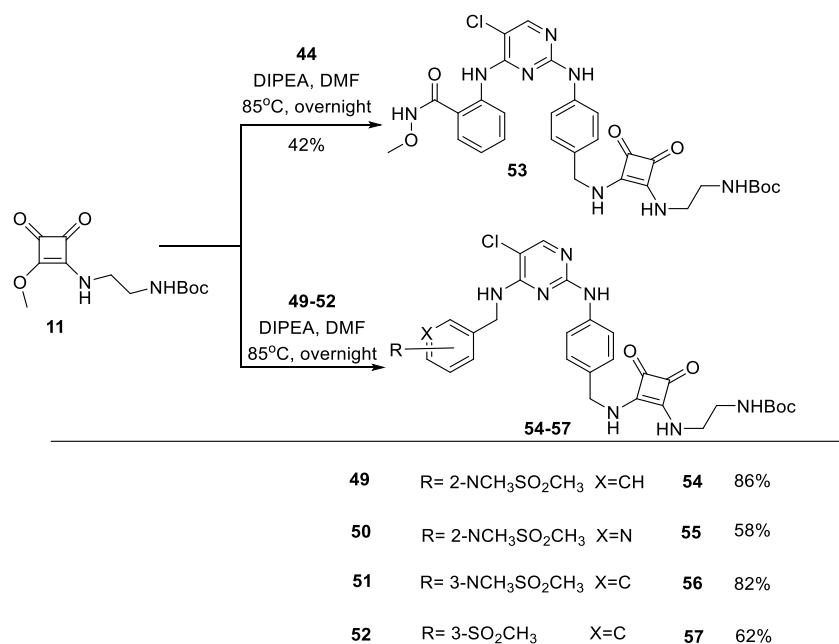


Scheme 28: Synthesis of compounds **49** – **53**.

The nucleophilic substitution of 2-chlorine in compounds **38** – **41** by arylamine **6** proceeded well under acidic conditions. The diaminosubstituted pyrimidines **45** – **48** were obtained in a yield of 55% - 88%. The deprotection was carried out according to a classical protocol¹⁵⁹ with $Pd(PPh_3)_4$ to give compounds **49** – **53** with yields of 81% - 94% (Scheme 28).

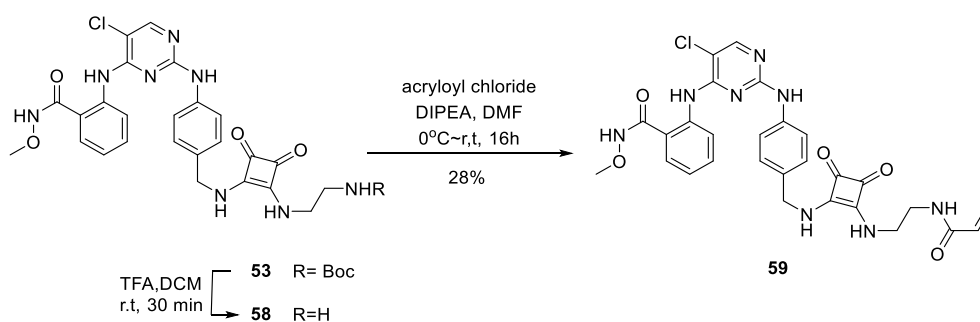
5) Coupling of the squaramide linker

With the same strategy in Part 1, the squaramide linker was directly coupled to the pyrimidine moiety. Squaramate **11** and compound **44** were condensed in DMF in the presence of DIPEA at 85 °C to give intermediate **53** in 42% yield. Compounds **54** – **57** were synthesized under the same conditions from **49** – **52** in a yield of 58% - 86% (**Scheme 29**).



Scheme 29: Coupling of squaramide linker

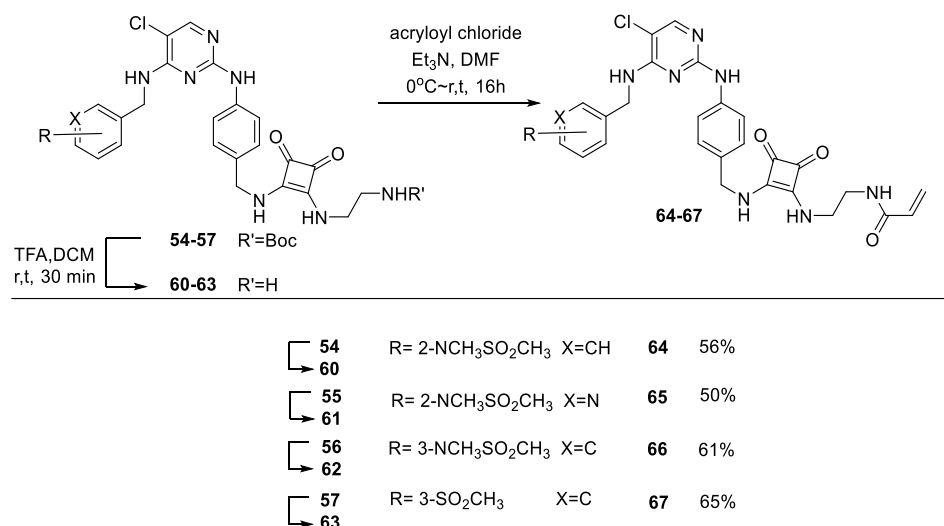
6) Incorporation of the electrophilic functional group.



Scheme 30: Synthesis of compound **59**.

Compound **53** was deprotected by TFA in DCM giving compound **58**. Afterwards, the

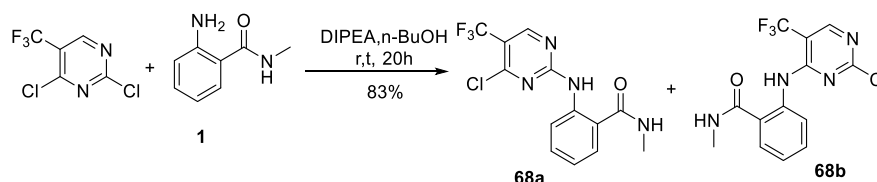
electrophilic functional group was incorporated to compound **58** through an acylation reaction to provide final product **59** (Scheme 30). As shown in Scheme 31, final products **64** – **67** were obtained following the same approach in a yield of 50% - 65%.



Scheme 31: Synthesis of compounds **64** – **67**.

3. Synthesis of irreversible inhibitor modified on the part B

1). Synthesis of 2,4-diaryl-amino-5-trifluoromethylpyrimidine



Scheme 32: *S_NAr* substitution of 2,4-dichloro-5-trifluoromethylpyrimidine

To synthesize 2,4-diaryl-amino-5-trifluoromethylpyrimidine, a base-catalyzed aromatic nucleophilic substitution protocol¹⁷⁴ was used (Scheme 32). Under the basic conditions, the substitution reaction gave two products. The ratio of these two compounds was about 1:1.6 determined by NMR (Figure 42). It was difficult to separate these two compounds by column, even after the use of several mixtures of eluents. With eluent of DCM/THF = 200/1, a small part of pure compound was separated. The NMR of each fraction showed that these two

compounds were products substituted in position 2 and position 4, respectively (**Figure 42**). From the subtle difference of chemical shift of the NH proton and the proton on pyrimidine, we proposed that fraction 1 was compound **68a** and fraction 2 was compound **68b**.

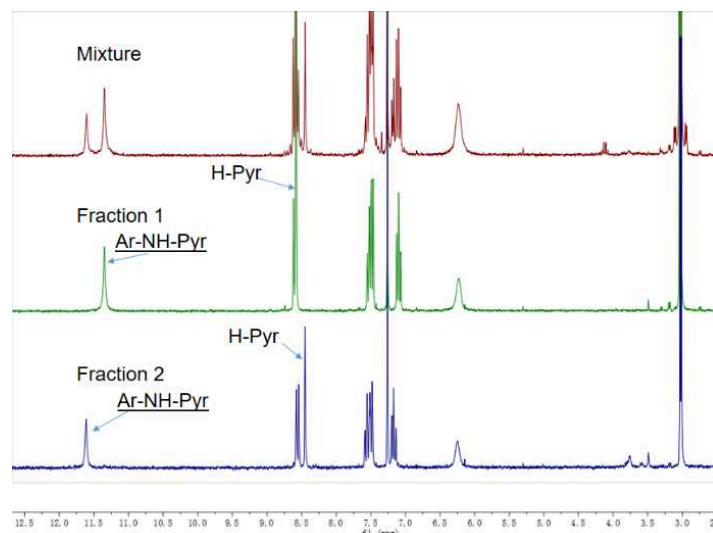
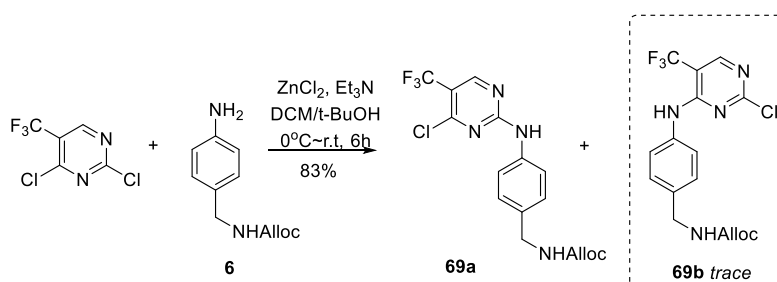


Figure 42: Superposition of ^1H NMR spectra of **68a** and **68b** in CDCl_3 (500 MHz).

Richter *et al*¹⁷⁵ reported the study of selective substitution of 2,4-dichloropyrimidines. The nucleophilic substitution of 2,4-dichloro-5-trifluoromethylpyrimidine was preferential to position 2 with Lewis acid additive ZnCl_2 . The authors mentioned that the 2-position substituted product was less polar than the 4-position substituted product, which was consistent with our analysis that compound **68a** was fraction 1.



Scheme 33: Substitution of 2,4-dichloro-5-trifluoromethylpyrimidine

According to Richter's protocol,¹⁷⁵ 2,4-dichloro-5-trifluoromethylpyrimidine and ZnCl_2 were mixed at 0°C in a solution of DCM and *t*-BuOH. After 1 h, arylamine **6** and Et_3N were

added to the mixture. The reaction was stirred at room temperature for 6 h (**Scheme 33**). With the addition of 1 equivalence of ZnCl_2 , we obtained **69a** and **69b** in a ratio about 5:1, and the ratio was increased to 10:1 with addition of two equivalent ZnCl_2 (**Figure 43**).

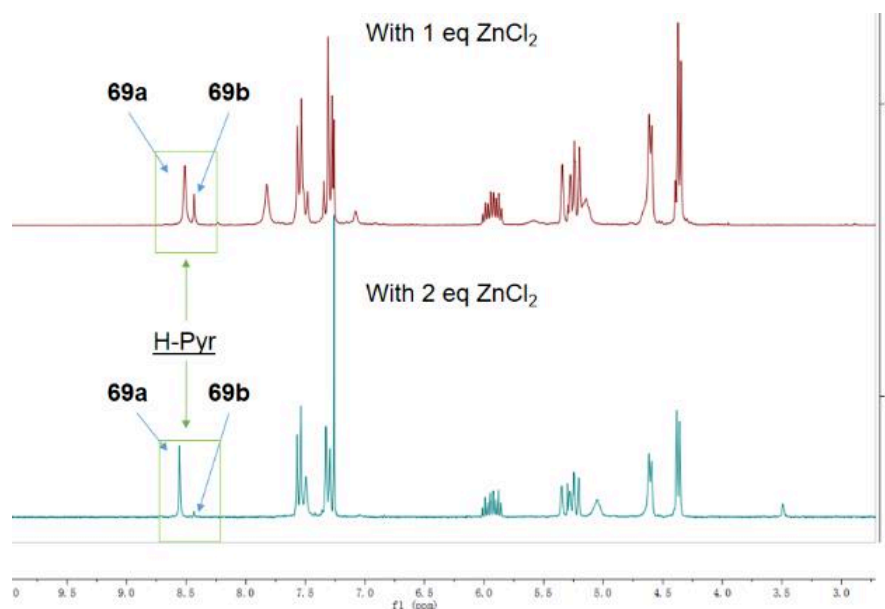
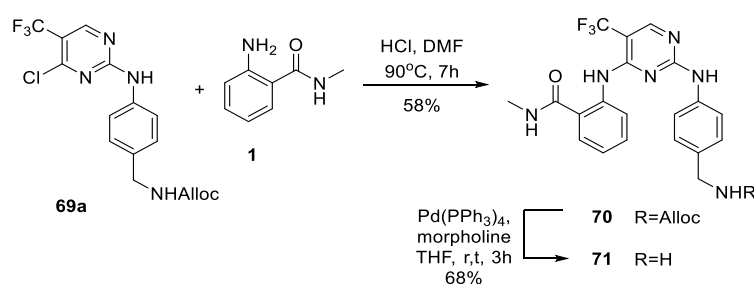


Figure 43: ^1H NMR spectra of compounds **69a** in CDCl_3 (500 MHz).

The substitution on the position 4 of **69a** by aniline **1** was achieved through an $\text{S}_{\text{N}}\text{Ar}$ reaction in the presence of HCl giving compound **70** in 58% yield. Then protecting group Alloc was removed to generate intermediate **71** in 68% yield (**Scheme 34**).

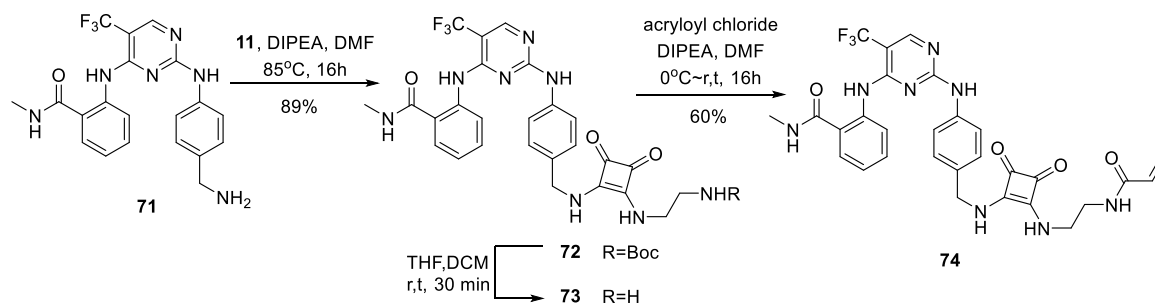


Scheme 34: Synthesis of compound **71**.

2). Coupling of squaramide linker and incorporation of electrophilic functional group

The condensation with squaramate **11** and deprotection were going smoothly under the conditions previously used to give intermediate **73**. Then the amino group was acylated by

acryloyl chloride to give the final product **74** in 60% yield (**Scheme 35**).



Scheme 35: Synthesis of compound **74**.

4. Design of reversible covalent inhibitors

4.1. Concept of reversible covalent inhibitor

Inspired by the fact that in the reaction between 2-cyanoacrylate and thiol, the addition reaction reached a fast equilibrium,¹⁷⁶ Serafimova and colleagues⁶⁷ developed 2-cyanoacrylate and 2-cyanoacrylamide as reversible electrophilic functional groups. The authors confirmed the reversibility of 2-cyanoacrylate and thiol adducts in physiological pH conditions by ¹H-NMR spectroscopy. As shown in **Figure 44**, cyanoacrylate **3** was treated with β-mercaptoethanol (βME) in a mixed solution of deuterium DMSO and PBS affording the thioether **6** quickly. The ratio of remaining compound **3** and product **6** formed was 15:85. However, when the solution was diluted 10 times, the reaction moved towards starting materials as the signal of cyanoacrylate **3** becomes more intense.⁶⁷ Through this NMR evidence, it's proved that the covalent adduct of thiol with cyanoacrylate could be recovered to Michael receptor and free thiol in biological low concentrations.

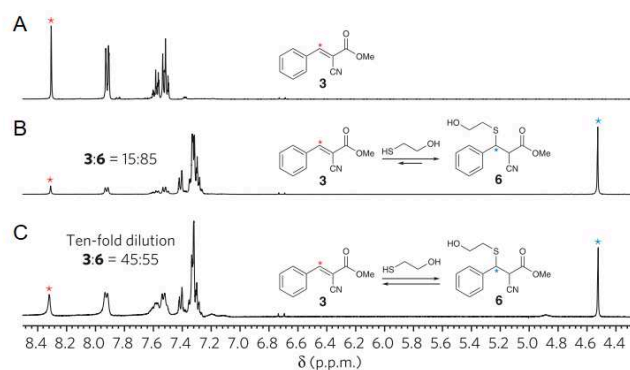


Figure 44: ¹H-NMR spectra showing reversible addition of βME to cyanoacrylate **3**. (A) Proton spectrum of cyanoacrylate **3**. (B) Cyanoacrylate **3** (90 mM) was treated with 100 mM βME in DMSO-*d*₆: PBS-*d* (3:1), affording a 15:85 mixture that favoured the βME adduct **6**. (C) Upon 10-fold dilution, the ratio of **3**:**6** turned to 45:55.⁶⁷

Then the authors demonstrated that the fusion of the 2-cyanoacrylamide structure with a known p90 ribosomal protein S6 kinase RSK2 inhibitor provided a reversible covalent inhibitor. Their experiments showed that the reversible inhibitor has a sustained and quasi-irreversible occupancy of RSK in cells. More importantly, the reversible inhibitor could be recycled after proteolytic digestion of the protein.⁶⁷

Therefore, no matter the irreversible or reversible covalent inhibitors, they both can form a covalent interaction with targeted cysteine in proteins. While the reversible one can reduce the risk of off-target labelling and immunogenic response (**Figure 45**).¹⁷⁷

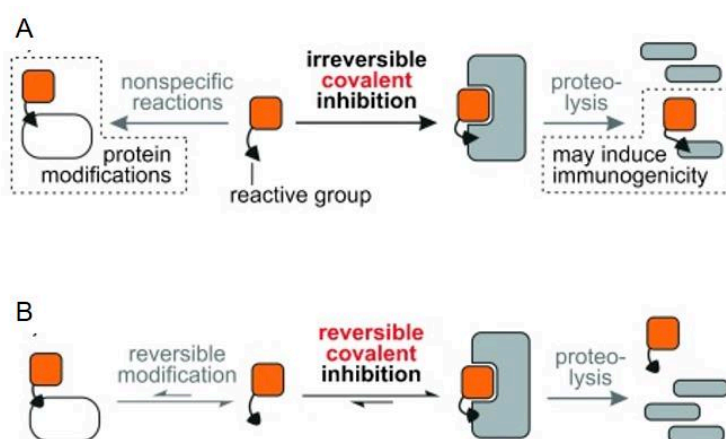


Figure 45: Representation of protein-targeting strategies. (A) Irreversible covalent inhibition by reactive ligands; (B) Reversible covalent inhibition by reactive ligands.¹⁷⁷

4.2. Design of reversible covalent inhibitors

Owing to the advantages of reversible covalent inhibition over irreversible covalent inhibition, the reversible covalent inhibitors were designed by the introduction of reversible electrophilic functional groups at the extremity of the linker (**Figure 46**).

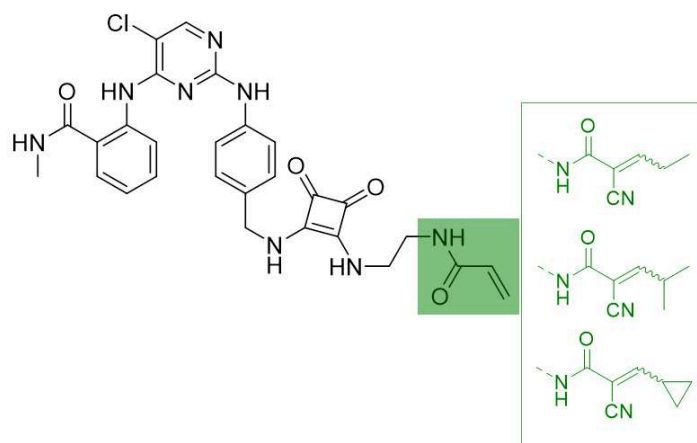
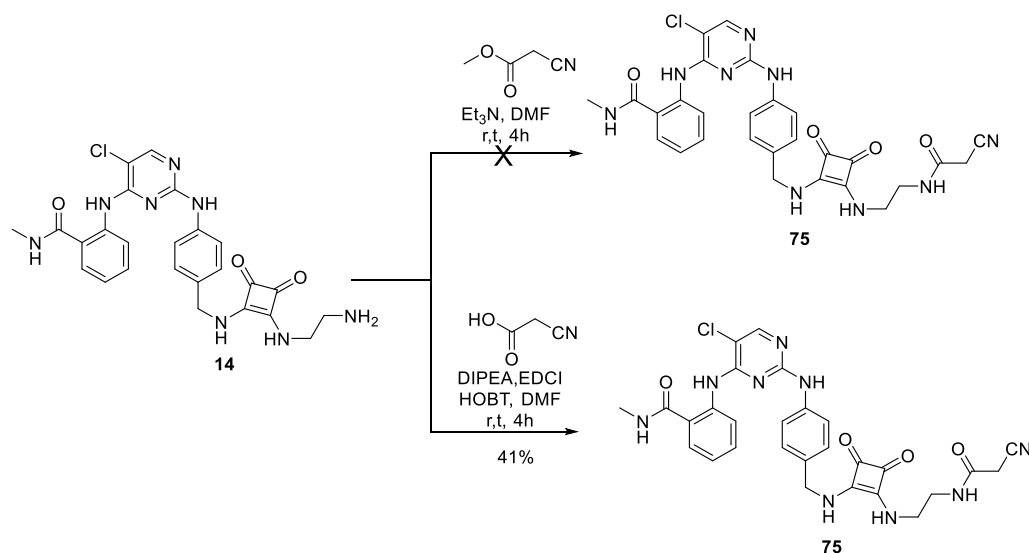


Figure 46: Structures of reversible covalent inhibitors.

5. Synthesis of reversible covalent inhibitors

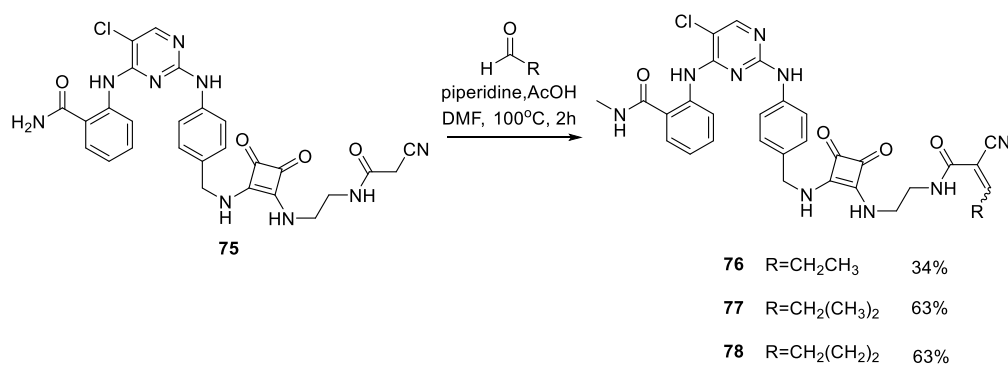
1) Synthesis of cyanoacetamide.



Scheme 36: Synthesis of compound **75**.

To synthesize compound **75**, two synthetic routes were attempted. An eco-friendly protocol to synthesize cyanoacetamides was reported by Pronença,¹⁷⁸ in which primary or secondary amines were directly mixed with methyl cyanoacetate without solvent and stirred for 2 h to give cyanoacetamide in high yield. We tried this method to prepare compound **75** with DMF as solvent because of poor solubility of compound **14**. After 4 hours at room temperature, no product was observed by TLC. In the second synthetic route, cyanoacetic acid was used to prepare compound **75** under peptide coupling conditions (EDCI, HOBT). The cyanoacetamide **75** was obtained in 41% yield.

2) Aldol condensation



Scheme 37: Synthesis of compounds **76** – **78**.

The aldol condensation of aliphatic aldehyde was achieved using the method described by Basu.¹⁷⁹ Compound **75** reacted with an appropriate aldehyde in a mixed solution of DMF and distilled acetic acid in the presence of piperidine to give the final products **76** – **78** with yields of 34% - 63% (**Scheme 37**).

74		CF ₃		6.8 ± 0.7
76		Cl		3.5 ± 0.2
77		Cl		1.2 ± 0.1
78		Cl		1.0 ± 0.1
15		Cl		0.6 ± 0.04 ^a
TAE-226	-	-	-	5.8 ± 0.6

^a, IC₅₀ value calculated before.

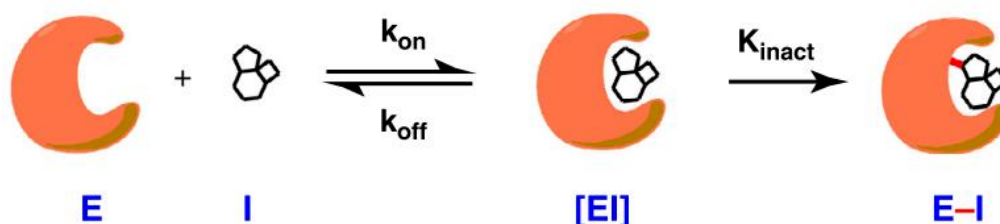
As shown in **Table 5**, the newly synthesized compounds significantly inhibited FAK enzymatic activity with IC₅₀ values ranging from 1.0 to 16.3 nM. In comparison with the irreversible covalent inhibitor **15**, introducing a benzohydroxamate group at 4-position of pyrimidine ring (**59**) is not favourable, giving an IC₅₀ value of 3.7 nM against FAK. The compounds **64** – **67** with a sulfonamide function group on the aromatic ring and containing a methylene spacer between the aromatic ring and 4-amino of pyrimidine were less potent than the reference compound **15**. Compound **15** had about 10-times higher anti-FAK activity than compounds **64** – **67**. However, compound **64** – **66** exhibited similar inhibitory potency as TAE-226. Furthermore, *N*-methylmethanesulfonamide substituent at position 3 of the aromatic ring (**66**, IC₅₀=4.9 nM) had better inhibition activity of FAK than methylsulfonyl substituent (**67**, IC₅₀=16.3 nM). The replacement of Cl with CF₃ group at position 5 of the pyrimidine ring caused a decrease of inhibitory activity on FAK, with an IC₅₀ value of 6.8

nM for compound **74** compared to 0.6 nM for compound **15**. The expected reversible covalent inhibitors **76** – **78** had improved anti-FAK activity compared with TAE-226. In addition, the compounds with an isopropyl (**77**) or a cyclopropyl (**78**) group on the electrophilic substituent showed strong inhibition of FAK activity with IC₅₀ values of 1.2 and 1.0 nM, respectively.

Kinetic analysis

In order to further evaluate the potency of covalent inhibitors, the enzymatic kinetics^{180,181} were studied by our collaborator YL Li in the Guangdong University of Technology.

The covalent inhibitors require a reversible interaction first and then undergoes the covalent bond formation (**Scheme 38**). In contrast to the conventional drugs, due to the resulting covalent bond, the biomolecular targets theoretically can be completely inhibited with sufficient time. As a result, the IC₅₀ values of covalent inhibitors can be time dependent. In order to better rank the covalent inhibitors, it is important to consider the rate of inactivation of a target (k_{inact}). The ability of non-covalent interaction in the first step was measured by K_i ($K_i = k_{on}/k_{off}$). The k_{inact}/K_i ratio describes the ability of a covalent irreversible inhibitor to interact with and neutralize a target, which is better than IC₅₀ values to reflect the potency of covalent inhibitors against the target.⁴⁸



Scheme 38: Covalent binding of inhibitor with its target.⁴⁸

Time-dependent half-maximal inhibitory concentration (IC₅₀(t)) was determined using ADP-Glo kinase kit and values of K_i and k_{inact} were calculated according to a reported procedure with following equations:¹⁸²

$$IC_{50}(t) = K_i \left(1 + \frac{S}{K_M} \right) \cdot \left(\frac{2 - 2e^{-\eta_{IC_{50}} \cdot K_{inact} \cdot t}}{\eta_{IC_{50}} \cdot K_{inact} \cdot t} - 1 \right)$$

$$\eta_{IC_{50}} = \frac{IC_{50}(t)}{K_i \left(1 + \frac{S}{K_M} \right) + IC_{50}(t)}$$

As shown in **Table 6**, compounds **15**, **77** and **78** had similar potencies with K_i / k_{inact} values ranging from $8.87 \mu\text{M}^{-1} \cdot \text{S}^{-1} \sim 11.6 \mu\text{M}^{-1} \cdot \text{S}^{-1}$. Compounds **77** and **78** had k_{inact} values about 1.5-fold that of compound **15**, which is consistent with the fact that α -cyanoacrylamide electrophile is more reactive than the acrylamide towards thiol. The compound **74** exhibited decreased values of K_i (2.64 nM), which implies that the introduction of the trifluoromethyl group at position 5 of pyrimidine reduced compound's affinity. In addition, the k_{inact} of compound **74** was 3-times lower than that of compound **15**, the introduction of trifluoromethyl group maybe is not benefit to the formation of the covalent bond between compound **74** and the Cys427. As a result, compound **74** had poor potency toward FAK with k_{inact}/K_i value of $0.3 \mu\text{M}^{-1} \cdot \text{S}^{-1}$.

Table 6: Determination of kinetic parameters K_i , k_{inact} , and k_{inact}/K_i for **15**, **74**, **77** and **78**.

Compounds	K_i (nM)	k_{inact} (min^{-1})	k_{inact}/K_i ($\mu\text{M}^{-1} \text{ s}^{-1}$)
15	0.23 ± 0.03	0.16 ± 0.02	11.6 ± 3.4
74	2.64 ± 0.4	0.047 ± 0.01	0.30 ± 0.12
77	0.47 ± 0.06	0.25 ± 0.03	8.87 ± 2.51
78	0.40 ± 0.05	0.24 ± 0.04	10.0 ± 3.33

6.2. In cell evaluation.

6.2.1. Effect of new inhibitors on oesophageal cancer cells.

It was reported that overexpression of FAK in oesophageal SCC cells was correlated to the tumour invasiveness and lymph node metastasis.^{183,184} Patients with overexpression of FAK had a poor prognosis and their 5-year survival rate (38%) was almost half of that of

patients without FAK overexpression (69%).¹⁸³

The effects of newly synthesized compounds on cell growth and cell cycle of human oesophageal cell lines including JH-eso-AD1 (AD1), Flo1, MFD1, OE33, OAC-P4C (P4C), and SKGT4 were evaluated by J. Dawson in Edinburgh cancer research centre. FAK inhibitor VS-4718 and chemotherapeutic drug Paclitaxel (Pac) were chosen as control.

Inhibition of cell growth

Table 7: Inhibition of cell growth in Oesophageal cancer cells.

Compound	Growth inhibition of Oesophageal cells (EC ₅₀ nM)					
	AD1	Flo1	MFD1	OE33	P4C	SKGT4
59	375.94	148.27	1844.62	1134.34	482.11	622.1
64	NA	NA	NA	NA	NA	NA
65	NA	NA	NA	NA	NA	NA
66	NA	NA	NA	NA	NA	NA
67	NA	NA	NA	NA	NA	NA
74	303.67	79.74	859.59	1411.82	849.18	680.7
76	613.78	300	1414.52	4069.89	1165.04	1295.85
77	664.61	160.4	1456.33	1088.88	1061.84	1129.99
78	226.54	17.39	748.31	166.88	384.42	582.61
15	367.73	107.12	786.24	1265.89	1094	1158.24
VS-4718	1316.5	581.4	2133.97	869.86	2160.68	1733.67
Pac	0.3	0.04	0.81	0.04	0.11	0.3

NA, no activity; Pac: Paclitaxel.

As shown in **Table 7**, most compounds (**15**, **74**, **76** – **78**) which have aminobenzamide substituent at position 4 of the pyrimidine ring showed good inhibitory effect on cell growth. However, the compounds with arylmethanamino substituent at 4-position of pyrimidine (**64** – **67**) did not inhibit the cell growth. In comparison with the reversible inhibitor VS-4718, compounds **15**, **74**, and **76** – **78** displayed equivalent or stronger inhibitory activity especially against AD1 and Flo1 cancer lines. Additionally, compound **78** was the most potent inhibitor

with EC₅₀ values of 17.39 nM ~ 748.31 nM. The Flo1 cells were the most sensitive oesophageal cancer lines to FAK inhibitors. The cell growth of Flo1 was significantly inhibited by compounds **74** and **78** with EC₅₀ values of 79.74 nM and 17.39 nM, respectively.

Influence on cell cycle

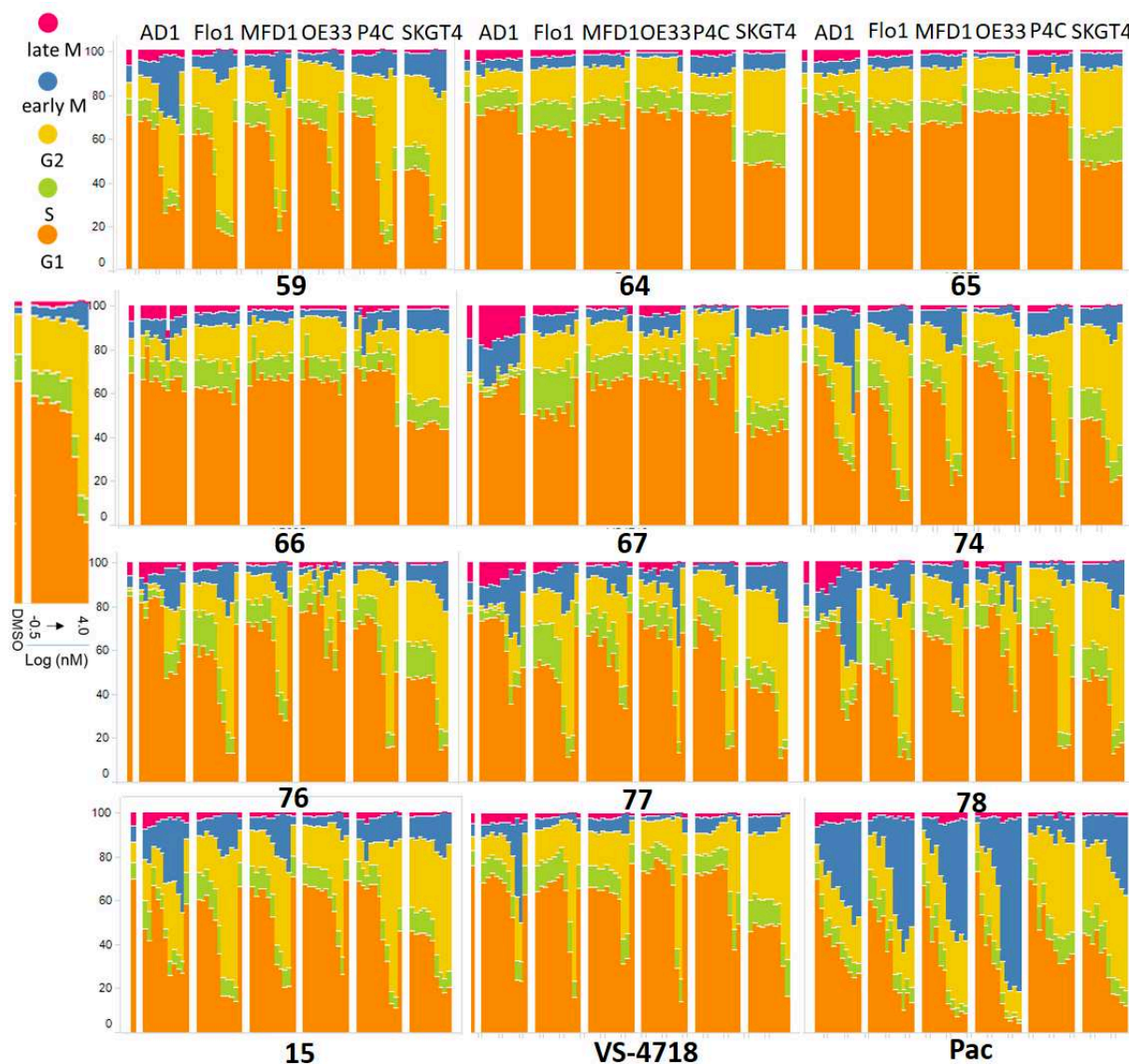


Figure 47: Percentage of cell cycle distribution.

The influence of each compound on the cell cycle distribution was measured under 10 concentrations (0.3nM ~ 10 μ M). As shown in **Figure 47**, compounds **15**, **74** and **76 – 78** showed a dose-dependent effect on cell cycle like VS-4718 and paclitaxel (Pac). The cell

cycle was blocked at the G2/M stage. However, compounds **64** – **67** didn't induce cell cycle arrest.

6.2.2. Effect of new inhibitors on glioblastoma cells.

Since a lot of studies have shown the association between FAK and grade of malignancy, proliferation and migration of gliomas, FAK is a promising therapeutic target for malignant gliomas.^{111,185} In addition, it was reported that TAE-226 treatment inhibited the glioma cell proliferation *in vitro* and *in vivo*.¹¹¹ Therefore, the anticancer activity of a subset of our compounds was evaluated on glioblastoma cells by our collaborators YL Li and C Tomkiewicz-Raulet, respectively.

Antiproliferation activity evaluation

In order to explore the antitumour activity of compounds **15**, **74**, **77** and **78**, which showed good inhibition of FAK *in vitro*, the ability of antiproliferation was evaluated using MTT assay on three glioblastoma cancer cell lines, including U87-MG, A172 and U251.

Table 8: Antiproliferative activity against glioblastoma cancer cells

Compound	IC ₅₀ (μM)		
	U87-MG	A172	U251
15	2.2 ± 0.1	0.65 ± 0.05	0.22 ± 0.01
74	3.3 ± 0.4	0.13 ± 0.01	0.15 ± 0.02
77	7.1 ± 0.6	1.3 ± 0.02	9.8 ± 0.8
78	7.2 ± 0.5	0.89 ± 0.07	1.2 ± 0.01
TAE-226	2.9 ± 0.4	8.3 ± 0.6	6.3 ± 0.5

As shown in **Table 8**, compound **15** (IC₅₀ = 2.2 μM) showed a slight improvement on inhibition of proliferation on U87-MG cells than that of TAE-226 (IC₅₀ = 2.9 μM), while

other compounds (**74**, **77** and **78**) were less potent than TAE-226. Our compounds **15**, **74**, **77**, and **78** ($IC_{50} = 0.13 \mu M \sim 1.3 \mu M$) showed improved antiproliferative activity against A172 in comparison with TAE-226 ($IC_{50} = 8.3 \mu M$). The proliferation of A172 cells was strongly inhibited by compound **74** with an IC_{50} value of $0.13 \mu M$. Compound **15** and **74** were about 30-fold potent than TAE-226 ($IC_{50} = 6.3 \mu M$) on antiproliferation of U251 cells with IC_{50} values of $0.22 \mu M$ and $0.15 \mu M$, respectively.

Influence on cell cycle of U87-MG cells

To further investigate the influence of FAK inhibitors on the cell cycle, the distribution of cell cycle was analyzed by flow cytometry. When U87-MG cells were exposed to FAK inhibitors (**15**, **74**, **77** or **78**) for 24 h, the number of cells in G₂-M greatly increased, which was consistent with the results of TAE-226 (**Figure 48**). It means that our inhibitors effectively block the G₂/M process.

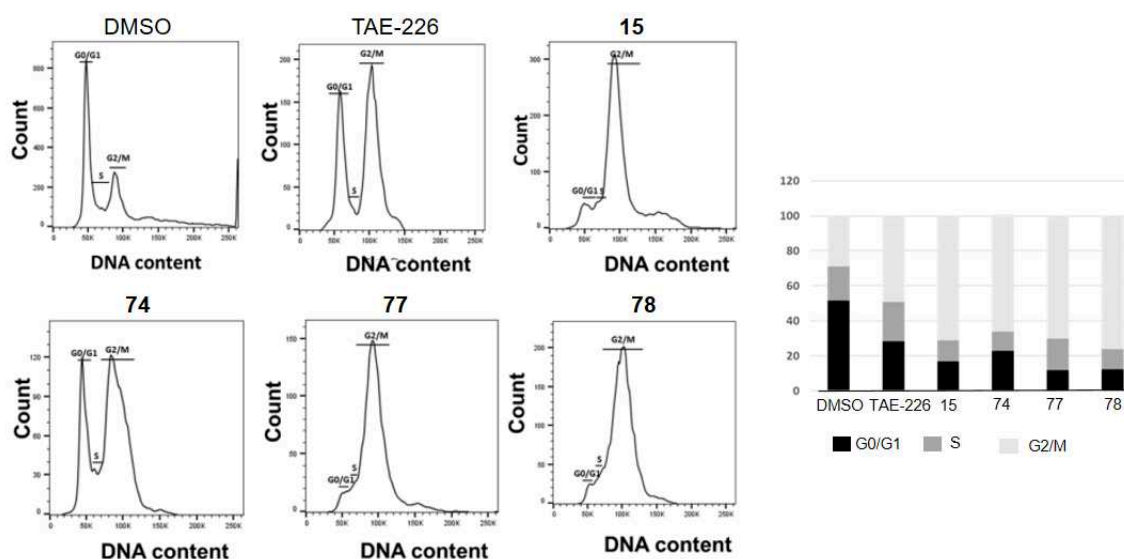


Figure 48: Cell cycle analysis was done on U87-MG cells treated with DMSO or corresponding inhibitors at $1 \mu M$ concentration, and the cell distribution at each phase was drawn in histograms.

Influence on cell apoptosis

Next, we investigated if compounds **15**, **64**, **65**, **74**, **77**, and **78** trigger apoptosis in U87-

MG cells by flow cytometry. The results (**Figure 49**) showed that none of the tested compounds induced significant apoptosis (< 12%) even at the concentration of 10 μ M. It was reported that TAE-226 couldn't induce massive apoptosis in U87-MG cells,¹¹¹ which was also observed in our experiments. Therefore, our compounds had a very similar anticancer effect in U87-MG cells to TAE-226.

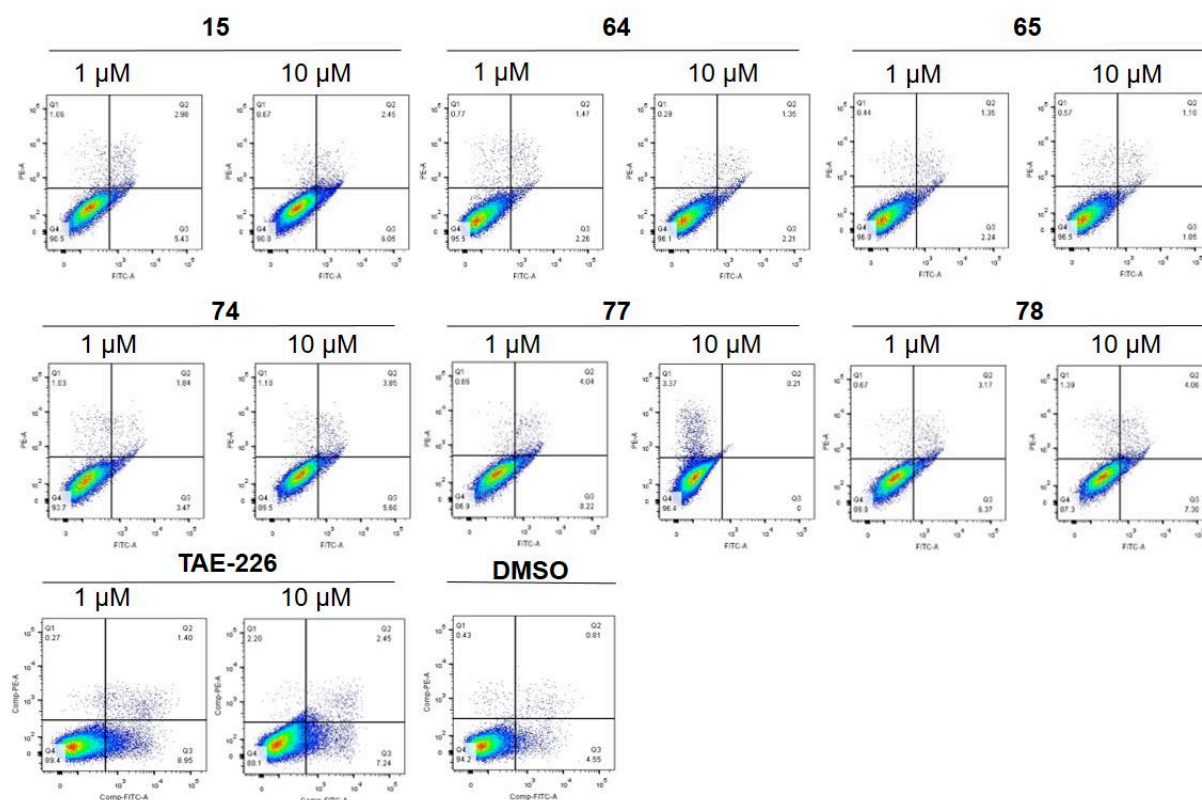


Figure 49: Analysis of cell apoptosis on U87-MG cells at concentrations of 1 μ M and 10 μ M.

Influence on cell morphology

The morphology of U87-MG cells was studied when the cells were exposed to 1 μ M FAK inhibitors for 48 h. As shown in **Figure 50**, the cells treated with compounds **15**, **74**, **77** and **78** exhibited obviously cellular morphologic change, which was similar to that of treated with TAE-226. The cells became bigger than the control group and double nucleus in cells was also observed. However, compounds **64** and **65** showed a limited effect on cellular morphology with a slight swell of cell volume observed.

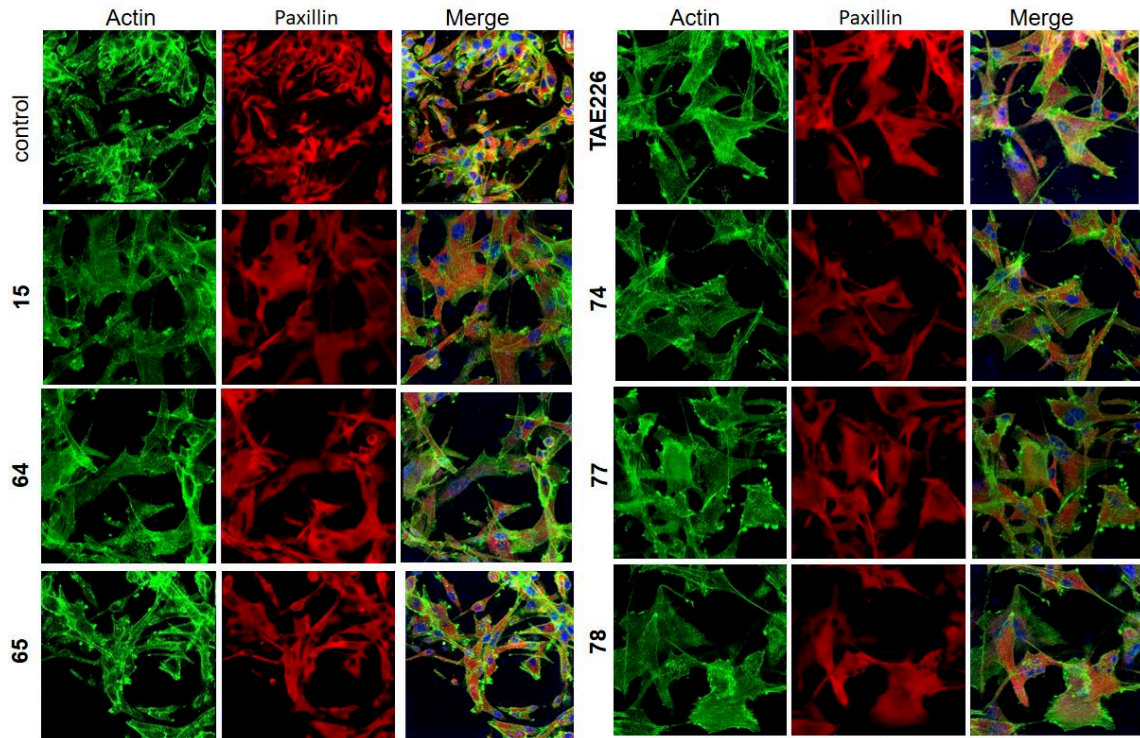


Figure 50: Cell morphologic change observed by confocal microscopy.

Influence on cell migration

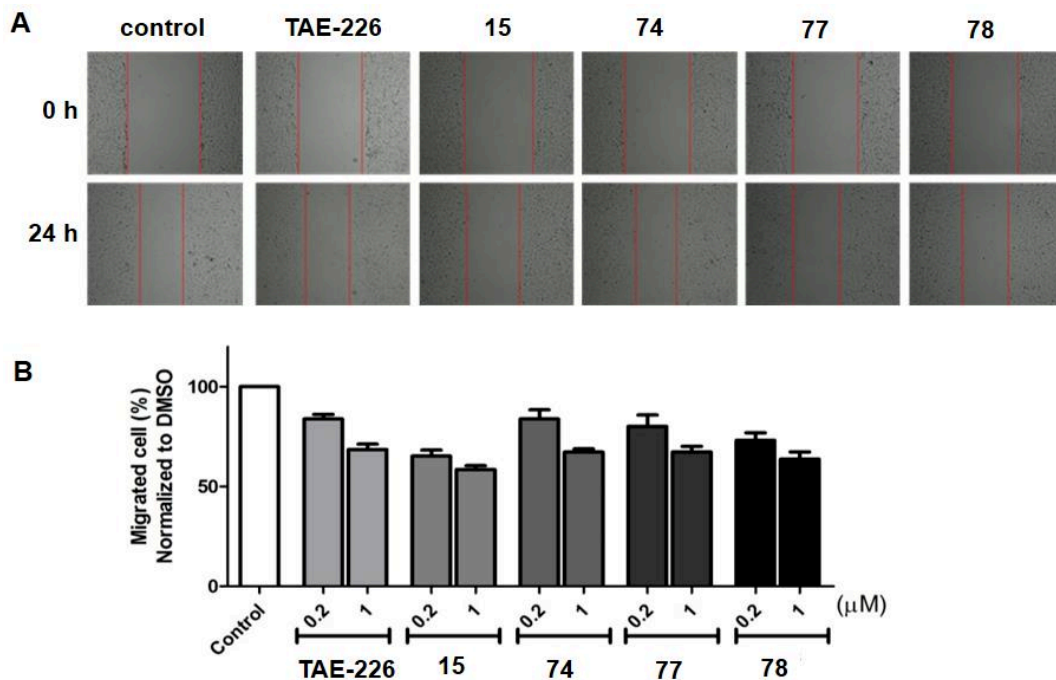


Figure 51: The ability of cell migration under each inhibitor treatment was determined by the scratch assay. (A) The pictures were taken immediately after making scratch (0 h) and at 24 h with or without 0.2 μ M inhibitors. (B) The percentage of cell migrated distance into the scratched areas was displayed in the histogram.

The effect of FAK inhibitors on the inhibition of cell migration was studied by scratch assay. Monolayer cultures of U87-MG cells were scratched (0 h) and then kept at 37 °C for another 24 h with FAK inhibitors or DMSO. The areas that were not occupied by migrated cells after 24 hours were shown in **Figure 51A**. The distance that cell migrated to the scratched areas was measured and the ratio to the control group was shown in histogram (**Figure 51B**). In comparison with vehicle DMSO, the tested compounds showed a negative effect on cell migration.

Influence on Tyr397 phosphorylation of FAK

To clarify if compounds with reversible electrophiles (**77** and **78**) could inhibit the phosphorylation of FAK in cancer cells, the U87-MG cells were exposed to each compound or DMSO for 48 h before determination of Tyr397 phosphorylation. As shown in **Figure 52A**, compounds **77** and **78** showed obvious inhibition of phosphorylation. Then the washout experiments were conducted to investigate the reversibility of the FAK autophosphorylation at Tyr397. After washout of inhibitors, cells treated with TAE-226 recovered the phosphorylation process, whereas the cells treated with compounds **15**, **77** and **78** maintained the potent inhibition of FAK phosphorylation (**Figure 52B**). These results demonstrated that compounds **77** and **78** had sustained occupancy of FAK in cells.

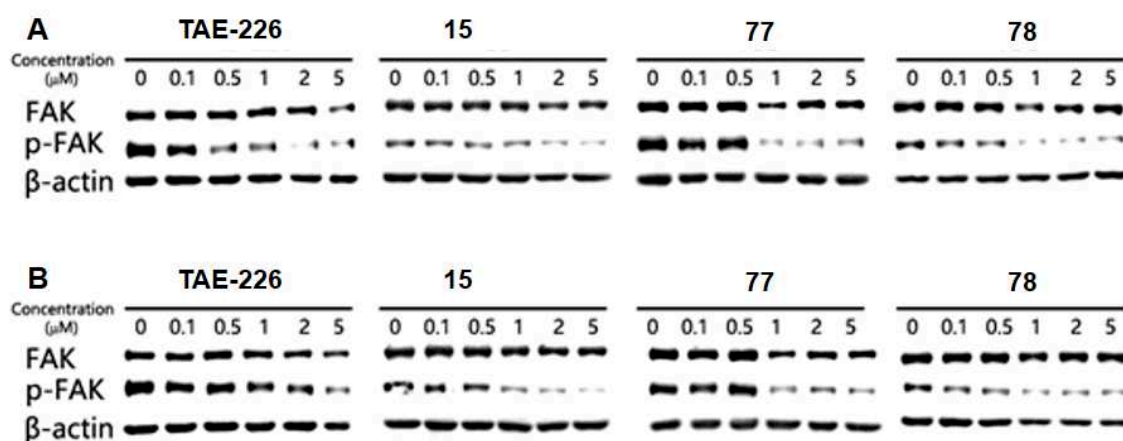


Figure 52: Inhibition of FAK phosphorylation on U87-MG cells. (A) Phosphorylation of FAK when U87-MG cells were exposed to FAK inhibitors for 48 h. (B) Phosphorylation of FAK when the inhibitors were washed out and fresh medium was added for 3 h.

6.3. Kinase selectivity profiling

Next, we investigated the kinase selectivity of 2 newly synthesized compounds with compound **15** as control. The kinase selectivity profiling was conducted by Eurofins on a panel of 9 kinases. The inhibition of each kinase for the corresponding compound at a concentration of 100 nM was shown in **Table 9**. The evaluation results revealed that compound **77** has improved kinase selectivity. Compared with compound **15**, compound **74** and **77** showed decreased inhibition of EGFR and PDGFR α . In addition, compound **77** showed significantly reduced inhibitory potency on PDGFR α , IR and Src.

Table 9: Inhibition of kinase activity (results were indicated as a mean of 2 experiments).

Kinase	Inhibition (at 100 nM)		
	15	74	77
FAK	98.1%	98.6%	94.1%
PyK2	97.6%	99.8%	97.5%
EGFR	47.2%	29.0%	25.1%
FGFR1	87.1%	88.3%	83.5%
IGF1R	91.5%	94.4%	71.9%
PDGFR α	91.0%	78.4%	67.5%
c-Kit	0.2%	0.1%	-5.9%
IR	57.6%	82.5%	32.4%
Src	52.1%	55.6%	31.1%

7. Conclusion and perspective

We synthesized 9 new covalent inhibitors of FAK. Among them, 6 compounds (group A and B) bear an irreversible electrophilic functional group and 3 compounds (group C) have a reversible electrophile (**Figure 53**).

In vitro enzymatic activity evaluation showed that these newly synthesized compounds

displayed significant inhibitory activity against FAK with IC₅₀ values ranging from 1.0 nM to 16.3 nM. Results of in cell evaluation revealed that the substituent at position 4 of the pyrimidine ring was important to the cellular anticancer activities. Compounds with arylamino substituents (**15**, **59**, **74**, **77** – **78**) showed better inhibition of cell growth on oesophageal cancer cells compared with VS-4718 and blocked the cell cycle at the G2/M stage. In contrast, compounds **64** – **66** which have arylmethanamino substituents neither had capacity to arrest cell cycle nor inhibited cell growth on oesophageal cancer cells.

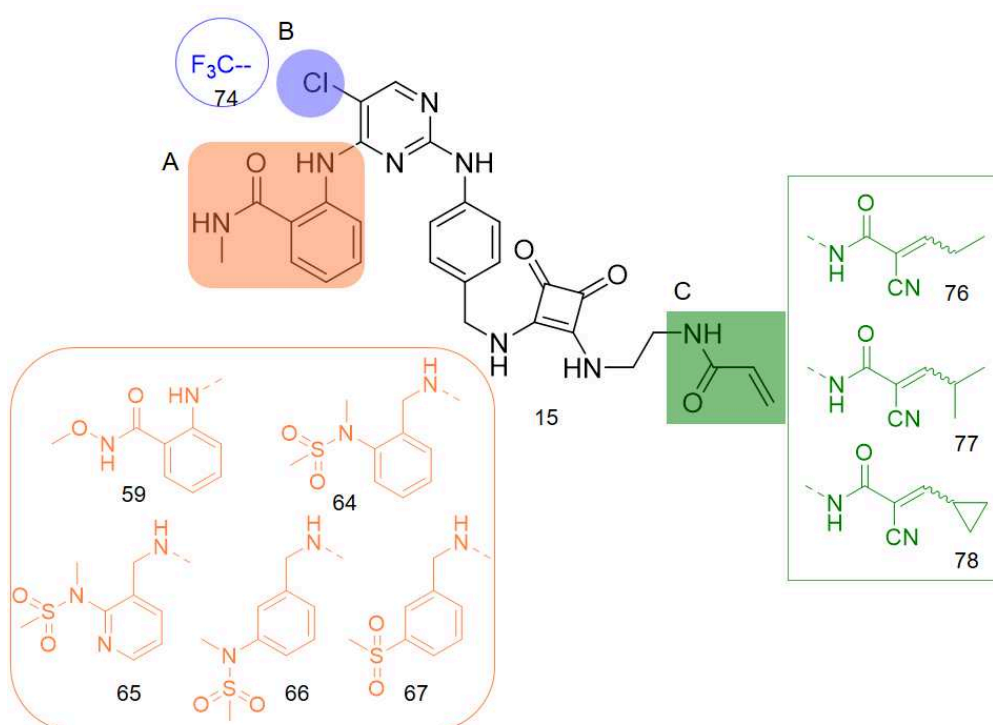


Figure 53: The chemical structures of newly synthesized compounds.

In addition, the anticancer activities on glioblastoma cells were investigated with selected compounds. Compounds **15**, **74**, **77** and **78** inhibited the proliferation of cancer cell lines U87-MG, A172 and U251 with IC₅₀ values range from 0.13 μ M to 9.8 μ M. Besides, these four compounds increased the number of cells in the G2/M stage in the cell cycle on U87-MG cells and induced morphologic change. However, none of the tested inhibitors induced apoptosis in U87-MG cells determined by flow cytometry.

The kinase selectivity evaluation showed that compound **77** had improved kinase

selectivity. In comparison with our first covalent inhibitor **15**, compound **77** exhibited less inhibitory activity against kinases such as EGFR, IGF1R, PDGFR α , IR and Scr.

The inhibitors **64** – **66** inhibited FAK enzymatic activity *in vitro*, but they didn't show anti-growth activity in cells. Similar results were also reported for FAK inhibitor VS-4718, which inhibits cell survival selectively in suspension culture, while it doesn't affect cell survival or proliferation under normally attached conditions.¹²⁰ In order to confirm their anticancer activity, it's necessary to evaluate their ability of inhibition of FAK autophosphorylation in cells. Moreover, evaluation of antiproliferation or cell survival in three-dimensional environments is also necessary.

On the other hand, in light of reversible covalent inhibition, the crystallization of our potential reversible covalent inhibitors (**76** – **78**) with FAK kinase domain is required to confirm the covalent bond formation. Otherwise, mass spectra of inhibitors with kinase can permit to observe the formation of covalent adducts.

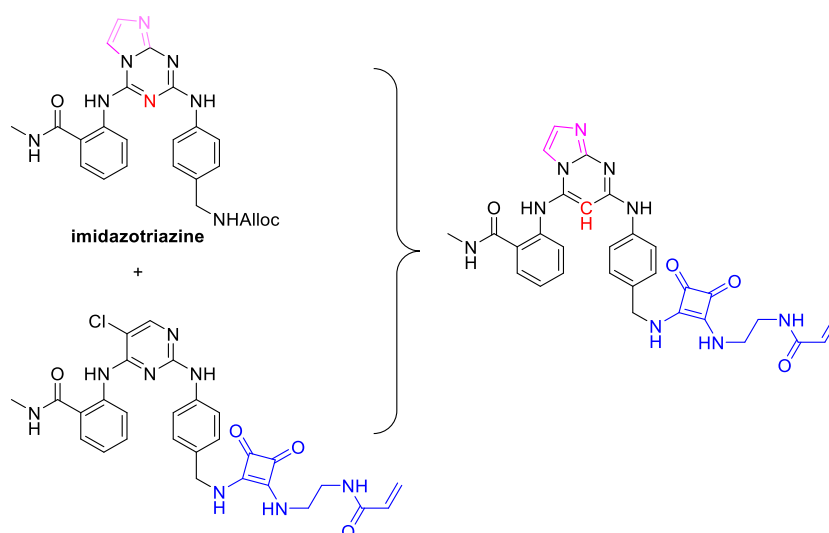
Furtherly, the *in vivo* anticancer activity assay of several candidate compounds (**15**, **77** and **78**) is under planning and the pharmacokinetic properties will be studied.

Part 3. Synthesis of imidazopyrimidine precursors for the development of bicyclic covalent inhibitor.

In this part, I will present the synthesis of imidazopyrimidine scaffold and discuss the cocrystal structure obtained with imidazopyrimidine precursor and FAK kinase.

1. Introduction

In 2015, our team reported an imidazotriazine compound as the FAK inhibitor with an IC_{50} value of 50 nM.¹³⁶ Kinase selectivity profiling showed that this compound only inhibits FAK over 50% at the concentration of 1 μ M on a panel of 32 kinases, including Pyk2, ABL1, AKT1, EGFR, IR and so on.¹³⁶ Molecular modelling showed that the binding mode of imidazotriazine was overlapped with TAE-226, and the imidazole ring has a hydrophobic interaction with the gatekeeper residue. Therefore, the replacement of pyrimidine ring in our covalent inhibitors by a bicyclic scaffold may provide a new approach to improve the selectivity. In consideration of solubility, we chose imidazopyrimidine scaffold to develop a new family of FAK inhibitors (**Scheme 39**).

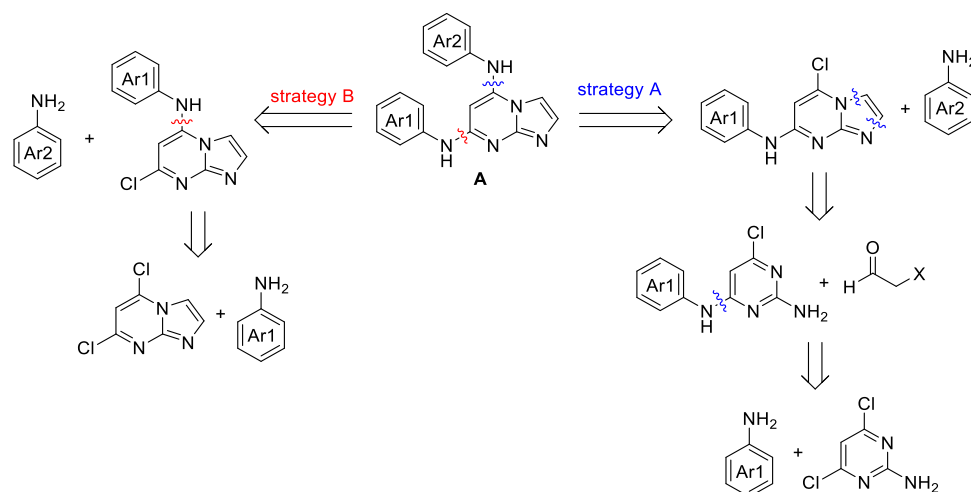


Scheme 39: Design of bicyclic covalent inhibitor.

2. Synthesis of imidazopyrimidine-based covalent inhibitor

1) Retrosynthetic analysis

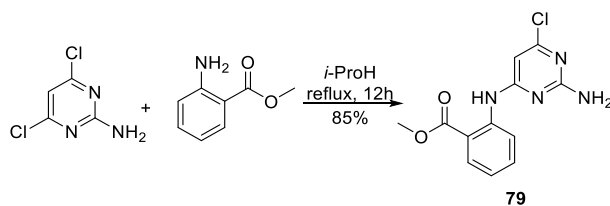
The retrosynthetic analysis of imidazopyrimidines was shown in **Scheme 40**. To synthesize the bicyclic covalent inhibitors, it was important to build the diarylaminoimidazopyrimidine intermediate **A**. One method to prepare intermediate **A** is shown as strategy A. Starting from 2-amino-4,6-dichloropyrimidine, the first chlorine is substituted by an arylamine using aromatic nucleophilic substitution. Then the cyclization step with 2-chloroacetaldehyde gives the imidazopyrimidine scaffold. Through another S_NAr reaction, the second arylamino group is introduced to generate the desired diaminosubstituted imidazopyrimidines. An alternative synthetic route (strategy B) is from 5,7-dichloroimidazo[1,2-a]pyrimidine. The chlorine at position 5 is firstly substituted by an arylamine, followed by another amination of arylamine to give intermediate **A**.



Scheme 40: Retrosynthetic analysis

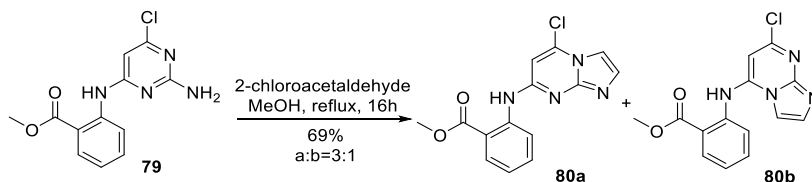
2) Construction of imidazo[1,2-a]pyrimidine core.

In order to introduce the first arylamino substituent, 2-amino-4,6-dichloropyrimidine and methyl anthranilate were refluxed in *iso*-propanol to give 4-position substituted product **79** through a nucleophilic substitution (**Scheme 41**).



Scheme 41: Synthesis of compound **79**.

The cyclization was achieved by refluxing **79** and 2-chloroacetaldehyde at 100 °C overnight in a sealed tube (**Scheme 42**).¹⁸⁶ As described in the synthesis of imidazo[1,2-a][1,3,5]triazine derivatives,¹⁸⁷ two regioisomers were obtained through cyclization in an isolated ratio of about 3:1 (a:b) because of the steric hindrance. These two regioisomers (**80a** and **80b**) had R_f values of 0.21 and 0.15 on TLC (eluent, DCM/MeOH=100/1), respectively. The regioisomer **80a** was a little less soluble than **80b** in DCM so that compound **80a** could be precipitated from the mixture. Then the filtrate was purified by column chromatography to give compound **80b**.



Scheme 42: Synthesis of compounds **80a** and **80b**.

In order to confirm the structure of these two regioisomers, the nuclear magnetic resonance spectroscopy was engaged. The peaks on the ¹H-NMR were fully assigned to corresponding protons in accordance with 2D-COSY, HSQC, and HMBC spectra. In the 2D-NOESY spectrum of compound **80a** (**Figure 54**), we observed cross peaks between H10 and H6. It seems that the benzoate substituent was not spatially close to the protons in the imidazo[1,2-a]pyrimidine scaffold in compound **80a**. However, in the 2D-NOESY spectrum of compound **80b** (**Figure 55**), the nuclear overhauser effects of protons H6-H6' and protons H10-H3 were observed, which were consistent with the structure that substitution at position

5 of the nitrogenous heterocycle.

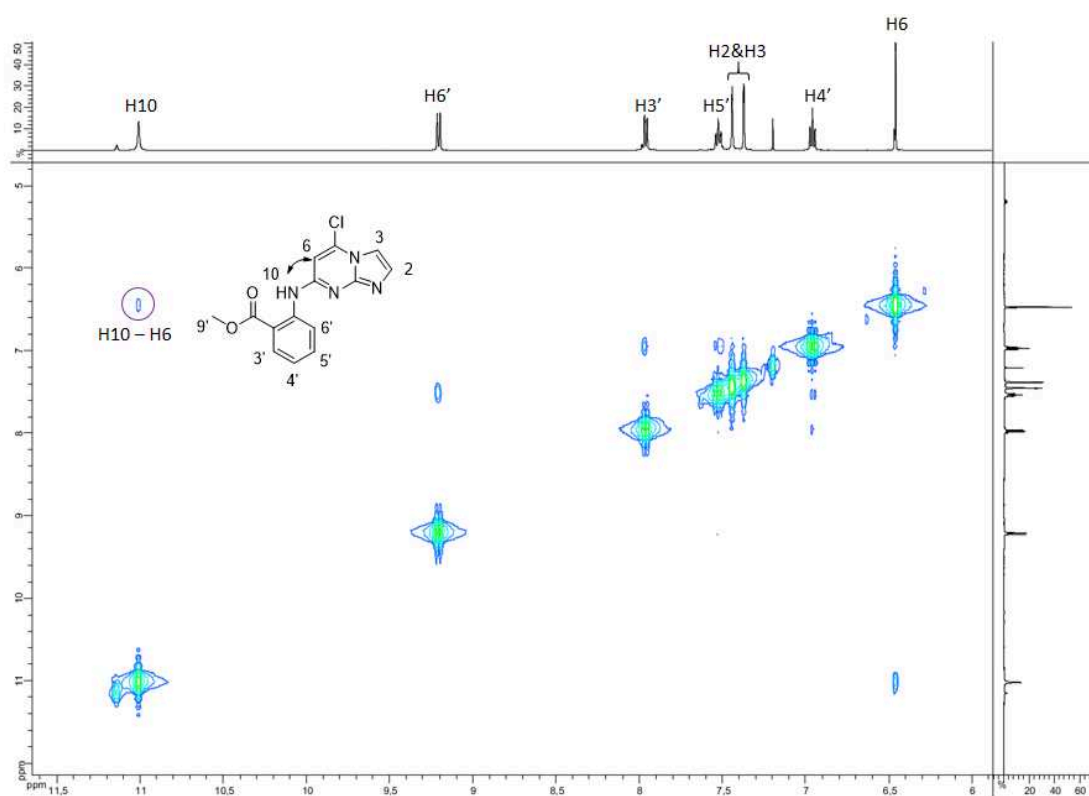


Figure 54: NMR 2D-NOESY spectrum of compound **80a** obtained in CDCl₃ (500 MHz).

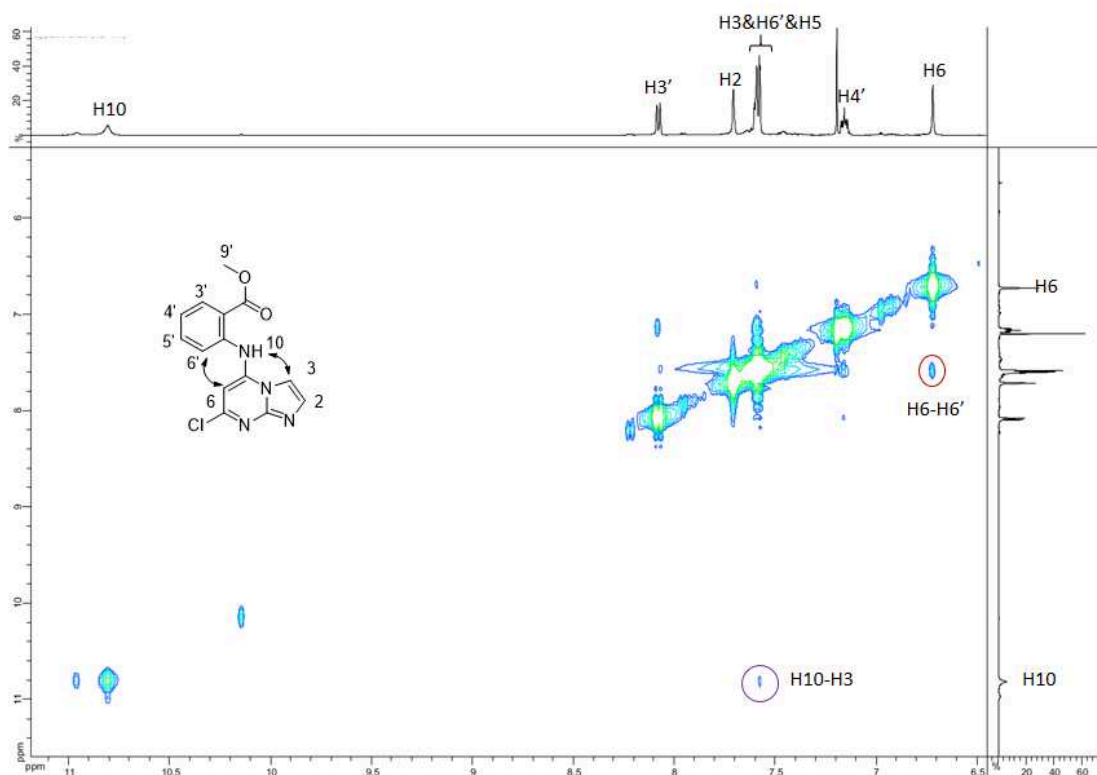
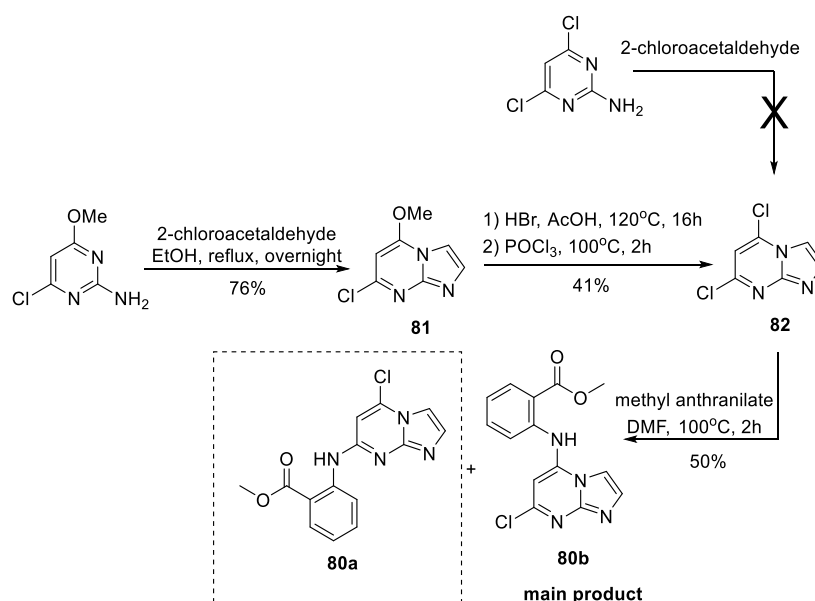


Figure 55: NMR 2D-NOESY spectrum of compound **80b** obtained in CDCl₃ (500 MHz).

The structure of compound **80b** was also double confirmed by direct substitution of compound **82** (**Scheme 43**). It was reported that the nucleophilic substitution of 5,7-dichloroimidazo[1,2-a]pyrimidine (**82**) was preferred on the position 5.^{188,189} As shown in **Scheme 43**, to synthesize the key intermediate **82**, the direct cyclization of 2-amino-4,6-dichloropyrimidine was attempted, but unfortunately the cyclization didn't occur. This could be attributed to the electron deficiency in the pyrimidine ring caused by the two chlorines. Then 2-amino-4-chloro-6-methoxypyrimidine was used as starting material. The cyclization with 2-chloroacetaldehyde gave compound **81** as main product in 76% yield.¹⁹⁰ Afterwards, intermediate **82** was prepared by demethylation and chlorination.¹⁸⁸ The substitution of **82** with methyl anthranilate gave the position 5 substituted compound as main product, which had identical NMR spectra to the compound **80b**. This synthetic route could be used to selectively prepare regioisomer **80b**.

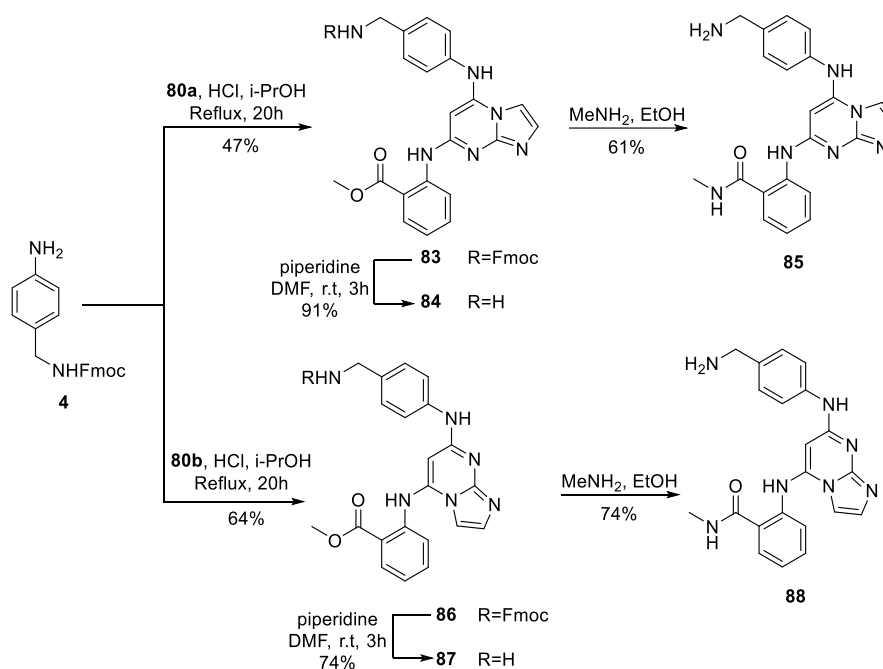


Scheme 43: Synthesis of compound **82** and its substitution

3) Synthesis of diaminosubstituted imidazopyrimidines

In order to introduce the second arylamino substituent, the nucleophilic substitution of regioisomer **80a** with arylamine **4** was performed under acidic conditions to generate

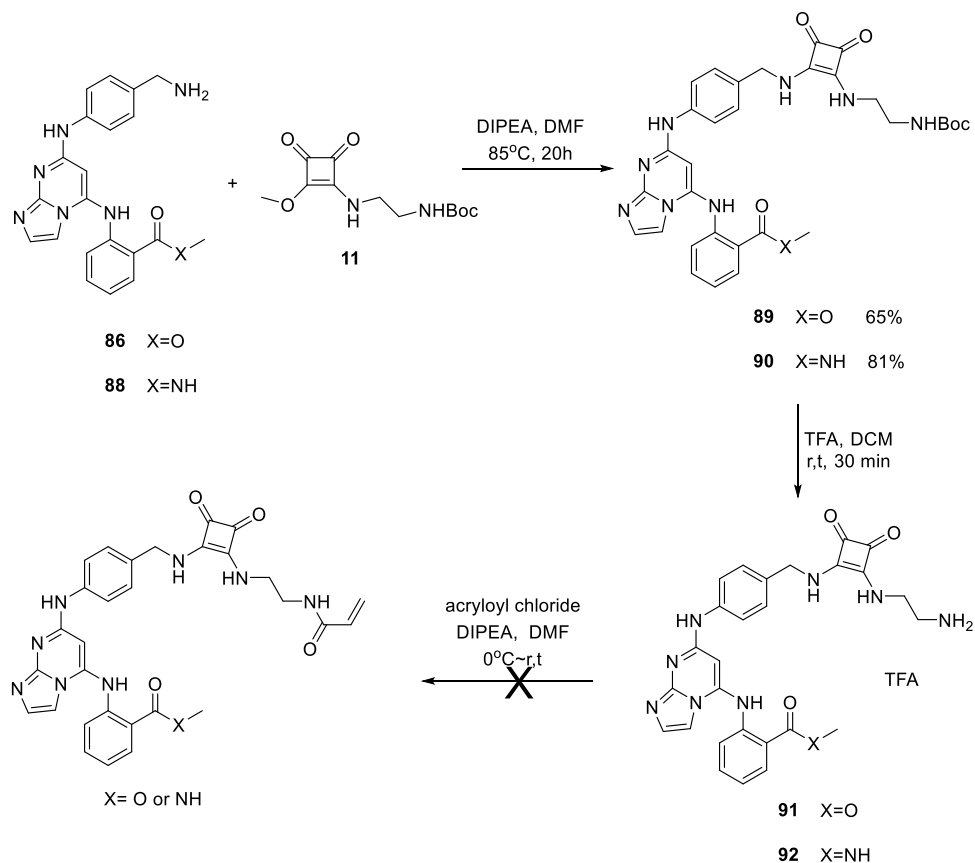
diaminosubstituted imidazo[1,2-a]pyrimidine **83**. Then the protecting group was removed by treatment of piperidine in DMF to give **84**. The final compound **85** was obtained in 61% yield by aminolysis of **84** in the solution of methylamine in ethanol at room temperature.¹⁹¹ Following the same procedure, from regioisomer **80b**, another desired compound **88** was also prepared in good yield (**Scheme 44**).



Scheme 44: Synthesis of compounds **85** and **88**.

4) Synthesis of bicyclic covalent inhibitors

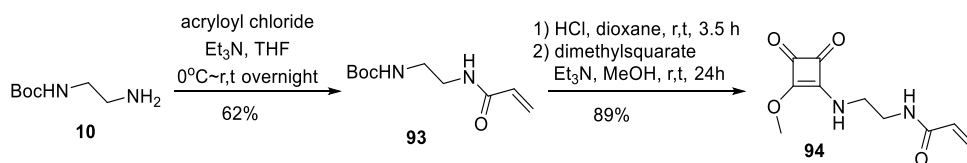
The squaramide linker was condensed with compounds **86** and **88** under the same conditions used before to give compounds **89** and **90** in 65% and 81% yield, respectively. The protecting group was removed by treatment with TFA giving intermediates **91** and **92** as trifluoroacetate salts. In the final step, acryloyl chloride was added to the solution of amine in DMF in the presence of DIPEA. Though this reaction worked well with pyrimidine compounds, unfortunately, we couldn't see any product on TLC (**Scheme 45**).



Scheme 45: Tentative synthesis of imidazopyrimidine-based covalent inhibitor.

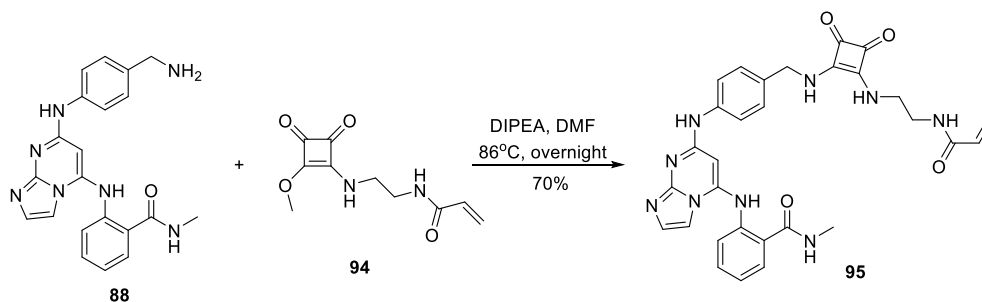
To obtain the desired molecule, a venturesome synthetic strategy was proposed. Owing to the difference in reactivity of mono-squaramide and acrylamide towards amine, we attempted to introduce the electrophile to the linker part before the condensation with compound **88**.

Starting from *N*-Boc-ethylenediamine **10**, an acylation step gave compound **93** in 62% yield. The Boc group was removed using Yung's method¹⁹² with 4 M HCl in 1,4-dioxane at room temperature. After concentration, the hydrochloride was neutralized with Et₃N and reacted with dimethylsquarate giving key intermediate **94** in 89% yield (**Scheme 46**).



Scheme 46: Synthesis of compound **94**.

Compounds **88** and **94** were added to a solution of DMF in the presence of DIPEA and stirred at 86 °C overnight. As expected, the reaction of the squaramate and the amine was favoured in this condition and the desired compound **95** was obtained in 70% yield (**Scheme 47**).



Scheme 47: Synthesis of compound **95**.

3. X-Ray crystallography

In order to confirm that the binding mode of imidazopyrimidine scaffold in the active site of FAK, compounds **85** and **88** were crystallized with the kinase domain of FAK. The crystallography experiments were conducted by D. Lietha at the Spanish National Cancer Research Center (CNIO).

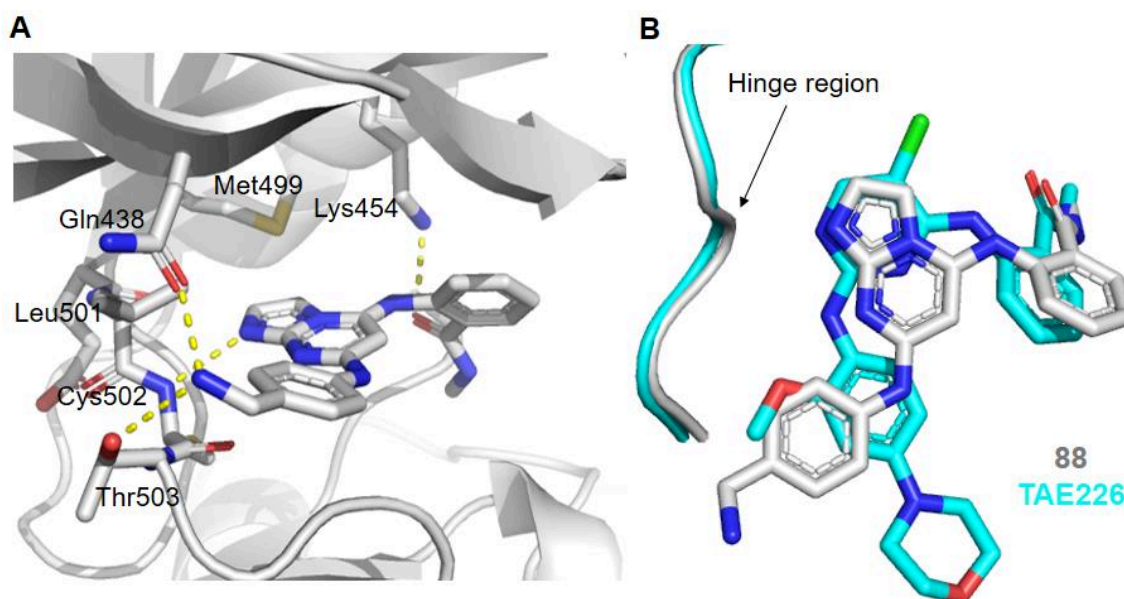


Figure 56: (A) Interactions of compound **88** with the FAK kinase domain, (B) Superposition of compound **88** and TAE-226.

Only the cocrystal structure of compound **88** with FAK was obtained. The compound **88** was able to enter the kinase active site and to form several hydrogen bonds with the residues in the ATP pocket (**Figure 56, A**). The N1 atom in the imidazole ring formed a hydrogen bond with the backbone NH group of Cys502. The oxygen on the carboxamide of **88** formed a hydrogen bond with the side chain of Lys454. The hydrogen bond interaction between the Lys454 and inhibitors was important to give a strong inhibition of FAK.¹³² Moreover, the terminal amino group on the *para*-aminomethylphenyl substituent formed two hydrogen bonds with the side chains of Gln438 and Thr503, respectively.

As shown in **Figure 56 B**, the superposition of compound **88** and TAE-226 showed that the pyrimidine ring of TAE-266 was overlapped with the imidazole ring in compound **88** rather than with the pyrimidine part. Moreover, the orientation of the arylamine substituent at position 7 on the bicyclic ring was towards the hinge region and it was almost orthogonal to the orientation of the 4-arylamino substituent of TAE-226.

4. Conclusion and perspective

We have established a feasible synthetic route to obtain 5,7-diaminosubstituted imidazo[1,2-a]pyrimidines and synthesized a potential bicyclic covalent inhibitor of FAK.

X-ray crystallography solved the binding mode of imidazo[1,2-a]pyrimidine in the active site of FAK. Interestingly, the bicyclic binds to the hinge region through the nitrogen of imidazole rather than the nitrogen of pyrimidine. Besides, the 4-aminomethylanilino substituent at position 7 of imidazopyrimidine pointed to the hinge region. As shown in **Figure 57**, the distance between Cys427 and the 7-aryl in **88** is about 8.9 Å. The *meta*-position seems better than the *para*-position for the installation of a linker to deliver the electrophilic functional group to the vicinity of Cys427 (**Figure 57**). Besides, the introduction of a small hydrophobic substituent on the position 2 or 3 of the imidazole ring which will have a hydrophobic interaction with the gatekeeper residue Met499 may improve the affinity.

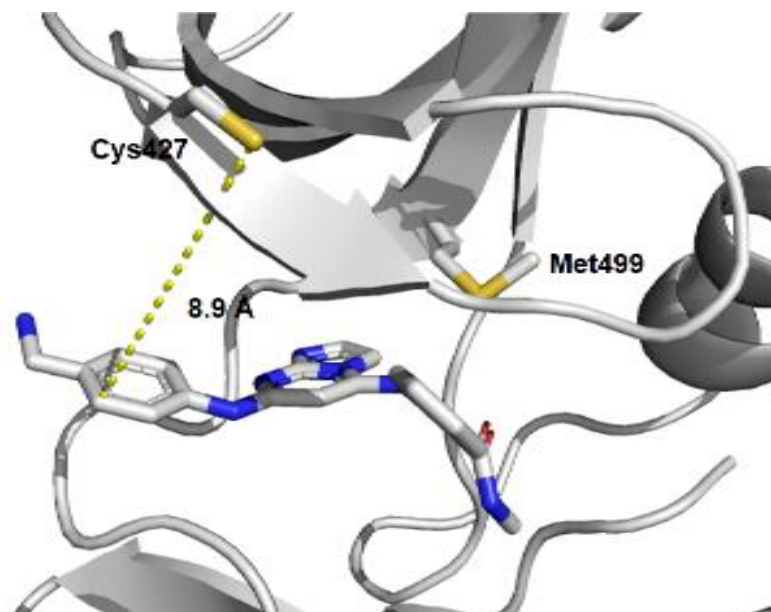


Figure 57: Crystal structure of compound **88** in FAK active site.

Chapter III. Study of microwave-assisted synthesis of 2,5-disubstituted pyrimidine derivatives

1. Introduction

FAK kinase exists in equilibrium between active and inactive states. The activation loop of FAK adopts different conformations between these two states (**Figure 58**). In the autoinhibited state, the activation loop occludes the catalytic cleft⁷⁷ and creates a hydrophobic pocket near to the ATP pocket. Type II inhibitors that bind to the inactive conformation of kinases have better selectivity than type I inhibitors. Hence, we are interested in the design of type II inhibitor of FAK.

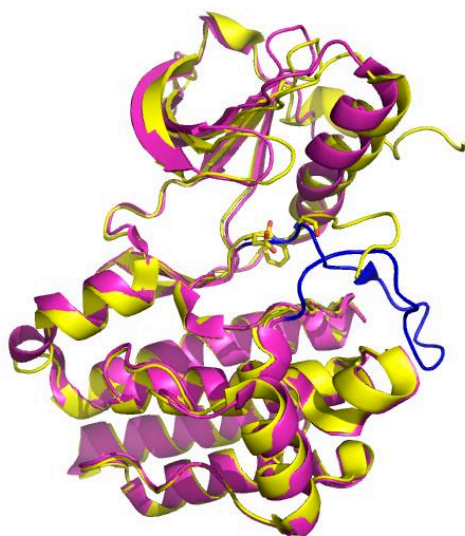


Figure 58: Superposition of active (purple) and inactive (yellow) FAK kinase domain structure. The activation loop in the active state was shown in blue. (PDB ID: 2J0L and 2J0J).

Molecular modelling with the inactive FAK kinase domain suggested that 2,5-disubstituted pyrimidine-based structures (**Figure 59**) could occupy the active site and allosteric pocket created by activation loop.

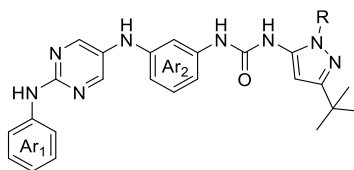
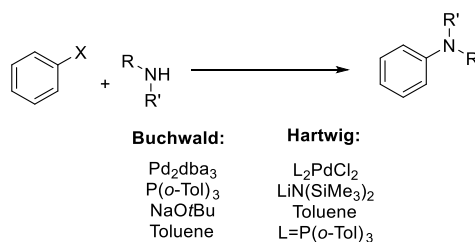


Figure 59: General structure of type II inhibitor of FAK.

To synthesize this kind of molecules, the amination on the 5-position of pyrimidine is a key step. In the previous work, we attempted Pd-catalysed amination. For the purpose of the total conversion of starting material, it's inevitable that the reaction needs to be heated at high temperature for a long time. Nevertheless, the yield was not satisfied. In addition, under this condition, some substrates with ester or amide functional groups were degraded. It's necessary to explore a new synthetic method for the preparation of 2,5-disubstituted pyrimidine.

1.1. The Pd-catalysed C-N coupling reaction

The palladium catalysed aromatic amination of aryl bromide with *N, N*-diethylamino-tributyltin was first reported as early as 1983.¹⁹³ Due to the limitation of substrate scope of the tin-reagent, this method didn't obtain extensive applications. About ten years later, Stephen L. Buchwald and John F. Hartwig reported directly Pd-catalysed amination of aromatic halide with amines without tin-reagents, respectively (**Scheme 48**).^{194,195} Then the Buchwald- Hartwig amination has been widely studied and became an important method for construction of C-N bond.



Scheme 48: Buchwald Hartwig amination conditions.

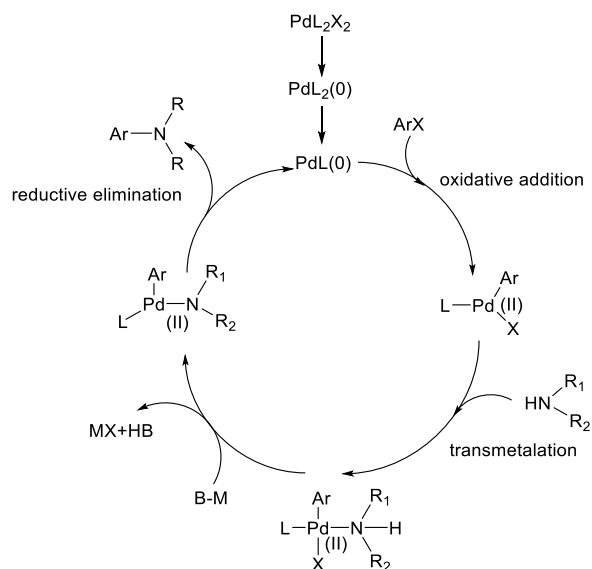
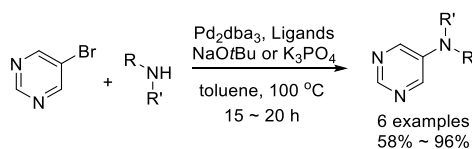


Figure 60: Catalytic cycle of Buchwald-Hartwig amination.

The catalytic mechanism involves 4 steps as shown in **Figure 60**. First, Pd(II) is reduced to Pd(0) by ligands. Then, Pd(0) loses one ligand and forms Pd(II) complex through oxidative addition. Next, amine attacks the Pd(II) and substitutes the X under the help of base. Afterwards, the product was produced through a reductive elimination and giving Pd(0) to continue the catalytic cycle.

The Pd-catalysed amination at position 5 of pyrimidine was rarely reported. In 2005, Buchwald *et al*¹⁹⁶ reported amination of 5-bromopyrimidine with 6 amines. This reaction was conducted in toluene at 100 °C for 15 to 20 hours and products were obtained in 58% - 96% yield (**Scheme 49**).

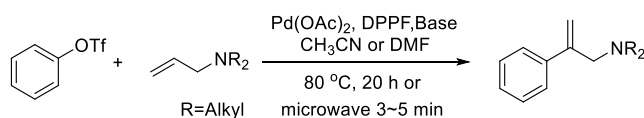


Scheme 49: Amination of 5-bromopyrimidine.

1.2. Microwave in organic reaction

The microwave heating is more efficient than traditional conductive heating. In the conductive heating such as oil bath or heating jacket, the temperature of the reaction vessel is usually higher than that in the reaction mixture, so that the transferring of energy is slow and inefficient. In contrast, microwave irradiation produces efficient internal heating by molecules' dipolar polarization and ionic conductance in chemical reactions.¹⁹⁷ In accordance with the dipolar polarization mechanism, the dipolar molecules will rotate to align with an oscillating electric field. With a suitable frequency, the re-orientation of dipole can't follow the phase change of applied field resulting in a phase difference between the orientation of the field and that of the dipole. This phase difference causes molecular friction and collision and energy released from the dipole producing dielectric heating.¹⁹⁷ The other energy source of heating in microwave irradiation is from the movement of ions through the solution in consequence of an electric field. The increased collisions of ions convert the kinetic energy to heat.¹⁹⁷

The main advantage of microwave irradiation is the shorter reaction time from days or hours to mere minutes or even seconds. For example, the Heck reaction between aryl triflate and *N,N*-dimethylallylamine need more than 20 hours to achieve the full conversion of aryl triflate with standard thermal heating, while under microwave irradiation the heck coupling could be finished within 5 min (**Scheme 50**).¹⁹⁸ Therefore, the reaction parameters such as reaction temperature and time, solvents, catalysts and additives can be investigated quickly to optimize the desired chemical reactions.



Scheme 50: Heck reaction between aryl triflate and *N,N*-dimethylallylamine.

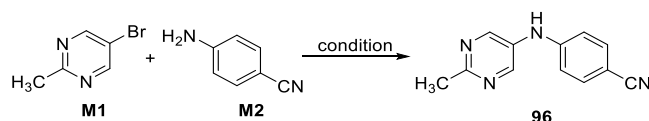
Microwave-assisted organic synthesis has been widely applied in present synthetic chemistry, including transition-metal catalysed carbon-carbon bond formation¹⁹⁹ or carbon-

heteroatom bond formation,²⁰⁰ heterocycles synthesis.²⁰¹ Nevertheless, the microwave-assisted Buchwald-Hartwig amination is relatively under-explored compared with the transition-metal catalysed C-C bond forming reactions.

Hence, we studied the Pd-catalysed amination of 2-substituted 5-bromopyrimidine under microwave irradiation and explored the substrate scope.

2. Optimization of coupling conditions

In order to study the Pd-catalysed amination for the synthesis of 2,5-disubstituted pyrimidine derivatives, we choose the reaction of 2-methyl-5-bromopyrimidine (**M1**) and *para*-aminobenzonitrile (**M2**) as a model for optimization of coupling conditions (**Scheme 51**). The microwave conditions were set as maximum temperature: 120 °C, heating as fast as possible and duration for 60 minutes.



Scheme 51: Model reaction.

1) Influence of Pd-catalysts and ligands.

The combination of palladium catalysts and ligands was important for the successful conversion of starting materials to corresponding products in C-N coupling reactions. Hence, we firstly screened a small scale of palladium catalysts and 5 ligands (**Figure 61**) which are frequently used in the Pd-catalysed aryl halide amination.

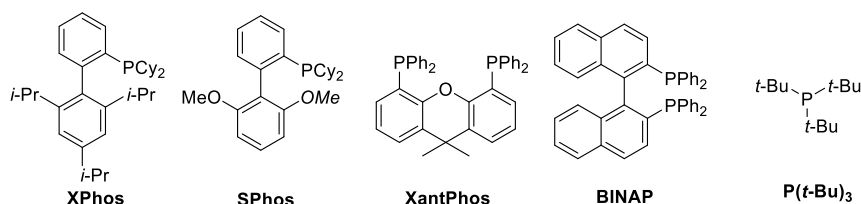


Figure 61: Chemical structure of ligands.

The initial experiment was conducted with Pd₂dba₃ and XPhos in the presence of Cs₂CO₃ in 1,4-dioxane (Entry 1, **Table 10**). Encouragingly, desired compound **96** was isolated in 65% yield. However, other palladium catalysts did not efficiently catalyze this reaction, such as Pd(OAc)₂ or Pd(PPh₃)₄ (Entry 2 and 3, **Table 10**). Next, the combination of Pd₂dba₃ and SPhos was employed resulting in a decrease of yield to 26% (Entry 4, **Table 10**). With XantPhos as ligand, the product was only separated in 14% yield (Entry 5, **Table 10**). Reactions with BINAP or P(t-Bu)₃ as ligands did not work well either affording a very small amount of product (Entry 6 and 7, **Table 10**). Therefore, Pd₂dba₃ in combination with XPhos was the most efficient reagents to catalyze the amination of 5-bromo-2-methylpyrimidine.

Table 10: Influence of catalyst and ligand^a

Entry	Catalyst	Ligand	Yield ^b
1	Pd₂dba₃	XPhos	65%
2	Pd(OAc) ₂	XPhos	29%
3	Pd(PPh ₃) ₄	XPhos	12%
4	Pd ₂ dba ₃	SPhos	26%
5	Pd ₂ dba ₃	XantPhos	14%
6	Pd ₂ dba ₃	BINAP	9%
7	Pd ₂ dba ₃	P(t-Bu) ₃	15%

a, Cs₂CO₃ was used as base and 1,4-dioxane was used as solvent; b, Isolated yield

2) Influence of base and solvent.

Given the fact that product **96** was delivered in 65% yield with Pd₂dba₃ and XPhos in the presence of Cs₂CO₃ in 1,4-dioxane (Entry 1, **Table 11**), then we investigated the influence of base and solvent. With K₃PO₄ as base, the yield of this reaction declined to 45% (Entry 2, **Table 11**). When base NaOtBu was used, the yield rose to 80% (Entry 3, **Table 11**). However, the change of solvents didn't give a better result than 80% yield in 1,4-dioxane (Entry 4 and 5, **Table 11**).

Table 11: Influence of base and solvent^a

Entry	Base	Solvent	Yield ^b
1	Cs ₂ CO ₃	1,4-Dioxane	65%
2	K ₃ PO ₄	1,4-Dioxane	45%
3	NaOtBu	1,4-Dioxane	80%
4	NaOtBu	Toluene	57%
5	NaOtBu	DMF	trace

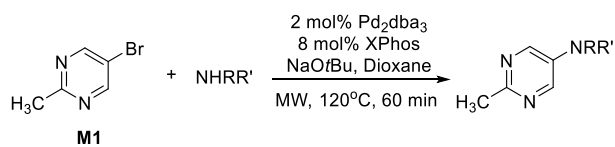
a, Pd₂dba₃ and XPhos were used as catalyst and ligand; b, Isolated yield

In conclusion, through a screening of catalysts, ligands, bases and solvents, the best conditions to promote this amination reaction appeared as the combination of 2 mol% Pd₂dba₃, 8 mol% XPhos and 1.1 eq NaOtBu in 1,4-dioxane.

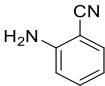
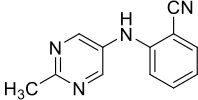
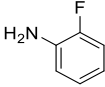
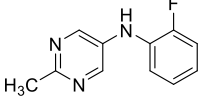
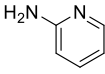
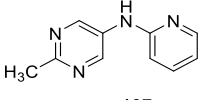
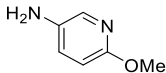
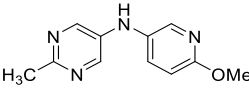
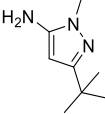
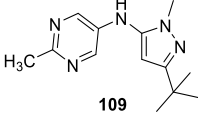
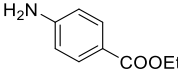
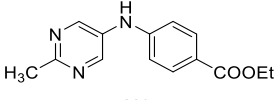
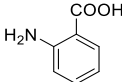
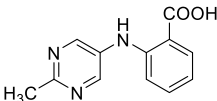
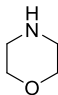
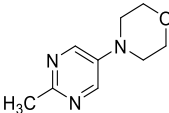
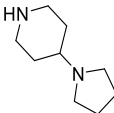
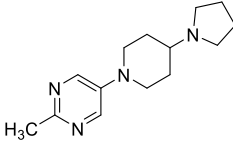
3. Expanding the scope of substrates

3.1. The substrate scope of amines.

Firstly, we investigated the substrate scope of amines. The compound **M1** and aniline reacted well under our optimal conditions giving the corresponding product in 82% yield (Entry 1, **Table 12**). Three different methoxyanilines all coupled to bromide **M1** in a yield 81% - 86% (Entry 2, 3, 4, **Table 12**), which means that electron-donating group on aromatic ring slightly favours the C-N coupling reaction. The product of reaction **M1** and 3-methylaniline was also obtained in 85% yield. However, the influence of electron-withdrawing substituent on arylamine depended on the position and property. The compound with a CF₃ group on the *meta* position of aniline was converted to the product in 82% yield (Entry 6, **Table 12**), while reaction with *para*-trifluoromethylaniline gave product in 59% yield (Entry 7, **Table 12**).

Table 12: Amination of 5-bromo-2-methylpyrimidine.

Entry	Amine	Product	Yield ^a
1			82%
2			86%
3			83%
4			81%
5			85%
6			82%
7			59%
8			69%

9		 105	37%
10		 106	98%
11		 107	23%
12		 108	64%
13		 109	84%
14		 110	52% ^b
15		 111	67%
16		 112	93%
17		 113	77%

a, isolated yield; b, reaction time 30 min.

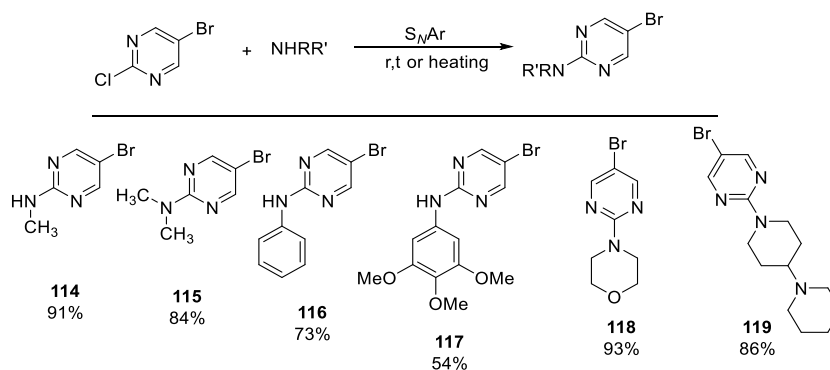
In addition, reaction of **M1** and 4-aminobenzonitrile (**M2**) that we studied as model generated product in 80% yield (Entry 3, **Table 11**), whereas with 3-aminobenzonitrile or 2-aminobenzonitrile as substrate the products were collected in a yield of 69% and 37%, respectively (Entry 8 and 9, **Table 12**). Nevertheless, 2-fluoroaniline was converted to products in 98% yield (Entry 10, **Table 12**). Then the substrate scope was expanded to heteroaryl amines and the products were generated in low to good yield. When pyridine-2-amine or 6-methoxypyridin-3-amine was used, the reaction gave the product in a yield of 23% and 64%, respectively (Entry 11, 12 **Table 12**), but the yield was very good (84%) for pyrazolyl-amine substrate (Entry 13, **Table 12**). Ester is an important functional group in the bioactive molecules. To investigate if the ester was tolerated in the microwave radiated condition, we chose the ethyl 4-aminobenzoate as substrate. Microwave irradiation for 60 minutes under the coupling conditions was long enough to hydrolyse the ester bond. The irradiation time was shortened to 30 minutes, the ethyl ester product was collected in 52% yield (Entry 14, **Table 12**). When 2-aminobenzoic acid was used as the substrate, the product was got in 67% yield (Entry 15, **Table 12**). At last, two aliphatic secondary amines were reacted with **M1** giving corresponding products in yield of 93% and 77% (Entry 16, 17, **Table 12**). In summary, this microwave-assisted amination method had a broad amine substrate scope including aryl amines, heteroaryl amines and aliphatic amines so that prepare a variety of 2,5-disubstituted pyrimidines.

3.2. The substrate scope of 5-bromo-2-substituted pyrimidines

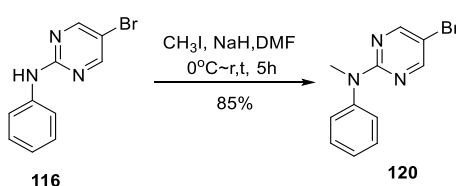
In order to study the influence of substituents at position 2 of pyrimidine on the coupling reaction, we prepared three kinds of 2-substituted-5-bromopyrimidine substrates and these substrates were used to react with 4-aminobenzonitrile (**M2**) under microwave-assisted palladium catalytic conditions.

3.2.1. Preparation of substrates

We firstly prepared 2-aminosubstituted-5-bromopyrimidines from 5-bromo-2-chloropyrimidine and appropriate amines through nucleophilic substitution. The substitution was prior at position 2 of the pyrimidine ring. In an optimized protocol of Li,²⁰² 5-bromo-2-chloropyrimidine was added to a solution of excessive amine in alcohol, the mixture was stirred at room temperature or heating to reflux giving corresponding 2-aminosubstituted-5-bromopyrimidines (**114** - **119**) with a yield of 54% - 93% (**Scheme 52**). The methylation of secondary amino in **116** was achieved by methyl iodide in the presence of sodium hydride giving **120** in 85% yield (**Scheme 53**).²⁰³

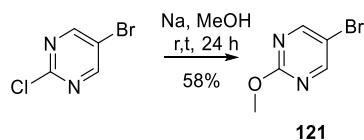


Scheme 52: Preparation of 2-aminosubstituted-5-bromopyrimidines.



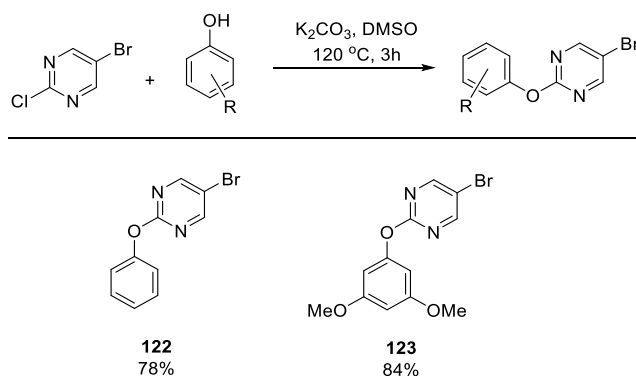
Scheme 53: Synthesis of compound **120**.

Then the substrates containing a methoxy or aryloxy at position 2 of 5-bromopyrimidine were prepared. 5-Bromo-2-methoxypyrimidine **121** was synthesized from 5-bromo-2-chloropyrimidine and freshly prepared sodium methoxide in 58% yield using a method described in the literature (**Scheme 54**).²⁰⁴



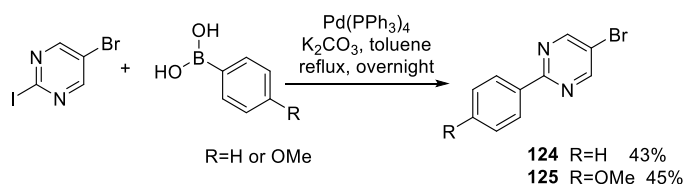
Scheme 54: Synthesis of compound **121**.

To prepare 2-aryloxy-5-bromopyrimidines (**122** – **123**), a method of Okada²⁰⁵ was employed. The chlorine of 5-bromo-2-chlorine-pyrimidine was substituted by phenol at 120°C in the presence of potassium carbonate giving 2-aryloxy-5-bromo-pyrimidine in 78% - 84% yield (**Scheme 55**).



Scheme 55: Synthesis of 2-aryloxy-5-bromopyrimidine.

2-Aryl-5-bromopyrimidines were synthesized through Suzuki coupling of 5-bromo-2-iodopyrimidine and aryl boric acid catalysed by $\text{Ph}(\text{PPh}_3)_4$ according to the protocol of Wong.²⁰⁶ Two compounds (**124**, **125**) were obtained in yields of 43% and 45%, respectively (**Scheme 56**).

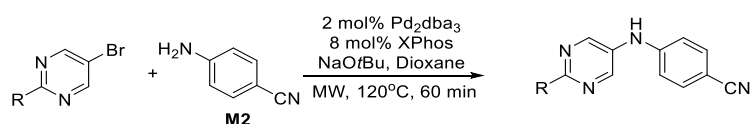


Scheme 56: Synthesis of 2-aryl-5-bromopyrimidines.

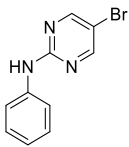
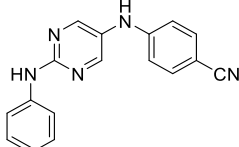
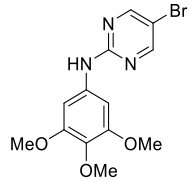
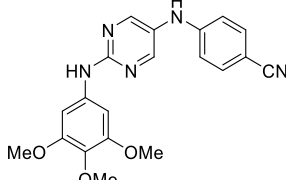
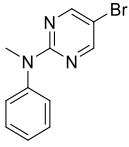
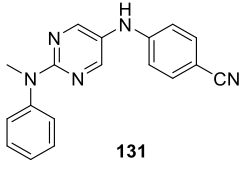
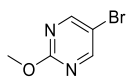
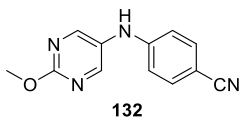
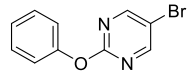
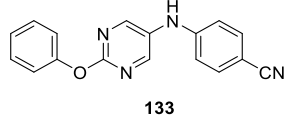
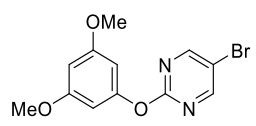
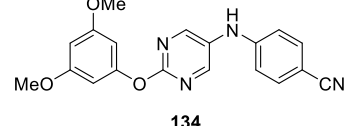
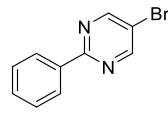
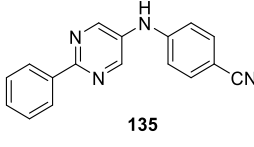
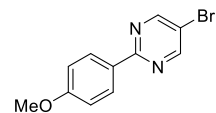
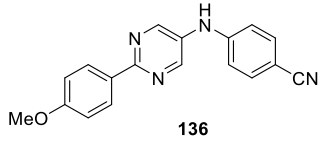
3.2.2. C-N coupling reaction of various 5-bromo-2-substituted pyrimidine

The C-N coupling of 5-bromo-2-substituted pyrimidine with 4-aminobenzonitrile (**M2**) was carried out under our optimal conditions, with Pd₂dba₃ as catalyst, XPhos as ligand, NaOtBu as base and 1,4-dioxane as solvent.

Table 13: C-N coupling of various 5-bromopyrimidines and 4-aminobenzonitrile.

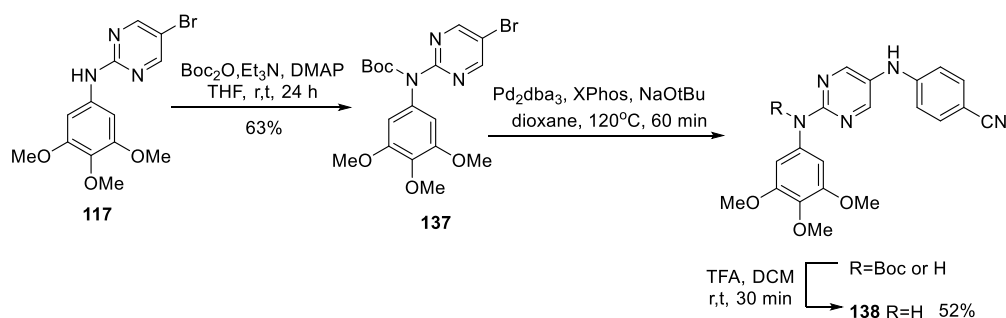


Entry	5-bromopyrimidine	Product	Yield
1		 126	84%
2		 127	44%
3		 128	81%
4		 129	99%
5		 130	89%

6			No product
7			No product
8			93%
9			65%
10			55%
11			51%
12			86%
13			90%

Firstly, we tried 5-bromopyrimidine as substrate, this coupling reaction gave the desired product in 84% isolated yield (Entry 1, **Table 13**). For *N*-substituted-2-amino-5-bromopyrimidines, the amination reaction was influenced by the substituents on the amine. Substrates with disubstituted amino group at position 2 of 5-bromo-pyrimidine generally gave the coupling product in good to high yields (80% - 99%) (Entry 3,4,5,8 **Table 13**), while the amination of substrates with monosubstituted amino group at position 2 of 5-bromopyrimidine was hindered (Entry 6,7 **Table 13**), only *N*-methyl-2-amino-5-bromopyrimidine gave product in 44% yield (Entry 2 **Table 13**). In the beginning, we thought that the low conversion of 2-arylamino-5-bromopyrimidine was due to the occupancy of palladium catalysts by the amino group. Hence, 10 mol% catalysts were loaded for the reaction of entry 6. Unfortunately, the reaction didn't get better monitored by TLC. For 5-bromopyrimidine with 2-methoxy or 2-aryloxy substituents, the yields of C-N coupling reaction under microwave irradiation were around 60% (Entry 9, 10, 11 **Table 13**), which was consistent with the yields of such reactions carried out in thermal conditions.²⁰⁷ The reaction of 2-aryl-5-bromo-pyrimidines and 4-aminobenzonitrile worked smoothly and afforded products in high yield (86% - 90%) (Entry 12, 13 **Table 13**).

In order to convert 2-arylamino-5-bromopyrimidine (**117**) into the aminated product, we protected the amino group with Boc_2O ²⁰⁸ giving intermediate **137**. Then compound **137** underwent the microwave-assisted amination giving products as a mixture with or without Boc group, then the mixture was treated by TFA to generate compound **138** in 52% yield for 2 steps (**Scheme 57**).



Scheme 57: Synthesis of compound **140**.

In summary, this microwave-assisted C-N coupling method could tolerate different substituents at position 2 of 5-bromopyrimidine as substrates including aliphatic amino, methoxy, aryloxy and phenyl. The reaction of 2-arylamino-5-bromopyrimidine was hindered, which could be circumvented by a Boc protecting strategy to give the desired compounds.

4. Conclusion

We studied the microwave-assisted Buchwald-Hartwig amination of 2-substituted 5-bromopyrimidine. Under the irradiation of microwave, the amination of 5-bromo-2-methyl pyrimidine could be fully achieved within 1 hour instead of over 20 hours under the conductive heating condition. With catalyst Pd₂dba₃, ligand XPhos, and base NaOtBu, this method had a broad substrate scope of amines including heteroaryl amines, arylamines, and aliphatic amines. In addition, we investigated the amination of 5-bromopyrimidines which bear various substituents at position 2 of the pyrimidine ring giving corresponding products in good to high yields. The efficient microwave-assisted synthesis of 2-5-disubstituted pyrimidine can be applied to the preparation of type II inhibitors of FAK. This work is under submission to the Tetrahedron Letters.

Chapter IV. Synthesis of fluorescent covalent binding tools of FAK

1. Introduction

Small molecule-based fluorescent probes are powerful and popular tools to visualize the biological processes because of their high resolution in space and time. Fluorescent chemical probes have been widely used in the tumour diagnosis²⁰⁹ and *in vivo* tumour imaging.²¹⁰ In addition, these probes are also very useful tools in biological experiments to study the kinase signalling transductions.²¹¹

Visualization of the specific protein in cells is an important strategy to analyze the role of a protein in the signal cascade. The antibody-based immunofluorescence and genetically encoded fluorescent reporters²¹² are general methods for monitoring selected proteins in cells, but these methods can't satisfy all the biological experiments. In comparison with antibody-based immunofluorescence, the fluorescent small molecules are able to enter cells without fixation and permeabilization and to provide visualization of dynamic cellular processes. In spite of genetically encoded fluorescent reporter is able to achieve live-cell imaging, this approach is limited to the systems in which genetic editing is available. Therefore, fluorescent small molecular probes that specifically target a protein can offer complementary information in biological experiments.

In the kinase cascades study, it's an effective strategy to inhibit the kinase activity with small molecules, which provide a dose-dependent response of kinase activity. However, this method sometimes gives ambiguous results because of the off-target effect and non-accurate concentration of inhibitors in cells, which are influenced by cell permeability, drug efflux, and cellular metabolism, etc.^{213,214} Blair and colleagues²¹⁵ demonstrated proof-of-concept of using fluorescent affinity probe to report the necessary fraction of EGFR kinase for cellular

signalling and to quantitate the relationship between EGFR stimulation and its downstream outputs. The targeted fluorescent probe can be used to quantitate the percentage of inhibited kinase and identify the most sensitive node in signalling pathway.

In order to study the enzyme occupancy of our covalent inhibitors in cells and related kinetic properties, a fluorescent covalent binding tool is required. On the other hand, FAK signalling is related to a number of downstream proteins. FAK targeted fluorescent probes are likely to be useful for the FAK cascade study. Moreover, it was reported that nuclear FAK reduces p53-mediated cell cycle arrest and enhances cell survival by promoting p53 ubiquitination and degradation.²¹⁶ The fluorescent probe is able to visualize FAK in living cells and to detect the nuclear FAK. Therefore, we are interested in the synthesis of fluorescence-labelled covalent inhibitors of FAK as imaging tools.

To maintain the strong affinity to FAK, the structural similarity between the fluorescent probe and the FAK inhibitor is important. 7-Nitrobenz-2-oxa-1,3-diazole (NBD) was selected as a fluorophore because its volume is similar to that of aniline substituent at position 2 of pyrimidine in the FAK inhibitors. Therefore, we introduced the NBD fluorophore to the pyrimidine scaffold through an amino group or an ethylenediamino linker (**Figure 62**).

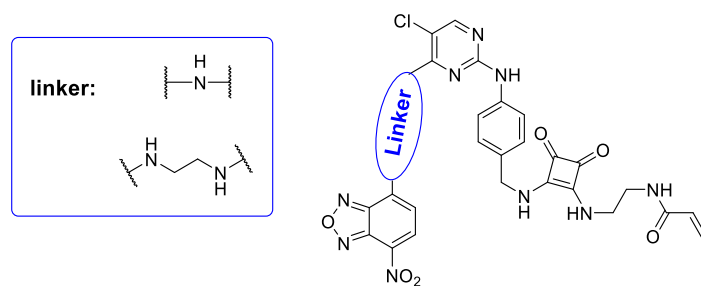


Figure 62: Expected fluorescent covalent inhibitors of FAK.

1.1. Fluorescence and nitrobenzoxadiazole (NBD) fluorophore.

Absorption of a photon can bring a molecule to its excited singlet electronic states (S_1^* , S_2^* ,...). The excited molecule will return to the ground state (S_0) via radiative and non-radiative pathways. One of the radiative pathways is that the molecule in S_1^* state directly returns to the S_0 state via emission of photons. This process is called fluorescence. Another radiative pathway is that the excited molecule undergoes an intersystem crossing (ISC) resulting in conversion to triplet states (T_1), and then the molecule is allowed to emit photons and go back to the ground state, which is referred to as phosphorescence. The excitation and de-excitation processes of fluorescent molecules are conveniently represented by the Perrin-Jablonski diagram (**Figure 63**).

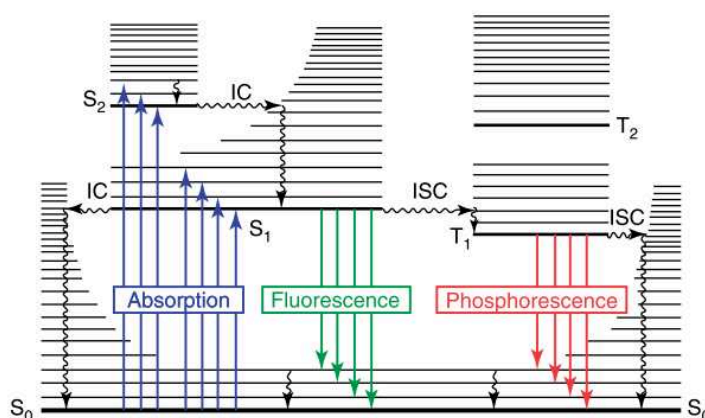


Figure 63: Perrin-Jablonski diagram. IC, internal conversion; ISC, intersystem crossing.²¹⁷

7-Chloro-4-nitrobenzo-2-oxa-1,3-diazole (NBD-Cl) was first reported as a fluorogenic reagent in 1968,²¹⁸ the 7-amino derivatives of NBD are excited by visible light and show strong green fluorescence. For example, 7-anilino-NBD in ethyl acetate (10 μ M) has excitation maximum at 464 nm and emission maximum at 537 nm.²¹⁸ Moreover, the fluorescence of NBD is affected by the polarity of the solvent. The fluorescence decay was observed in polar and protic solvents, whereas high fluorescence activity is retained in nonpolar environments.²¹⁹ This property can amplify the signal-to-noise ratio when the NBD fluorophore is used to visualize proteins in cells. Due to its accessibility of preparation and

highly fluorescent, NBD fluorophore has been widely used in the fluorescent probes.

Hansen and colleagues²²⁰ introduced fluorophore NBD to the FFA2 antagonist via a diamino linker affording a fluorescent tool (**TUG-1609**, **Figure 64**) for investigating the binding of natural and synthetic ligands to the free fatty acid receptor 2 (FFA2). This compound showed favourable spectroscopic properties ($\lambda_{\text{ex}} = 492$ nm and $\lambda_{\text{em}} = 557$ nm in PBS buffer) and high affinity with a K_d of 65 nM. It was demonstrated that this fluorescent tracer was used to determine the thermodynamic and kinetic binding parameters of unlabelled FFA2 ligands.

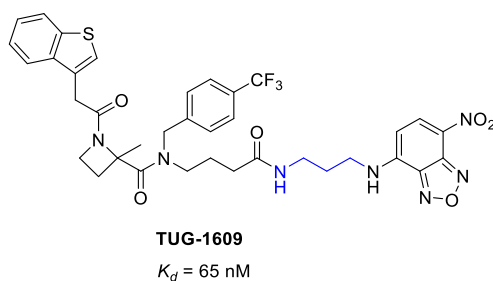


Figure 64: Chemical structure of TUG-1609 and its dissociation constant.

NBD labelled COX-2 inhibitors were also used for the COX-2 imaging in cancer cells. Tietz *et al*²²¹ synthesized 3 conjugates of pyrimidine based COX-2 inhibitor with NBD fluorophore (compound **6**, **8**, **10**, **Figure 65**). These compounds displayed a selective inhibition of COX-2 between COX-1 and COX-2 isomers. In the imaging study, compound **6** effectively stained COX-2 positive HCA-7 colon cancer cells, while HCT-116 cancer cells which don't express COX-2 were not labelled.

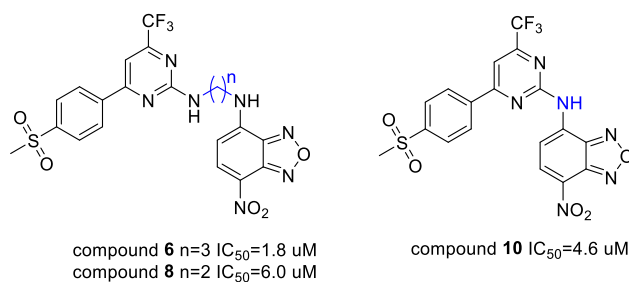
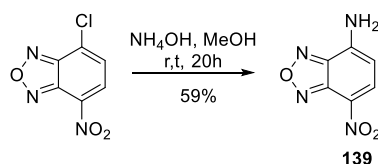


Figure 65: Chemical structures of fluorescent COX-2 inhibitors.

2. Synthesis of Fluorescent compounds

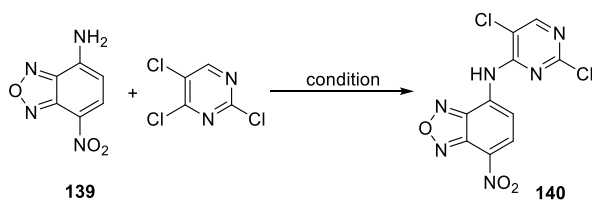
2.1. Synthesis of compounds with a fluorophore connected to pyrimidine through an amino group

In order to introduce the NBD fluorophore to the pyrimidine ring, the 7-chloro-4-nitrobenzo-2-oxa-1,3-diazole (NBD-Cl) was converted to NBD-NH₂ (**139**) through a nucleophilic substitution in MeOH (Scheme 58).²²¹



Scheme 58: Synthesis of NBD-NH₂

For the nucleophilic substitution on 2,4,5-trichloropyrimidine, the previous protocol of refluxing in ethanol in the presence of NaHCO₃ was firstly attempted, but no product was obtained (Entry 1 Scheme 59). Afterwards, increasing reaction temperature up to 140 °C caused decomposition of starting materials (Entry 2 Scheme 59). Changing base to Cs₂CO₃, this reaction neither rendered product (Entry 3 Scheme 59). Because of the electron-deficiency in NBD, this amine had very low nucleophilicity. NaH was used to deprotonate NBD-NH₂, which then reacted with trichloropyrimidine. In THF the desired product **140** was obtained in 20% yield (Entry 4, Scheme 59). The yield slightly increased to 27% when this reaction was conducted at 80 °C in DMF (Entry 5, Scheme 59). We also attempted Pd-catalyzed amination, which led to decomposition (Entry 6, Scheme 59). As microwave irradiation usually efficiently facilitated the reaction, the two reagents in butanol were heated in microwave at 150 °C for 30 min, but no reaction happened (Entry 7 Scheme 59). Heated to 180 °C the starting materials were decomposed (Entry 8 Scheme 59). Therefore, the condition in entry 5 was employed to prepare compound **140**.



Scheme 59: Synthesis of **140**.

Entry	condition	yield
1	NaHCO ₃ , EtOH, reflux, 1 day	SM
2	Et ₃ N, DMF, 140 °C, 16 h	decomposition
3	Cs ₂ CO ₃ , EtOH, reflux, 1 day	SM
4	NaH, THF, reflux, overnight	20%
5	NaH, DMF, 80 °C, overnight	27%
6	Pd ₂ dba ₃ , Xphos, Cs ₂ CO ₃ , 1,4-dioxane, overnight	decomposition
7	DIPEA, n-BuOH, 150°C, 30 min (microwave)	SM
8	DIPEA, n-BuOH, 180°C, 30 min (microwave)	decomposition

The preparation of diarylamino pyrimidine intermediate **145** is shown in **Scheme 60**. With 4-aminosubstituted pyrimidine **140** in hand, the second nucleophilic substitution was achieved in modest yield with aniline **4** (**Figure 66**). However, the deprotection of Fmoc with piperidine failed and caused decomposition. Afterwards, intermediate **142** was prepared from aniline **6** and compound **140**. Like compound **141**, the compound **142** degraded during deprotection process. We supposed that the decomposition was attributed to the basic condition for deprotection. Therefore, we prepared aniline **143** (**Figure 66**) from 4-aminobenzylamine,²²² which could release free amine in acidic condition. Substitution reaction between compounds **140** and **143** afforded intermediate **144** in 71% yield. Then the deprotection was performed in HCl-MeOH solution at 65 °C using the protocol of King.²²³ After stirring overnight the desired product **145** was collected as hydrochloride. In addition,

deprotection of compound **144** using 5% NaOH solution in methanol²²⁴ also led to the degradation of compound **144**, which was in consistence with our hypothesis.

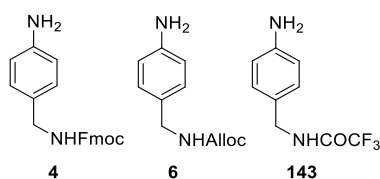
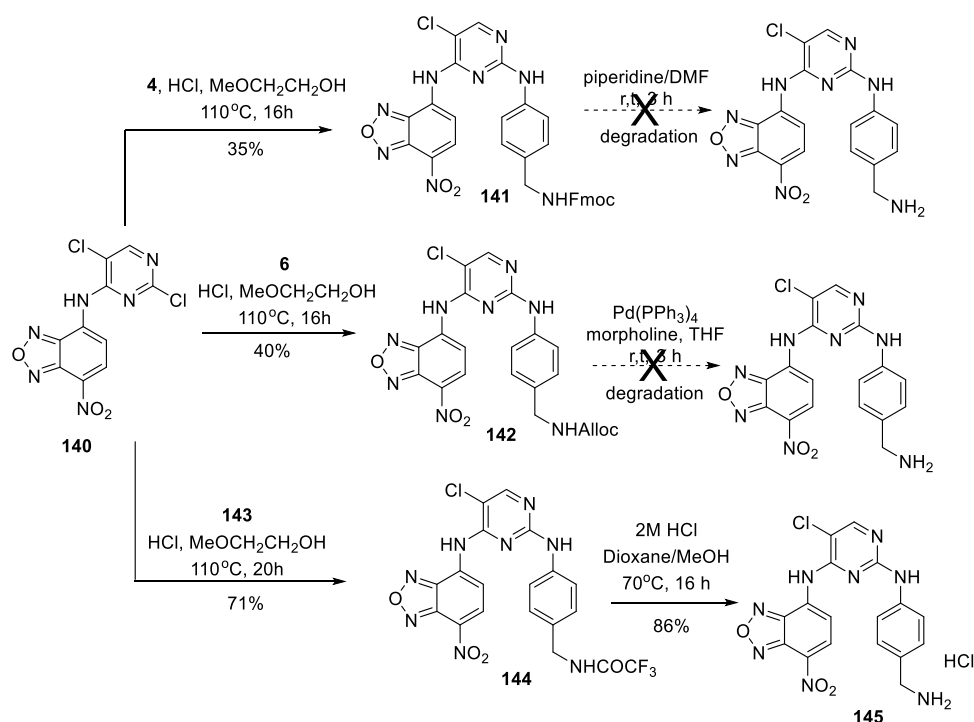
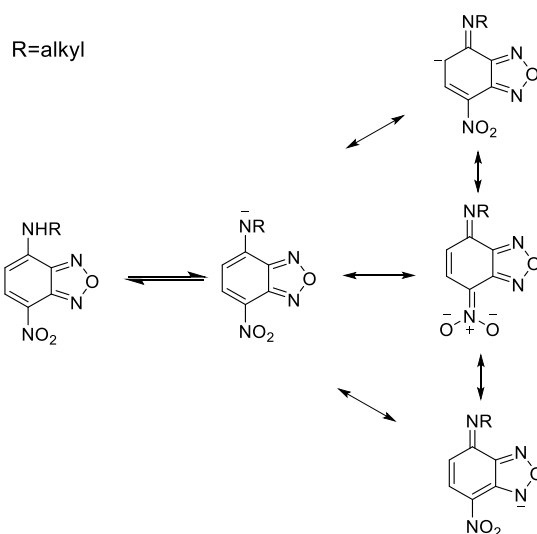


Figure 66: Chemical structures of **4**, **6** and **143**.



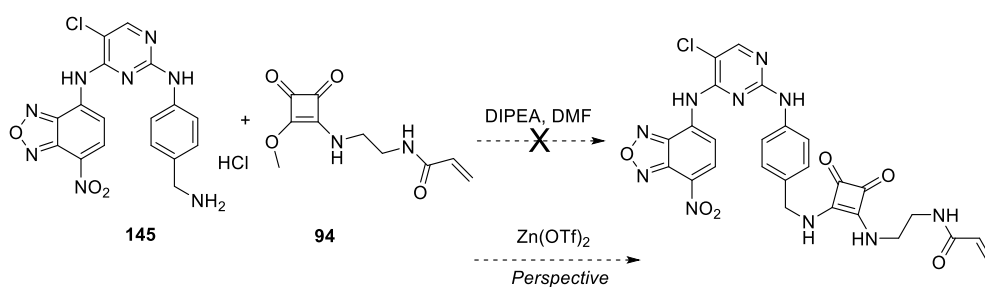
Scheme 60: Synthesis of compound **145**.

It was reported that 7-alkylamino-4-nitrobenzo-2-oxa-1,3-diazoles (NBD-amines) were reasonably strong acids with pK_a values of around 10.²²⁵ The C-N bond at position 7 of NBD-amino derivatives had a partial double bond property with a bond length of 1.336 Å which was apparently shorter than a pure C-N single bond (1.467 Å).²²⁶ In addition, the negative charge on the nitrogen atom of NBD-amine conjugate base could be stabilized by resonance²²⁵ (**Scheme 61**) making it a good leaving group from pyrimidine.



Scheme 61: Resonance of NBD-amines.

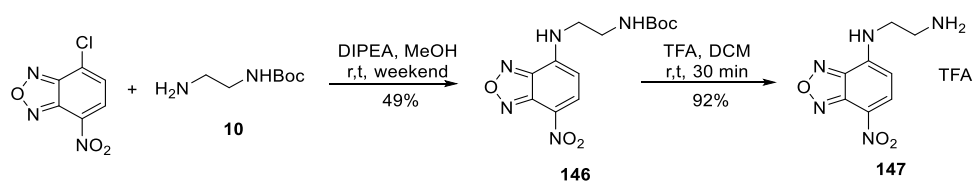
For condensation with the mono-squaramide linker, the synthesis work encountered the same problem. Usually the second substitution of mono-squaramide need base to promote the formation of the product. We attempted it at room temperature with 2 equivalent DIPEA, the starting materials were stable but no product was formed. When the reaction was heated to 80 °C, the base caused decomposition of **145**. For the preparation of the desired compound in a non-basic condition, it might be achieved by activating the squarate. Rostami²²⁷ reported a Lewis-acid catalyzed method for condensation of anilines and squarate ester, which may be an alternative solution. (**Scheme 62**)



Scheme 62: condensation of the linker.

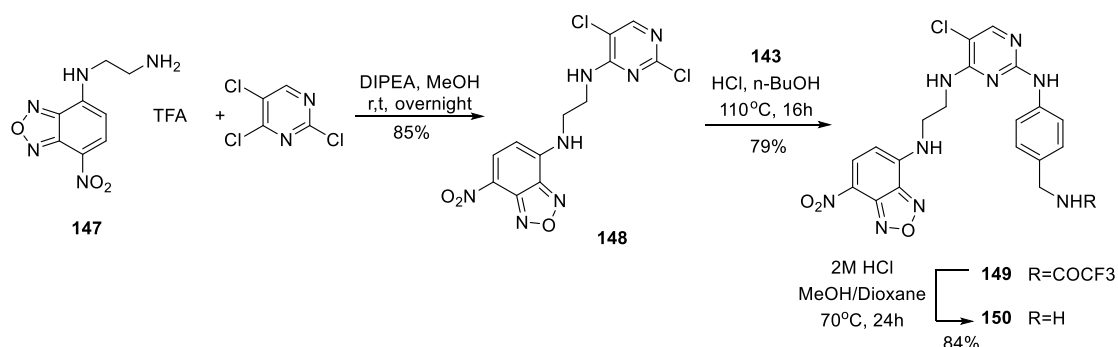
2.2. Synthesis of compounds with a fluorophore connected to pyrimidine through an aliphatic linker

To introduce the linker part, the *N*-boc-ethylenediamine **10** reacted with NBD-Cl in MeOH giving NBD-amine **146** in 49% yield, followed by treatment of TFA offering intermediate **147** as a salt of trifluoroacetate (**Scheme 63**).



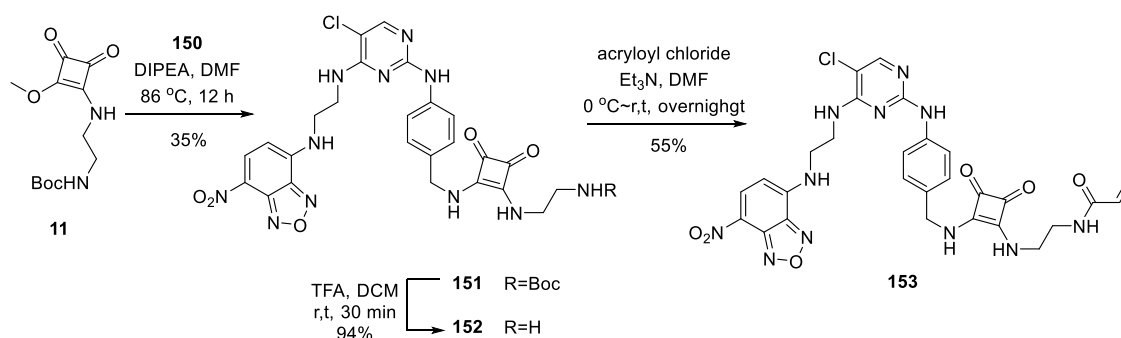
Scheme 63: Synthesis of NBD-amine **147**.

The diaminopyrimidine intermediate **149** was obtained through two aromatic nucleophilic substitutions. In the first substitution, amine **147** substituted the chlorine at position 4 of 2,4,5-trichloropyrimidine under a mild basic condition giving product **148** in 85% yield. In the second substitution, compound **148** and aniline **143** reacted under conditions of refluxing in *n*-BuOH in the presence of HCl to give the compound **149**. The deprotection of **149** with 2 M HCl gave amine **150** as the hydrochloride salt in 84% yield (**Scheme 64**).



Scheme 64: Synthesis of compound **150**.

Then the condensation between compound **150** and linker **11** was catalyzed by DIPEA at 86 °C in DMF giving product **151** in 35% yield. Removal of Boc with TFA gave amine **152**, which was acylated with acryloyl chloride affording the desired compound **153** in 55% yield (Scheme 65).



Scheme 65: Synthesis of fluorescent compound **153**.

3. Fluorescence properties and biological evaluation

3.1. Absorption and fluorescence spectra.

The Absorption and fluorescence spectra of compound **153** were recorded in PBS at 10 μ M, 20 μ M and 40 μ M concentrations (Figure 67). In the PBS buffer, the maximum excitation of compound **153** was observed at 490 nm. Then the fluorescence spectrum was measured with an excitation wavelength of 490 nm. The fluorescent compound **153** exhibited maximum emission at 560 nm with a Stokes shift of 70 nm.

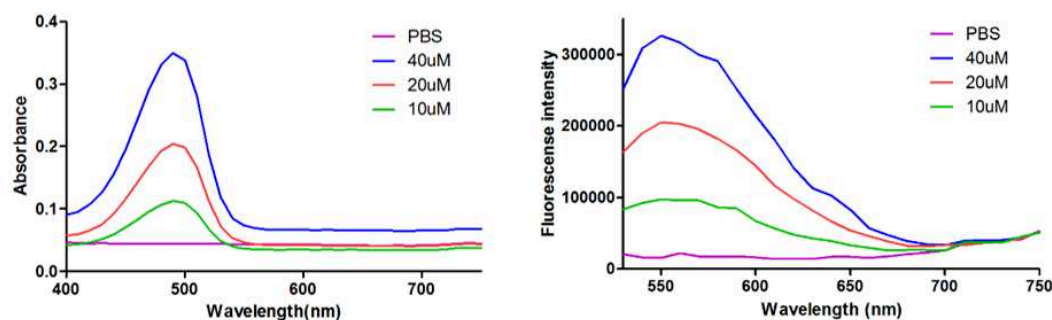
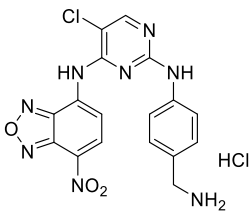
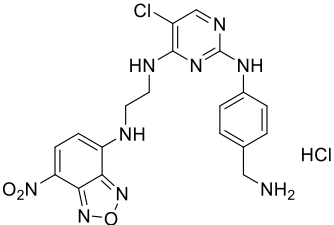
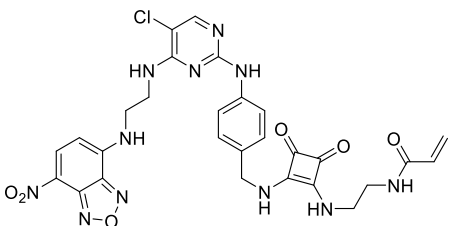


Figure 67: Absorption and fluorescence spectra of compound **153** in PBS.

3.2. In vitro enzymatic activity

The inhibitory activity against FAK of newly synthesized fluorescent compounds was evaluated using the ADP-Glo kinase kit. The results are shown in **Table 14**. The anti-FAK activity of fluorescent inhibitors markedly dropped in comparison with covalent inhibitor **15** ($IC_{50}=0.6$ nM). Compounds **145** and **150** showed modest inhibition of FAK with IC_{50} values of 3.3 μ M and 2.87 μ M, respectively. However, compound **153** displayed very low potency on inhibition of FAK ($IC_{50}=14.27$ μ M).

Table 14: *In vitro* inhibition of FAK.

compound	Inhibition of FAK (IC_{50})
 145	3.3 μ M
 150	2.87 μ M
 153	14.27 μ M

4. Conclusion and perspective

We synthesized 3 compounds with an NBD fluorophore. The small fluorophore NBD was chosen to replace the aniline substituent at position 2 of pyrimidine in covalent FAK inhibitor. The preliminary enzymatic activity evaluation showed that these fluorescent compounds had modest inhibition against FAK, which suggested that in the ATP binding site, the NBD fluorophore is not tolerated. Maybe the fluorescent group can be introduced through a longer linker into the *para*-position of arylamino substituent at the position 2 of pyrimidine.

General conclusion

Targeted therapy is a promising therapeutic strategy to cure cancer, which is one of the most threats to human health. The non-receptor tyrosine kinase FAK attracted our attention due to its important biological function in cancer cells and its overexpression in many cancers, such as glioblastoma, oesophageal carcinoma. This thesis is dedicated to the design and synthesis of selective FAK inhibitors for the development of targeted anticancer drugs. Three parallel projects were described in the manuscript.

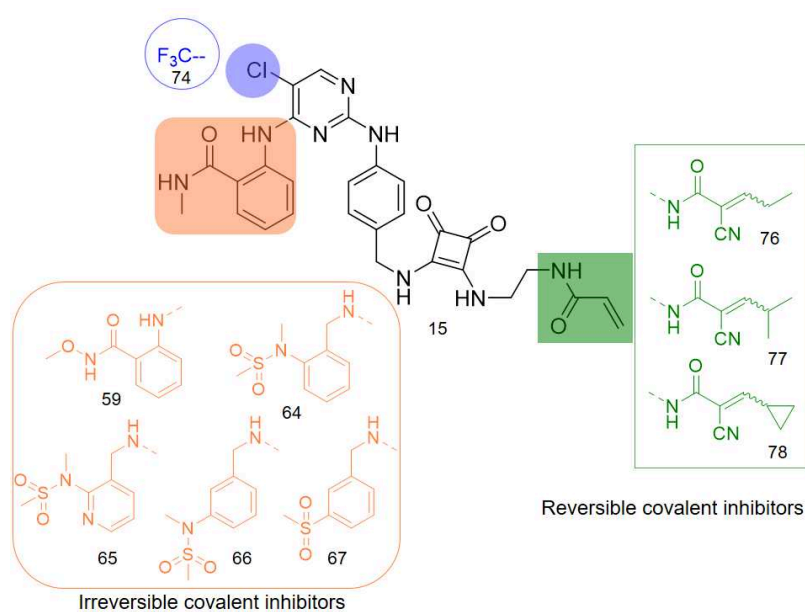
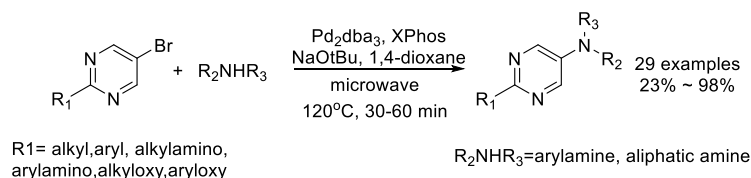


Figure 68: Chemical structures of compound **15** and modified analogues.

In chapter II, I continued the development of covalent inhibitors of FAK (**Figure 68**). The acrylamide electrophile was incorporated to the diaminosubstituted pyrimidine scaffold through squaramide linker or triazole linker. The synthetic route was optimized to permit obtaining the desired compounds in good yield. Through the biochemical evaluation and X-Ray crystallography, the first irreversible covalent inhibitor (**15**) was characterized. Then, in order to improve the kinase selectivity, I conducted the structural modification giving 9 new compounds including irreversible and reversible covalent inhibitors. All the compounds showed excellent inhibitory activity against FAK *in vitro*. In cells a subset of compounds with 2-amino *N*-methyl benzamide group at 2-position of pyrimidine showed good

anticancer activity. On the other hand, 5,7-disubstituted imidazo[1.2-a]pyrimidines were synthesized and the binding mode of the bicyclic structure in the active site was resolved by X-ray crystallography. The distinct binding mode will be used to design new selective FAK inhibitors.



Scheme 66: microwave-assisted amination of 5-bromo-2-substituted pyrimidine.

In chapter III, the efforts were contributed to the microwave-assisted amination of 5-bromo-2-substituted pyrimidine. The 2,5-disubstituted pyrimidine scaffold is an important fragment in the pharmacophore of type II inhibitor of FAK. The synthesis of 2,5-disubstituted pyrimidine is usually hindered because of the low reactivity of 5-halid pyrimidine. In this chapter, I optimized the conditions of Pd-catalysed Buchwald-Hartwig reaction. Under the optimal conditions, 29 derivatives were prepared in good to high yield (**Scheme 66**). Therefore, our microwave-assisted amination of 5-bromo-2-substituted pyrimidine approach will be used to synthesize new type II inhibitors of FAK.

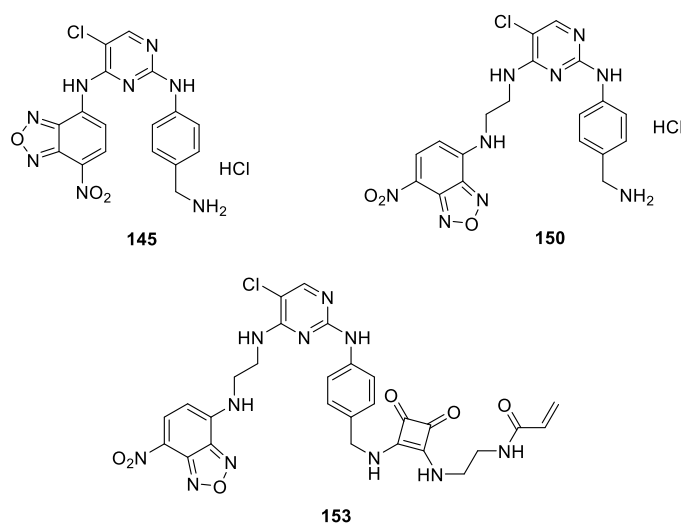


Figure 69: Chemical structures of fluorescent compounds.

In the last chapter, I prepared fluorescent FAK inhibitors, which will be used to visualize FAK in cells and study the FAK kinase cascade. Fluorophore NBD was introduced to the 2-position of pyrimidine-based inhibitors through an amino group or ethylenediamino spacer. Two reversible fluorescent inhibitors (**145**, **150**) and one fluorescent compound bearing an electrophile were successfully prepared (**153**) (**Figure 69**). The preliminary in vitro evaluation showed that these compounds had modest inhibition of FAK.

EXPERIMENTAL PART

General experimental methods: Commercially available reagents and solvents were used without further purification if it's not noted. CH₂Cl₂, DMF, 1,4-dioxane, Et₃N and DIPEA were distilled over calcium hydride, THF was distilled from sodium benzophenone. The reaction was monitored by thin layer chromatography carried out on 60F-254 silica gel plates and visualized under UV light at 254 and 365 nm. Column chromatography was performed with silica gel 60 (Merck 40 – 63 μM) and eluents were given in v/v. The yield refers to isolated and purified products. Chemical shifts (δ) of ¹H and ¹³C NMR are reported in ppm, and the residual proton resonance of the solvents was used as reference. The coupling constants are given in Hz. Multiplets are indicated with following abbreviations, s = singlet, d = doublet, t = triplet, q = quadruplet, bs = broad singlet, m = multiplet. Mass spectra (MS) were recorded with an ion trap mass analyzer under electrospray ionization (ESI) in positive or negative ionization mode detection. High resolution mass spectra (HRMS) were recorded with a TOF mass analyzer under electrospray ionization (ESI) in positive or negative mode detection. Microwave reaction was carried out in Anton Paar monowave 400 reactor.

General procedure A: reduction of nitriles to primary amines

The compounds **33**, **34**, **35**, and **36** were prepared according to the general procedure A.

A PaarTM reaction bottle (250 mL) was charged with a solution of the corresponding benzonitrile in 7 M ammonia in methanol and 10% palladium on carbon (0.1 equivalent). The reaction mixture was vacuumed and charged with hydrogen (50 psi). Then the bottle was shaken on the Paar apparatus for 3 h. The mixture was filtered through a pad of celite and evaporated to give the corresponding amine.

General procedure B: Substitution of chlorine at position 4 of 2,4,5-trichloropyrimidine.

The compounds **38**, **39**, **40**, and **41** were prepared according to the general procedure B.

Appropriate amine (1.1 eq) was added to a solution of 2,4,5-trichloropyrimidine (1 eq) in THF at room temperature, followed by the addition of DIPEA (1.5 eq). The mixture was stirred overnight. The solution was diluted with ethyl acetate and washed with water and brine. The organic phase was dried over MgSO₄ and concentrated under reduced pressure. The residue was purified by silica column chromatography to give the desired product.

General procedure C: Substitution of chlorine at position 2 of 4-aminosubstituted-2,5-dichloropyrimidine with allyl (4-aminobenzyl)carbamate (**6**)

The compounds **45**, **46**, **47**, and **48** were prepared according to the general procedure C.

To a solution of appropriate 4-aminosubstituted 2,5-dichloropyrimidine (1.0 eq) in *n*-BuOH, aniline **6** (1.0 eq) and HCl (4M in 1,4-dioxane, 1.0 eq) were added. The mixture was stirred at 100 °C overnight. After cooled to room temperature, the solution was diluted with DCM, and washed with 1M Na₂CO₃, brine and dried over MgSO₄. The organic phase was concentrated under reduced pressure. The residue was purified through silica gel column chromatography to give the desired product.

General procedure D: removing the Alloc protecting group

The compounds **49**, **50**, **51**, **52**, and **71** were prepared according to the general procedure D.

To a solution of corresponding Alloc protected compounds (1.0 eq) in anhydrous THF or DMF, morpholine (10 eq) and Pd(PPh₃)₄ (0.1 eq ~ 0.5 eq) were added under an inert atmosphere. The mixture was stirred at room temperature for 3 h. After completion of the reaction monitored by TLC, the solvent was concentrated under reduced pressure. The residue was purified through silica gel column chromatography to give the desired product.

General procedure E: removing the Boc protecting group

The compounds **14**, **44**, **58**, **60**, **61**, **62**, **63**, **72**, **91**, and **92** were prepared according to the general procedure E.

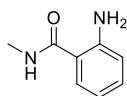
The Boc protected compound (1 eq) was added to a mixed solution of DCM and TFA (v/v =1:1) at room temperature. The mixture was stirred for 30 minutes before removing the solvent *in vacuo*. Then diethyl ether was added to the residue and filtered to give the desired compound as the salt of trifluoroacetate. The compound was directly used without further purification.

General procedure F: condensation of amines with squaramate linker **11**

The compounds **53**, **54**, **55**, **56**, **57**, **89**, and **90** were prepared according to the general procedure F.

To a solution of appropriate amine (1.0 eq) in dry DMF were added squaramate **11** (1.0 eq) and DIPEA (1.0 eq). The mixture was stirred at 75°C overnight. After removal of the solvent, the crude product was purified by flash silica gel chromatography to give the desired product as solid.

2-Amino-*N*-methylbenzamide (**1**)¹⁵⁵

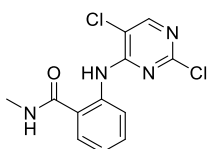


Chemical Formula: C₈H₁₀N₂O
Molecular Weight: 150.18

Methylamine (6 mL, 11.77 mmol, 2 M in THF) was added to a stirred suspension of isatoic anhydride (1.0 g, 5.88 mmol) in water at room temperature and the reaction was left to stir at this temperature for 3 h. The solution was extracted with ethyl acetate 3 times. Combined organic phases were washed with brine and dried over MgSO₄, and the solvent was removed under reduced pressure to give the title compound as off-white solid (0.87 g, 99%).

¹H NMR (250 MHz, Chloroform-*d*) δ 7.37 – 7.27 (m, 1H), 7.22 (ddd, *J* = 8.4, 7.1, 1.5 Hz, 1H), 6.76 – 6.69 (m, 1H), 6.68 – 6.61 (m, 1H), 6.14 (s, 1H), 5.52 (s, 2H), 2.98 (d, *J* = 4.9 Hz, 3H).

2-((2,5-Dichloropyrimidin-4-yl)amino)-*N*-methylbenzamide (**2**)¹⁵⁰

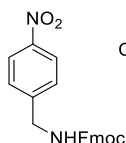


Chemical Formula: C₁₂H₁₀Cl₂N₄O
Molecular Weight: 297.1390

Trichloropyrimidine (282 μL, 2.4 mmol) was added to a stirred solution of **1** (397 mg, 2.64 mmol) and NaHCO₃ (242 mg, 2.9 mmol) in anhydrous EtOH (5 mL) at room temperature. The resulted mixture was heated to reflux and stirred overnight. The reaction mixture was cooled to room temperature and the precipitate was filtered out, washed with water giving the title compound as yellowish solid (660 mg, 93%).

¹H NMR (250 MHz, DMSO-*d*₆) δ 12.24 (s, 1H), 8.96 (d, *J* = 4.7 Hz, 1H), 8.54 (dd, *J* = 8.5, 1.1 Hz, 1H), 8.50 (s, 1H), 7.84 (dd, *J* = 7.8, 1.5 Hz, 1H), 7.69 – 7.54 (m, 1H), 7.31 – 7.16 (m, 1H), 2.82 (d, *J* = 4.5 Hz, 3H).

(9H-Fluoren-9-yl)methyl (4-nitrobenzyl)carbamate (**3**)¹⁵⁶

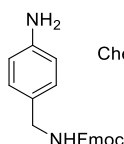


Chemical Formula: C₂₂H₁₈N₂O₄
Molecular Weight: 374.40

To a solution of 4-Nitrobenzylamine hydrochloride (1.0 g, 5.1 mmol) in anhydrous DCM (40 mL), DIPEA (4.4 mL, 25 mmol) and Fmoc-Cl (1.5 g, 5.6 mmol) were added at room temperature. The mixture was stirred for 12 h. Subsequently, the reaction was diluted, washed with water and brine, the DCM layer was dried over MgSO₄, filtered and concentrated *in vacuo*. The crude product was purified by column chromatography (Cyclohexane: EA= 6:1~0:1) to give the desired compound as white solid (1.9 g, 99%).

¹H NMR (250 MHz, Chloroform-*d*) δ 8.21 (d, *J* = 8.3 Hz, 2H), 7.80 (d, *J* = 7.5 Hz, 2H), 7.62 (d, *J* = 7.4 Hz, 2H), 7.41 (m, 6H), 5.19 (s, 1H), 4.57 (d, *J* = 6.4 Hz, 3H), 4.49 (d, *J* = 6.3 Hz, 2H), 4.25 (t, *J* = 6.4 Hz, 1H)

(9H-Fluoren-9-yl)methyl (4-aminobenzyl)carbamate (**4**)¹⁵⁶



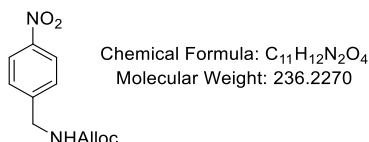
Chemical Formula: C₂₂H₂₀N₂O₂
Molecular Weight: 344.41

To a solution of **3** (490 mg, 1.3 mmol) in MeOH and DCM (250 mL v/v=4:1), Pd/C (5%, 25 mg) was added under H₂ atmosphere, the mixture was stirred at room temperature for 3 h with an H₂ balloon. Subsequently, the mixture was filtered through celite, and the filtrate was concentrated *in vacuo* to give the desired compound as off-white solid (460 mg, 98%).

¹H NMR (250 MHz, Chloroform-*d*) δ 7.79 (dd, *J* = 7.4, 1.2 Hz, 2H), 7.62 (d, *J* = 7.5 Hz, 2H), 7.38 (m, 5H), 7.10 (d, *J* = 8.0 Hz, 2H), 6.77 – 6.56 (m, 2H), 4.98 (s, 1H), 4.47 (d, *J*

= 6.9 Hz, 2H), 4.27 (m, 3H), 3.69 (s, 2H).

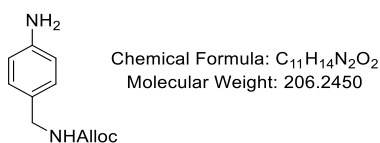
Allyl (4-nitrobenzyl)carbamate (**5**)¹⁵⁷



To a solution of 4-nitrobenzylamine hydrochloride (400 mg, 2.06 mmol) in mixed EtOAc and water (v/v= 1/1) was added K₂CO₃ (853 mg, 6.18 mmol) and allyl chloroformate (264 μL, 2.47 mmol). The resultant biphasic solution was stirred vigorously at room temperature for 16 h. The mixture was extracted with EtOAc 3 times. The combined organic layers were washed with water, brine and dried over MgSO₄. After filtration, the solution was evaporated *in vacuo* to give the title compound as white solid (481 mg, 99%).

¹H NMR (250 MHz, Chloroform-*d*) δ 8.23 (d, *J* = 8.7 Hz, 2H), 7.49 (d, *J* = 8.6 Hz, 2H), 6.04 – 5.88 (m, 1H), 5.43 – 5.21 (m, 3H, NH, =CH₂), 4.64 (d, *J* = 5.7 Hz, 2H), 4.51 (d, *J* = 6.3 Hz, 2H).

Allyl (4-aminobenzyl)carbamate (**6**)¹⁵⁸



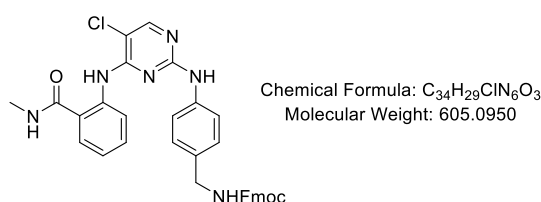
The solution ethanol containing **5** (478 mg, 2.02 mmol) and tin (II) chloride dihydrate (3.58 g, 16 mmol) was refluxed for 2 h. After cooling to room temperature, the solution was poured to 100 mL water. Then 2 M NaOH solution was added to adjust pH to 14 to get a milk-like solution. After filtration through celite, the filtrate was extracted with EtOAc 3 times. The organic layer was washed with water, brine and dried over MgSO₄.

The solvent was filtered and concentrated under reduced pressure to give the crude product. The crude product was purified through a flash column (eluent: Cy/EA= 4/1 ~ 1/1) to give the title compound as oil (353 mg, 85%).

^1H NMR (500 MHz, Chloroform-*d*) δ 7.07 (d, J = 7.9 Hz, 2H), 6.64 (d, J = 8.4 Hz, 2H), 5.92 (td, J = 10.8, 5.2 Hz, 1H), 5.30 (dd, J = 17.2, 1.6 Hz, 1H), 5.20 (dd, J = 10.5, 1.5 Hz, 1H), 4.94 (s, 1H), 4.58 (d, J = 4.8 Hz, 2H), 4.24 (d, J = 5.8 Hz, 2H), 3.66 (s, 2H).

^{13}C NMR (126 MHz, Chloroform-*d*) δ 156.3, 146.0, 133.1, 129.0, 128.4, 117.7, 115.3, 65.7, 44.9.

(9*H*-Fluoren-9-yl)methyl (4-((5-chloro-4-((2-(methylcarbamoyl)phenyl)amino)pyrimidin-2-yl)amino)benzyl)carbamate (**7**)

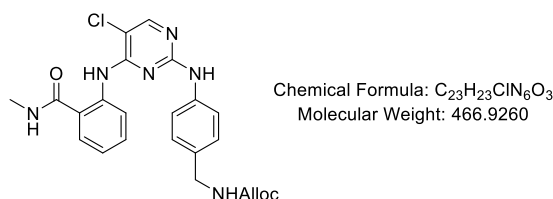


HCl solution (50 μL , 4 M in 1,4-dioxane) was added to a stirred suspension of **4** (345 mg, 1.0 mmol) and **2** (298 mg, 1.0 mmol) in *n*-BuOH (20 mL). The mixture was heated to 120°C and stirred at this temperature for 20 h before the mixture was concentrated *in vacuo*. The residual material was purified by column chromatography (DCM: MeOH, 50:1~10:1) to give the desired product as off-white solid (316 mg, 52%).

^1H NMR (250 MHz, DMSO-*d*₆) δ 11.65 (s, 1H), 9.48 (s, 1H), 8.77 (dd, J = 9.7, 6.7 Hz, 2H), 8.23 (s, 1H), 7.96 – 7.67 (m, 6H), 7.60 (d, J = 8.2 Hz, 2H), 7.44 (dq, J = 17.5, 9.8, 8.7 Hz, 4H), 7.31 (d, J = 7.3 Hz, 2H), 7.12 (dd, J = 16.6, 8.0 Hz, 3H), 4.36 (d, J = 6.8 Hz, 2H), 4.24 (t, J = 6.8 Hz, 1H), 4.16 (d, J = 6.1 Hz, 1H), 2.82 (d, J = 4.4 Hz, 3H).

HRMS: (ESI) m/z [M+Na]⁺, C₃₄H₂₉ClN₆NaO₃, calcul. 627.1887, found, 627.1867.

Allyl (4-((5-chloro-4-((2-(methylcarbamoyl)phenyl)amino)pyrimidin-2-yl)amino)benzyl) carbamate (**8**)



To a solution of **2** (600 mg, 2.02 mmol) in *n*-BuOH, **6** (416 mg, 2.02 mmol) and HCl (505 μ L, 4 M in 1,4-dioxane) were added. The mixtures were heated at 120 °C overnight. After cooled to room temperature, the solution was diluted with DCM, and washed with 1M K₂CO₃, brine and dried over MgSO₄. The organic phase was concentrated under reduced pressure. The residue was purified through silica gel column chromatography to give the desired compound as white solid (419 mg, 44%).

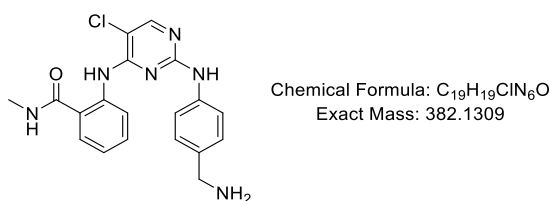
¹H NMR (500 MHz, DMSO-*d*₆) δ 11.60 (s, 1H), 9.42 (s, 1H), 8.79 – 8.68 (m, 2H), 8.21 (s, 1H), 7.76 (dd, *J* = 8.0, 1.6 Hz, 1H), 7.70 (t, *J* = 6.2 Hz, 1H), 7.62 – 7.57 (m, 2H), 7.48 (ddd, *J* = 8.7, 7.3, 1.6 Hz, 1H), 7.19 – 7.10 (m, 3H), 5.93 (ddt, *J* = 17.3, 10.6, 5.3 Hz, 1H), 5.34 – 5.13 (m, 2H), 4.50 (dt, *J* = 5.4, 1.6 Hz, 2H), 4.15 (d, *J* = 6.2 Hz, 2H), 2.81 (d, *J* = 4.5 Hz, 3H).

¹³C NMR (126 MHz, DMSO-*d*₆) δ 168.9, 157.7, 156.1, 154.9, 154.6, 139.3, 138.9, 133.8, 133.1, 131.4, 127.9, 127.2, 121.9, 121.4, 120.7, 119.6, 116.8, 105.0, 64.3, 43.5, 26.3.

HRMS (ESI) *m/z* calcd. for C₂₃H₂₄O₃N₆Cl [M+H]⁺: 467.15984, found:467.16043.

Melting point: 229 °C.

2-((2-((4-(Aminomethyl)phenyl)amino)-5-chloropyrimidin-4-yl)amino)-*N*-methylbenzamide (**9**)



Synthetic route A: A solution of compound **7** (570 mg, 1.06 mmol) in DMF and piperidine (12 mL, v/v=5/1) was stirred at room temperature for 2 h. The solution was concentrated *in vacuo*. Ethyl ether was added to the resulted syrup and filtered to give the crude product as off-white solid (214 mg, 53%). The crude product was used directly for the next step without further purification.

Synthetic route B: To a solution of **8** (836 mg, 1.79 mmol) in anhydrous THF, morpholine (3 mL, 34.8 mmol) and Pd(PPh₃)₄ (103 mg, 0.09 mmol) were added under an inert atmosphere. The mixture was stirred at room temperature without light for 3h. After the completion monitored with TLC, the solvent was concentrated under reduced pressure. The residue was purified through silica gel column chromatography (eluent: DCM/MeOH, 10:1+1% NH₄OH) to give the desired product as white solid (580 mg, 85%).

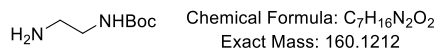
¹H NMR (250 MHz, DMSO-*d*₆) δ 11.61 (s, 1H), 9.43 (s, 1H), 8.77 (d, J = 7.9 Hz, 2H), 8.22 (s, 1H), 7.77 (d, J = 7.9 Hz, 1H), 7.62 (d, J = 8.2 Hz, 2H), 7.52 (t, J = 7.9 Hz, 1H), 7.26 (d, J = 8.2 Hz, 2H), 7.16 (t, J = 7.4 Hz, 1H), 3.73 (s, 2H), 2.82 (d, J = 4.2 Hz, 3H).

¹³C NMR (126 MHz, DMSO-*d*₆) δ 168.9, 157.7, 154.9, 154.6, 139.3, 138.6, 136.5, 131.4, 127.4, 127.2, 121.9, 121.4, 120.7, 119.5, 104.9, 44.9, 26.3.

HRMS (ESI) *m/z* calcd for C₁₉H₂₀ClN₆O: 383.1387, found: 383.1380.

Melting point: 205 °C.

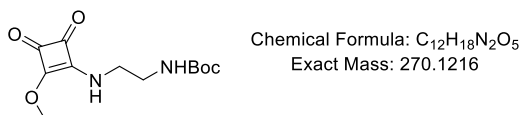
N-Boc-ethylenediamine (**10**)²²⁸



A solution of di-*tert*-butyl dicarbonate (1.06 g 4.7 mmol) in DCM was dropped to the flask containing ethylenediamine (2 g, 32.9 mmol) in DCM with stirring at room temperature. The mixture was stirred for 48 h followed by filtration to remove the white precipitate. The filtrate was concentrated. Subsequently, 2 mL of water was added to the residue and filtered. The water solution was saturated by NaCl and extracted with DCM (5 times). The combined organic phase was dried over MgSO₄. After filtration, the solution was concentrated to give the titled compound as a colourless oil (581 mg, 91%).

¹H NMR (250 MHz, Chloroform-*d*) δ 4.86 (br, 1H), 3.16 (q, *J* = 5.9 Hz, 2H), 2.79 (t, *J* = 5.9 Hz, 2H), 1.44 (s, 9H), 1.39 (s, 2H).

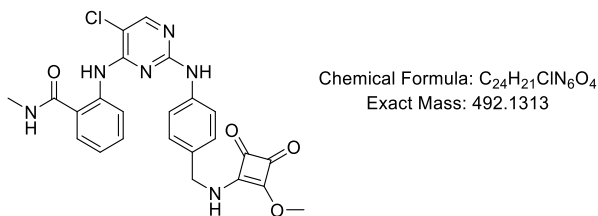
tert-Butyl (2-((2-methoxy-3,4-dioxocyclobut-1-en-1-yl)amino)ethyl)carbamate (**11**)



To a solution of dimethylsquarate (1278 mg, 9.06 mmol) in MeOH was added the solution of **1** (1320 mg, 8.23 mmol) in MeOH dropwise. After stirring at room temperature overnight, the mixture was concentrated and purified by silica column chromatography (DCM/MeOH= 50/1~30/1) to give the title compound as white solid (1451 mg, 65%).

¹H NMR (250 MHz, Chloroform-*d*) δ 4.90 (s, 1H), 4.39 (s, 3H), 3.76 (s, 1H), 3.54(s, 1H), 3.35 (q, *J* = 5.8 Hz, 2H), 1.43 (s, 9H).

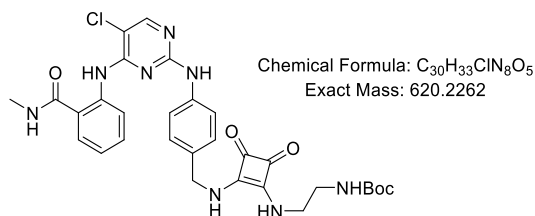
2-((5-Chloro-2-((4-(((2-methoxy-3,4-dioxocyclobut-1-en-1-yl)amino)methyl)phenyl)amino)pyrimidin-4-yl)amino)-*N*-methylbenzamide (**12**)



Compound **9** (200 mg, 0.52 mmol) was dissolved in dry DMF (3 mL) and dropped to a solution of dimethyl squarate (91 mg, 0.63 mmol) and DIPEA (0.1 mL, 0.52 mmol) in dry DMF (5 mL) at room temperature. The mixture was left to stir for 24 h and the solution was removed *in vacuo*. Subsequently, DCM was added to the residue to give the product as a pale solid (207 mg, 81%). The crude product was used directly for the next step without further purification.

¹H NMR (250 MHz, DMSO-*d*₆) δ 11.62 (s, 1H), 9.51 (s, 1H), 8.74 (d, *J* = 11.2 Hz, 2H), 8.23 (s, 1H), 7.77 (d, *J* = 7.8 Hz, 1H), 7.65 (d, *J* = 8.1 Hz, 2H), 7.52 – 7.43 (m, 1H), 7.27 – 7.07 (m, 3H), 4.68 – 4.37 (m, 2H), 4.32 (d, *J* = 10.1 Hz, 3H), 2.82 (d, *J* = 4.4 Hz, 3H).

tert-Butyl (2-((2-((4-((5-chloro-4-((2-(methylcarbamoyl)phenyl)amino)pyrimidin-2-yl)amino) benzyl)amino)-3,4-dioxocyclobut-1-en-1-yl)amino)ethyl)carbamate (**13**)



Route 1. A solution of compound **12** (91 mg, 0.81 mmol), **10** (58 mg, 0.36 mmol) and DIPEA (43 μL, 0.2 mmol) in dry DMF (2 mL) was stirred at 70 °C for 8 h. Subsequently, the reaction mixture was concentrated *in vacuo* to afford the crude product which was

purified by column chromatography (DCM: MeOH=20: 1). The desired compound was obtained as a white solid (83 mg, 72%).

Route 2. To a solution of **9** (580 mg, 1.51 mmol) in dry DMF were added compound **11** (409 mg, 1.51 mmol) and DIPEA (256 μ M, 1.51 mmol). The mixture was stirred at 75°C for overnight. After removal of the solvent, the crude product was purified by flash silica gel chromatography to give the desired product as white solid (724 mg, 77%).

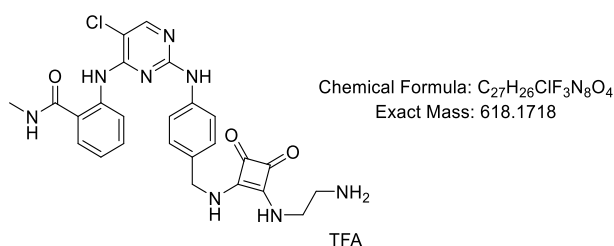
^1H NMR (250 MHz, DMSO- d_6) δ 11.62 (s, 1H), 9.51 (s, 1H), 8.74 (d, J = 8.3 Hz, 2H), 8.23 (s, 1H), 7.77 (d, J = 7.8 Hz, 1H), 7.66 (d, J = 8.2 Hz, 2H), 7.47 (t, J = 7.9 Hz, 1H), 7.26 (d, J = 8.2 Hz, 2H), 7.14 (t, J = 7.5 Hz, 1H), 6.91 (s, 1H), 4.66 (d, J = 5.9 Hz, 2H), 3.52 (s, 2H), 3.10 (d, J = 6.1 Hz, 2H), 2.82 (d, J = 4.3 Hz, 3H), 1.36 (s, 9H).

^{13}C NMR (126 MHz, DMSO- d_6) δ 182.6, 182.4, 168.8, 162.2, 157.6, 155.7, 154.9, 154.5, 139.5, 139.2, 132.0, 131.3, 127.9, 127.8, 121.9, 121.4, 120.7, 119.8, 105.1, 77.8, 46.5, 43.2, 41.1, 28.1, 26.2.

HRMS (ESI) m/z calcd. for $\text{C}_{30}\text{H}_{33}\text{ClN}_8\text{O}_5$ $[\text{M}+\text{H}]^+$: 621.2341, found: 621.2308.

Melting point: 226 °C.

2-((2-((4-(((2-((2-Aminoethyl)amino)-3,4-dioxocyclobut-1-en-1-yl)amino)methyl)phenyl)amino)-5-chloropyrimidin-4-yl)amino)-N-methylbenzamide trifluoroacetate salt
(14)



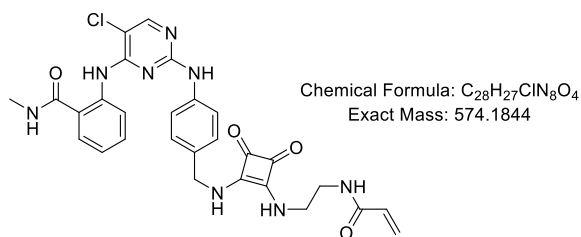
Following the general procedure E, from compound **13** (716 mg, 1.15 mmol), the title compound was obtained as solid (983 mg, quant).

^1H NMR (250 MHz, $\text{DMSO-}d_6$) δ 11.67 (s, 1H), 9.55 (s, 1H), 8.75 (d, $J = 10.6$ Hz, 2H), 8.24 (s, 1H), 7.87 (s, 2H), 7.77 (d, $J = 7.8$ Hz, 1H), 7.66 (d, $J = 8.3$ Hz, 3H), 7.48 (t, $J = 7.8$ Hz, 1H), 7.26 (d, $J = 8.1$ Hz, 2H), 7.14 (t, $J = 7.6$ Hz, 1H), 3.72 (d, $J = 6.9$ Hz, 2H), 3.03 (d, $J = 6.1$ Hz, 2H), 2.82 (d, $J = 4.4$ Hz, 3H).

^{13}C NMR (126 MHz, $\text{DMSO-}d_6$) δ 182.8, 182.3, 168.7, 168.2, 155.7, 155.6, 155.4, 150.8, 138.5, 138.2, 133.5, 131.5, 128.0, 127.9, 122.8, 121.8, 121.2, 120.9, 105.3, 46.4, 40.8, 39.3, 26.3.

HRMS (ESI) m/z calcd. for $\text{C}_{25}\text{H}_{26}\text{ClN}_8\text{O}_3$ $[\text{M}+\text{H}]^+$: 521.1816, found: 521.1803.

2-((2-((4-(((2-((2-Acrylamidoethyl)amino)-3,4-dioxocyclobut-1-en-1-yl)amino)methyl)phenyl) amino)-5-chloropyrimidin-4-yl)amino)-*N*-methylbenzamide (**15**)



To an ice-cooled solution of compound **14** (40 mg, 0.063 mmol) in dry DMF (0.8 mL) was added Et_3N (23 μL , 0.157 mmol) and acryloyl chloride (8 μL , 0.095 mmol). The mixture was stirred at room temperature for 12 h. The solvent was removed *in vacuo* and the crude product was purified by column chromatography (DCM:MeOH=20:1~10:1) to give the desired compound as white solid (20 mg, 55%).

^1H NMR (250 MHz, $\text{DMSO-}d_6$) δ 11.62 (s, 1H), 9.50 (s, 1H), 8.74 (d, $J = 8.9$ Hz, 2H), 8.28 (s, 1H), 8.23 (s, 1H), 7.76 (d, $J = 7.8$ Hz, 1H), 7.66 (d, $J = 8.2$ Hz, 2H), 7.47 (t, $J = 7.9$ Hz, 1H), 7.25 (d, $J = 8.3$ Hz, 2H), 7.14 (t, $J = 7.6$ Hz, 1H), 6.30 – 6.00 (m, 2H), 5.59 (dd, $J = 9.5, 2.8$ Hz, 1H), 4.67 (s, 2H), 3.58 (s, 2H), 2.82 (d, $J = 4.5$ Hz, 3H), 2.62 (s, 2H).

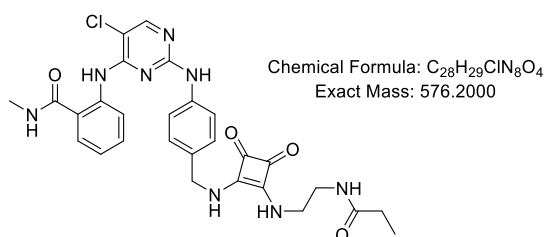
^{13}C NMR (126 MHz, $\text{DMSO-}d_6$) δ 182.7, 182.5, 168.9, 165.0, 157.6, 155.0, 154.6, 139.5, 139.2, 131.6, 131.4, 127.9, 127.8, 125.3, 121.9, 121.4, 120.8, 119.8, 105.1, 46.5, 42.8,

40.1, 26.3.

HRMS (ESI) m/z calcd. for $C_{28}H_{28}ClN_8O_4$ $[M+H]^+$: 575.1922, found: 575.1910.

Melting point: 258 °C.

2-((5-Chloro-2-((4-(((3,4-dioxo-2-((2-propionamidoethyl)amino)cyclobut-1-en-1-yl)amino) methyl)phenyl)amino)pyrimidin-4-yl)amino)-*N*-methylbenzamide (**16**)



To a solution of compound **14** (50 mg, 0.079 mmol) in dry DMF (1 mL) was added DIPEA (83 μ L, 0.23 mmol) and propionyl chloride (14 μ L, 0.157 mmol). The mixture was stirred at room temperature for 5 h. The solvent was removed *in vacuo* and the crude product was purified by column chromatography (DCM:MeOH=20:1~10:1) to give the desired compound as white solid (23 mg, 51%).

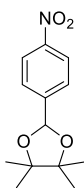
1H NMR (500 MHz, Methanol- d_4) δ 8.58 (d, J = 8.4 Hz, 1H), 7.95 (s, 1H), 7.81 (s, 1H), 7.54 (dd, J = 7.9, 1.5 Hz, 1H), 7.48 (d, J = 8.0 Hz, 2H), 7.36 (td, J = 7.4, 1.6 Hz, 1H), 7.17 (d, J = 8.1 Hz, 2H), 7.00 (td, J = 7.6, 1.1 Hz, 1H), 6.14 – 6.09 (m, 2H), 5.55 (dd, J = 7.8, 4.2 Hz, 1H), 4.34 (t, J = 7.0 Hz, 2H), 3.81 (s, 2H), 3.71 (s, 2H), 3.18 (t, J = 6.7 Hz, 2H), 2.82 (s, 3H), 2.03 (p, J = 6.9 Hz, 2H).

^{13}C NMR (500 MHz, Methanol- d_4) δ 171.7, 168.4, 159.4, 157.1, 155.3, 140.8, 140.4, 132.8, 131.9, 130.1, 128.8, 126.8, 124.8, 123.6, 123.5, 123.2, 121.4, 107.1, 53.2, 49.6, 43.9, 37.5, 31.1, 26.9.

HRMS (ESI) m/z calcd. for $C_{28}H_{29}ClN_8NaO_4$ $[M+H]^+$: 599.1898, found: 599.1908.

Melting point: > 260°C.

4,4,5,5-Tetramethyl-2-(4-nitrophenyl)-1,3-dioxolane (**17**)¹⁶¹

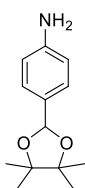


Chemical Formula: C₁₃H₁₇NO₄
Exact Mass: 251.1158

A mixture of 4-nitrobenzaldehyde (1.51 g, 10.0 mmol) and pinacol (2.36 g, 20.0 mmol) and *p*-toluenesulfonic acid (57 mg, 0.3 mmol) was refluxed in dry toluene (30 mL) for 4 h. After cooling to room temperature, a solution of NaOH (80 mg, 2.0 mmol) in ethanol (2 mL) was added to the mixture and stirred for 30 min. The suspension was filtered and the residue was washed with toluene. The filtrate was washed with brine, dried over MgSO₄ and finally concentrated *in vacuo* to give the desired compound as solid (2.23 g, 92%).

¹H NMR (250 MHz, Chloroform-*d*) δ 8.25 (d, *J* = 8.8 Hz, 2H), 7.69 (d, *J* = 8.6 Hz, 2H), 6.04 (s, 1H), 1.36 (s, 6H), 1.25 (s, 6H).

4-(4,4,5,5-Tetramethyl-1,3-dioxolan-2-yl)aniline (**18**)¹⁶¹

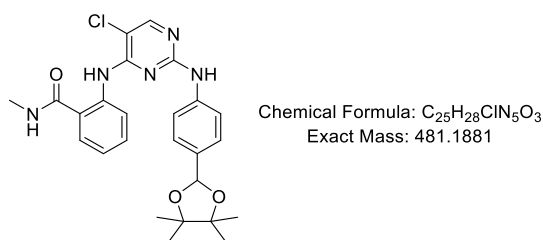


Chemical Formula: C₁₃H₁₉NO₂
Exact Mass: 221.1416

A mixture of **17** (1.0 g, 3.98 mmol) and 10% Pd/C in degassed THF (30 mL) under a hydrogen atmosphere was stirred for 7 h. The mixture was filtrated through a pad of celite and the filtrate was concentrated *in vacuo* to give the desired compound as white solid (870 mg, 99%).

¹H NMR (250 MHz, Chloroform-*d*) δ 7.30 (d, *J* = 8.3 Hz, 2H), 6.69 (d, *J* = 8.4 Hz, 2H), 5.92 (s, 1H), 3.75 (s, 2H), 1.33 (s, 6H), 1.31 (s, 7H).

2-((5-Chloro-2-((4-(4,4,5,5-tetramethyl-1,3-dioxolan-2-yl)phenyl)amino)pyrimidin-4-yl)amino)-N-methylbenzimidamide (**19**)

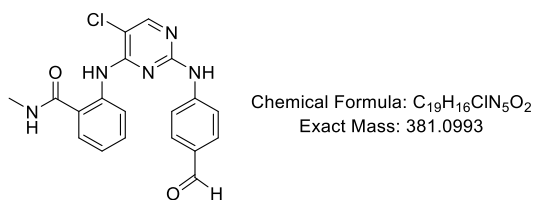


A sealed tube was charged with **2** (272 mg, 1.23 mmol), **18** (36.6 mg, 1.23 mmol), Pd₂(dba)₃ (23 mg, 2 mol%), XPhos (47 mg, 8 mol%) and Cs₂CO₃ (400 mg, 1.23 mmol) and degassed 1,4-dioxane (7 mL) under N₂ atmosphere. The tube was evacuated and backfilled 3 times with argon and stirred at room temperature for 10 min. Then the mixture was heated at 100 °C for 20 h. After cooling to room temperature, the reaction mixture was diluted and filtered through a celite pad and concentrated *in vacuo*. The crude residues were purified by column chromatography (DCM:MeOH=100:1) to give the title compound as yellow solid (337 mg, 57%).

¹H NMR (500 MHz, DMSO-*d*₆) δ 11.62 (s, 1H), 9.55 (s, 1H), 8.81 – 8.72 (m, 2H), 8.24 (s, 1H), 7.76 (dd, *J* = 8.0, 1.6 Hz, 1H), 7.70 – 7.64 (m, 2H), 7.49 (td, *J* = 7.2, 1.6 Hz, 1H), 7.37 – 7.30 (m, 2H), 7.16 (td, *J* = 7.6, 1.2 Hz, 1H), 5.86 (s, 1H), 2.82 (d, *J* = 4.5 Hz, 3H), 1.24 (d, *J* = 17.2 Hz, 12H).

¹³C NMR (126 MHz, DMSO-*d*₆) δ 168.9, 157.6, 155.0, 154.5, 140.5, 139.2, 132.8, 131.4, 127.9, 126.6, 122.0, 121.5, 120.8, 119.0, 105.3, 99.1, 81.9, 26.3, 24.2, 22.0.

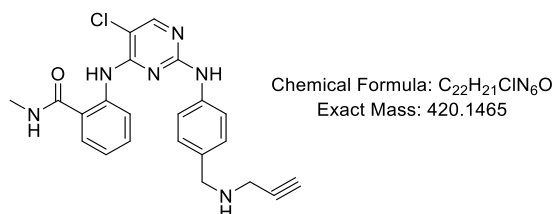
2-((5-Chloro-2-((4-formylphenyl)amino)pyrimidin-4-yl)amino)-*N*-methylbenzamide (**20**)



Compound **19** was treated with 10% HCl solution in THF (20 mL) overnight at room temperature. Then the solution of NaOH (2 M) was added till pH=14. Then the mixture was filtered to give the title compound as a yellow solid (228 mg, 86%).

¹H NMR (250 MHz, DMSO-*d*₆) δ 11.66 (s, 1H), 10.04 (s, 1H), 9.85 (s, 1H), 8.79 (s, 1H), 8.71 (d, *J* = 8.3 Hz, 1H), 8.34 (s, 1H), 7.95 (d, *J* = 8.5 Hz, 2H), 7.81 (d, *J* = 7.8 Hz, 3H), 7.58 (t, *J* = 7.9 Hz, 1H), 7.21 (t, *J* = 7.6 Hz, 1H), 2.82 (d, *J* = 4.4 Hz, 3H).

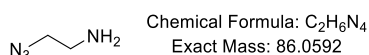
2-((5-Chloro-2-((4-((prop-2-yn-1-ylamino)methyl)phenyl)amino)pyrimidin-4-yl)amino)-*N*-methylbenzamide (**21**)



A solution of compound **20** (110 mg, 0.29 mmol), propargylamine (57 μL, 0.87 mmol) and a drop of AcOH in distilled DMF (4 mL) was stirred at room temperature under Argon atmosphere for 8 h. Then NaBH₃CN (91 mg, 1.45 mmol) was added. The stirring was maintained for 12 h. After quenched with H₂O, the mixture was extracted with DCM 3 times. The combined organic phase was dried over MgSO₄, filtered and concentrated *in vacuo*. The crude residue was purified by column chromatography (DCM: MeOH = 50:1~20:1) to give the title compound as yellowish solid (30 mg, 25%).

^1H NMR (250 MHz, DMSO- d_6) δ 11.59 (s, 1H), 9.43 (s, 1H), 8.81 – 8.69 (m, 2H), 8.22 (s, 1H), 7.82 – 7.70 (m, 1H), 7.60 (d, J = 8.3 Hz, 2H), 7.50 (t, J = 7.9 Hz, 1H), 7.28 – 7.08 (m, 3H), 3.70 (s, 2H), 3.58 (s, 1H), 3.28 (d, J = 2.4 Hz, 3H), 3.10 (t, J = 2.4 Hz, 1H), 2.82 (d, J = 4.4 Hz, 3H).

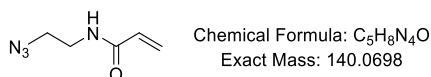
2-Azidoethan-1-amine (**22**)¹⁶⁴



Sodium azide (1.8 g, 27.7 mmol) was added to a solution of 2-bromoethan-1-amine hydrobromide (2.5 g, 12.2 mmol) in water (30 mL). The mixture was stirred for 20 h at 80°C. Subsequently, NaOH solution (2 M, 15 mL) was added and the mixture aqueous solution was saturated with NaCl and extracted with DCM for 3 times. The combined DCM layers were dried over MgSO₄, filtered, and concentrated *in vacuo* to give the title compound as oil (1.0 g, 96%).

^1H NMR (250 MHz, Chloroform- d) δ 3.36 (t, J = 5.7 Hz, 2H), 2.94 – 2.81 (m, 2H), 1.34 (s, 2H).

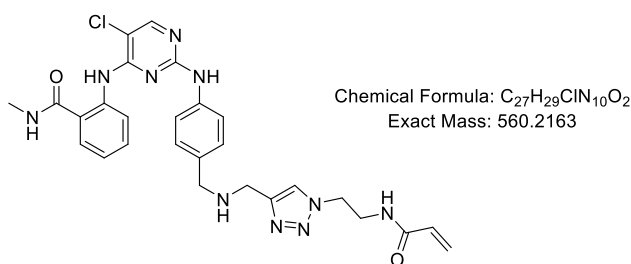
N-(2-Azidoethyl)acrylamide (**23**)



To a solution of **22** (340 mg, 3.95 mmol) in anhydrous DCM (10 mL) was added DIPEA (697 μL , 4.0 mmol) and acryloyl chloride (334 μL , 3.95 mmol) dropwise. The mixture was stirred at room temperature for 14 h and quenched with H₂O. The mixture was washed with saturated brine. The organic phase was dried over MgSO₄, filtered and concentrated *in vacuo*. The crude product was purified by column chromatography (Cyclohexane: EA= 4:1) to give the title compound as light yellow oil (255 mg, 48%).

^1H NMR (250 MHz, Chloroform-*d*) δ 6.34 (dd, $J = 17.0, 1.5$ Hz, 1H), 6.13 (dd, $J = 17.0, 10.1$ Hz, 1H), 5.93 (s, 1H), 5.72 (dd, $J = 10.2, 1.5$ Hz, 1H), 3.57 – 3.45 (m, 4H).

2-((2-((4-(((1-(2-Acrylamidoethyl)-1*H*-1,2,3-triazol-4-yl)methyl)amino)methyl)phenyl)amino)-5-chloropyrimidin-4-yl)amino)-*N*-methylbenzamide (**24**)

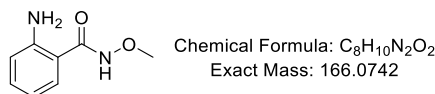


To a solution of compound **21** (30 mg, 0.07 mmol) and compound **23** (19 mg, 0.11 mmol) in DMF and water (1.5 mL, v/v=3:2) was added CuSO_4 (3.4 mg, 0.02 mmol) and sodium ascorbate (8.5 mg, 0.04 mmol). The mixture was stirred at room temperature for 24 h. The heterogeneous mixture was concentrated *in vacuo* and purified by column chromatography (DCM: MeOH = 20:1~10:1) to give the title compound as white solid (13 mg, 33%).

^1H NMR (250 MHz, DMSO-*d*₆) δ 11.59 (s, 1H), 9.42 (s, 1H), 8.74 (d, $J = 7.4$ Hz, 2H), 8.37 – 8.12 (m, 2H), 7.94 (s, 1H), 7.75 (d, $J = 7.9$ Hz, 1H), 7.60 (d, $J = 8.5$ Hz, 2H), 7.49 (t, $J = 7.8$ Hz, 1H), 7.23 (d, $J = 8.4$ Hz, 2H), 7.13 (t, $J = 7.7$ Hz, 1H), 6.25 – 5.98 (m, 2H), 5.57 (dt, $J = 9.6, 2.5$ Hz, 1H), 4.44 (t, $J = 5.9$ Hz, 2H), 4.08 (s, 1H), 3.74 (s, 2H), 3.66 (s, 2H), 3.59 (t, $J = 6.3$ Hz, 2H), 2.87 – 2.74 (m, 3H).

^{13}C NMR (126 MHz, Methanol-*d*₄) δ 171.7, 168.5, 159.4, 157.1, 155.3, 140.9, 140.4, 132.8, 131.7, 130.3, 130.2, 128.8, 127.2, 123.6, 123.4, 123.2, 121.4, 107.1, 50.6, 49.9, 40.5, 26.9.

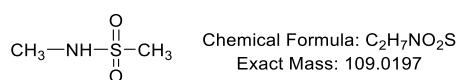
2-Amino-N-methoxybenzamide (**25**)¹⁶⁸



To an ice-cooled solution of *O*-methyl hydroxylamine hydrochloride (500 mg, 6.0 mmol) in H₂O (1.5 mL) was added NaOH (aq) (2 M, 3 mL). Then isatoic anhydride (326 mg, 2.0 mmol) was added in one portion. The mixture was stirred at room temperature overnight. The solution was diluted by ethyl acetate and washed with water and saturated brine solution. Then the organic layer was dried over MgSO₄ and concentrated *in vacuo*. The residue was purified through silica gel column (eluent: DCM/MeOH = 50/1) to give the title compound as white solid (331 mg, 90%).

¹H NMR (500 MHz, DMSO-*d*₆) δ 12.05 (s, 1H), 11.34 (s, 1H), 8.47 (s, 1H), 8.40 (d, *J* = 8.4 Hz, 1H), 7.69 – 7.56 (m, 2H), 7.23 (td, *J* = 7.6, 1.2 Hz, 1H), 3.72 (s, 3H).

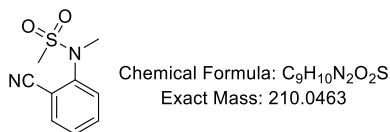
N-Methylmethanesulfonamide (**26**)¹⁶⁹



To a solution of Methylamine (10 mL, 40% in H₂O) in an ice bath, methane sulfonyl chloride (3 mL, 38.76 mmol) was dropped slowly and maintained the internal temperature was below 25 °C. Then the mixture was stirred at room temperature overnight. The solution was saturated by adding NaCl (3.6 g) and stirred for 30 min followed by extraction with DCM (3 times). The organic phase was dried over MgSO₄ and filtered. The solvent was removed *in vacuo* to give colourless oil 6.5 g, yield 77%.

¹H NMR (250 MHz, Chloroform-*d*) δ 4.43 (s, 1H), 2.94 (s, 3H), 2.82 (d, *J* = 3.3 Hz, 3H).

N-(2-Cyanophenyl)-*N*-methylmethanesulfonamide (**27**)

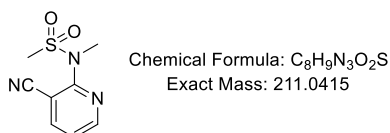


To a solution of potassium carbonate (3.0 g, 21.8 mmol) in DMF (30 mL) at room temperature was added **26** (1.19 g, 10.9 mmol) and 2-fluorobenzonitrile (777 μ L, 7.3 mmol). The mixture was stirred at 100 °C for 20 hours and then was diluted with 100 mL EtOAc and washed by water (50 mL x 3) and brine (50 mL). The organic phase was dried over MgSO₄ and evaporated. The resulting residue was purified by flash chromatography on silica gel (Cyclohexane / EtOAc = 2/1) to afford the desired product as white solid (787 mg, 51%).

¹H NMR (500 MHz, Chloroform-*d*) δ 7.71 (dd, *J* = 7.8, 1.6 Hz, 1H), 7.66 (td, *J* = 7.9, 1.6 Hz, 1H), 7.55 (dd, *J* = 8.2, 1.2 Hz, 1H), 7.46 (td, *J* = 7.6, 1.2 Hz, 1H), 3.38 (s, 3H), 3.11 (s, 3H).

¹³C NMR (126 MHz, Chloroform-*d*) δ 143.9, 134.1, 133.8, 130.7, 128.8, 116.8, 113.0, 39.2, 38.6.

N-(3-Cyanopyridin-2-yl)-*N*-methylmethanesulfonamide (**28**)



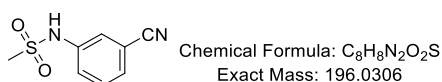
To a solution of potassium carbonate (1.7 g, 12.6 mmol) in DMF (30 mL) at room temperature was added **26** (830 mg, 7.6 mmol), and 2-chloronicotinonitrile (960 mg, 6.3 mmol). The reaction mixture was stirred at 86 °C for 18 hours. Then the mixture was diluted with 100 mL EtOAc and washed by water (50 mL x 3) and brine (50 mL). The organic phase was dried over MgSO₄ and evaporated. The resulting residue was purified

by flash chromatography on silica gel (eluent, Cyclohexane / EtOAc = 2/1 ~ 1/1) to afford the desired product as white solid (355 mg, 27%).

^1H NMR (500 MHz, Chloroform-*d*) δ 8.65 (dd, $J = 4.9, 2.0$ Hz, 1H), 8.05 (dd, $J = 7.8, 1.9$ Hz, 1H), 7.39 (dd, $J = 7.7, 4.9$ Hz, 1H), 3.39 (s, 3H), 3.19 (s, 3H).

^{13}C NMR (126 MHz, Chloroform-*d*) δ 156.1, 152.0, 142.6, 122.6, 115.2, 109.4, 37.9, 37.2.

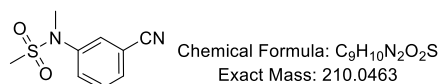
N-(3-Cyanophenyl)methanesulfonamide (**29**)



To a cold solution of 3-aminobenzonitrile (1.18 g, 10.0 mmol) in pyridine (20 mL) was added methanesulfonyl chloride (770 μL , 9.9 mmol) dropwise and the mixture was stirred at room temperature overnight. The solution was removed and the residue was partitioned between 1 *N* aqueous HCl and ethyl acetate. The organic layer was washed with brine, dried over MgSO_4 and filtered. The filtrate was concentrated to give the desired compound as a pale orange solid (1.6 g, 82%).

^1H NMR (250 MHz, Methanol-*d*₄) δ 7.60 – 7.45 (m, 4H), 3.05 (s, 3H).

N-(3-Cyanophenyl)-*N*-methylmethanesulfonamide (**30**)



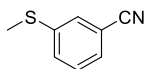
Sodium hydride (220 mg, 60% dispersion in mineral oil, 5.5 mmol) was carefully added to a solution of **29** (900 mg, 4.59 mmol) in distilled DMF (15 mL). After 20 min, methyl iodide (428 μL , 6.88 mmol) was added, and the reaction mixture was stirred at room temperature for 18 h. Then the reaction mixture was poured into ice water and extracted with ethyl acetate (20 mL x 3). The combined organic layers were dried over MgSO_4 and

concentrated *in vacuo*. Purification of the residue by silica gel chromatography (eluent, cyclohexane/ethyl acetate= 3/1~ 2/1) provided the title product as white solid (880 mg, 91%).

^1H NMR (250 MHz, Chloroform-*d*) δ 7.68 – 7.64 (m, 2H), 7.60 – 7.46 (m, 2H), 3.35 (s, 3H), 2.87 (s, 3H).

^{13}C NMR (126 MHz, Chloroform-*d*) δ 142.4, 130.6, 130.5, 130.4, 128.9, 117.9, 113.5, 37.8, 35.9.

3-(Methylthio)benzonitrile (**31**)¹⁷¹

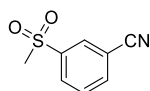


Chemical Formula: C₈H₇NS
Exact Mass: 149.0299

3-Aminobenzonitrile (500 mg, 4.23 mmol) was added to dimethyl disulfide (4 mL) and the mixture was stirred magnetically. After heating to about 100 °C, *tert*-BuONO (744 μL , 6.34 mmol) was added in five portions over 10 min. After a further 20 min stirring, the mixture was cooled to room temperature and the solvent was removed *in vacuo* (*Stench!*). The residue was purified by silica column chromatography (eluent, cyclohexane/ethyl acetate= 20/1) to give the title compound as lemon yellow solid (438 mg, 69%).

^1H NMR (250 MHz, Chloroform-*d*) δ 7.54 – 7.34 (m, 4H), 2.51 (s, 3H).

3-(Methylsulfonyl)benzonitrile (**32**)¹⁷¹



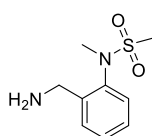
Chemical Formula: C₈H₇NO₂S
Exact Mass: 181.0197

To a cooled solution of **31** (420 mg, 2.8 mmol) in acetone and water (10 mL, 1:1), was added Oxone (2KHSO₅·KHSO₄·K₂SO₄) (2.6 g, 4.2 mmol) and the mixture was stirred overnight. On completion, the reaction mixture was diluted with water (30 mL) and

extracted with DCM (10 mL x 3). The combined organic layers were washed with brine and dried over MgSO₄ and concentrated to give the title compound as white solid (443 mg, 87%).

¹H NMR (250 MHz, Chloroform-*d*) δ 8.26 (t, *J* = 1.4 Hz, 1H), 8.19 (dt, *J* = 7.9, 1.5 Hz, 1H), 7.95 (dt, *J* = 7.8, 1.4 Hz, 1H), 7.75 (td, *J* = 7.8, 0.6 Hz, 1H), 3.10 (s, 3H).

N-(2-(Aminomethyl)phenyl)-*N*-methylmethanesulfonamide (**33**)



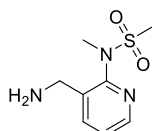
Chemical Formula: C₉H₁₄N₂O₂S
Exact Mass: 214.0776

Following the general procedure A from **27** (740 mg, 3.52 mmol) afforded title compound as a colourless oil (763 mg, 100%).

¹H NMR (500 MHz, Chloroform-*d*) δ 7.52 (dd, *J* = 7.6, 1.6 Hz, 1H), 7.35 (td, *J* = 7.5, 1.4 Hz, 1H), 7.28 (td, *J* = 7.6, 1.7 Hz, 1H), 7.22 (dd, *J* = 7.9, 1.4 Hz, 1H), 3.97 (s, 2H), 3.23 (s, 3H), 2.95 (s, 3H), 1.99 (s, 2H).

¹³C NMR (126 MHz, Chloroform-*d*) δ 143.3, 139.3, 130.0, 129.2, 128.0, 126.6, 42.1, 39.3, 36.1.

N-(3-(Aminomethyl)pyridin-2-yl)-*N*-methylmethanesulfonamide (**34**)



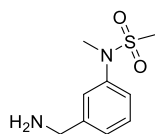
Chemical Formula: C₈H₁₃N₃O₂S
Exact Mass: 215.0728

Following the general procedure A from **27** (311 mg, 1.47 mmol) afforded title compound as a colourless oil (294 mg, 94%).

^1H NMR (500 MHz, Chloroform-*d*) δ 8.34 (dd, $J = 4.7, 1.9$ Hz, 1H), 7.88 (dd, $J = 7.7, 1.9$ Hz, 1H), 7.29 (dd, $J = 7.6, 4.7$ Hz, 1H), 3.99 (s, 2H), 3.21 (s, 3H), 3.04 (s, 3H).

^{13}C NMR (126 MHz, Chloroform-*d*) δ 152.6, 147.5, 138.7, 138.1, 124.4, 41.8, 37.8, 35.9.

N-(3-(Aminomethyl)phenyl)-*N*-methylmethanesulfonamide (**35**)

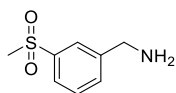


Chemical Formula: $\text{C}_9\text{H}_{14}\text{N}_2\text{O}_2\text{S}$
Exact Mass: 214.0776

Following the general procedure A from **30** (350 mg, 1.66 mmol) afforded title compound as a colourless oil (344 mg, 97%).

^1H NMR (250 MHz, Chloroform-*d*) δ 7.40 – 7.26 (m, 4H), 3.92 (s, 2H), 3.35 (s, 3H), 2.88 (s, 3H).

(3-(Methylsulfonyl)phenyl)methanamine (**36**)

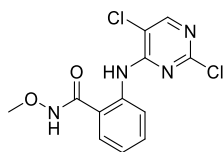


Chemical Formula: $\text{C}_8\text{H}_{11}\text{NO}_2\text{S}$
Exact Mass: 185.0510

Following the general procedure A from **32** (443 mg, 2.44 mmol) afforded title compound as a colourless oil (429 mg, 95%).

^1H NMR (250 MHz, Chloroform-*d*) δ 7.91 (d, $J = 1.8$ Hz, 1H), 7.82 (dt, $J = 7.6, 1.7$ Hz, 1H), 7.63 (d, $J = 7.8$ Hz, 1H), 7.53 (t, $J = 7.6$ Hz, 1H), 3.98 (s, 2H), 3.06 (s, 3H).

2-((2,5-Dichloropyrimidin-4-yl)amino)-*N*-methoxybenzamide (**37**)



Chemical Formula: C₁₂H₁₀Cl₂N₄O₂
Exact Mass: 312.0181

2,4,5-Trichloropyrimidine (178 μ L, 1.52 mmol) was added to a stirred solution of aniline **25** (252 mg, 1.52 mmol) and NaHCO₃ (153 mg, 1.8 mmol) in anhydrous EtOH at room temperature. The resulted mixture was heated to reflux and stirred overnight before cooled to room temperature. The precipitate was filtered out, washed with water give the title compound as white solid (367 mg, 77%).

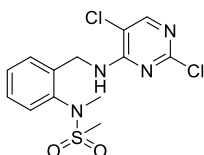
¹H NMR (500 MHz, DMSO-*d*₆) δ 12.05 (s, 1H), 11.34 (s, 1H), 8.47 (s, 1H), 8.40 (d, *J* = 8.4 Hz, 1H), 7.69 – 7.56 (m, 2H), 7.23 (td, *J* = 7.6, 1.2 Hz, 1H), 3.72 (s, 3H).

¹³C NMR (126 MHz, DMSO-*d*₆) δ 165.5, 156.6, 156.3, 155.4, 137.8, 132.1, 127.9, 123.5, 121.7, 120.2, 114.8, 63.3.

HRMS (ESI) *m/z* calcd. for C₁₂H₁₁Cl₂N₄O₂ [M+H]⁺: 313.02504, found: 313.02536.

Melting point: 222 °C.

N-(2-(((2,5-Dichloropyrimidin-4-yl)amino)methyl)phenyl)-*N*-methylmethanesulfonamide (**38**)



Chemical Formula: C₁₃H₁₄Cl₂N₄O₂S
Exact Mass: 360.0215

Following the general procedure B, from amine **33** (700 mg, 3.27 mmol) and 2,4,5-trichloropyrimidine (610 mg, 3.26 mmol), the title compound was obtained as white solid (1.034 g, 88%).

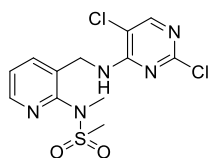
^1H NMR (500 MHz, Chloroform-*d*) δ 7.97 (s, 1H), 7.60 – 7.57 (m, 1H), 7.38 – 7.35 (m, 2H), 7.30 – 7.27 (m, 1H), 4.51 (d, J = 15.7 Hz, 2H), 3.31 (s, 3H), 3.00 (s, 3H).

^{13}C NMR (126 MHz, CDCl_3) δ 158.8, 158.3, 153.6, 140.1, 138.4, 131.7, 129.6, 129.4, 126.3, 113.6, 40.4, 39.6, 35.6.

HRMS (ESI) m/z calcd. for $\text{C}_{13}\text{H}_{15}\text{O}_2\text{N}_4\text{Cl}_2\text{S}$ $[\text{M}+\text{H}]^+$: 361.02873, found: 361.02857.

Melting point: 177 °C.

N-(3-(((2,5-Dichloropyrimidin-4-yl)amino)methyl)pyridin-2-yl)-*N*-methylmethanesulfonamide (**39**)



Chemical Formula: $\text{C}_{12}\text{H}_{13}\text{Cl}_2\text{N}_5\text{O}_2\text{S}$
Exact Mass: 361.0167

Following the general procedure B, from amine **34** (280 mg, 1.3 mmol) and 2,4,5-trichloropyrimidine (224 mg, 1.2 mmol) the title compound obtained as white solid (401 mg, 92%).

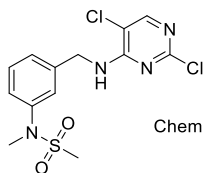
^1H NMR (500 MHz, Chloroform-*d*) δ 8.45 (dd, J = 4.7, 1.9 Hz, 1H), 8.00 (s, 1H), 7.96 (dd, J = 7.7, 1.9 Hz, 1H), 7.32 (dd, J = 7.7, 4.7 Hz, 1H), 4.87 (s, 2H), 3.31 (s, 3H), 3.06 (s, 3H).

^{13}C NMR (126 MHz, Chloroform-*d*) δ 158.8, 158.3, 153.9, 153.2, 149.0, 140.6, 133.3, 124.7, 113.7, 40.4, 38.0, 35.5.

HRMS (ESI) m/z calcd. for $\text{C}_{12}\text{H}_{14}\text{O}_2\text{N}_5\text{Cl}_2\text{S}$ $[\text{M}+\text{H}]^+$: 362.02398, found: 362.02335.

Melting point: 190 °C.

N-(3-(((2,5-Dichloropyrimidin-4-yl)amino)methyl)phenyl)-*N*-methylmethanesulfonamide (**40**)



Following the general procedure B, from amine **35** (320 mg, 1.5 mmol) and 2,4,5-trichloropyrimidine (281 mg, 1.5 mmol) the title compound was obtained as white solid (413 mg, 76%).

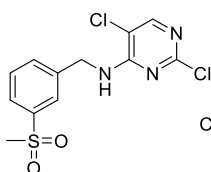
¹H NMR (500 MHz, Chloroform-*d*) δ 7.90 (s, 1H), 7.27 – 7.21 (m, 2H), 7.19 – 7.10 (m, 2H), 5.77 (t, *J* = 5.9 Hz, 1H), 4.56 (d, *J* = 5.9 Hz, 2H), 3.18 (s, 3H), 2.70 (s, 3H).

¹³C NMR (126 MHz, Chloroform-*d*) δ 158.8, 158.5, 154.0, 142.0, 138.8, 129.9, 127.0, 126.2, 125.4, 113.4, 44.9, 38.2, 35.6.

HRMS (ESI) *m/z* calcd. for C₁₃H₁₅O₂N₄Cl₂S [M+H]⁺: 361.02873, found: 361.02863.

Melting point: 154 °C.

2,5-Dichloro-*N*-(3-(methylsulfonyl)benzyl)pyrimidin-4-amine (**41**)



Following the general procedure B, from amine **36** (357 mg, 1.93 mmol) and 2,4,5-trichloropyrimidine (361 mg, 1.93 mmol) the title compound was obtained as white solid (535 mg, 83%).

¹H NMR (500 MHz, Chloroform-*d*) δ 8.03 (s, 1H), 7.91 (d, *J* = 1.7 Hz, 1H), 7.84 (dt, *J* = 7.9, 1.4 Hz, 1H), 7.65 (d, *J* = 7.7 Hz, 1H), 7.54 (t, *J* = 7.7 Hz, 1H), 4.78 (d, *J* = 6.0 Hz,

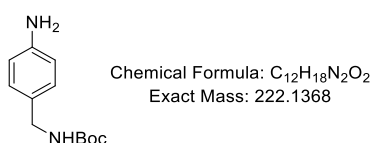
2H), 3.05 (s, 3H).

¹³C NMR (126 MHz, Chloroform-*d*) δ 158.8, 158.4, 154.1, 141.0, 139.4, 133.4, 130.0, 126.8, 126.7, 113.5, 44.5, 44.5.

HRMS (ESI) *m/z* calcd. for C₁₂H₁₂O₂N₃Cl₂S [M+H]⁺: 332.00218, found: 332.00168.

Melting point: 148 °C.

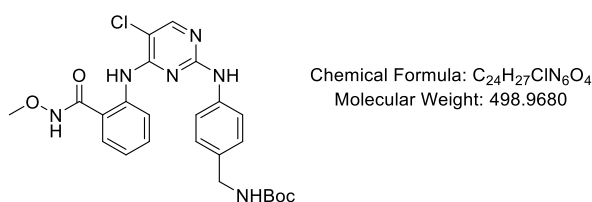
tert-Butyl (4-aminobenzyl)carbamate (**42**)²²⁹



To a solution of 4-aminobenzylamine (200 mg, 1.6 mmol) in distilled DCM was added Boc₂O (360 mg, 1.6 mmol). The mixture was stirred at room temperature for 2 h. The solution was concentrated and the residue was dissolved in DCM and was washed with water brine, dried over MgSO₄. After concentration in vacuo, the crude product was purified through column chromatography (eluent cyclohexane/ethyl acetate=2/1) to give the title compound as light yellow solid (277 mg, 78%).

¹H NMR (250 MHz, Chloroform-*d*) δ 7.08 (d, *J* = 8.2 Hz, 2H), 6.65 (d, *J* = 8.4 Hz, 2H), 4.18 (d, *J* = 5.7 Hz, 2H), 1.45 (s, 9H).

tert-Butyl (4-((5-chloro-4-((2-(methoxycarbonyl)phenyl)amino)pyrimidin-2-yl)amino)benzyl) carbamate (**43**)



In an argon charged sealed tube, to a solution of **37** (337 mg, 1.08 mmol) in 1,4-dioxane (6 mL) was added Pd₂(dba)₃ (99 mg, 10% mmol), XantPhos (128 mg, 20% mmol) and Cs₂CO₃ (420 mg, 1.29 mmol), followed by addition of **42** (240 mg, 1.08 mmol). The mixture was stirred at room temperature for 10 minutes, then stirred at 105 °C for 24 h. Subsequently, the solvent was concentrated and the resulting residue was purified by silica gel chromatography (eluent: DCM/MeOH= 100/1) to give the title compound as white solid (231 mg, 43%).

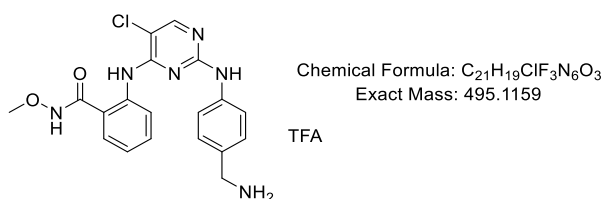
¹H NMR (500 MHz, DMSO-*d*₆) δ 11.98 (s, 1H), 10.89 (s, 1H), 9.42 (s, 1H), 8.68 (d, *J* = 8.4 Hz, 1H), 8.22 (s, 1H), 7.66 – 7.60 (m, 1H), 7.57 (d, *J* = 8.2 Hz, 2H), 7.54 – 7.47 (m, 1H), 7.30 (t, *J* = 6.3 Hz, 1H), 7.17 – 7.10 (m, 3H), 4.08 (d, *J* = 6.2 Hz, 2H), 3.74 (s, 3H), 1.40 (s, 9H).

¹³C NMR (126 MHz, DMSO-*d*₆) δ 166.0 157.7, 155.7, 154.9, 154.7, 139.1, 138.7, 133.6, 131.8, 127.8, 127.1, 122.1, 121.9, 119.6, 119.1, 104.8, 77.6, 63.3, 43.0, 28.2.

HRMS (ESI) *m/z* calcd. for C₂₄H₂₈O₄N₆Cl [M+H]⁺: 499.18551, found: 499.18489.

Melting point: 216 °C.

2-((2-((4-(Aminomethyl)phenyl)amino)-5-chloropyrimidin-4-yl)amino)-*N*-methoxybenzamide trifluoroacetate (**44**)



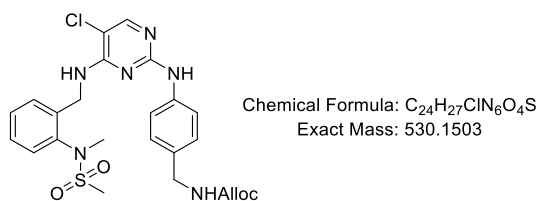
Following the general procedure E, from compound **43** (350 mg, 0.7 mmol) the titled compound was obtained as white solid (464 mg, quantitative). This compound was used in next step without further purification.

^1H NMR (250 MHz, Methanol- d_4) δ 8.57 (d, $J = 8.4$ Hz, 2H), 8.17 (s, 2H), 7.66 (dd, $J = 8.6, 6.6$ Hz, 6H), 7.64 – 7.49 (m, 1H), 7.40 (d, $J = 8.5$ Hz, 4H), 7.32 – 7.17 (m, 2H), 4.10 (s, 4H), 3.82 (s, 6H).

HRMS (ESI) m/z calcd for $\text{C}_{19}\text{H}_{20}\text{ClN}_6\text{O}_2$ 399.13308, found: 399.13248.

Melting point: 240 °C.

Allyl (4-((5-chloro-4-((2-(*N*-methylmethylsulfonamido)benzyl)amino)pyrimidin-2-yl)amino)benzyl)carbamate (**45**)



Following the general procedure C, from **38** (400 mg, 1.11 mmol), aniline **6** (229 mg, 1.08 mmol) and HCl (280 μL , 1.11 mmol), the title compound was obtained as pale solid (375 mg, 64%).

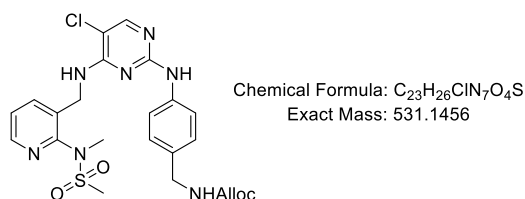
^1H NMR (500 MHz, Chloroform- d) δ 7.88 (s, 1H), 7.55 – 7.47 (m, 3H), 7.38 – 7.27 (m, 3H), 7.22 – 7.15 (m, 3H), 6.17 (t, $J = 6.1$ Hz, 1H), 5.92 (ddt, $J = 16.3, 10.8, 5.6$ Hz, 1H), 5.34 – 5.19 (m, 2H), 5.07 (t, $J = 6.2$ Hz, 2H), 4.64 (br, 1H), 4.59 (d, $J = 5.7$ Hz, 2H), 4.30 (d, $J = 5.9$ Hz, 2H), 3.27 (s, 3H), 2.99 (s, 3H).

^{13}C NMR (126 MHz, Chloroform- d) δ 158.1, 157.9, 156.3, 153.2, 139.9, 139.4, 139.4, 133.0, 132.1, 130.9, 129.4, 129.0, 128.3, 126.5, 119.5, 117.8, 105.3, 65.7, 44.9, 40.6, 39.5, 35.7.

HRMS (ESI) m/z calcd. for $\text{C}_{24}\text{H}_{28}\text{O}_4\text{N}_6\text{ClS}$ $[\text{M}+\text{H}]^+$: 531.15758, found: 531.15652.

Melting point: 110 °C.

Allyl (4-((5-chloro-4-(((2-(*N*-methylmethylsulfonamido)pyridin-3-yl)methyl)amino)pyrimidin-2-yl)amino)benzyl)carbamate (**46**)



Following the general procedure C, from **39** (389 mg, 1.07mmol), aniline **6** (222 mg, 1.08mmol) and HCl (270 μ L, 1.08mmol), the title compound was obtained as pale foamy solid (493 mg, 86%).

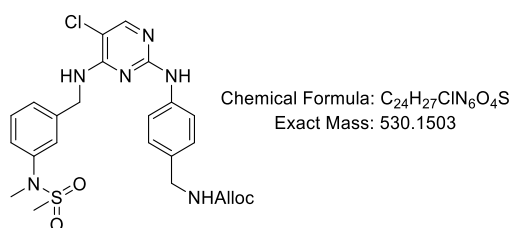
¹H NMR (500 MHz, Methanol-*d*₄) δ 8.40 (dd, *J* = 4.8, 1.8 Hz, 1H), 7.86 (s, 1H), 7.77 (dd, *J* = 7.7, 1.8 Hz, 1H), 7.35 – 7.28 (m, 3H), 7.05 (d, *J* = 8.2 Hz, 2H), 5.94 (ddd, *J* = 15.5, 10.5, 5.2 Hz, 1H), 5.34 – 5.25 (m, 1H), 5.21 – 5.13 (m, 1H), 4.84 (s, 2H), 4.58 – 4.52 (m, 2H), 4.18 (s, 2H), 3.18 (s, 3H), 3.12 (s, 3H).

¹³C NMR (126 MHz, Methanol-*d*₄) δ 159.6, 158.8, 154.0, 153.9, 148.7, 140.5, 139.0, 135.9, 134.5, 134.1, 128.6, 125.3, 120.7, 117.5, 116.6, 105.6, 66.4, 45.1, 41.5, 37.9, 36.4.

HRMS (ESI) *m/z* calcd. for C₂₃H₂₇O₄N₇ClS [M+H]⁺: 532.15283, found: 532.15167.

Melting point: 100 °C.

Allyl (4-((5-chloro-4-((3-(*N*-methylmethylsulfonamido)benzyl)amino)pyrimidin-2-yl)amino)benzyl)- carbamate (**47**)



Following the general procedure C, from **40** (394 mg, 1.09 mmol), aniline **6** (242 mg, 1.17

mmol) and HCl (270 μ L, 1.08 mmol), the title compound was obtained as white solid (360 mg, 62%).

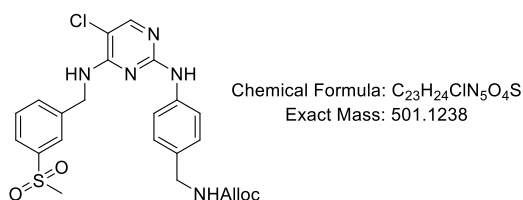
^1H NMR (500 MHz, DMSO- d_6) δ 7.96 (s, 1H), 7.81 (t, J = 6.2 Hz, 1H), 7.63 (s, 1H), 7.52 (d, J = 8.4 Hz, 2H), 7.41 (t, J = 2.0 Hz, 1H), 7.35 (t, J = 7.8 Hz, 1H), 7.26 (dt, J = 7.5, 2.1 Hz, 2H), 7.07 (d, J = 8.3 Hz, 2H), 5.91 (ddd, J = 16.1, 10.7, 5.3 Hz, 1H), 5.31 – 5.14 (m, 2H), 4.63 (d, J = 5.9 Hz, 2H), 4.49 (dt, J = 5.4, 1.7 Hz, 2H), 4.09 (d, J = 5.7 Hz, 2H), 3.16 (s, 3H), 2.86 (s, 3H).

^{13}C NMR (126 MHz, DMSO- d_6) δ 157.9, 157.34 156.1, 153.2, 141.6, 140.7, 139.4, 133.8, 132.2, 128.9, 127.1, 125.6, 125.0, 124.6, 118.5, 116.9, 103.4, 64.3, 43.4, 43.3, 37.7, 34.9.

HRMS (ESI) m/z calcd. for $\text{C}_{24}\text{H}_{28}\text{O}_4\text{N}_6\text{ClS}$ $[\text{M}+\text{H}]^+$: 531.15758, found: 531.15627.

Melting point: 177 $^\circ\text{C}$.

Allyl (4-((5-chloro-4-((3-(methylsulfonyl)benzyl)amino)pyrimidin-2-yl)amino)benzyl) carbamate (**48**)



Following the general procedure C, from **41** (530 mg, 1.60 mmol), aniline **6** (329 mg, 1.60 mmol) and HCl (400 μ L, 1.60 mmol), the title compound was obtained as white solid (443 mg, 55%).

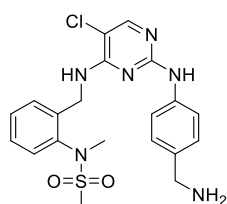
^1H NMR (500 MHz, Chloroform- d) δ 7.93 (s, 1H), 7.92 (d, J = 1.8 Hz, 1H), 7.84 (dt, J = 7.8, 1.5 Hz, 1H), 7.62 (dt, J = 8.0, 1.3 Hz, 1H), 7.55 (t, J = 7.7 Hz, 1H), 7.44 – 7.37 (m, 2H), 7.18 (d, J = 8.1 Hz, 2H), 7.05 (s, 1H), 5.93 (ddt, J = 17.2, 10.4, 5.6 Hz, 1H), 5.80 (t, J = 6.1 Hz, 1H), 5.34 – 5.18 (m, 3H), 4.77 (d, J = 6.1 Hz, 2H), 4.59 (d, J = 5.6 Hz, 2H), 4.31 (d, J = 6.0 Hz, 2H), 2.96 (s, 3H).

^{13}C NMR (126 MHz, Chloroform-*d*) δ 158.0, 157.8, 156.4, 153.7, 141.1, 140.5, 138.9, 133.1, 132.7, 132.6, 129.9, 128.3, 126.5, 126.5, 119.6, 117.7, 105.0, 66.0, 44.8, 44.5, 44.5.

HRMS (ESI) m/z calcd. for $\text{C}_{23}\text{H}_{25}\text{O}_4\text{N}_5\text{ClS}$ $[\text{M}+\text{H}]^+$: 502.13103, found: 502.13037.

Melting point: 169 °C.

N-(2-(((2-((4-(Aminomethyl)phenyl)amino)-5-chloropyrimidin-4-yl)amino)methyl)phenyl)-*N*-methylmethanesulfonamide (**49**)



Chemical Formula: $\text{C}_{20}\text{H}_{23}\text{ClN}_6\text{O}_2\text{S}$
Exact Mass: 446.1292

Following the general procedure D, from **45** (360 mg, 0.68 mmol), the title compound was obtained as white solid (255 mg, 84%).

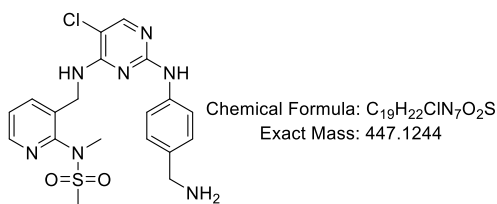
^1H NMR (500 MHz, DMSO-*d*₆) δ 9.06 (s, 1H), 7.98 (s, 1H), 7.55 (dd, $J = 7.0, 2.0$ Hz, 1H), 7.47 (t, $J = 6.0$ Hz, 1H), 7.43 (d, $J = 8.2$ Hz, 2H), 7.38 – 7.30 (m, 3H), 7.06 (d, $J = 8.2$ Hz, 2H), 4.78 (d, $J = 32.3$ Hz, 2H), 3.59 (s, 2H), 3.19 (s, 3H), 3.11 (s, 3H).

^{13}C NMR (126 MHz, DMSO-*d*₆) δ 158.1, 157.6, 153.2, 139.6, 139.2, 138.8, 136.5, 128.3, 127.9, 127.8, 127.0, 127.0, 118.4, 103.3, 45.2, 40.1, 38.6, 36.0.

HRMS (ESI) m/z calcd. for $\text{C}_{20}\text{H}_{24}\text{O}_2\text{N}_6\text{ClS}$ $[\text{M}+\text{H}]^+$: 447.13645, found: 447.13549.

Melting point: 218 °C.

N-(3-(((2-((4-(Aminomethyl)phenyl)amino)-5-chloropyrimidin-4-yl)amino)methyl)pyridin-2-yl)-*N*-methylmethanesulfonamide (**50**)



Following the general procedure D, from **46** (471 mg, 0.89 mmol), the title compound was obtained as white solid (377 mg, 94%).

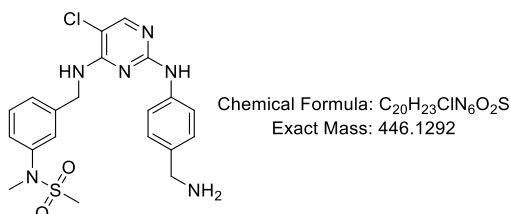
¹H NMR (250 MHz, Methanol-*d*₄) δ 8.43 – 8.41 (m, 1H), 7.93 – 7.87 (m, 1H), 7.81 (dd, *J* = 7.7, 1.9 Hz, 1H), 7.46 – 7.32 (m, 3H), 7.14 (d, *J* = 8.6 Hz, 2H), 4.87 (s, 2H), 3.74 (s, 2H), 3.22 (s, 3H), 3.13 (s, 3H).

¹³C NMR (126 MHz, Methanol-*d*₄) δ 159.6, 154.0, 153.9, 148.8, 140.8, 139.2, 135.9, 135.1, 129.1, 125.3, 120.7, 116.6, 105.7, 45.8, 41.3, 37.9, 36.4.

HRMS (ESI) *m/z* calcd. for C₁₉H₂₃O₂N₇ClS [M+H]⁺: 448.13170, found: 448.13054.

Melting point: 124 °C.

N-(3-(((2-((4-(Aminomethyl)phenyl)amino)-5-chloropyrimidin-4-yl)amino)methyl)phenyl)-*N*-methylmethanesulfonamide (**51**)



Following the general procedure D, from **47** (200 mg, 0.38 mmol), the title compound was obtained as white solid (138 mg, 81%).

¹H NMR (500 MHz, DMSO-*d*₆) δ 9.11 (s, 1H), 7.97 (s, 1H), 7.81 (t, *J* = 6.2 Hz, 1H), 7.55

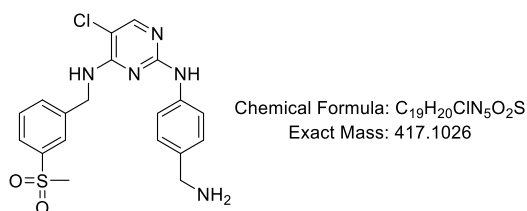
– 7.51 (m, 2H), 7.42 (m, 1H), 7.38 (t, $J = 7.7$ Hz, 1H), 7.30 – 7.26 (m, 2H), 7.17 – 7.12 (m, 2H), 4.64 (d, $J = 6.1$ Hz, 2H), 3.64 (s, 2H), 3.17 (s, 3H), 2.88 (s, 3H).

^{13}C NMR (126 MHz, $\text{DMSO-}d_6$) δ 157.9, 157.3, 153.2, 141.6, 140.8, 138.9, 136.4, 128.9, 127.0, 125.7, 125.1, 124.5, 118.5, 103.3, 45.1, 43.2, 37.8, 34.9.

HRMS (ESI) m/z calcd. for $\text{C}_{20}\text{H}_{24}\text{O}_2\text{N}_6\text{ClS}$ $[\text{M}+\text{H}]^+$: 447.13645, found: 447.13558.

Melting point: 176 °C.

N^2 -(4-(Aminomethyl)phenyl)-5-chloro- N^4 -(3-(methylsulfonyl)benzyl)pyrimidine-2,4-diamine (**52**)



Following the general procedure D, from **48** (380mg, 0.76 mmol), the title compound was obtained as white solid (262 mg, 86.5%).

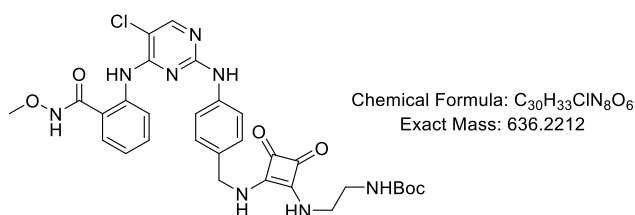
^1H NMR (500 MHz, $\text{DMSO-}d_6$) δ 9.15 (s, 1H), 7.98 (s, 1H), 7.95 – 7.91 (m, 2H), 7.81 (d, $J = 7.7$ Hz, 1H), 7.69 (d, $J = 7.7$ Hz, 1H), 7.62 (t, $J = 7.7$ Hz, 1H), 7.48 (d, $J = 8.1$ Hz, 2H), 7.14 (d, $J = 8.2$ Hz, 2H), 4.71 (d, $J = 6.0$ Hz, 2H), 3.65 (s, 2H), 3.14 (s, 3H).

^{13}C NMR (126 MHz, $\text{DMSO-}d_6$) δ 157.9, 157.3, 153.4, 141.4, 140.8, 139.0, 135.4, 132.0, 129.4, 127.2, 125.3, 125.1, 118.5, 103.3, 44.8, 43.5, 43.3.

HRMS (ESI) m/z calcd. for $\text{C}_{19}\text{H}_{21}\text{O}_2\text{N}_5\text{ClS}$ $[\text{M}+\text{H}]^+$: 418.10990, found: 418.10920.

Melting point: 216 °C.

tert-Butyl (2-((2-((4-((5-chloro-4-((2-(methoxycarbonyl)phenyl)amino)pyrimidin-2-yl)amino)benzyl)amino)-3,4-dioxocyclobut-1-en-1-yl)amino)ethyl)carbamate (**53**)



Following the general procedure F, from compound **44** (464 mg, 0.74 mmol) and compound **11** (200 mg, 0.74 mmol), the title compound was obtained as white solid (196 mg, 42%).

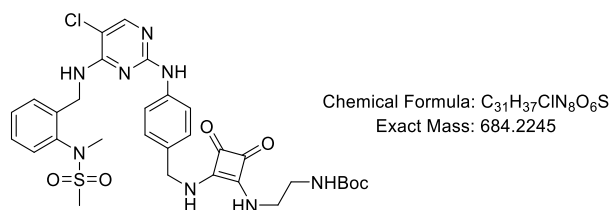
¹H NMR (500 MHz, DMSO-*d*₆) δ 11.97 (s, 1H), 10.91 (s, 1H), 9.49 (s, 1H), 8.67 (d, *J* = 8.3 Hz, 1H), 8.23 (s, 1H), 7.63 (t, *J* = 8.4 Hz, 3H), 7.53 – 7.47 (m, 1H), 7.29 – 7.22 (m, 2H), 7.14 (td, *J* = 7.6, 1.2 Hz, 1H), 6.88 (t, *J* = 5.7 Hz, 1H), 4.71 – 4.57 (m, 2H), 3.73 (s, 3H), 3.51 (s, 2H), 3.09 (q, *J* = 5.9 Hz, 2H), 1.35 (s, 9H).

¹³C NMR (126 MHz, DMSO-*d*₆) δ 182.6, 182.5, 168.1, 167.4, 165.9, 157.6, 155.7, 154.9, 154.7, 139.4, 139.0, 132.1, 131.8, 127.8, 127.8, 122.2, 121.8, 119.8, 119.2, 105.0, 77.8, 63.3, 46.5, 43.2, 41.1, 28.2.

HRMS (ESI) *m/z* calcd. for C₃₀H₃₄O₆N₈Cl [M+H]⁺: 637.22843 found: 637.22760

Melting point: 206 °C.

tert-Butyl (2-((2-((4-((5-chloro-4-((2-(*N*-methylmethylsulfonamido)benzyl)amino)pyrimidin-2-yl)amino)benzyl)amino)-3,4-dioxocyclobut-1-en-1-yl)amino)ethyl)carbamate (**54**)



Following the general procedure F from **49** (230 mg, 0.51 mmol) and **11** (230 mg, 0.51 mmol), the title compound was obtained as white solid (302 mg, 86%).

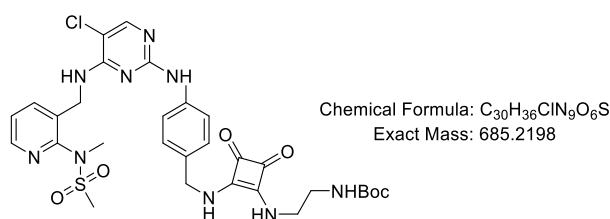
¹H NMR (500 MHz, DMSO-*d*₆) δ 9.19 (s, 1H), 8.00 (s, 1H), 7.53 (t, *J* = 4.5 Hz, 2H), 7.48 (d, *J* = 8.1 Hz, 2H), 7.37 – 7.32 (m, 2H), 7.30 (d, *J* = 5.4 Hz, 1H), 7.06 (d, *J* = 8.2 Hz, 2H), 6.89 (d, *J* = 5.9 Hz, 1H), 4.85 – 4.72 (m, 2H), 4.65 – 4.51 (m, 2H), 3.52 (s, 2H), 3.17 (s, 3H), 3.11 – 3.08 (m, 5H), 1.36 (s, 9H).

¹³C NMR (126 MHz, DMSO-*d*₆) δ 182.6, 182.4, 168.0, 167.4, 157.9, 157.7, 155.7, 153.2, 140.0, 139.6, 139.2, 131.1, 128.4, 127.9, 127.8, 127.7, 127.0, 118.5, 103.6, 77.8, 46.4, 43.2, 41.1, 38.6, 35.9, 28.2.

HRMS (ESI) *m/z* calcd. for C₃₁H₃₈O₆N₈ClS [M+H]⁺: 685.23181, found: 685.23068.

Melting point: 237 °C.

tert-Butyl(2-((2-((4-((5-chloro-4-(((2-(*N*-methylmethylsulfonamido)pyridin-3-yl)methyl)amino)pyrimidin-2-yl)amino)benzyl)amino)-3,4-dioxocyclobut-1-en-1-yl)amino)ethyl) carbamate (**55**)



Following the general procedure F, from **50** (300 mg, 0.67 mmol) and **11** (181 mg, 0.67 mmol), the title compound was obtained as beige solid (267 mg, 58%).

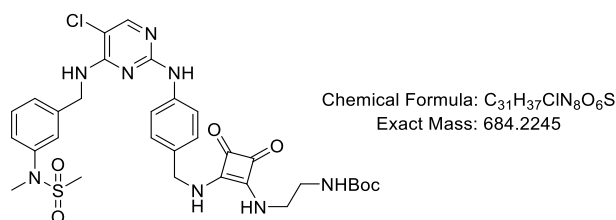
¹H NMR (500 MHz, DMSO-*d*₆) δ 9.18 (s, 1H), 8.43 (dd, *J* = 4.7, 1.9 Hz, 1H), 8.01 (s, 1H), 7.73 – 7.68 (m, 1H), 7.66 (t, *J* = 6.0 Hz, 1H), 7.45 – 7.39 (m, 3H), 7.04 (d, *J* = 8.1 Hz, 2H), 6.87 (d, *J* = 5.8 Hz, 1H), 4.76 (d, *J* = 5.9 Hz, 2H), 4.63 – 4.52 (m, 2H), 3.51 (s, 2H), 3.15 (s, 6H), 3.09 (q, *J* = 6.0 Hz, 2H), 1.35 (s, 9H).

^{13}C NMR (126 MHz, $\text{DMSO-}d_6$) δ 182.6, 182.4, 168.0, 167.3, 157.9, 157.7, 155.7, 153.3, 152.2, 147.3, 139.9, 137.1, 133.9, 131.2, 127.7, 124.0, 118.5, 103.7, 77.8, 46.4, 43.2, 41.1, 37.1, 36.0, 28.2.

HRMS (ESI) m/z calcd. for $\text{C}_{30}\text{H}_{37}\text{O}_6\text{N}_9\text{ClS}$ $[\text{M}+\text{H}]^+$: 686.22705 found: 686.22590.

Melting point: 209 °C.

tert-Butyl (2-((2-((4-((5-chloro-4-((3-(*N*-methylmethylsulfonamido)benzyl)amino)pyrimidin-2-yl)amino)benzyl)amino)-3,4-dioxocyclobut-1-en-1-yl)amino)ethyl)carbamate (**56**)



Following the general procedure F, from **51** (200 mg, 0.45 mmol) and **11** (122 mg, 0.45 mmol), the title compound was obtained as white solid (252 mg, 82%).

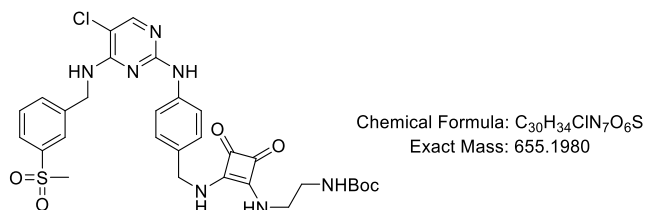
^1H NMR (500 MHz, $\text{DMSO-}d_6$) δ 9.22 (s, 1H), 7.98 (s, 1H), 7.83 (t, $J = 6.1$ Hz, 1H), 7.59 (d, $J = 8.4$ Hz, 2H), 7.42 (t, $J = 1.9$ Hz, 1H), 7.37 (t, $J = 7.8$ Hz, 1H), 7.30 – 7.24 (m, 2H), 7.16 (d, $J = 8.3$ Hz, 2H), 6.88 (t, $J = 5.7$ Hz, 1H), 4.63 (m, 4H), 3.52 (s, 2H), 3.32 (s, 2H), 3.18 (s, 3H), 3.10 (q, $J = 6.0$ Hz, 2H), 2.88 (s, 3H), 1.37 (s, 9H).

^{13}C NMR (126 MHz, $\text{DMSO-}d_6$) δ 182.6, 182.4, 168.0, 167.3, 157.8, 157.4, 155.7, 153.2, 141.6, 140.7, 140.0, 131.1, 128.9, 127.7, 125.7, 125.0, 124.5, 118.7, 103.6, 77.8, 46.5, 43.2, 41.2, 37.8, 34.9, 28.2.

HRMS (ESI) m/z calcd. for $\text{C}_{31}\text{H}_{38}\text{O}_6\text{N}_8\text{ClS}$ $[\text{M}+\text{H}]^+$: 685.23181, found: 685.23092.

Melting point: 234 °C.

tert-Butyl(2-((2-((4-((5-chloro-4-((3-(methylsulfonyl)benzyl)amino)pyrimidin-2-yl)amino)benzyl)amino)-3,4-dioxocyclobut-1-en-1-yl)amino)ethyl)carbamate (**57**)



Following the general procedure F, from **52** (260 mg, 0.6 mmol) and **11** (162 mg, 0.60 mmol), the title compound was obtained as white solid (269 mg, 68%).

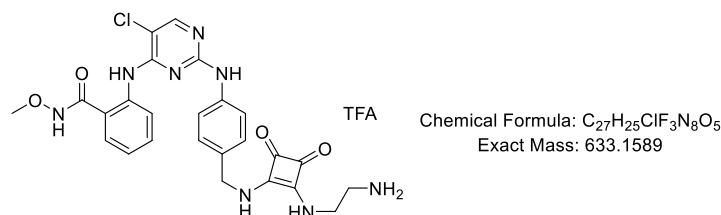
¹H NMR (500 MHz, DMSO-*d*₆) δ 9.23 (s, 1H), 8.00 (s, 1H), 7.97 – 7.89 (m, 2H), 7.80 (d, *J* = 7.6 Hz, 1H), 7.69 (d, *J* = 7.7 Hz, 1H), 7.61 (t, *J* = 7.7 Hz, 1H), 7.55 (d, *J* = 8.2 Hz, 2H), 7.15 (d, *J* = 8.2 Hz, 2H), 6.88 (t, *J* = 5.7 Hz, 1H), 4.72 (d, *J* = 6.1 Hz, 2H), 4.61 (d, *J* = 5.9 Hz, 2H), 3.52 (s, 2H), 3.14 (s, 3H), 3.10 (q, *J* = 6.0 Hz, 2H), 1.36 (s, 9H).

¹³C NMR (126 MHz, DMSO-*d*₆) δ 182.6, 182.4, 168.0, 167.4, 157.9, 157.3, 155.7, 153.3, 141.3, 140.8, 139.9, 132.1, 131.2, 129.4, 127.7, 125.3, 125.1, 118.7, 103.6, 77.8, 46.5, 43.4, 43.3, 41.1, 28.2.

HRMS (ESI) *m/z* calcd. for C₃₀H₃₅O₆N₇ClS [M+H]⁺: 656.20526, found: 656.20439.

Melting point: 186 °C.

2-((2-((4-(((2-((2-Aminoethyl)amino)-3,4-dioxocyclobut-1-en-1-yl)amino)methyl)phenyl)amino)-5-chloropyrimidin-4-yl)amino)-*N*-methoxybenzamide trifluoroacetate salt (**58**)



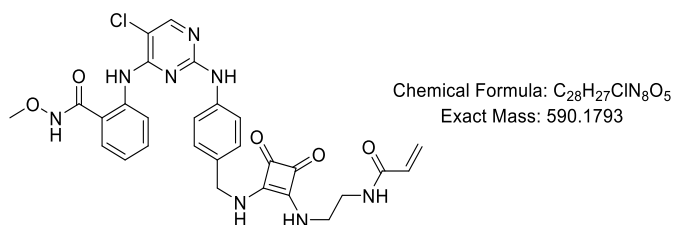
Following the general procedure E, from compound **53** (193 mg, 0.3 mmol) the titled compound was obtained as solid (245 mg, quant). The product was directly used for the next step without further purification.

^1H NMR (500 MHz, DMSO- d_6) δ 12.02 (s, 1H), 10.99 (s, 1H), 9.66 (s, 1H), 8.63 (d, J = 8.3 Hz, 1H), 8.26 (s, 1H), 8.15 (s, 1H), 7.92 (s, 3H), 7.77 (s, 1H), 7.63 (t, J = 7.7 Hz, 3H), 7.49 (t, J = 8.0 Hz, 1H), 7.26 (d, J = 8.2 Hz, 2H), 7.15 (t, J = 7.6 Hz, 1H), 4.67 (s, 2H), 3.73 (d, J = 10.5 Hz, 5H), 3.03 (q, J = 6.0 Hz, 2H).

^{13}C NMR (126 MHz, DMSO- d_6) δ 182.9, 182.5, 168.0, 165.9, 157.0, 155.2, 153.5, 139.1, 138.8, 132.6, 131.8, 127.9, 127.9, 122.6, 122.1, 120.2, 119.5, 117.0, 114.7, 105.2, 63.4, 46.5, 41.0.

HRMS (ESI) m/z calcd. for $\text{C}_{25}\text{H}_{26}\text{ClN}_8\text{O}_4$ 537.17601 found 537.17561.

2-((2-((4-(((2-((2-Acrylamidoethyl)amino)-3,4-dioxocyclobut-1-en-1-yl)amino)methyl)phenyl)amino)-5-chloropyrimidin-4-yl)amino)-*N*-methoxybenzamide (**59**)



To an ice-cooled solution of **58** (100 mg, 0.13 mmol) in dry DMF was added DIPEA (113 μL , 0.65 mmol) and acryloyl chloride (17 μL , 0.2 mmol). The mixture was stirred at room temperature for 12 h. The solvent was removed *in vacuo* and the crude product was purified by column chromatography (eluent, DCM/MeOH=10/1) to give the title compound as white solid (21.6 mg, 28%)

^1H NMR (500 MHz, DMSO- d_6) δ 8.62 (d, J = 8.3 Hz, 1H), 8.20 (s, 1H), 7.60 (t, J = 7.0 Hz, 3H), 7.48 (t, J = 8.0 Hz, 1H), 7.23 (d, J = 8.1 Hz, 2H), 7.13 (t, J = 7.6 Hz, 1H), 6.23

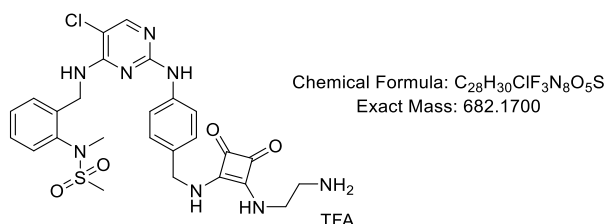
– 6.04 (m, 2H), 5.59 (dd, $J = 9.9, 2.2$ Hz, 1H), 4.64 (s, 2H), 3.72 (s, 3H), 3.59 (s, 2H), 3.30 (t, $J = 6.1$ Hz, 2H).

^{13}C NMR (126 MHz, DMSO- d_6) δ 182.8, 182.6, 168.2, 167.6, 166.2, 165.5, 157.8, 155.2, 154.9, 139.52 139.0, 132.4, 132.1, 131.5, 128.1, 128.0, 125.9, 122.7, 122.2, 120.1, 119.5, 105.2, 63.7, 46.6, 43.0, 42.0.

HRMS (ESI) m/z calcd. for $[\text{M}-\text{H}]^-$: $\text{C}_{28}\text{H}_{26}\text{ClN}_8\text{O}_5$, 589.17092, found: 589.17023.

Melting point: 234 °C.

N-(2-(((2-(((4-(((2-((2-Aminoethyl)amino)-3,4-dioxocyclobut-1-en-1-yl)amino)methyl)phenyl)amino)-5-chloropyrimidin-4-yl)amino)methyl)phenyl)-*N*-methylmethanesulfonamide trifluoroacetate salt (**60**)



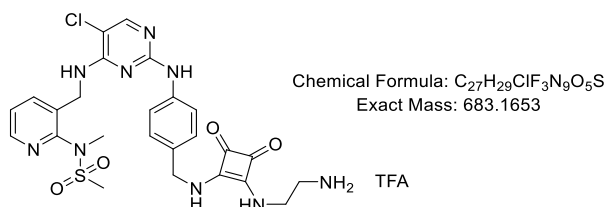
Following the general procedure E, from compound **54** (209 mg, 0.3 mmol) the titled compound was obtained as white solid (249 mg, quantitative). The product was directly used for next step without further purification.

^1H NMR (500 MHz, Methanol- d_4) δ 8.00 (s, 1H), 7.52 (d, $J = 7.8$ Hz, 1H), 7.42 (td, $J = 7.6, 1.8$ Hz, 1H), 7.39 – 7.30 (m, 4H), 7.26 (d, $J = 8.2$ Hz, 2H), 4.96 (d, $J = 15.9$ Hz, 2H), 4.74 (d, $J = 8.7$ Hz, 2H), 3.87 (t, $J = 6.0$ Hz, 2H), 3.20 (t, $J = 6.0$ Hz, 2H), 3.13 (s, 3H), 3.04 (s, 3H).

^{13}C NMR (126 MHz, Methanol- d_4) δ 184.2, 184.0, 169.8, 169.3, 160.7, 153.2, 142.1, 141.4, 138.6, 137.7, 130.0, 130.0, 129.7, 129.6, 128.3, 123.4, 119.2, 106.6, 48.2, 43.0, 42.5, 41.5, 39.4, 35.9.

HRMS (ESI) m/z calcd. for $\text{C}_{26}\text{H}_{30}\text{O}_4\text{N}_8\text{ClS}$ $[\text{M}+\text{H}]^+$: 585.17938, found: 585.17836.

N-(3-(((2-(((4-(((2-((2-Aminoethyl)amino)-3,4-dioxocyclobut-1-en-1-yl)amino)methyl)phenyl)amino)-5-chloropyrimidin-4-yl)amino)methyl)pyridin-2-yl)-*N*-methylmethanesulfonamide trifluoroacetate salt (**61**)



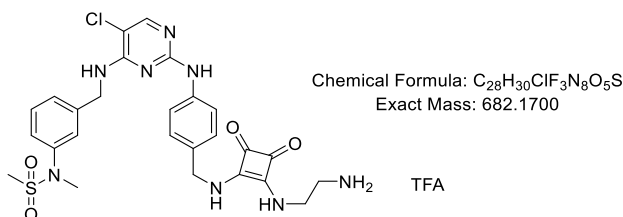
Following the general procedure E, from compound **55** (178 mg, 0.28 mmol) the titled compound was obtained as pale white solid (241 mg, quantitative). The product was directly used for next step without further purification.

¹H NMR (500 MHz, Methanol-*d*₄) δ 8.44 (dd, *J* = 4.7, 1.8 Hz, 1H), 8.00 (s, 1H), 7.73 (dd, *J* = 7.8, 1.8 Hz, 1H), 7.36 (dd, *J* = 7.8, 5.0 Hz, 3H), 7.26 (d, *J* = 8.3 Hz, 2H), 4.90 (s, 2H), 4.74 (s, 2H), 3.88 (t, *J* = 6.0 Hz, 2H), 3.21 (t, *J* = 5.9 Hz, 2H), 3.12 (s, 3H), 3.10 (s, 3H).

¹³C NMR (126 MHz, Methanol-*d*₄) δ 184.2, 184.0, 169.8, 169.2, 160.8, 154.1, 154.0, 149.3, 143.6, 139.1, 138.0, 134.0, 129.6, 125.4, 123.2, 119.2, 106.6, 44.6, 42.5, 42.4, 41.5, 37.9, 36.3.

HRMS (ESI) *m/z* calcd. for C₂₅H₂₉O₄N₉ClS [M+H]⁺: 586.17463, found: 586.17391.

N-(3-(((2-(((4-(((2-((2-Aminoethyl)amino)-3,4-dioxocyclobut-1-en-1-yl)amino)methyl)phenyl)amino)-5-chloropyrimidin-4-yl)amino)methyl)phenyl)-*N*-methylmethanesulfonamide trifluoroacetate salt (**62**)



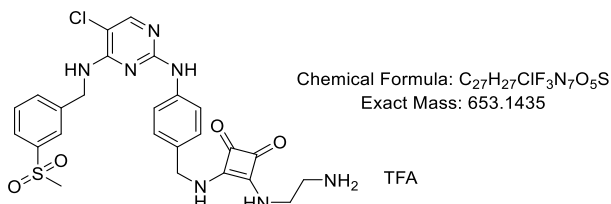
Following the general procedure E, from compound **56** (230 mg, 0.34 mmol) the titled compound was obtained as pale white solid (309 mg, quantitative). The product was directly used for next step without further purification.

¹H NMR (500 MHz, Methanol-*d*₄) δ 7.90 (s, 1H), 7.32 – 7.20 (m, 8H), 7.13 (dt, *J* = 7.6, 1.4 Hz, 1H), 4.68 (s, 2H), 4.62 (s, 2H), 3.77 (s, 2H), 3.70 – 3.66 (m, 1H), 3.12 (d, *J* = 5.4 Hz, 6H), 2.68 (s, 3H).

¹³C NMR (126 MHz, DMSO-*d*₆) δ 182.6, 182.4, 168.0, 167.3, 157.8, 157.4, 155.7, 153.2, 141.6, 140.7, 140.0, 131.1, 128.9, 127.7, 125.7, 125.0, 124.5, 118.7, 103.6, 77.8, 46.5, 43.3, 43.2, 41.1, 37.8, 34.9, 28.2.

HRMS (ESI) *m/z* calcd. for C₂₆H₃₀O₄N₈ClS [M+H]⁺ : 585.17938, found: 585.17886.

3-((2-Aminoethyl)amino)-4-((4-((5-chloro-4-((3-(methylsulfonyl)benzyl)amino)pyrimidin-2-yl)amino)benzyl)amino)cyclobut-3-ene-1,2-dione trifluoroacetate salt (**63**)

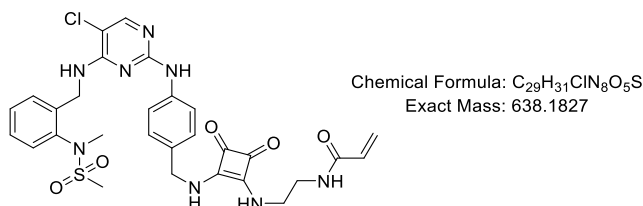


Following the general procedure E, from compound **57** (50 mg, 0.08 mmol) the titled compound was obtained as pale white solid (70 mg, quantitative). The product was directly used for next step without further purification.

¹H NMR (250 MHz, Methanol-*d*₄) δ 7.91 – 7.81 (m, 2H), 7.64 – 7.57 (m, 2H), 7.41 – 7.33 (m, 3H), 4.84 – 4.73 (m, 4H), 3.88 (t, *J* = 6.0 Hz, 2H), 3.20 (t, *J* = 6.0 Hz, 2H), 3.02 (s, 3H).

HRMS (ESI) *m/z* calcd. for C₂₅H₂₇O₄N₇ClS [M+H]⁺ : 556.15283, found: 556.15204.

N-(2-((2-((4-((5-Chloro-4-((2-(*N*-methylmethylsulfonamido)benzyl)amino)pyrimidin-2-yl)amino)benzyl)amino)-3,4-dioxocyclobut-1-en-1-yl)amino)ethyl)acrylamide (**64**)



To an ice-cooled solution of compound **60** (150 mg, 0.17 mmol) in dry DMF was added Et₃N (119 μL, 0.85 mmol) and acryloyl chloride (22 μL, 0.26 mmol). The mixture was stirred at room temperature for 9 h. The solvent was removed *in vacuo* and the crude product was purified by column chromatography (eluent, DCM/MeOH = 20/1) to give the title compound as white solid (59 mg, 56%).

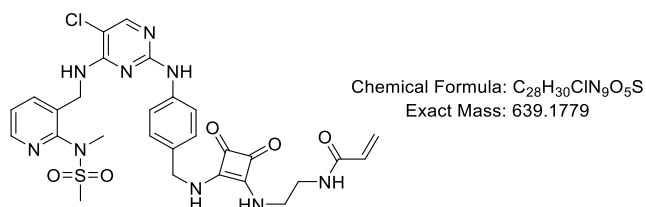
¹H NMR (500 MHz, DMSO-*d*₆) δ 9.22 (s, 1H), 8.26 (t, *J* = 5.6 Hz, 1H), 8.01 (s, 1H), 7.58 (t, *J* = 6.0 Hz, 1H), 7.55 – 7.51 (m, 1H), 7.46 (d, *J* = 8.1 Hz, 2H), 7.35 (dt, *J* = 5.5, 2.0 Hz, 2H), 7.30 (d, *J* = 5.5 Hz, 1H), 7.06 (d, *J* = 8.1 Hz, 2H), 6.19 (dd, *J* = 17.1, 10.1 Hz, 1H), 6.08 (dd, *J* = 17.1, 2.3 Hz, 1H), 5.59 (dd, *J* = 10.0, 2.3 Hz, 1H), 4.78 (t, *J* = 7.3 Hz, 2H), 4.58 (s, 2H), 3.73 – 3.53 (m, 2H), 3.31 (q, *J* = 5.8 Hz, 2H), 3.16 (s, 3H), 3.11 (s, 3H).

¹³C NMR (126 MHz, DMSO-*d*₆) δ 182.6, 182.4, 167.9, 167.4, 165.0, 157.7, 152.8, 139.8, 139.5, 139.1, 131.5, 131.2, 128.4, 127.8, 127.8, 127.6, 127.0, 125.3, 118.6, 103.6, 46.4, 42.8, 40.3, 38.6, 35.9.

HRMS (ESI) *m/z* calcd. for C₂₉H₃₂O₅N₈ClS [M+H]⁺: 639.18994, found: 639.18772.

Melting point: 219 °C (degradation).

N-(2-((2-((4-((5-Chloro-4-(((2-(*N*-methylmethylsulfonamido)pyridin-3-yl)methyl)amino) pyrimidin-2-yl)amino)benzyl)amino)-3,4-dioxocyclobut-1-en-1-yl)amino)ethyl) acrylamide (**65**)



To an ice-cooled solution of compound **61** (115 mg, 0.13 mmol) in dry DMF was added Et₃N (91 μL, 0.65 mmol) and acryloyl chloride (22 μL, 0.26 mmol). The mixture was stirred at room temperature for 9 h. The solvent was removed *in vacuo* and the crude product was purified by column chromatography (eluent, DCM/MeOH = 20/1) to give the title compound as white solid (42 mg, 50%).

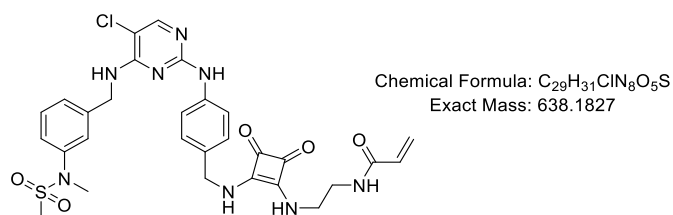
¹H NMR (500 MHz, DMSO-*d*₆) δ 9.24 (s, 1H), 8.43 (d, *J* = 4.7 Hz, 1H), 8.26 (t, *J* = 5.8 Hz, 1H), 8.02 (s, 1H), 7.76 – 7.69 (m, 2H), 7.41 (dd, *J* = 12.6, 7.9 Hz, 3H), 7.04 (d, *J* = 8.2 Hz, 2H), 6.19 (dd, *J* = 17.1, 10.1 Hz, 1H), 6.08 (dd, *J* = 17.2, 2.3 Hz, 1H), 5.58 (dd, *J* = 10.0, 2.3 Hz, 1H), 4.76 (d, *J* = 5.9 Hz, 2H), 4.64 – 4.48 (m, 2H), 3.58 (s, 2H), 3.31 (q, *J* = 6.6, 6.2 Hz, 2H), 3.14 (s, 6H).

¹³C NMR (126 MHz, DMSO-*d*₆) δ 182.6, 182.5, 167.9, 167.4, 165.0, 157.7, 157.5, 152.7, 152.2, 147.3, 139.6, 137.1, 133.8, 131.5, 127.7, 125.3, 124.0, 118.6, 103.7, 46.4, 42.8, 40.1, 37.1, 36.0.

HRMS (ESI) *m/z* calcd. for C₂₈H₂₉O₅N₉ClS [M-H]⁻: 638.16954, found: 638.16895.

Melting point: 179 °C.

N-(2-((2-((4-((5-Chloro-4-((3-(*N*-methylmethylsulfonamido)benzyl)amino)pyrimidin-2-yl)amino)benzyl)amino)-3,4-dioxocyclobut-1-en-1-yl)amino)ethyl)acrylamide (**66**)



To an ice-cooled solution of compound **62** (150 mg, 0.17 mmol) in dry DMF was added Et₃N (119 μ L, 0.85 mmol) and acryloyl chloride (22 μ L, 0.26 mmol). The mixture was stirred at room temperature for 13 h. The solvent was removed *in vacuo* and the crude product was purified by column chromatography (eluent, DCM/MeOH = 40/1 ~ 20/1) to give the title compound as pale white solid (67 mg, 61%).

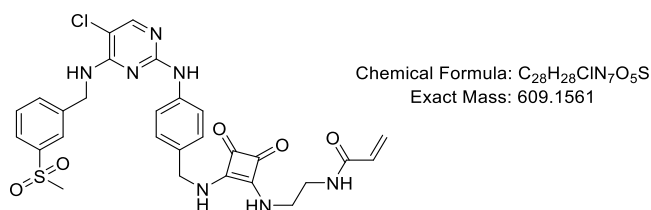
¹H NMR (500 MHz, DMSO-*d*₆) δ 9.22 (s, 1H), 8.26 (t, *J* = 6.0 Hz, 1H), 7.98 (s, 1H), 7.84 (t, *J* = 6.1 Hz, 1H), 7.59 (d, *J* = 8.2 Hz, 2H), 7.41 (s, 1H), 7.36 (t, *J* = 7.8 Hz, 1H), 7.30 – 7.25 (m, 2H), 7.16 (d, *J* = 8.2 Hz, 2H), 6.20 (dd, *J* = 17.1, 10.1 Hz, 1H), 6.09 (dd, *J* = 17.1, 2.3 Hz, 1H), 5.59 (dd, *J* = 10.0, 2.3 Hz, 1H), 4.63 (m, 4H), 3.59 (s, 2H), 3.32 (d, *J* = 6.2 Hz, 2H), 3.17 (s, 3H), 2.88 (s, 3H).

¹³C NMR (126 MHz, DMSO-*d*₆) δ 182.6, 182.5, 168.0, 167.4, 165.0, 157.8, 157.4, 153.2, 141.6, 140.7, 140.0, 131.5, 131.2, 128.9, 127.8, 125.7, 125.3, 125.1, 124.6, 118.7, 103.6, 46.5, 43.3, 42.8, 37.8, 34.9.

HRMS (ESI) *m/z* calcd. for C₂₉H₃₂O₅N₈ClS [M+H]⁺: 639.18994, found: 639.18925.

Melting point: 153 °C.

N-(2-((2-((4-((5-Chloro-4-((3-(methylsulfonyl)benzyl)amino)pyrimidin-2-yl)amino)benzyl)amino)-3,4-dioxocyclobut-1-en-1-yl)amino)ethyl)acrylamide (**67**)



To an ice-cooled solution of compound **63** (70 mg, 0.07 mmol) in dry DMF was added Et₃N (50 μL, 0.35 mmol) and acryloyl chloride (10 μL, 0.11 mmol). The mixture was stirred at room temperature for 16 h. The solvent was removed *in vacuo* and the crude product was purified by column chromatography (eluent, DCM/MeOH = 20/1 ~ 15/1) to give the title compound as white solid (28 mg, 65%).

¹H NMR (500 MHz, DMSO-*d*₆) δ 9.23 (s, 1H), 8.25 (t, *J* = 5.9 Hz, 1H), 7.99 (s, 1H), 7.94 (t, *J* = 6.2 Hz, 1H), 7.91 (s, 1H), 7.79 (d, *J* = 7.7 Hz, 1H), 7.68 (d, *J* = 7.7 Hz, 1H), 7.60 (t, *J* = 7.7 Hz, 1H), 7.54 (d, *J* = 8.1 Hz, 2H), 7.14 (d, *J* = 8.1 Hz, 2H), 6.24 – 6.03 (m, 2H), 5.58 (dd, *J* = 10.0, 2.3 Hz, 1H), 4.71 (d, *J* = 6.1 Hz, 2H), 4.66 – 4.54 (m, 2H), 3.58 (s, 2H), 3.31 (d, *J* = 6.0 Hz, 2H), 3.13 (s, 3H).

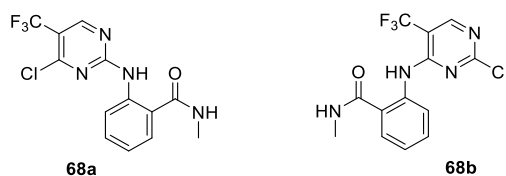
¹³C NMR (126 MHz, DMSO-*d*₆) δ 182.6, 182.4, 168.0, 167.43 165.0, 157.8, 157.4, 153.3, 141.3, 140.8, 139.9, 132.1, 131.5, 131.3, 129.4, 127.7, 125.3, 125.3, 125.1, 118.7, 103.6, 46.5, 43.4, 43.3, 42.8, 40.1.

HRMS (ESI) *m/z* calcd. for C₂₈H₂₉O₅N₇ClS [M+H]⁺ : 610.16449, found: 610.16272.

Melting point: 198 °C.

2-((4-Chloro-5-(trifluoromethyl)pyrimidin-2-yl)amino)-*N*-methylbenzamide (**68a**)

2-((2-Chloro-5-(trifluoromethyl)pyrimidin-4-yl)amino)-*N*-methylbenzamide (**68b**)



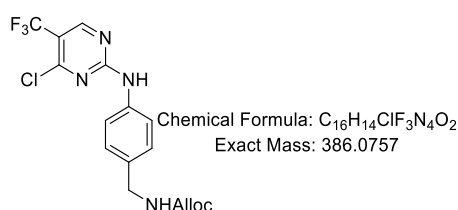
Chemical Formula: C₁₃H₁₀ClF₃N₄O
Exact Mass: 330.0495

To a solution of 2,4-dichloro-5-trifluoropyrimidine (180 μ L, 1.33 mmol) in *n*-BuOH (3 mL) was added compound **1** (200 mg, 1.33 mmol) and DIPEA (290 μ L, 1.66 mmol) at room temperature. The mixture was stirred at room temperature overnight. The mixture was diluted by DCM, washed with water and brine. The organic layer was dried over MgSO₄ and concentrated under reduced pressure. The residue was purified by column chromatography (eluent, cyclohexane/ethyl acetate = 4/1) to give titled compounds as white solid (365 mg, 83%).

68a: ¹H NMR (250 MHz, Chloroform-*d*) δ 11.35 (s, 1H), 8.63 – 8.54 (m, 2H), 7.57 – 7.43 (m, 2H), 7.10 (td, *J* = 7.6, 1.1 Hz, 1H), 6.23 (s, 1H), 3.03 (d, *J* = 4.9 Hz, 3H).

68b: ¹H NMR (250 MHz, Chloroform-*d*) δ 11.61 (s, 1H), 8.56 (dd, *J* = 8.5, 1.1 Hz, 1H), 8.45 (q, *J* = 1.0 Hz, 1H), 7.61 – 7.44 (m, 2H), 7.21 – 7.11 (m, 1H), 6.25 (s, 1H), 3.02 (d, *J* = 4.9 Hz, 3H).

Allyl (4-((4-chloro-5-(trifluoromethyl)pyrimidin-2-yl)amino)benzyl)carbamate (**69a**)



To a solution of 2,4-dichloro-5-(trifluoromethyl)pyrimidine (200 μ L, 1.48 mmol) in mixed *t*-BuOH/DCM (v/v=1/1, 10 mL) was added zinc chloride (403 mg, 2.96 mmol) at 0 °C.

After 1 h, compound **6** (305 mg, 1.48 mmol) was added followed by dropwise addition of triethylamine (207 μ L, 1.48 mmol). After stirring for 6 hours, the mixture was diluted with DCM and washed with water and brine. The organic layer was dried over MgSO_4 . After filtration, the organic solution was concentrated *in vacuo*, and the residue was purified through silica gel chromatography (eluent: DCM/MeOH = 150/1) to give the titled compound as white solid (477 mg, 83%).

^1H NMR (500 MHz, Chloroform-*d*) δ 8.53 (s, 1H), 7.65 (s, 1H), 7.55 (d, $J = 8.3$ Hz, 2H), 7.30 (d, $J = 8.3$ Hz, 2H), 5.99 – 5.89 (m, 1H), 5.31 (dq, $J = 17.3, 1.7$ Hz, 1H), 5.22 (dp, $J = 10.5, 1.3$ Hz, 1H), 5.09 (s, 1H), 4.61 (d, $J = 5.6$ Hz, 2H), 4.37 (d, $J = 6.0$ Hz, 2H).

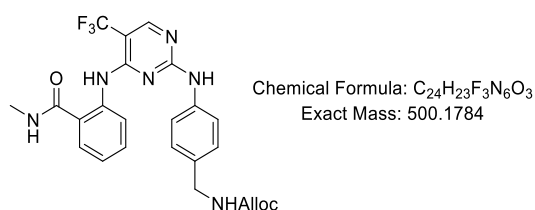
^{13}C NMR (126 MHz, Chloroform-*d*) δ 160.6, 157.5, 156.4, 136.9, 134.9, 132.9, 128.5, 123.8, 122.9, 121.6, 120.8, 117.9, 65.9, 44.7.

^{19}F NMR (471 MHz, Chloroform-*d*) δ -61.8.

HRMS (ESI) m/z calcd. for $\text{C}_{16}\text{H}_{15}\text{O}_2\text{N}_4\text{ClF}_3$ $[\text{M}+\text{H}]^+$: 387.08356, found: 387.08279.

Melting point: 154 $^\circ\text{C}$.

Allyl (4-((4-((2-(methylcarbamoyl)phenyl)amino)-5-(trifluoromethyl)pyrimidin-2-yl)amino)benzyl)carbamate (**70**)



To a solution **69b** (380 mg, 0.98 mmol) in DMF (5 mL) was added compound **1** (147 mg, 0.98 mmol) followed by addition of HCl (250 μ L, 4 M in 1,4-dioxane). The mixture was stirred at 90 $^\circ\text{C}$ for 7 hours. Then the solvent was removed *in vacuo*. DCM was added to the residue. Through filtration, the title compound was obtained as white solid (286 mg, 58%).

^1H NMR (500 MHz, DMSO-*d*₆) δ 11.35 (s, 1H), 9.81 (s, 1H), 8.79 (q, $J = 4.6$ Hz, 1H),

8.42 (s, 1H), 7.76 – 7.72 (m, 2H), 7.58 (d, $J = 8.0$ Hz, 2H), 7.45 (t, $J = 8.0$ Hz, 1H), 7.17 – 7.15 (m, 3H), 5.96 – 5.89 (m, 1H), 5.35 – 5.22 (m, 1H), 5.18 (d, $J = 10.5$ Hz, 1H), 4.50 (d, $J = 5.0$ Hz, 2H), 4.15 (d, $J = 6.2$ Hz, 2H), 2.78 (d, $J = 4.4$ Hz, 3H).

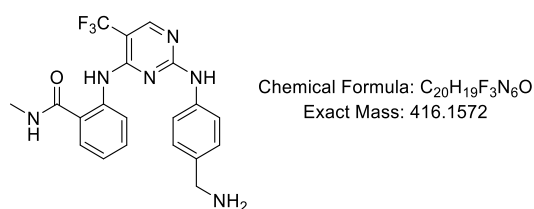
^{13}C NMR (126 MHz, DMSO- d_6) δ 168.8, 160.8, 156.1, 155.9, 138.6, 138.0, 134.0, 133.8, 131.1, 127.9, 127.2, 125.7, 123.5, 122.5, 120.5, 116.9, 64.3, 43.4, 26.2.

^{19}F NMR (471 MHz, DMSO- d_6) δ -59.9.

HRMS (ESI) m/z calcd. for $\text{C}_{24}\text{H}_{24}\text{O}_3\text{N}_6\text{F}_3$ $[\text{M}+\text{H}]^+$: 501.18620, found: 501.18442.

Melting point: 251 °C.

2-((2-((4-(Aminomethyl)phenyl)amino)-5-(trifluoromethyl)pyrimidin-4-yl)amino)-*N*-methylbenzamide (**71**)



Following the general procedure D, from compound **70** (260 mg, 0.52 mmol), $\text{Pd}(\text{PPh}_3)_4$ (88 mg, 0.076 mmol), morpholine (450 μL , 5.2 mmol) in mixed solution of THF (1 mL) and DMF (1.6 mL), titled compound was obtained as white solid (147 mg, 68%).

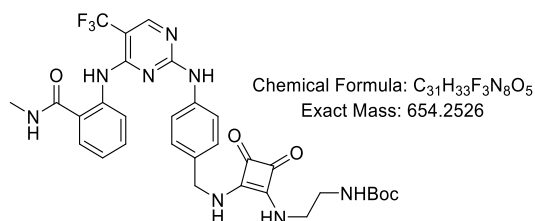
^1H NMR (500 MHz, Methanol- d_4) δ 8.37 (d, $J = 8.6$ Hz, 1H), 8.30 (d, $J = 1.1$ Hz, 1H), 7.63 (dd, $J = 7.9, 1.6$ Hz, 1H), 7.56 – 7.51 (m, 2H), 7.45 (ddd, $J = 8.6, 7.4, 1.7$ Hz, 1H), 7.25 (d, $J = 8.5$ Hz, 2H), 7.18 (td, $J = 7.6, 1.2$ Hz, 1H), 3.80 (d, $J = 3.0$ Hz, 2H), 2.89 (d, $J = 1.3$ Hz, 3H).

^{13}C NMR (126 MHz, Methanol- d_4) δ 171.6, 162.3, 158.1, 156.5, 139.5, 139.3, 132.5, 129.0, 128.8, 126.9, 125.1, 125.0, 124.8, 124.5, 122.4, 68.4, 26.9.

HRMS (ESI) m/z calcd. for $\text{C}_{20}\text{H}_{20}\text{ON}_6\text{F}_3$ $[\text{M}+\text{H}]^+$: 417.16507, found: 417.16470.

Melting point: 180 °C.

tert-Butyl (2-((2-((4-((2-(methylcarbamoyl)phenyl)amino)-5-(trifluoromethyl)pyrimidin-2-yl)amino)benzyl)amino)-3,4-dioxocyclobut-1-en-1-yl)amino)ethyl carbamate (**72**)



To a solution of **71** (132 mg, 0.32 mmol) and **11** (86 mg, 0.32 mmol) in dry DMF (1.5 mL) was added DIPEA (56 μ L, 0.32 mmol) at room temperature. Then the mixture was heated to 80 °C and stirred overnight. The solvent was removed under reduced pressure. MeOH was added to the residue and was filtered to give white solid. Then the filtrate was concentrated and purified by column chromatography (eluent: DCM/MeOH= 30/1 ~ 15/1) to give white solid. Two white solids were combined and dried (185 mg, 89%).

¹H NMR (500 MHz, DMSO-*d*₆) δ 11.34 (s, 1H), 9.84 (s, 1H), 8.71 (q, *J* = 4.6 Hz, 1H), 8.43 (s, 1H), 7.72 (dd, *J* = 7.9, 1.6 Hz, 1H), 7.63 (d, *J* = 8.1 Hz, 2H), 7.43 (t, *J* = 7.9 Hz, 1H), 7.36 (q, *J* = 5.0 Hz, 1H), 7.24 (d, *J* = 8.1 Hz, 2H), 7.15 (t, *J* = 7.6 Hz, 1H), 6.88 (t, *J* = 5.7 Hz, 1H), 4.66 (s, 2H), 3.58 – 3.45 (m, 2H), 3.10 (q, *J* = 6.0 Hz, 2H), 2.79 (d, *J* = 4.5 Hz, 3H), 1.35 (s, 9H).

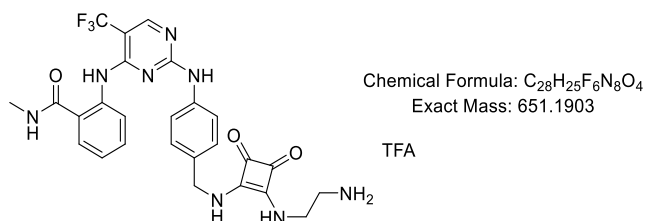
¹³C NMR (125 MHz, DMSO-*d*₆) δ 182.6, 182.5, 168.7, 168.1, 167.4, 160.7, 156.1, 155.9, 155.7, 138.6, 133.1, 132.5, 131.1, 127.8, 125.6, 124.4, 123.5, 123.1, 122.6, 122.1, 120.7, 77.8, 46.4, 43.2, 41.1, 28.2, 26.2.

¹⁹F NMR (471 MHz, DMSO-*d*₆) δ -59.9.

HRMS (ESI) *m/z* calcd. for C₃₁H₃₄O₅N₈F₃ [M+H]⁺: 655.26043, found: 655.26227.

Melting point: 258 °C.

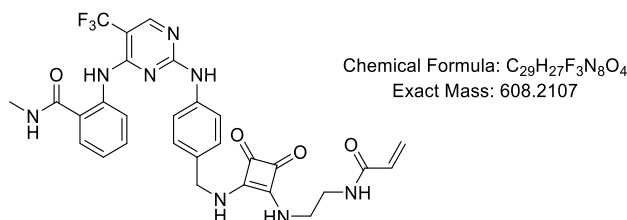
2-((2-((4-(((2-((2-Aminoethyl)amino)-3,4-dioxocyclobut-1-en-1-yl)amino)methyl)phenyl)amino)-5-(trifluoromethyl)pyrimidin-4-yl)amino)-N-methylbenzamide trifluoroacetate salt (**73**)



Following the general procedure E, from compound **72** (153 mg, 0.23 mmol) the titled compound was obtained as white solid (190 mg, quantitative). This compound was directly used in next step without further purification.

¹H NMR (500 MHz, DMSO-*d*₆) δ 11.35 (s, 1H), 9.86 (s, 1H), 8.73 (q, *J* = 4.5 Hz, 1H), 8.43 (s, 1H), 8.13 (d, *J* = 7.2 Hz, 1H), 7.90 (s, 3H), 7.72 (dd, *J* = 7.9, 1.6 Hz, 2H), 7.63 (d, *J* = 8.1 Hz, 2H), 7.44 (t, *J* = 8.0 Hz, 1H), 7.24 (d, *J* = 8.2 Hz, 2H), 7.15 (td, *J* = 7.6, 1.2 Hz, 1H), 4.66 (s, 2H), 3.72 (q, *J* = 6.2 Hz, 2H), 3.02 (p, *J* = 5.9 Hz, 2H), 2.78 (d, *J* = 4.6 Hz, 3H).

2-((2-((4-(((2-((2-Acrylamidoethyl)amino)-3,4-dioxocyclobut-1-en-1-yl)amino)methyl)phenyl)amino)-5-(trifluoromethyl)pyrimidin-4-yl)amino)-N-methylbenzamide (**74**)



To an ice-cooled solution of compound **73** (120 mg, 0.142 mmol) in dry DMF was added Et₃N (100 μL, 0.71 mmol) and acryloyl chloride (18 μL, 0.213 mmol). The mixture was stirred at room temperature for 16 h. The solvent was removed *in vacuo* and the crude

product was purified by column chromatography (eluent, DCM/MeOH = 20/1 ~ 15/1) to give the title compound as white solid (52 mg, 60%).

^1H NMR (500 MHz, DMSO- d_6) δ 11.33 (s, 1H), 9.85 (s, 1H), 8.79 – 8.65 (m, 1H), 8.43 (s, 2H), 8.27 (s, 1H), 7.72 (d, J = 7.9 Hz, 1H), 7.63 (d, J = 8.1 Hz, 2H), 7.43 (t, J = 7.9 Hz, 1H), 7.24 (d, J = 8.1 Hz, 2H), 7.15 (t, J = 7.6 Hz, 1H), 6.27 – 6.00 (m, 2H), 5.58 (d, J = 10.2 Hz, 1H), 4.66 (s, 2H), 3.59 (s, 2H), 2.79 (d, J = 4.6 Hz, 3H).

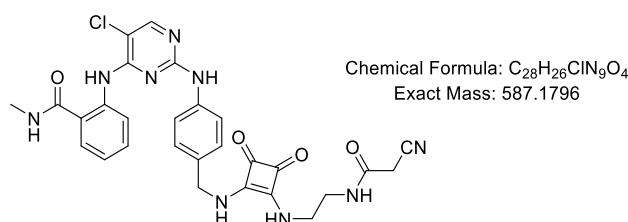
^{13}C NMR (126 MHz, DMSO- d_6) δ 182.7, 182.5, 168.7, 168.1, 167.5, 165.0, 160.8, 156.1, 155.9, 138.6, 133.1, 131.5, 131.1, 127.8, 125.6, 125.3, 123.5, 123.1, 122.6, 122.1, 120.7, 46.4, 42.8, 39.8, 26.2.

^{19}F NMR (471 MHz, DMSO- d_6) δ -59.9.

HRMS (ESI) m/z calcd. for $\text{C}_{29}\text{H}_{28}\text{O}_4\text{N}_8\text{F}_3$ $[\text{M}+\text{H}]^+$: 609.21856, found: 609.21967.

Melting point: 179 °C.

2-((5-Chloro-2-(((4-(((2-((2-cyanoacetamido)ethyl)amino)-3,4-dioxocyclobut-1-en-1-yl)amino)methyl)phenyl)amino)pyrimidin-4-yl)amino)-N-methylbenzamide (**75**)



To an ice-cold solution of **14** (500 mg, 0.67 mmol) in dry DMF (3 mL) was added DIPEA (700 μL , 4.01 mmol), EDCI (257 mg, 1.34 mmol), HOBT (181 mg, 1.34 mmol), followed by addition of cyanoacetic acid (114mg, 1.34 mmol). The mixture was stirred at 0 °C for 30 mins, then stirred at room temperature overnight. The solvent was removed *in vacuo*, then the residue was purified through silica gel column chromatography (eluent: DCM/MeOH= 20/1~10/1) to give the title compound as yellow solid (293 mg, 74%).

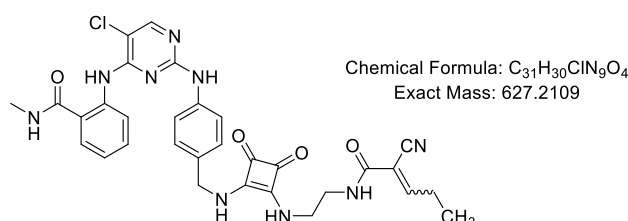
^1H NMR (500 MHz, $\text{DMSO-}d_6$) δ 11.61 (s, 1H), 9.49 (s, 1H), 8.74 (t, $J = 5.9$ Hz, 2H), 8.40 (t, $J = 5.7$ Hz, 1H), 8.22 (s, 1H), 7.76 (d, $J = 7.8$ Hz, 1H), 7.66 (d, $J = 8.2$ Hz, 2H), 7.47 (t, $J = 7.9$ Hz, 1H), 7.26 (d, $J = 8.1$ Hz, 2H), 7.14 (t, $J = 7.6$ Hz, 1H), 4.66 (s, 2H), 3.58 (s, 2H), 3.58 – 3.52 (m, 2H), 3.26 (q, $J = 6.0$ Hz, 2H), 2.82 (d, $J = 4.4$ Hz, 3H).

^{13}C NMR (126 MHz, $\text{DMSO-}d_6$) δ 182.7, 182.5, 168.9, 168.0, 167.5, 162.5, 157.7, 155.0, 154.6, 139.5, 139.2, 132.0, 131.4, 127.9, 127.9, 121.9, 121.4, 120.8, 119.8, 116.0, 105.2, 46.5, 42.6, 40.4, 26.3, 25.3.

HRMS (ESI) m/z calcd. for $\text{C}_{28}\text{H}_{27}\text{O}_4\text{N}_9\text{Cl}$ $[\text{M}+\text{H}]^+$: 588.18745, found:588.18890.

Melting point: 258 °C

2-((5-Chloro-2-(((4-(((2-((2-cyanopent-2-enamido)ethyl)amino)-3,4-dioxocyclobut-1-en-1-yl)amino)methyl)phenyl)amino)pyrimidin-4-yl)amino)-*N*-methylbenzamide (**76**)



Compound **20** (50 mg, 0.09 mmol), propionaldehyde (9 μL , 0.13 mmol) and piperidine (13 μL , 0.13 mmol) were added to a mixed solution of DMF and acetic acid ($v/v=1/1$). The solution was heated to 100 °C and stirred for 2 hours. After cooling to room temperature, the solvent was removed *in vacuo*. Subsequently, the crude product was purified through silica gel column chromatography (eluent: $\text{DCM}/\text{MeOH}= 20/1 \sim 15/1$) to give the desired product as off white solid (19 mg, 34%).

^1H NMR (500 MHz, $\text{DMSO-}d_6$) δ 11.61 (s, 1H), 9.49 (s, 1H), 8.80 – 8.68 (m, 2H), 8.46 (s, 1H), 8.22 (s, 1H), 7.76 (d, $J = 7.9$ Hz, 1H), 7.65 (d, $J = 8.1$ Hz, 2H), 7.47 (t, $J = 7.9$ Hz, 1H), 7.40 (t, $J = 7.7$ Hz, 1H), 7.25 (d, $J = 8.1$ Hz, 2H), 7.13 (t, $J = 7.6$ Hz, 1H), 4.66 (s,

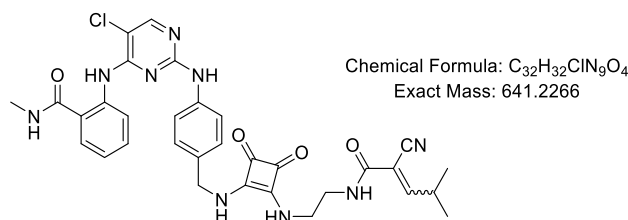
2H), 3.61 (s, 2H), 3.38 – 3.34 (m, 2H), 2.82 (d, $J = 4.5$ Hz, 3H), 2.42 (q, $J = 7.5$ Hz, 2H), 1.24 (s, 1H), 1.06 (t, $J = 7.5$ Hz, 2H).

^{13}C NMR (126 MHz, DMSO- d_6) δ 182.7, 182.4, 168.9, 168.1, 167.5, 160.7, 159.4, 157.7, 155.0, 154.6, 139.5, 139.2, 132.1, 131.4, 127.9, 127.8, 121.9, 121.4, 120.8, 119.8, 114.5, 111.3, 105.2, 46.5, 42.6, 40.7, 26.3, 24.8, 12.1.

HRMS (ESI) m/z calcd. for $\text{C}_{31}\text{H}_{31}\text{O}_4\text{N}_9\text{Cl}$ $[\text{M}+\text{H}]^+$: 628.21875, found: 628.22015.

Melting point: 194 °C.

2-((5-Chloro-2-(((4-(((2-((2-cyano-4-methylpent-2-enamido)ethyl)amino)-3,4-dioxocyclobut-1-en-1-yl)amino)methyl)phenyl)amino)pyrimidin-4-yl)amino)-*N*-methylbenzamide (**77**)



Compound **20** (100 mg, 0.17 mmol), isobutyraldehyde (23 μL , 0.26 mmol) and piperidine (25 μL , 0.26 mmol) were added to a mixed solution of DMF (0.5 mL) and acetic acid (0.5 mL). The solution was heated to 100 °C and stirred for 2 hours. After cooling to room temperature, the solvent was removed *in vacuo*. Subsequently, the crude product was purified through silica gel column chromatography (eluent: DCM/MeOH= 20/1 ~ 15/1) to give the desired product as off white solid (69 mg, 63%).

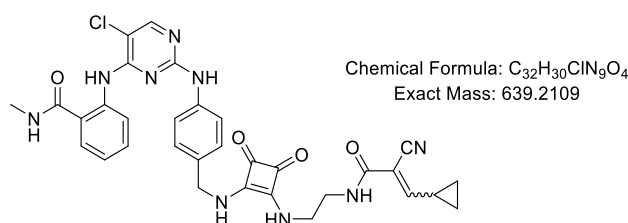
^1H NMR (500 MHz, DMSO- d_6) δ 11.60 (s, 1H), 9.47 (s, 1H), 8.87 – 8.65 (m, 2H), 8.46 (t, $J = 5.8$ Hz, 1H), 8.21 (s, 1H), 7.75 (d, $J = 7.9$ Hz, 1H), 7.65 (d, $J = 8.1$ Hz, 2H), 7.46 (t, $J = 7.8$ Hz, 1H), 7.25 (d, $J = 7.9$ Hz, 2H), 7.13 (t, $J = 7.5$ Hz, 1H), 4.66 (s, 2H), 3.60 (s, 2H), 3.37 – 3.33 (m, 2H), 2.81 (d, $J = 4.5$ Hz, 3H), 2.76 (dd, $J = 8.2, 4.8$ Hz, 1H), 1.68 (d, $J = 19.8$ Hz, 1H), 1.06 (d, $J = 6.6$ Hz, 5H).

^{13}C NMR (126 MHz, $\text{DMSO-}d_6$) δ 182.7, 182.5, 168.9, 168.1, 167.5, 163.4, 160.8, 157.7, 155.0, 154.6, 139.5, 139.2, 132.1, 131.4, 127.9, 127.8, 127.8, 121.9, 121.4, 120.8, 119.8, 114.5, 109.7, 105.2, 46.5, 42.6, 40.7, 31.2, 26.3, 21.1.

HRMS (ESI) m/z calcd. for $\text{C}_{32}\text{H}_{33}\text{O}_4\text{N}_9\text{Cl}$ $[\text{M}+\text{H}]^+$: 642.23440, found: 642.23553.

Melting point: 236 °C.

2-((5-Chloro-2-((4-(((2-((2-(2-cyano-3-cyclopropylacrylamido)ethyl)amino)-3,4-dioxocyclobut-1-en-1-yl)amino)methyl)phenyl)amino)pyrimidin-4-yl)amino)-*N*-methylbenzamide (**78**)



Compound **20** (100 mg, 0.17 mmol), cyclopropanecarbaldehyde (19 μL , 0.26 mmol) and piperidine (25 μL , 0.26 mmol) were added to a mixed solution of DMF (0.5 mL) and acetic acid (0.5 mL). The solution was heated to 100 °C and stirred for 2 hours. After cooling to room temperature, the solvent was removed *in vacuo*. Subsequently, the crude product was purified through silica gel column chromatography (eluent: DCM/MeOH= 20/1 ~ 15/1) to give the desired product as off white solid (69 mg, 63%).

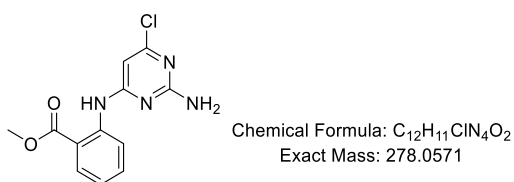
^1H NMR (500 MHz, $\text{DMSO-}d_6$) δ 11.62 (s, 1H), 9.49 (s, 1H), 8.75 (q, $J = 4.0$ Hz, 2H), 8.28 (t, $J = 5.7$ Hz, 1H), 8.23 (s, 1H), 7.77 (dd, $J = 8.0, 1.6$ Hz, 1H), 7.66 (d, $J = 8.1$ Hz, 2H), 7.47 (t, $J = 7.7$ Hz, 1H), 7.26 (d, $J = 8.3$ Hz, 2H), 7.14 (t, $J = 7.5$ Hz, 1H), 6.90 (d, $J = 11.1$ Hz, 1H), 4.67 (s, 2H), 3.68 – 3.52 (m, 2H), 3.35 (d, $J = 6.0$ Hz, 2H), 2.82 (d, $J = 4.5$ Hz, 3H), 1.89 (dtt, $J = 11.9, 7.9, 4.2$ Hz, 1H), 1.22 (dt, $J = 7.7, 3.7$ Hz, 2H), 0.97 – 0.86 (m, 2H).

^{13}C NMR (126 MHz, $\text{DMSO-}d_6$) δ 182.7, 182.5, 168.9, 168.1, 167.5, 164.0, 160.8, 157.7, 155.0, 154.6, 139.5, 139.2, 132.1, 131.4, 129.9, 127.8, 121.9, 121.4, 120.7, 119.8, 115.6, 107.5, 105.2, 46.5, 42.6, 40.6, 26.3, 15.4, 10.4.

HRMS (ESI) m/z calcd. for $\text{C}_{32}\text{H}_{31}\text{O}_4\text{N}_9\text{Cl}$ $[\text{M}+\text{H}]^+$: 640.21875, found: 640.21960.

Melting point: 248 °C.

Methyl 2-((2-amino-6-chloropyrimidin-4-yl)amino)benzoate (**79**)



A suspension of 2-amino-4,6-dichloropyrimidine (1 g, 6.0 mmol) and methyl 2-aminobenzoate (0.78 mL, 6.0 mmol) in *i*-PrOH (30 mL) was heated and refluxed for 12 h. The solvent was removed under reduced pressure and the residue was triturated with DCM (5 mL). The precipitate was filtered off to give the title compound as yellow solid (1.46 g, 85%).

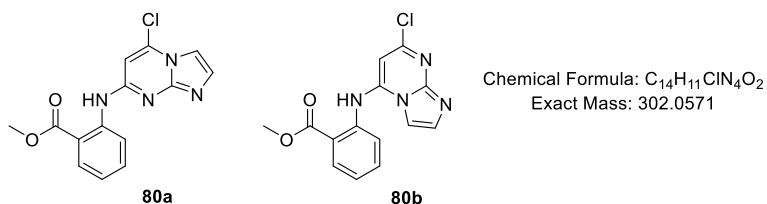
^1H NMR (250 MHz, $\text{DMSO-}d_6$) δ 10.17 (s, 1H), 8.23 (dd, $J = 8.4, 1.1$ Hz, 1H), 7.91 (dd, $J = 7.9, 1.7$ Hz, 1H), 7.59 (ddd, $J = 8.6, 7.3, 1.7$ Hz, 1H), 7.19 (td, $J = 7.6, 1.2$ Hz, 1H), 6.71 (s, 2H), 6.24 (s, 1H), 3.83 (s, 3H).

HRMS (ESI) calcd. for $\text{C}_{12}\text{H}_{12}\text{ClN}_4\text{O}_2$ $[\text{M}+\text{H}]^+$ 279.0649; found 279.0644.

Melting point: 224 °C.

Methyl 2-((5-chloroimidazo[1,2-a]pyrimidin-7-yl)amino)benzoate (**80a**)

Methyl 2-((7-chloroimidazo[1,2-a]pyrimidin-5-yl)amino)benzoate (**80b**)



Method A: In a sealed tube chloroacetaldehyde (7 mL, 50% in water, 55 mmol) was added to a solution of **79** (1.43 g, 5.14 mmol) in MeOH (15 mL). The mixture was stirred and refluxed for 14 h. After cooling to room temperature, saturated NaHCO₃ solution (50 mL) was added, and the mixture was extracted with ethyl acetate (50 mL*3). The combined organic phases were dried over MgSO₄ and concentrated. Subsequently, DCM (10 mL) was added to the residue and filtered to give the most part of **80a**. The filtrate was concentrated and purified by column chromatography (eluent: DCM/MeOH=80/1 ~50/1) give **80a** and **80b**. After the combination of two parts of the product, the title compound **80a** was obtained as white solid (797 mg, 51%) and **80b** was obtained as beige solid (274 mg, 18%).

Method B: To a solution of **82** (416 mg, 2.2 mmol) in dry DMF (10 mL) was added methyl 2-aminobenzoate (344 μL, 2.65 mmol). The solution was stirred at 100 °C for 2 h. After cooling to room temperature, NaOH solution (0.5 M, 20 mL) was added, the mixture was extracted with ethyl acetate (20 mL*3). The organic layer was washed with brine and dried over MgSO₄. Then the solvent was concentrated and the residue was purified by column chromatography (eluent: DCM/MeOH=100/1 ~ 50/1) to give title compound **80a** (42 mg, 6%) and **80b** (331 mg, 50%).

(**80a**): ¹H NMR (250 MHz, Chloroform-*d*) δ 10.91 (s, 1H), 8.17 (dt, *J* = 8.0, 1.1 Hz, 1H), 7.80 (d, *J* = 1.6 Hz, 1H), 7.74 – 7.62 (m, 4H), 7.33 – 7.18 (m, 2H), 6.81 (s, 1H), 5.32 (s, 1H), 4.01 (s, 3H).

¹³C NMR (126 MHz, Chloroform-*d*) δ 169.4, 152.7, 149.0, 142.7, 136.2, 135.0, 133.0,

131.0, 121.5, 120.5, 114.2, 108.8, 102.0, 52.4.

Melting point: 220 °C.

R_f (DCM/MeOH: 100/1): 0.21.

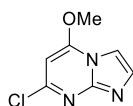
(80b): ¹H NMR (250 MHz, Chloroform-*d*) δ 11.13 (s, 1H), 9.34 (dd, *J* = 8.6, 1.2 Hz, 1H), 8.08 (dd, *J* = 8.0, 1.7 Hz, 1H), 7.64 (ddd, *J* = 8.8, 7.2, 1.7 Hz, 1H), 7.56 (d, *J* = 1.7 Hz, 1H), 7.49 (d, *J* = 1.7 Hz, 1H), 7.07 (ddd, *J* = 8.3, 7.3, 1.2 Hz, 1H), 6.58 (s, 1H), 3.98 (s, 3H).

¹³C NMR (126 MHz, Chloroform-*d*) δ 168.9, 152.5, 148.8, 143.6, 140.8, 135.2, 134.9, 134.6, 132.2, 123.7, 119.3, 106.0, 90.8, 53.0

Melting point: 184 °C.

R_f (DCM/MeOH: 100/1):0.15.

7-Chloro-5-methoxyimidazo[1,2-*a*]pyrimidine (**81**)



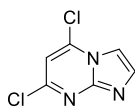
Chemical Formula: C₇H₆ClN₃O
Exact Mass: 183.0199

To a solution of 2-amino-4-chloro-6-methoxypyrimidine (500 mg, 3.13 mmol) in anhydrous ethanol (15 mL) was added chloroacetaldehyde (4 mL, 50%wt in H₂O). The mixture was heated at 100 °C overnight. Subsequently, the solvent was concentrated in vacuo. DCM was added to dissolve the residue. The organic solution was washed with 1 M NaOH solution, water, and brine. After drying over with MgSO₄, DCM was removed in vacuo to give the crude product. The crude residue was purified by silica gel chromatography (eluent: DCM/MeOH=80/1~50/1) to give the title compound as yellow oil (439 mg, 76%).

¹H NMR (500 MHz, Methanol-*d*₄) δ 7.70 (d, *J* = 1.8 Hz, 1H), 7.49 (d, *J* = 1.7 Hz, 1H), 6.80 (s, 1H), 4.03 (s, 3H).

¹³C NMR (126 MHz, Methanol-*d*₄) δ 164.8, 149.5, 139.1, 132.6, 110.7, 101.9, 55.1.

5,7-Dichloroimidazo[1,2-a]pyrimidine (**82**)



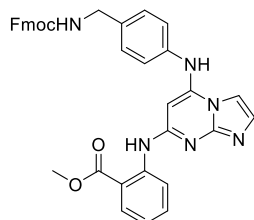
Chemical Formula: C₆H₃Cl₂N₃
Exact Mass: 186.9704

In a sealed tube **81** (439 mg, 2.39 mmol) was dissolved in a mixed solution of HBr (48% in water, 5.5 mL) and acetic acid (5 mL), The mixture was stirred at 120 °C for 1 day. Subsequently, the solution was removed in vacuo. Then POCl₃ (3 mL) was added to the flask containing the residue. The suspension was heated at 80 °C for 2 h. After cooling to room temperature, the solvent was removed under reduced pressure. The residue was dissolved in cooled water and pH was adjusted to 8 with 1 M NaOH solution. The solution was extracted with ethyl acetate. The organic phases were combined, washed with water and brine, and dried over MgSO₄. After concentration, the residue was purified by column chromatography (eluent: DCM/MeOH= 80/1) to give the title compound as beige solid (170 mg, 38%).

¹H NMR (500 MHz, Chloroform-*d*) δ 7.74 (d, *J* = 2.5 Hz, 1H), 7.64 (d, *J* = 2.6 Hz, 1H), 6.98 (s, 1H).

¹³C NMR (126 MHz, Chloroform-*d*) δ 150.0, 147.1, 137.3, 135.9, 110.2, 109.2.

Methyl 2-((5-((4-(((9H-fluoren-9-yl)methoxy)carbonyl)amino)methyl)phenyl)amino)imidazo[1,2-a]pyrimidin-7-yl)amino)benzoate (**83**)



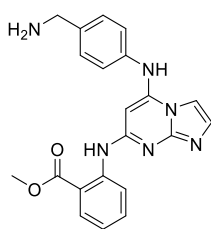
Chemical Formula: C₃₆H₃₀N₆O₄
Exact Mass: 610.2329

To a suspension of **80a** (200 mg, 0.66 mmol) in *i*-PrOH (8 mL) was added compound **4** (228 mg, 0.66 mmol) and HCl (20 μL, 4 M in 1,4-dioxane) at room temperature. The

mixture was refluxed for 20 h with stirring. After cooling to room temperature, the solvent was removed under reduced pressure, and the residue was purified by silica gel chromatography (eluent: DCM/MeOH=100/1~20/1) to give the title compound as white solid (189 mg, 47%).

¹H NMR (250 MHz, Chloroform-*d*) δ 10.58 (s, 1H), 9.11 (d, *J* = 8.5 Hz, 1H), 7.93 (dd, *J* = 8.0, 1.7 Hz, 1H), 7.76 – 7.74 (m, 3H), 7.60 (d, *J* = 7.4 Hz, 2H), 7.41 – 7.26 (m, 13H), 6.87 (t, *J* = 7.6 Hz, 1H), 5.76 (s, 1H), 4.48 (d, *J* = 6.8 Hz, 2H), 4.38 (d, *J* = 6.0 Hz, 2H), 4.23 (t, *J* = 6.6 Hz, 1H), 3.83 (s, 3H).

Methyl 2-((5-((4-(aminomethyl)phenyl)amino)imidazo[1,2-*a*]pyrimidin-7-yl)amino)benzoate (**84**)



Chemical Formula: C₂₁H₂₀N₆O₂
Exact Mass: 388.1648

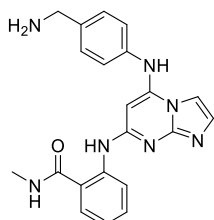
Compound **83** (184 mg, 0.3 mmol) was added to the mixed solution of DMF (2 mL) and piperidine (0.5 mL). The mixture stirred at room temperature for 3 h. Subsequently, the solvent was removed under reduced pressure. Ethyl ether was added to the remained residue and filtered to give the crude product as beige solid, then purification by silica gel chromatography (DCM/MeOH/NH₄OH = 10/1/0.01) to give the title compound as off-white solid (106 mg, 91%).

¹H NMR (500 MHz, DMSO-*d*₆) δ 10.11 (s, 1H), 8.78 (d, *J* = 8.5 Hz, 1H), 7.93 – 7.84 (m, 2H), 7.64 – 7.56 (m, 1H), 7.47 (d, *J* = 8.1 Hz, 2H), 7.37 – 7.31 (m, 3H), 7.03 (t, *J* = 7.6 Hz, 1H), 5.64 (s, 1H), 3.81 (s, 3H), 3.78 (s, 2H).

¹³C NMR (126 MHz, DMSO-*d*₆) δ 168.1, 154.4, 149.3, 146.4, 142.5, 141.4, 135.9, 133.9, 131.4, 130.5, 128.3, 124.2, 120.5, 120.1, 115.0, 106.2, 77.3, 52.2, 45.0.

Melting point: 164 °C.

2-((5-((4-(Aminomethyl)phenyl)amino)imidazo[1,2-a]pyrimidin-7-yl)amino)-N-methylbenzamide (**85**)



Chemical Formula: C₂₁H₂₁N₇O
Exact Mass: 387.1808

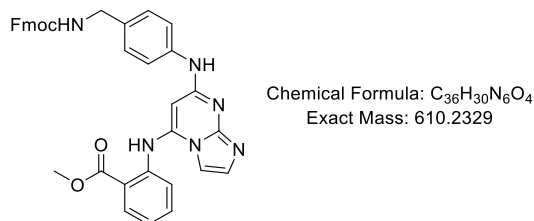
Compound **84** (66 mg, 0.17 mmol) was added to a solution of MeNH₂ in ethanol (wt 33%, 5 mL). The mixture was stirred at room temperature overnight. Subsequently, the solvent was removed under reduced pressure. The residue was purified by silica gel chromatography (eluent: DCM/MeOH/NH₄OH = 10/1/0.01) to give the product as white solid (40mg, 61%).

¹H NMR (500 MHz, DMSO-*d*₆) δ 10.90 (s, 1H), 8.86 (d, *J* = 8.5 Hz, 1H), 8.70 (q, *J* = 4.5 Hz, 1H), 7.93 – 7.83 (m, 1H), 7.67 (d, *J* = 7.9 Hz, 1H), 7.48 (d, *J* = 7.7 Hz, 3H), 7.42 – 7.32 (m, 3H), 6.99 (t, *J* = 7.5 Hz, 1H), 5.50 (s, 1H), 3.79 (s, 2H), 2.75 (d, *J* = 4.5 Hz, 3H).
¹³C NMR (126 MHz, DMSO-*d*₆) δ 169.2, 154.5, 149.5, 146.3, 141.4, 141.1, 135.9, 131.6, 131.2, 128.3, 127.9, 124.3, 120.2, 119.8, 119.2, 106.1, 77.1, 45.0, 26.2.

HRMS (ESI) calcd. for C₂₁H₂₂N₇O [M+H]⁺ : 388.1886; found 388.1884.

Melting point: over 260 °C .

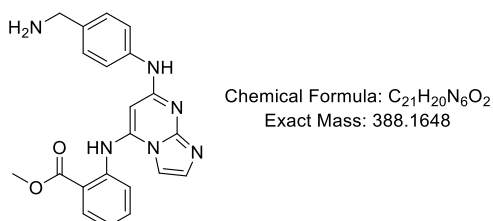
Methyl 2-((7-((4-(((9H-fluoren-9-yl)methoxy)carbonyl)amino)methyl)phenyl)amino)imidazo[1,2-a]pyrimidin-5-yl)amino)benzoate (**86**)



To a suspension of **80b** (150 mg, 0.5 mmol) in *i*-PrOH (8 mL) was added compound **4** (171 mg, 0.5 mmol) and HCl (15 μ L, 4 M in 1,4-dioxane) at room temperature. The mixture was refluxed for 20 h with stirring. After cooling to room temperature, the solvent was removed under reduced pressure, and the residue was purified by silica gel chromatography (eluent: DCM/MeOH=100/1~20/1) to give the title compound as white solid (192 mg, 64%).

¹H NMR (500 MHz, Chloroform-*d*) δ 10.42 (s, 1H), 7.97 (d, *J* = 7.6 Hz, 1H), 7.67 (dd, *J* = 7.7, 2.8 Hz, 2H), 7.58 – 7.36 (m, 8H), 7.33 – 7.24 (m, 3H), 7.25 – 7.17 (m, 2H), 7.10 – 7.02 (m, 2H), 6.97 (d, *J* = 8.5 Hz, 1H), 6.38 – 6.33 (m, 1H), 4.35 (dd, *J* = 7.1, 2.9 Hz, 2H), 4.23 (d, *J* = 4.9 Hz, 2H), 4.14 (q, *J* = 6.8, 6.0 Hz, 1H), 3.87 (d, *J* = 3.5 Hz, 3H).

Methyl 2-((7-((4-(aminomethyl)phenyl)amino)imidazo[1,2-a]pyrimidin-5-yl)amino)benzoate (**87**)



Compound **86** (192 mg, 0.3 mmol) was added to the mixed solution of DMF (3 mL) and piperidine (0.6 mL). The mixture stirred at room temperature for 3 h. Subsequently, the

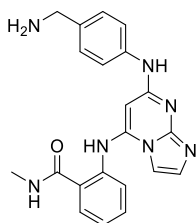
solvent was removed under reduced pressure. Ethyl ether was added to the remained residue and filtered to give the crude product as beige solid, then purification by silica gel chromatography (DCM/MeOH/NH₄OH = 10/1/0.01) to give the title compound as off-white solid (90 mg, 74%).

¹H NMR (500 MHz, DMSO-*d*₆) δ 9.10 (s, 1H), 8.00 (d, *J* = 7.9 Hz, 1H), 7.76 – 7.67 (m, 4H), 7.60 (d, *J* = 8.1 Hz, 1H), 7.37 (t, *J* = 7.6 Hz, 1H), 7.33 (d, *J* = 1.6 Hz, 1H), 7.23 (d, *J* = 8.2 Hz, 2H), 5.83 (s, 1H), 3.77 (s, 3H), 3.66 (s, 2H).

¹³C NMR (126 MHz, DMSO-*d*₆) δ 166.7, 155.4, 149.7, 144.7, 139.6, 139.3, 136.3, 133.9, 131.3, 130.7, 127.3, 124.9, 124.7, 122.7, 118.5, 105.5, 78.8, 52.3, 45.0.

Melting point: 174 °C.

2-((7-((4-(Aminomethyl)phenyl)amino)imidazo[1,2-*a*]pyrimidin-5-yl)amino)-*N*-methylbenzamide (**88**)



Chemical Formula: C₂₁H₂₁N₇O
Exact Mass: 387.1808

Compound **87** (25 mg, 0.06 mmol) was added to a solution of MeNH₂ in ethanol (wt 33%, 1 mL). The mixture was stirred at room temperature overnight. Subsequently, the solvent was removed under reduced pressure. The residue was purified by silica gel chromatography (eluent: DCM/MeOH/NH₄OH = 10/1/0.01) to give the product as white solid (20mg, 74%).

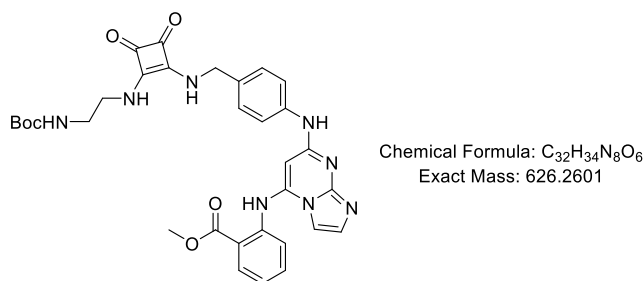
¹H NMR (500 MHz, DMSO-*d*₆) δ 8.98 (s, 1H), 7.91 (d, *J* = 7.9 Hz, 1H), 7.71 – 7.67 (m, 2H), 7.59 (d, *J* = 1.8 Hz, 1H), 7.47 (d, *J* = 4.1 Hz, 2H), 7.29 (d, *J* = 1.7 Hz, 1H), 7.27 – 7.22 (m, 2H), 7.09 (dt, *J* = 8.1, 4.1 Hz, 1H), 5.87 (s, 1H), 3.74 (s, 2H), 2.77 (d, *J* = 2.8 Hz,

3H).

^{13}C NMR (126 MHz, DMSO- d_6) δ 167.3, 158.5, 145.9, 145.7, 139.2, 135.7, 131.8, 129.6, 129.1, 128.9, 128.7, 126.2, 125.3, 120.0, 119.1, 108.0, 80.7, 41.8, 26.2.

Melting point: 179 °C.

Methyl 2-((7-((4-(((2-((tert-butoxycarbonyl)amino)ethyl)amino)-3,4-dioxocyclobut-1-en-1-yl)amino)methyl)phenyl)amino)imidazo[1,2-a]pyrimidin-5-yl)amino)benzoate
(89)

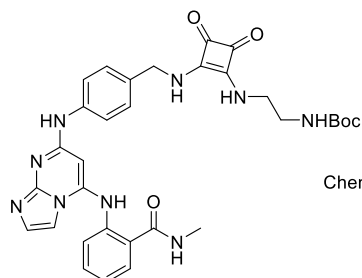


Following the general procedure F, from compound **86** (50 mg, 0.13 mmol), compound **11** (35 mg, 0.13 mmol) and DIPEA (23 μL , 0.13 mmol), the title compound was obtained as off-white solid (53 mg, 65%).

^1H NMR (500 MHz, Chloroform- d) δ 10.56 (s, 1H), 9.09 (s, 1H), 8.68 (s, 1H), 7.94 (d, J = 8.0 Hz, 1H), 7.55 – 7.46 (m, 1H), 7.38 – 7.31 (m, 4H), 6.94 (t, J = 7.1 Hz, 1H), 6.78 (s, 2H), 6.58 (s, 1H), 5.97 (s, 1H), 4.48 (s, 2H), 3.91 (s, 3H), 3.68 (s, 2H), 3.30 – 3.08 (m, 2H), 1.25 (s, 9H).

^{13}C NMR (126 MHz, Chloroform- d) δ 182.9, 182.5, 169.1, 168.4, 156.8, 156.3, 150.7, 141.9, 139.2, 134.7, 131.7, 130.5, 127.7, 121.9, 121.6, 118.3, 115.5, 105.4, 83.4, 78.9, 52.7, 48.0, 44.2, 41.8, 28.4.

tert-Butyl (2-((2-((4-((5-((2-(methylcarbamoyl)phenyl)amino)imidazo[1,2-a]pyrimidin-7-yl)amino)benzyl)amino)-3,4-dioxocyclobut-1-en-1-yl)amino)ethyl)carbamate (**90**)



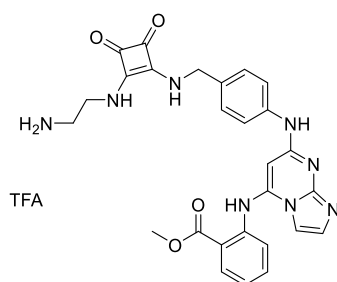
Chemical Formula: C₃₂H₃₅N₉O₅
Exact Mass: 625.2761

Following the general procedure F, from compound **88** (72 mg, 0.185 mmol), compound **11** (50 mg, 0.185 mmol) and DIPEA (33 μ L, 0.189 mmol), the title compound was obtained as off-white solid (94 mg, 81%).

¹H NMR (500 MHz, Methanol-*d*₄) δ 7.73 – 7.70 (m, 3H), 7.55 (d, *J* = 8.2 Hz, 1H), 7.49 – 7.42 (m, 2H), 7.33 (d, *J* = 1.9 Hz, 1H), 7.21 – 7.11 (m, 3H), 4.68 (s, 2H), 3.64 (s, 2H), 3.22 (t, *J* = 5.9 Hz, 2H), 2.89 (s, 3H), 1.37 (s, 9H).

¹³C NMR (126 MHz, Methanol-*d*₄) δ 183.9, 183.7, 171.0, 169.9, 169.1, 158.5, 157.9, 151.6, 145.0, 141.4, 140.7, 133.2, 132.8, 129.7, 129.2, 124.4, 124.4, 122.2, 120.8, 106.5, 80.3, 49.8, 45.2, 42.4, 28.7 (3C), 26.8.

Methyl 2-((7-((4-(((2-((2-aminoethyl)amino)-3,4-dioxocyclobut-1-en-1-yl)amino) methyl)phenyl)amino)imidazo[1,2-a]pyrimidin-5-yl)amino)benzoate trifluoroacetate salt (**91**)



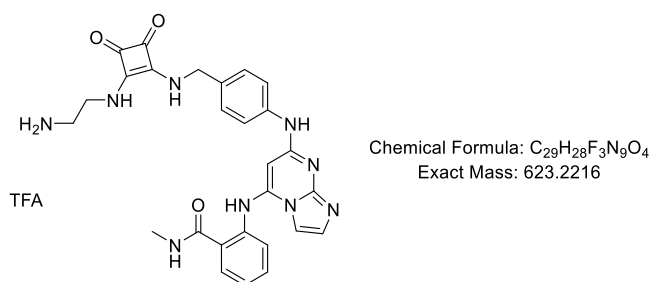
Chemical Formula: C₂₉H₂₆F₃N₈O₅
Exact Mass: 623.1978

TFA

Following the general procedure E, from compound **89** (40 mg, 0.06 mmol) the titled compound was obtained as beige solid (43 mg, quantitative). The product was directly used in next step without further purification.

¹H NMR (500 MHz, Methanol-*d*₄) δ 8.16 (dd, *J* = 8.0, 1.6 Hz, 1H), 7.92 (d, *J* = 2.8 Hz, 1H), 7.80 – 7.72 (m, 1H), 7.72 – 7.62 (m, 4H), 7.44 (t, *J* = 7.6 Hz, 1H), 7.36 (d, *J* = 8.6 Hz, 2H), 6.21 (s, 1H), 3.91 (s, 3H), 3.89 (t, *J* = 6.2 Hz, 2H), 3.20 (t, *J* = 6.1 Hz, 2H).

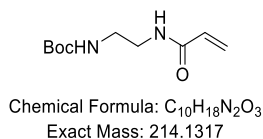
2-((7-((4-(((2-((2-Aminoethyl)amino)-3,4-dioxocyclobut-1-en-1-yl)amino)methyl)phenyl)amino)imidazo[1,2-a]pyrimidin-5-yl)amino)-N-methylbenzamide trifluoroacetate salt (**92**)



Following the general procedure E, from compound **90** (92 mg, 0.15 mmol) the titled compound was obtained as beige solid (93 mg, quantitative). The product was directly used in next step without further purification.

¹H NMR (250 MHz, DMSO-*d*₆) δ 13.63 (s, 1H), 10.60 (s, 1H), 10.05 (s, 1H), 8.61 (d, *J* = 3.8 Hz, 1H), 8.17 (s, 1H), 8.02 (d, *J* = 2.7 Hz, 1H), 7.82 (d, *J* = 2.5 Hz, 2H), 7.78 (d, *J* = 1.5 Hz, 1H), 7.69 – 7.59 (m, 4H), 7.44 (td, *J* = 7.4, 1.5 Hz, 1H), 7.32 (d, *J* = 8.4 Hz, 2H), 6.03 (s, 1H), 4.67 (d, *J* = 6.1 Hz, 2H), 3.70 (d, *J* = 6.3 Hz, 2H), 3.09 – 2.97 (m, 2H), 2.73 (d, *J* = 4.5 Hz, 3H).

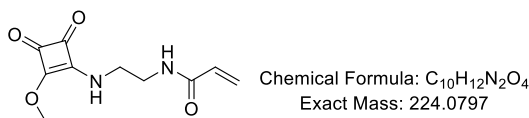
tert-Butyl (2-acrylamidoethyl)carbamate (**93**)



Acryloyl chloride (282 μ L, 3.32 mmol) in 5 mL THF was added dropwise into an ice-cooled anhydrous THF (15 mL) containing compound **10** (483 mg, 3.02 mmol) and Et₃N (445 μ L, 3.32 mmol) in 10 mins under stirring. The mixture was stirred for another 2 h in ice water, and then at room temperature overnight. After removal of the white precipitate by filtration, THF was removed *in vacuo*. The residual powder was dissolved into 40 mL chloroform and washed subsequently by citrate buffer solution (80 mL, pH 5.0), saturated NaHCO₃ solution and saturated brine. The organic layer was collected and dried over MgSO₄. After concentration *in vacuo*, the crude residue was purified by column (eluent: DCM/MeOH= 60/1~50/1) to give the title compound as colourless oil (400 mg, 62%).

¹H NMR (500 MHz, Chloroform-*d*) δ 6.40 (s, 1H, NH), 6.25 (d, *J* = 17.0 Hz, 1H), 6.09 (dd, *J* = 17.1, 10.3 Hz, 1H), 5.63 (d, *J* = 10.3 Hz, 1H), 4.93 (s, 1H, NH), 3.43 (t, *J* = 5.7 Hz, 2H), 3.31 (t, *J* = 5.6 Hz, 2H), 1.43 (s, 9H).

N-(2-((2-Methoxy-3,4-dioxocyclobut-1-en-1-yl)amino)ethyl)acrylamide (**94**)



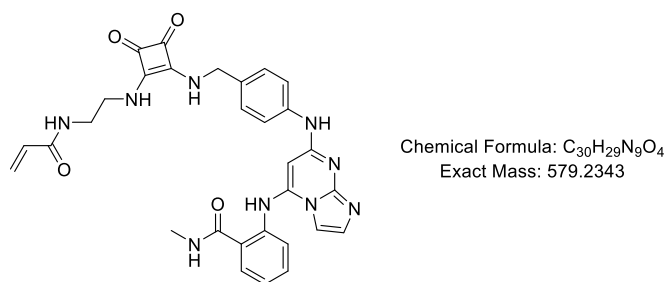
A solution of HCl (2.5 mL, 4 M in 1,4-dioxane) was injected into a 25 mL flask and compound **93** (400 mg, 1.87 mmol). After stirring at room temperature for 4 h, the solvent was removed *in vacua* to give the deprotected intermediate as colourless oil. The oil and Et₃N (521 μ L, 3.74 mmol) were dissolved in MeOH (10 mL). The mixture was added dropwise to the solution of dimethyl squarate (293 mg, 2.06 mmol). Then the mixture was

stirred at room temperature for 3 h. The solvent was removed under reduced pressure and the residue was purified through silica gel column (eluent: DCM/MeOH=30/1) to give the title compound as white solid (377 mg, 90%).

^1H NMR (500 MHz, Methanol- d_4) δ 6.27 – 6.14 (m, 2H), 5.72 – 5.60 (m, 1H), 4.34 (s, 3H), 3.70 (t, $J = 5.9$ Hz, 1H), 3.52 (t, $J = 5.6$ Hz, 1H), 3.48 – 3.40 (m, 2H).

^{13}C NMR (126 MHz, Methanol- d_4) δ 188.4, 183.7, 176.7, 173.6, 167.1, 130.5, 125.6, 59.8, 43.7, 39.6.

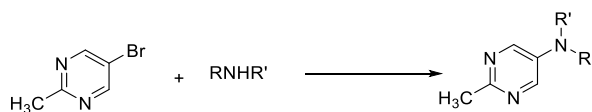
2-(((7-(((4-(((2-((2-Acrylamidoethyl)amino)-3,4-dioxocyclobut-1-en-1-yl)amino)methyl)phenyl)amino)imidazo[1,2-a]pyrimidin-5-yl)amino)-N-methylbenzamide (**95**))



To a solution of compound **88** (20 mg, 0.05 mmol) in DMF (0.5 mL) was added compound **94** (12 mg, 0.05 mmol) and DIPEA (10 μL , 0.05 mmol). The mixture was stirred at 86 $^\circ\text{C}$ overnight. Then the solvent was removed in vacuo. The residue was purified by silica gel column chromatography (eluent: DCM/MeOH/ $\text{NH}_4\text{OH} = 10/1/0 \sim 10/1/0.01$) to give the title compound as off-white solid (24 mg, 70%).

^1H NMR (500 MHz, DMSO- d_6) δ 9.27 (s, 1H), 8.27 (t, $J = 5.7$ Hz, 1H), 7.93 – 7.83 (m, 1H), 7.79 – 7.62 (m, 3H), 7.56 (s, 2H), 7.41 (d, $J = 1.9$ Hz, 1H), 7.28 – 7.16 (m, 3H), 6.20 (dd, $J = 17.1, 10.1$ Hz, 1H), 6.09 (dd, $J = 17.1, 2.3$ Hz, 1H), 5.60 (dd, $J = 10.1, 2.3$ Hz, 1H), 4.65 (s, 2H), 3.58 (s, 2H), 3.31 (s, 2H), 2.78 (d, $J = 4.5$ Hz, 3H).

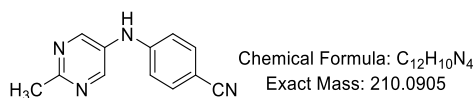
General procedure for compound **96** – **113**



RNHR' = Arylamine or heterocyclic amine

A G10 microwave vial equipped with a stir-bar was charged with 5-bromo-2-methylpyrimidine (42 mg, 0.3 mmol), corresponding amine (0.33 mmol), Pd₂dba₃ (5.5 mg, 2 mol%), XPhos (11.8 mg, 8 mol%), NaO^tBu (42 mg, 0.42 mmol) and anhydrous 1,4-dioxane (2 mL). The vial was purged with argon, then was heated in Anton Paar monowave reactor to 120 °C. The reaction was maintained at this temperature for 1 h and then cooled to room temperature. The reaction mixture was directly concentrated under reduced pressure and the crude residue purified by flash chromatography (eluent: cyclohexane/ethylacetate = 10/1 ~ 0/1) to corresponding products.

4-((2-Methylpyrimidin-5-yl)amino)benzonitrile (**96**)



White solid (50.4 mg, 80%).

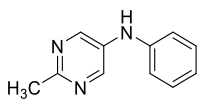
¹H NMR (500 MHz, Chloroform-*d*) δ 8.56 (s, 2H), 7.54 – 7.50 (m, 2H), 6.97 – 6.94 (m, 2H), 6.31 (s, 1H), 2.72 (s, 3H).

¹³C NMR (126 MHz, Chloroform-*d*) δ 163.3, 149.9, 147.0, 134.2, 133.0, 119.4, 115.3, 103.4, 25.3.

HRMS (ESI) *m/z* calcd. for C₁₂H₁₁N₄ [M+H]⁺ : 211.09837, found: 211.09799.

Melting point: 174 °C.

2-Methyl-*N*-phenylpyrimidin-5-amine (**97**)



Chemical Formula: C₁₁H₁₁N₃
Exact Mass: 185.0953

White solid (45 mg, 82%).

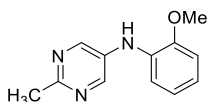
¹H NMR (500 MHz, Chloroform-*d*) δ 8.45 (s, 2H), 7.29 (t, *J* = 7.7 Hz, 2H), 7.04 – 6.97 (m, 3H), 5.78 (s, 1H), 2.66 (s, 3H).

¹³C NMR (126 MHz, Chloroform-*d*) δ 160.5, 146.5, 141.7, 135.5, 129.8, 122.4, 117.9, 25.1.

HRMS (ESI) *m/z* calcd. for C₁₁H₁₂N₃ [M+H]⁺ : 186.10312, found: 186.10250.

Melting point: 136 °C.

N-(2-Methoxyphenyl)-2-methylpyrimidin-5-amine (**98**)



Chemical Formula: C₁₂H₁₃N₃O
Exact Mass: 215.1059

White solid (55.5 mg, 86%).

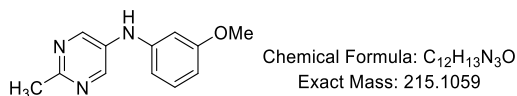
¹H NMR (500 MHz, Chloroform-*d*) δ 8.49 (s, 2H), 7.14 (dd, *J* = 7.6, 1.6 Hz, 1H), 6.95 – 6.86 (m, 3H), 6.02 (s, 1H), 3.89 (s, 3H), 2.67 (s, 3H).

¹³C NMR (126 MHz, Chloroform-*d*) δ 160.6, 148.8, 147.1, 135.1, 131.4, 121.6, 121.1, 114.8, 111.0, 55.7, 25.1.

HRMS (ESI) *m/z* calcd. for C₁₂H₁₄N₃O [M+H]⁺ : 216.11369, found: 216.11282.

Melting point: 132 °C.

N-(3-Methoxyphenyl)-2-methylpyrimidin-5-amine (**99**)



White solid (53.3 mg, 82.5%).

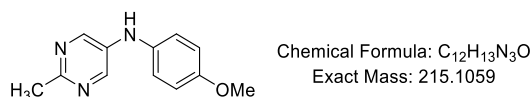
¹H NMR (500 MHz, Chloroform-*d*) δ 8.44 (s, 2H), 7.17 (t, *J* = 8.1 Hz, 1H), 6.59 (ddd, *J* = 7.9, 2.2, 0.8 Hz, 1H), 6.58 – 6.48 (m, 2H), 6.01 (s, 1H), 3.74 (s, 3H), 2.65 (s, 3H).

¹³C NMR (126 MHz, Chloroform-*d*) δ 161.0, 160.5, 146.8, 143.2, 135.3, 130.6, 110.1, 107.5, 103.6, 55.3, 25.0.

HRMS (ESI) *m/z* calcd. for C₁₂H₁₄N₃O [M+H]⁺ : 216.11369, found: 216.11275.

Melting point: 110 °C.

N-(4-Methoxyphenyl)-2-methylpyrimidin-5-amine (**100**)



White solid (52.7 mg, 81%).

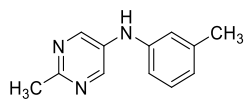
¹H NMR (500 MHz, Chloroform-*d*) δ 8.29 (s, 2H), 7.06 – 7.00 (m, 2H), 6.90 – 6.84 (m, 2H), 5.54 (s, 1H), 3.79 (s, 3H), 2.62 (s, 3H).

¹³C NMR (126 MHz, Chloroform-*d*) δ 159.1, 156.2, 144.3, 137.2, 134.0, 122.3, 115.1, 55.7, 25.0.

HRMS (ESI) *m/z* calcd. for C₁₂H₁₄N₃O [M+H]⁺ : 216.11369, found: 216.11317.

Melting point: 126 °C.

2-Methyl-*N*-(*m*-tolyl)pyrimidin-5-amine (**101**)



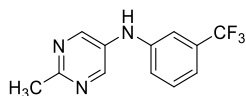
Chemical Formula: C₁₂H₁₃N₃
Exact Mass: 199.1109

White solid (50 mg, 85%).

¹H NMR (500 MHz, Chloroform-*d*) δ 8.44 (s, 2H), 7.17 (t, *J* = 7.7 Hz, 1H), 6.86 – 6.80 (m, 3H), 5.73 (s, 1H), 2.66 (s, 3H), 2.30 (s, 3H).

¹³C NMR (126 MHz, Chloroform-*d*) δ 160.3, 146.5, 141.6, 139.8, 135.6, 129.6, 123.3, 118.5, 115.1, 25.1, 21.6.

2-Methyl-*N*-(3-(trifluoromethyl)phenyl)pyrimidin-5-amine (**102**)



Chemical Formula: C₁₂H₁₀F₃N₃
Exact Mass: 253.0827

White solid (62.5 mg, 82%).

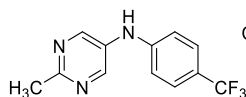
¹H NMR (500 MHz, Chloroform-*d*) δ 8.47 (s, 2H), 7.41 – 7.29 (m, 1H), 7.25 – 7.10 (m, 3H), 6.31 (s, 1H), 2.66 (s, 3H).

¹³C NMR (126 MHz, Chloroform-*d*) δ 161.6, 147.6, 142.8, 134.6, 132.5, 130.3, 124.9, 119.9, 118.4, 113.6, 25.1.

HRMS (ESI) *m/z* calcd. for C₁₂H₁₁F₃N₃ [M+H]⁺: 254.09051, found: 254.08949.

Melting point: 114 °C.

2-Methyl-*N*-(4-(trifluoromethyl)phenyl)pyrimidin-5-amine (**103**)



Chemical Formula: C₁₂H₁₀F₃N₃
Exact Mass: 253.0827

Off-white solid (45 mg, 59%).

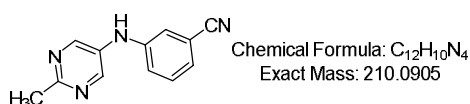
^1H NMR (500 MHz, Chloroform-*d*) δ 8.47 (s, 2H), 7.44 (d, $J = 8.3$ Hz, 2H), 6.96 – 6.93 (m, 2H), 5.87 (s, 1H), 2.64 (s, 3H).

^{13}C NMR (126 MHz, Chloroform-*d*) δ 162.6, 148.9 (2C), 145.6, 133.8, 127.3 (q, $J=127$ Hz), 125.5, 123.4, 115.6 (2C), 25.3.

HRMS (ESI) m/z calcd. for $\text{C}_{12}\text{H}_9\text{F}_3\text{N}_3$ $[\text{M}-\text{H}]^-$: 252.07486, found: 252.07523.

Melting point: 146 °C.

3-((2-Methylpyrimidin-5-yl)amino)benzonitrile (**104**)



White solid (43.5 mg, 69%).

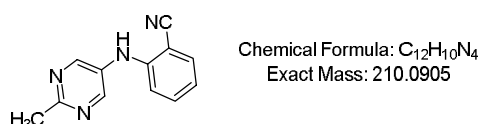
^1H NMR (500 MHz, Chloroform-*d*) δ 8.48 (s, 2H), 7.38 – 7.31 (m, 1H), 7.22 – 7.15 (m, 3H), 6.38 (s, 1H), 2.67 (s, 3H).

^{13}C NMR (126 MHz, Chloroform-*d*) δ 162.2, 148.4, 143.5, 134.0, 130.7, 124.9, 120.6, 119.3, 118.7, 113.6, 25.2.

HRMS (ESI) m/z calcd. $\text{C}_{12}\text{H}_{11}\text{N}_4$ $[\text{M}+\text{H}]^+$: 211.09837, found: 211.09750.

Melting point: 136 °C.

2-((2-Methylpyrimidin-5-yl)amino)benzonitrile (**105**)



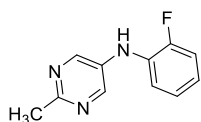
Yellow solid (31 mg, 37%).

^1H NMR (500 MHz, $\text{DMSO-}d_6$) δ 8.57 (s, 2H), 7.73 (dd, $J = 7.8, 1.5$ Hz, 1H), 7.34 (tt, $J = 7.2, 1.6$ Hz, 1H), 7.18 (ddd, $J = 8.4, 4.1, 1.0$ Hz, 1H), 6.87 (ddd, $J = 7.8, 4.7, 1.8$ Hz, 1H), 2.56 (s, 3H).

^{13}C NMR (126 MHz, $\text{DMSO-}d_6$) δ 170.9, 160.3, 148.5, 144.0, 143.8, 134.0, 132.3, 129.4, 118.8, 114.6, 24.8.

HRMS (ESI) m/z calcd. for $\text{C}_{12}\text{H}_9\text{N}_4$ $[\text{M-H}]^-$: 209.0827, found: 209.08313.

N-(2-Fluorophenyl)-2-methylpyrimidin-5-amine (**106**)



Chemical Formula: $\text{C}_{11}\text{H}_{10}\text{FN}_3$
Exact Mass: 203.0859

Off-white solid (59.8 mg, 98%).

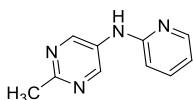
^1H NMR (500 MHz, $\text{Chloroform-}d$) δ 8.47 (s, 2H), 7.16 (td, $J = 8.2, 1.6$ Hz, 1H), 7.11 (ddd, $J = 11.2, 8.2, 1.4$ Hz, 1H), 7.05 (tt, $J = 7.9, 1.0$ Hz, 1H), 6.93 (tdd, $J = 7.7, 5.0, 1.6$ Hz, 1H), 5.77 (s, 1H), 2.68 (s, 3H).

^{13}C NMR (126 MHz, $\text{Chloroform-}d$) δ 161.4, 154.4, 147.3, 134.6, 130.3, 124.8, 122.4, 117.4, 116.1, 25.2.

HRMS (ESI) m/z calcd. for $\text{C}_{11}\text{H}_{11}\text{FN}_3$ $[\text{M+H}]^+$: 204.09370, found: 204.09242.

Melting point: 110 °C.

2-Methyl-*N*-(pyridin-2-yl)pyrimidin-5-amine (**107**)



Chemical Formula: $\text{C}_{10}\text{H}_{10}\text{N}_4$
Exact Mass: 186.0905

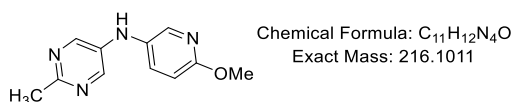
White solid (13 mg, 23%).

^1H NMR (500 MHz, Chloroform-*d*) δ 8.86 (s, 2H), 8.23 (dd, $J = 5.0, 1.9$ Hz, 1H), 7.55 (ddd, $J = 8.4, 7.2, 1.9$ Hz, 1H), 6.82 (ddd, $J = 7.3, 5.0, 0.9$ Hz, 1H), 6.73 (dd, $J = 8.2, 1.0$ Hz, 1H), 6.55 (s, 1H), 2.70 (s, 3H).

^{13}C NMR (126 MHz, Chloroform-*d*) δ 161.6, 154.8, 148.3, 148.2, 138.1, 133.3, 116.3, 109.5, 25.3.

Melting point: 184 °C.

N-(6-Methoxypyridin-3-yl)-2-methylpyrimidin-5-amine (**108**)



Pale gray solid (41.3 mg, 64%).

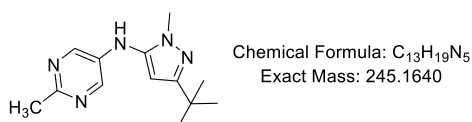
^1H NMR (500 MHz, Chloroform-*d*) δ 8.26 (s, 2H), 7.99 (d, $J = 2.8$ Hz, 1H), 7.40 (dd, $J = 8.8, 2.8$ Hz, 1H), 6.75 (d, $J = 8.7$ Hz, 1H), 5.51 (s, 1H), 3.92 (s, 3H), 2.63 (s, 3H).

^{13}C NMR (126 MHz, Chloroform-*d*) δ 161.2, 159.7, 144.2, 140.3, 137.0, 133.1, 131.2, 111.7, 53.8, 25.0.

HRMS (ESI) m/z calcd. for $\text{C}_{11}\text{H}_{13}\text{N}_4\text{O}$ $[\text{M}+\text{H}]^+$: 217.10894, found: 217.10853.

Melting point: 144 °C.

N-(3-(*tert*-Butyl)-1-methyl-1*H*-pyrazol-5-yl)-2-methylpyrimidin-5-amine (**109**)



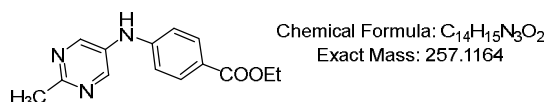
Yellow oil (62 mg, 84%).

^1H NMR (500 MHz, Chloroform-*d*) δ 8.07 (s, 2H), 5.83 (s, 1H), 5.76 (s, 1H), 3.54 (s, 3H), 2.50 (s, 3H), 1.15 (s, 9H).

^{13}C NMR (126 MHz, Chloroform-*d*) δ 161.3, 159.7, 143.5, 139.0, 136.8, 94.7, 34.7, 32.3, 30.4, 24.8.

HRMS (ESI) m/z calcd. for $\text{C}_{13}\text{H}_{20}\text{N}_5$ $[\text{M}+\text{H}]^+$: 246.17187, found: 246.17118

Ethyl 4-((2-methylpyrimidin-5-yl)amino)benzoate (**110**)



White solid (42.5 mg, 55%).

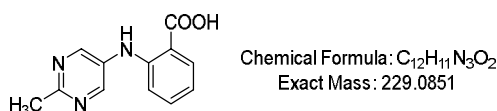
^1H NMR (500 MHz, Chloroform-*d*) δ 8.55 (s, 2H), 7.96 – 7.92 (m, 2H), 6.98 – 6.94 (m, 2H), 6.17 (s, 1H), 4.34 (q, $J = 7.1$ Hz, 2H), 2.70 (s, 3H), 1.37 (t, $J = 7.1$ Hz, 3H).

^{13}C NMR (126 MHz, CDCl_3) δ 166.3, 162.5, 149.0, 146.7, 133.7, 131.8, 123.2, 114.9, 60.8, 25.3, 14.5.

HRMS (ESI) m/z calcd. for $\text{C}_{14}\text{H}_{14}\text{N}_3\text{O}_2$ $[\text{M}-\text{H}]^-$: 256.10860, found: 256.10909.

Melting point: 176 °C.

2-((2-Methylpyrimidin-5-yl)amino)benzoic acid (**111**)



Beige solid (46 mg, 67%).

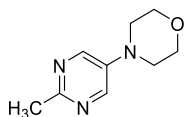
^1H NMR (500 MHz, $\text{DMSO}-d_6$) δ 8.65 (s, 2H), 7.93 (dd, $J = 7.9, 1.7$ Hz, 1H), 7.41 (ddd, $J = 8.7, 7.1, 1.8$ Hz, 1H), 7.14 – 7.11 (m, 1H), 6.88 – 6.84 (m, 1H), 2.60 (s, 3H).

^{13}C NMR (126 MHz, $\text{DMSO}-d_6$) δ 169.6, 161.4, 150.3, 146.2, 134.2, 133.4, 131.9, 118.4, 113.8, 113.6, 24.9.

HRMS (ESI) m/z calcd. for $\text{C}_{12}\text{H}_{10}\text{N}_3\text{O}_2$ $[\text{M}-\text{H}]^-$: 228.07730, found: 228.07739.

Melting point: 246 °C.

4-(2-Methylpyrimidin-5-yl)morpholine (**112**)



Chemical Formula: C₉H₁₃N₃O
Exact Mass: 179.1059

White solid (50 mg, 93%).

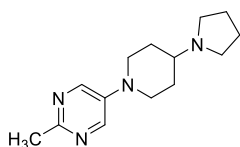
¹H NMR (500 MHz, Chloroform-*d*) δ 8.22 (s, 2H), 3.82 – 3.78 (m, 4H), 3.12 – 3.08 (m, 4H), 2.58 (s, 3H).

¹³C NMR (126 MHz, Chloroform-*d*) δ 159.3, 144.3, 142.1, 66.6, 48.3, 24.9.

HRMS (ESI) *m/z* calcd. for C₉H₁₄N₃O [M+H]⁺ : 180.11369, found: 180.11292.

Melting point: 104 °C.

2-methyl-5-(4-(pyrrolidin-1-yl)piperidin-1-yl)pyrimidine (**113**)



Chemical Formula: C₁₄H₂₂N₄
Exact Mass: 246.1844

White solid (57 mg, 77%).

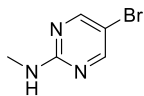
¹H NMR (500 MHz, Chloroform-*d*) δ 8.28 (s, 2H), 3.69 – 3.63 (m, 2H), 2.81 (td, *J* = 12.1, 2.8 Hz, 5H), 2.62 (s, 3H), 2.42 (s, 1H), 2.08 (dd, *J* = 10.4, 5.8 Hz, 2H), 2.00 – 1.75 (m, 7H).

¹³C NMR (126 MHz, Chloroform-*d*) δ 158.1, 144.5, 142.1, 61.1, 51.4, 47.3, 30.6, 24.7, 23.3.

HRMS (ESI) *m/z* calcd. for C₁₄H₂₃N₄ [M+H]⁺ : 247.19227, found: 247.19130.

Melting point: 140 °C.

5-Bromo-*N*-methylpyrimidin-2-amine (**114**)



Chemical Formula: C₅H₆BrN₃
Exact Mass: 186.9745

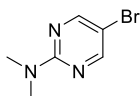
5-Bromo-2-chloropyrimidine (500 mg, 2.6 mmol) was added to the methylamine solution (33% Wt in ethanol, 700 μ L). The mixture was stirred at 80 °C overnight. After cooling to room temperature, the solvent was concentrated *in vacuo*. The residue was purified by silica gel column chromatography (eluent: cyclohexane/ethyl acetate = 20/1 ~ 2/1) to give the title compound as white solid (443 mg, 91%).

¹H NMR (500 MHz, Chloroform-*d*) δ 8.24 (s, 2H), 5.74 (s, 1H), 2.93 (d, *J* = 5.1 Hz, 3H).

¹³C NMR (126 MHz, Chloroform-*d*) δ 161.3, 158.2, 106.1, 28.6.

MS ESI⁺: 188.0 [M+H]

5-Bromo-*N,N*-dimethylpyrimidin-2-amine (**115**)



Chemical Formula: C₆H₈BrN₃
Exact Mass: 200.9902

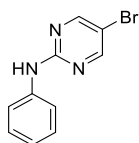
5-Bromo-2-chloropyrimidine (1.0 g, 5.1 mmol) was added to the dimethylamine solution (2 M in THF, 15 mL). The mixture was stirred at room temperature overnight. NaOH solution (1 M) was added to the reaction. The mixture was extracted with DCM. The organic phase was dried over MgSO₄ and concentrated *in vacuo*. The residue was purified by silica gel column chromatography (eluent: cyclohexane/ethyl acetate = 40/1 ~ 20/1) to give the title compound as white solid (878 mg, 84%).

¹H NMR (500 MHz, Chloroform-*d*) δ 8.26 (s, 2H), 3.13 (s, 6H).

¹³C NMR (126 MHz, Chloroform-*d*) δ 160.6, 157.8, 105.2, 37.4.

MS ESI⁺: 202.3 [M+H]

5-Bromo-*N*-phenylpyrimidin-2-amine (**116**)



Chemical Formula: C₁₀H₈BrN₂
Exact Mass: 248.9902

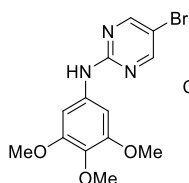
To a solution of 5-bromo-2-chloropyrimidine (400 mg, 2.02 mmol) in n-BuOH (10 mL) was added aniline (370 μ L, 4.0 mmol). The mixture was stirred at 120 °C overnight. After cooling to room temperature, the solvent was removed *in vacuo*. The residue was dissolved in ethyl acetate and washed with NaOH (0.5 M), water, brine. The organic phase was concentrated under reduced pressure. The residue was purified by silica gel column chromatography (eluent, cyclohexane/ethyl acetate= 16/10) to give the title compound as beige solid (366 mg, 73%).

¹H NMR (500 MHz, Chloroform-*d*) δ 8.42 (s, 2H), 7.59 – 7.55 (m, 2H), 7.38 – 7.33 (m, 2H), 7.08 (tt, *J* = 7.3, 1.1 Hz, 1H).

¹³C NMR (126 MHz, CDCl₃) δ 158.5, 158.4, 138.9, 129.2, 123.4, 119.7, 108.6.

MS ESI⁺: 250.2 [M+H]

5-Bromo-*N*-(3,4,5-trimethoxyphenyl)pyrimidin-2-amine (**117**)



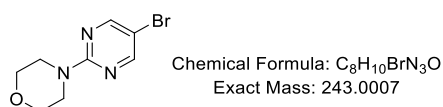
Chemical Formula: C₁₃H₁₄BrN₂O₃
Exact Mass: 339.0219

To a solution of 5-bromo-2-chloropyrimidine (400 mg, 2.02 mmol) in n-BuOH (10 mL) was added 3,4,5-trimethoxyaniline (732 mg, 4.0 mmol). The mixture was stirred at 120 °C overnight. After cooling to room temperature, the solvent was removed *in vacuo*. The residue was dissolved in ethyl acetate and washed with NaOH (0.5 M), water, brine. The organic phase was concentrated under reduced pressure. The residue was purified by silica

gel column chromatography (eluent, cyclohexane/ethyl acetate= 2/1) to give the title compound as beige solid (367 mg, 54%).

^1H NMR (500 MHz, Chloroform-*d*) δ 8.42 (s, 2H), 7.11 (s, 1H), 6.86 (s, 2H), 3.87 (s, 6H), 3.83 (s, 3H).

4-(5-Bromopyrimidin-2-yl)morpholine (**118**)



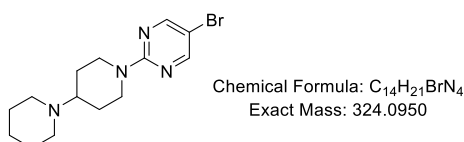
To a solution of 5-bromo-2-chloropyrimidine (200 mg, 1.0 mmol) in *n*-BuOH (5 mL) was added morpholine (262 μL , 3.0 mmol). The mixture was stirred at 100°C overnight. After cooling to room temperature, the mixture was diluted by ethyl acetate. The mixture was washed by water, brine. The organic phase was dried over MgSO_4 and concentrated *in vacuo*. The residue was purified by silica gel column chromatography (eluent: cyclohexane/ethyl acetate = 10/1 ~ 5/1) to give the title compound as white solid (229 mg, 93%).

^1H NMR (500 MHz, Chloroform-*d*) δ 8.30 (s, 2H), 3.75 (d, $J = 2.6$ Hz, 8H).

^{13}C NMR (126 MHz, Chloroform-*d*) δ 160.1, 158.0, 106.3, 66.8, 44.5.

MS ESI⁺ : 244.2 [M+H]

1'-(5-Bromopyrimidin-2-yl)-1,4'-bipiperidine (**119**)



To a solution of 5-bromo-2-chloropyrimidine (500 mg, 2.59 mmol) in ethanol (5 mL) was added 1,4'-bipiperidine (970 mg, 5.18 mmol). The mixture was stirred at 80°C overnight.

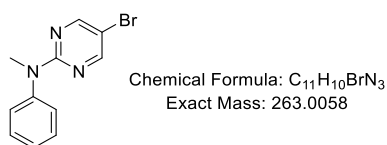
After cooling to room temperature, the mixture was diluted by ethyl acetate. The mixture was washed by water, brine. The organic phase was dried over MgSO₄ and concentrated *in vacuo*. The residue was purified by silica gel column chromatography (eluent: ethyl acetate/MeOH = 1/0 ~ 10/1) to give the title compound as white solid (729 mg, 86%).

¹H NMR (500 MHz, Chloroform-*d*) δ 8.25 (s, 2H), 4.72 (dt, *J* = 13.4, 2.5 Hz, 2H), 2.87 – 2.79 (m, 2H), 2.51 (d, *J* = 4.8 Hz, 5H), 1.92 – 1.84 (m, 2H), 1.58 (p, *J* = 5.6 Hz, 4H), 1.52 – 1.39 (m, 4H).

¹³C NMR (126 MHz, Chloroform-*d*) δ 159.9, 158.0, 105.4, 63.0, 50.4, 44.1, 27.9, 26.5, 24.9.

MS ESI⁺:325.2 [M+H]

5-Bromo-*N*-methyl-*N*-phenylpyrimidin-2-amine (**120**)



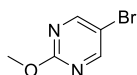
Compound 116 (250 mg, 1.0 mmol) in anhydrous DMF (2 mL) was added to a suspension of sodium hydride (120 mg, 60 wt% in mineral oil, 3.0 mmol) in anhydrous DMF (2 mL) at 0 °C. After stirring at this temperature for 30 minutes iodomethane (125 μL, 2.0 mmol) was added dropwise and the solution was allowed to warm to room temperature and stir for 4 h. The reaction was quenched by the addition of a saturated NaHCO₃ solution (5 mL) and the solution was extracted with ethyl acetate (3 x 5 mL). The combined organic extracts were dried over MgSO₄, filtered and the volatiles were removed under reduced pressure. The residue was purified by column chromatography on silica (eluent: cyclohexane/ethyl acetate= 1/0 ~ 20/1) to give the title compound as white solid (225 mg, 85%).

¹H NMR (500 MHz, Chloroform-*d*) δ 8.32 (s, 2H), 7.43 – 7.39 (m, 2H), 7.30 – 7.23 (m,

4H), 3.50 (s, 3H).

¹³C NMR (126 MHz, Chloroform-*d*) δ 160.4, 158.0, 145.3, 129.4, 126.6, 126.4, 107.2, 39.1.

5-Bromo-2-methoxypyrimidine (**121**)



Chemical Formula: C₅H₅BrN₂O
Exact Mass: 187.9585

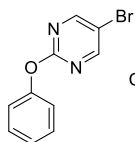
To a solution of NaOMe freshly prepared by dissolving Na metal (350 mg) in dry methanol, was added 2-bromo-5-chloropyrimidine (500 mg, 2.59 mmol), and the solution stirred at room temperature overnight. The reaction was monitored by TLC and quenched after 24 h by addition of water and extraction with ethyl acetate. The combined organic extracts were washed with brine, dried over MgSO₄ and concentrated *in vacuo*. The residue was purified by silica gel column chromatography (eluent: cyclohexane/ethyl acetate= 20/1) to give the title compound as white solid (283 mg, 58%).

¹H NMR (500 MHz, Chloroform-*d*) δ 8.50 (s, 1H), 3.97 (s, 2H).

¹³C NMR (126 MHz, Chloroform-*d*) δ 164.2, 159.5, 111.8, 55.4.

HRMS (ESI) *m/z* calcd. for C₅H₆BrN₂O [M+H]⁺: 188.9664, found: 188.96593.

5-Bromo-2-phenoxyypyrimidine (**122**)



Chemical Formula: C₁₀H₇BrN₂O
Exact Mass: 249.9742

To a solution of 5-bromo-2-chloropyrimidine (400 mg, 2.03 mmol) in DMSO (6 mL) was added phenol (191 mg, 2.03 mmol) and K₂CO₃ (560 mg, 4.06 mmol). The mixture was heated at 120 °C for 3 h. After cooling to room temperature, the mixture was poured into water and extracted with ethyl acetate. The combined organic phase was washed with

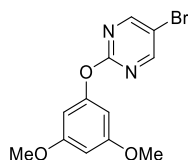
water and brine. Then the organic layer was dried over MgSO_4 , and concentrated under reduced pressure. The residue was purified by silica gel column chromatography (eluent: cyclohexane/ethyl acetate= 50/1) to give the title compound as white solid (398 mg, 78%).

^1H NMR (500 MHz, Chloroform-*d*) δ 8.55 (s, 2H), 7.42 (dd, $J = 8.5, 7.3$ Hz, 2H), 7.26 (t, $J = 6.8$ Hz, 1H), 7.20 – 7.15 (m, 2H).

^{13}C NMR (126 MHz, Chloroform-*d*) δ 164.1, 160.1, 152.8, 129.8, 125.9, 121.6, 113.3.

HRMS (ESI) m/z calcd. for $\text{C}_{10}\text{H}_8\text{BrN}_2\text{O}$ $[\text{M}+\text{H}]^+$: 250.9820, found: 250.98157.

5-Bromo-2-(3,5-dimethoxyphenoxy)pyrimidine (**123**)



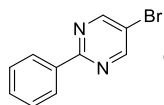
Chemical Formula: $\text{C}_{12}\text{H}_{11}\text{BrN}_2\text{O}_3$
Exact Mass: 309.9953

To a solution of 5-bromo-2-chloropyrimidine (400 mg, 2.03 mmol) in DMSO (6 mL) was added 3,5-dimethoxyphenol (320 mg, 2.03 mmol) and K_2CO_3 (560 mg, 4.06 mmol). The mixture was heated at 120 °C for 3 h. After cooling to room temperature, the mixture was poured into water and extracted with ethyl acetate. The combined organic phase was washed with water and brine. Then the organic layer was dried over MgSO_4 , and concentrated under reduced pressure. The residue was purified by silica gel column chromatography (eluent: cyclohexane/ethyl acetate= 50/1) to give the title compound as colourless oil (532 mg, 84%).

^1H NMR (500 MHz, Chloroform-*d*) δ 8.57 (s, 2H), 6.38 (t, $J = 2.2$ Hz, 1H), 6.34 (d, $J = 2.2$ Hz, 2H), 3.78 (s, 6H).

^{13}C NMR (126 MHz, Chloroform-*d*) δ 164.0, 161.6, 160.2, 154.4, 113.4, 100.2, 98.2, 55.6.

5-Bromo-2-phenylpyrimidine (**124**)



Chemical Formula: C₁₀H₇BrN₂
Exact Mass: 233.9793

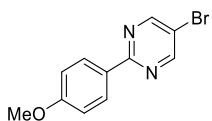
Phenylboronic acid (126 mg, 1.03 mmol), 5-bromo-2-iodopyrimidine (300 mg, 1.03 mmol), K₂CO₃ (2 M in H₂O, 1.03 mL), and Pd(PPh₃)₄ (12 mg, 1 mol%) in argon saturated toluene (2 mL). The mixture was refluxed overnight under argon. The resulting mixture was allowed to cool to room temperature, diluted with chloroform and extracted with brine. The combined organic solution was dried over MgSO₄. The concentrated crude product was isolated by column chromatography on silica gel (eluent: cyclohexane/ethyl acetate= 50/1) to give the title compound as white solid (104 mg, 43%).

¹H NMR (500 MHz, Chloroform-*d*) δ 8.83 (s, 2H), 8.42 – 8.39 (m, 2H), 7.51 – 7.47 (m, 3H).

¹³C NMR (126 MHz, Chloroform-*d*) δ 163.0, 158.0, 136.6, 131.3, 128.8, 128.3, 118.4.

HRMS (ESI) *m/z* calcd. for C₁₀H₈BrN₂ [M+H]⁺: 234.9871, found: 234.98663.

5-Bromo-2-(4-methoxyphenyl)pyrimidine (**125**)



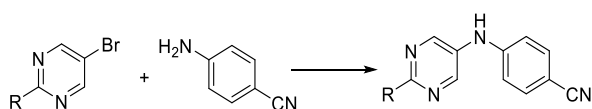
Chemical Formula: C₁₁H₉BrN₂O
Exact Mass: 263.9898

4-Methoxyphenylboronic acid (247 mg, 1.54 mmol), 5-bromo-2-iodopyrimidine (300 mg, 1.03 mmol), K₂CO₃ (2M in H₂O, 1.03 mL), and Pd(PPh₃)₄ (59 mg, 5 mol%) in argon saturated toluene (4 mL). The mixture was refluxed overnight under argon. The resulting mixture was allowed to cool to room temperature, diluted with chloroform and extracted with brine. The combined organic solution was dried over MgSO₄. The concentrated crude product was isolated by column chromatography on silica gel (eluent: cyclohexane/ethyl acetate= 50/1) to give the title compound as white solid (123 mg, 45%).

^1H NMR (500 MHz, Chloroform-*d*) δ 8.77 (s, 2H), 8.36 (d, J = 8.9 Hz, 2H), 6.99 (d, J = 8.9 Hz, 2H), 3.88 (s, 3H).

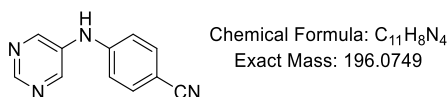
^{13}C NMR (126 MHz, Chloroform-*d*) δ 162.7, 162.2, 157.7, 129.9, 129.2, 117.3, 114.0, 55.4.

General procedure for **126** – **136**.



A G10 microwave vial equipped with a stir-bar was charged with 5-bromo-2-substituted pyrimidine (0.3 mmol), 4-aminobenzonitrile (40 mg, 0.33 mmol), Pd_2dba_3 (5.5 mg, 2 mol%), XPhos (11.8 mg, 8 mol%), NaO^tBu (42 mg, 0.42 mmol) and anhydrous 1,4-dioxane (2 mL). The vial was purged with argon, then was heated in Anton Paar monowave reactor to 120 °C. The reaction was maintained at this temperature for 1 h and then cooled to room temperature. The reaction mixture was directly concentrated under reduced pressure and the crude residue purified by flash chromatography (eluent: cyclohexane/ethylacetate = 10/1 ~ 0/1) to corresponding products.

4-(Pyrimidin-5-ylamino)benzonitrile (**126**)



White solid (51.1 mg, 87%).

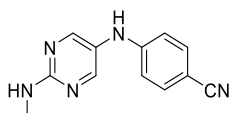
^1H NMR (500 MHz, DMSO-*d*₆) δ 9.16 (s, 1H), 8.81 (s, 1H), 8.69 (s, 2H), 7.70 – 7.62 (m, 2H), 7.22 – 7.14 (m, 2H).

^{13}C NMR (126 MHz, DMSO-*d*₆) δ 151.7, 147.1, 146.6, 136.4, 133.8, 119.5, 115.5, 101.2.

HRMS (ESI) m/z calcd. for $C_{11}H_7N_4$ $[M-H]^-$: 195.06707, found: 195.0669.

Melting point: 230 °C.

4-((2-(Methylamino)pyrimidin-5-yl)amino)benzonitrile (**127**)



Chemical Formula: $C_{12}H_{11}N_5$
Exact Mass: 225.1014

White solid (29.7 mg, 44%).

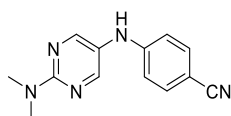
1H NMR (500 MHz, Chloroform-*d*) δ 8.23 (s, 2H), 7.44 (d, J = 8.8 Hz, 2H), 6.67 (d, J = 8.8 Hz, 2H), 5.60 (s, 1H), 3.03 (d, J = 5.0 Hz, 3H).

^{13}C NMR (126 MHz, Chloroform-*d*) δ 161.3, 156.6, 150.2, 133.9, 124.3, 119.8, 113.4, 101.2, 28.7.

HRMS (ESI) m/z calcd. for $C_{12}H_{12}N_5$ $[M+H]^+$: 226.10927, found: 226.10863.

Melting point: 173 °C.

4-((2-(Dimethylamino)pyrimidin-5-yl)amino)benzonitrile (**128**)



Chemical Formula: $C_{13}H_{13}N_5$
Exact Mass: 239.1171

White solid (70 mg, 80.5%).

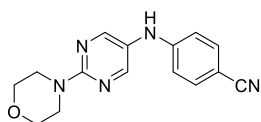
1H NMR (500 MHz, Chloroform-*d*) δ 8.21 (s, 2H), 7.39 (d, J = 8.8 Hz, 2H), 6.65 (d, J = 8.8 Hz, 2H), 5.86 (s, 1H), 3.19 (s, 6H).

^{13}C NMR (126 MHz, Chloroform-*d*) δ 160.6, 156.2, 150.6, 133.9, 123.0, 120.0, 113.3, 100.6, 37.5.

HRMS (ESI) m/z calcd. for $C_{13}H_{14}N_5$ $[M+H]^+$: 240.12492, found: 240.12461.

Melting point: 178 °C.

4-((2-Morpholinopyrimidin-5-yl)amino)benzonitrile (**129**)



Chemical Formula: C₁₅H₁₅N₅O
Exact Mass: 281.1277

Light yellow solid (84.3 mg, 99%).

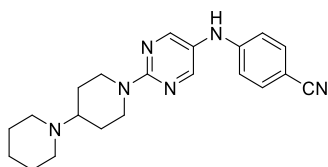
¹H NMR (500 MHz, Chloroform-*d*) δ 8.25 (s, 2H), 7.46 – 7.40 (m, 2H), 6.72 – 6.65 (m, 2H), 5.78 (s, 1H), 3.81 – 3.76 (m, 8H).

¹³C NMR (126 MHz, Chloroform-*d*) δ 160.0, 156.0, 150.2, 134.0, 124.3, 119.9, 113.5, 101.1, 66.9, 44.6.

HRMS (ESI) *m/z* calcd. for C₁₅H₁₆N₅O [M+H]⁺ : 282.13549, found: 282.13527.

Melting point: 154 °C.

4-((2-([1,4'-Bipiperidin]-1'-yl)pyrimidin-5-yl)amino)benzonitrile (**130**)



Chemical Formula: C₂₁H₂₆N₆
Exact Mass: 362.2219

Solid (96.9 mg, 89%).

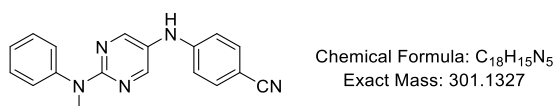
¹H NMR (500 MHz, Chloroform-*d*) δ 8.16 (s, 2H), 7.35 (d, *J* = 8.7 Hz, 2H), 6.64 (d, *J* = 8.8 Hz, 2H), 6.17 (s, 1H), 4.74 (dp, *J* = 13.5, 2.2 Hz, 2H), 2.82 (td, *J* = 13.0, 2.6 Hz, 3H), 2.50 – 2.43 (m, 5H), 1.87 (dt, *J* = 13.8, 2.4 Hz, 2H), 1.54 (q, *J* = 5.7 Hz, 4H), 1.48 – 1.34 (m, 4H).

¹³C NMR (126 MHz, Chloroform-*d*) δ 159.6, 155.9, 150.4, 133.8, 123.4, 120.0, 113.3, 100.3, 62.9, 50.2, 44.0, 27.8, 26.2, 24.7.

HRMS (ESI) m/z calcd. for $C_{21}H_{27}N_6$ $[M+H]^+$: 363.22972, found: 363.22878.

Melting point: 78 °C.

4-((2-(Methyl(phenyl)amino)pyrimidin-5-yl)amino)benzonitrile (**131**)



Off-white solid (86.6 mg, 93%).

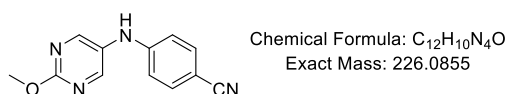
1H NMR (500 MHz, Methanol- d_4) δ 8.24 (s, 2H), 7.47 (d, J = 8.8 Hz, 2H), 7.41 (dd, J = 8.4, 7.3 Hz, 2H), 7.32 (dd, J = 8.5, 1.3 Hz, 2H), 7.25 (td, J = 7.3, 1.3 Hz, 1H), 6.83 (d, J = 8.8 Hz, 2H), 3.52 (s, 3H).

^{13}C NMR (126 MHz, Chloroform- d) δ 159.9, 155.3, 149.9, 145.3, 133.9, 129.3, 126.5, 126.1, 124.9, 119.9, 113.5, 100.8, 39.0.

HRMS (ESI) m/z calcd. for $C_{18}H_{14}N_5$ calcd. $[M-H]^-$: 300.12492, found: 300.12548.

Melting point: 119 °C.

4-((2-Methoxypyrimidin-5-yl)amino)benzonitrile (**132**)



White solid (44.2 mg, 65%).

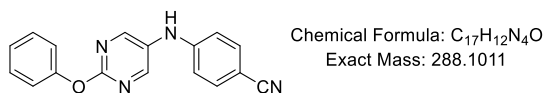
1H NMR (500 MHz, DMSO- d_6) δ 8.81 (s, 1H), 8.58 (s, 2H), 7.63 (d, J = 8.9 Hz, 2H), 6.99 (d, J = 8.8 Hz, 2H), 3.98 (s, 3H).

^{13}C NMR (126 MHz, DMSO- d_6) δ 161.5, 153.6, 149.0, 133.7, 130.2, 119.7, 113.7, 99.3, 54.6.

HRMS (ESI) m/z calcd. for $C_{12}H_{11}N_4O$ $[M+H]^+$: 227.09329, found: 227.09316.

Melting point: 197 °C.

4-((2-Phenoxy)pyrimidin-5-yl)amino)benzonitrile (**133**)



Off-white solid (47.6 mg, 55%).

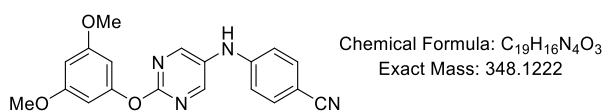
¹H NMR (500 MHz, Chloroform-*d*) δ 8.47 (s, 2H), 7.49 (d, *J* = 8.8 Hz, 2H), 7.44 (dd, *J* = 8.5, 7.4 Hz, 2H), 7.30 – 7.24 (m, 1H), 7.20 (dd, *J* = 8.6, 1.2 Hz, 2H), 6.86 (d, *J* = 8.8 Hz, 2H), 6.17 (s, 1H).

¹³C NMR (126 MHz, Chloroform-*d*) δ 162.3, 154.7, 153.1, 148.0, 134.1, 130.9, 129.8, 125.8, 121.6, 119.5, 114.5, 102.7.

HRMS (ESI) *m/z* calcd. for C₁₇H₁₃N₄O [M+H]⁺ : 289.10894, found: 289.10806.

Melting point: 163 °C.

4-((2-(3,5-Dimethoxyphenoxy)pyrimidin-5-yl)amino)benzonitrile (**134**)



Off-white solid (55.2 mg, 51%).

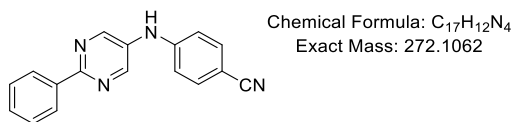
¹H NMR (500 MHz, Chloroform-*d*) δ 8.49 (s, 2H), 7.51 (d, *J* = 8.7 Hz, 2H), 6.86 (d, *J* = 8.8 Hz, 2H), 6.38 (s, 3H), 5.89 (s, 1H), 3.79 (s, 6H).

¹³C NMR (126 MHz, Chloroform-*d*) δ 162.3, 161.6, 154.9, 154.7, 147.9, 134.2, 130.8, 119.4, 114.6, 103.1, 100.3, 98.0, 55.6.

HRMS (ESI) *m/z* calcd. for C₁₉H₁₇N₄O₃ [M+H]⁺ : 349.13007, found: 349.12931.

Melting point: 132 °C.

4-((2-Phenylpyrimidin-5-yl)amino)benzonitrile (**135**)



White solid (70 mg, 85.7%).

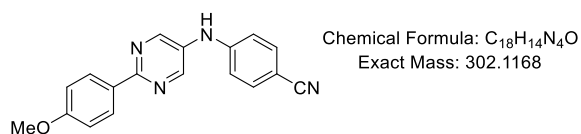
¹H NMR (500 MHz, Chloroform-*d*) δ 8.71 (s, 2H), 8.42 – 8.38 (m, 2H), 7.57 (d, *J* = 8.8 Hz, 2H), 7.52 – 7.47 (m, 3H), 7.05 (d, *J* = 8.7 Hz, 2H), 6.04 (s, 1H).

¹³C NMR (126 MHz, Chloroform-*d*) δ 160.2, 149.5, 146.4, 137.1, 134.2, 133.5, 130.6, 128.8, 127.9, 119.3, 115.7, 104.0.

HRMS (ESI) calcd. for C₁₇H₁₃N₄ [M+H]⁺ : 273.11402, found: 273.11386.

Melting point: 209 °C.

4-((2-(4-Methoxyphenyl)pyrimidin-5-yl)amino)benzonitrile (**136**)



White solid (81.6 mg, 90%).

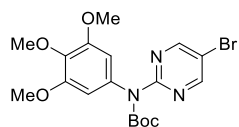
¹H NMR (500 MHz, DMSO-*d*₆) δ 9.18 (s, 1H), 8.75 (s, 2H), 8.28 (d, *J* = 8.9 Hz, 2H), 7.66 (d, *J* = 8.8 Hz, 2H), 7.19 (d, *J* = 8.8 Hz, 2H), 7.06 (d, *J* = 8.9 Hz, 2H), 3.84 (s, 3H).

¹³C NMR (126 MHz, DMSO-*d*₆) δ 160.8, 157.1, 148.0, 147.0, 133.8, 133.9, 129.6, 128.6, 119.6, 115.2, 114.0, 100.7, 55.2.

HRMS (ESI) *m/z* calcd. for C₁₈H₁₅N₄O [M+H]⁺ : 303.12459, found: 303.12380.

Melting point: 207 °C.

tert-Butyl (5-bromopyrimidin-2-yl)(3,4,5-trimethoxyphenyl)carbamate (**137**)



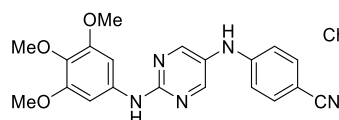
Chemical Formula: C₁₈H₂₂BrN₃O₅
Exact Mass: 439.0743

To a solution of compound **117** (240 mg, 0.7 mmol) in anhydrous THF (5 mL) was added Boc₂O (238 mg, 1.06 mmol), Et₃N (293 μL, 2.1 mmol) and DMAP (25 mg, 0.21 mmol). The mixture was stirred at room temperature for overnight. The solvent was concentrated in vacuo. The residue was purified by silica gel column chromatography (eluent: cyclohexane/ethyl acetate = 4/1 ~ 1/1) to give the title compound as white solid (194 mg, 63%).

¹H NMR (500 MHz, Chloroform-*d*) δ 8.67 (s, 2H), 6.44 (s, 2H), 3.84 (s, 3H), 3.80 (s, 6H), 1.46 (s, 9H).

¹³C NMR (126 MHz, Chloroform-*d*) δ 159.6, 158.8, 153.4, 153.0, 137.2, 136.4, 115.2, 105.4, 82.5, 60.8, 56.1, 28.1.

4-((2-((3,4,5-Trimethoxyphenyl)amino)pyrimidin-5-yl)amino)benzonitrile (**138**)



Chemical Formula: C₂₀H₁₉N₅O₃
Exact Mass: 377.1488

A G10 microwave vial equipped with a stir-bar was charged with **137** (117 mg, 0.26 mmol), 4-aminobenzonitrile (35 mg, 0.29 mmol), Pd₂dba₃ (4.8 mg, 2 mol%), XPhos (10.2 mg, 8 mol%), NaOtBu (42 mg, 0.36 mmol) and anhydrous 1,4-dioxane (2 mL). The vial was purged with argon, then was heated in Anton Paar monowave reactor to 120 °C. The reaction was maintained at this temperature for 1 h and then cooled to room temperature. The solvent was diluted with MeOH and filtered through celite pad. The filtrate was concentrated *in vacuo*. Then DCM (1 mL) and TFA (1 mL) was added to the residue and stirred at room temperature for 30 min. The reaction mixture was directly

concentrated under reduced pressure and the residue diluted by DCM and washed with NaOH solution (1M) and brine. The organic phase was dried over MgSO₄ and concentrated *in vacuo* and purified by flash chromatography (eluent: cyclohexane/ethylacetate = 5/1 ~ 0/1) to give the product as white solid (51 mg, 98%).

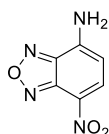
¹H NMR (500 MHz, Chloroform-*d*) δ 8.34 (s, 2H), 7.46 (d, *J* = 8.8 Hz, 2H), 7.24 (s, 1H), 6.91 (s, 2H), 6.75 (d, *J* = 8.8 Hz, 2H), 5.84 (s, 1H), 3.87 (s, 6H), 3.83 (s, 3H).

¹³C NMR (126 MHz, Chloroform-*d*) δ 158.0, 155.5, 153.5, 149.5, 135.4, 134.1, 126.6, 119.8, 113.8, 101.7, 97.6, 61.1, 56.3.

HRMS (ESI) *m/z* calcd. for C₂₀H₁₉N₅O₃ [M+H]⁺: 378.15661, found: 378.15670.

Melting point: 178 °C.

7-Nitrobenzo[*c*][1,2,5]oxadiazol-4-amine (**139**)²²¹

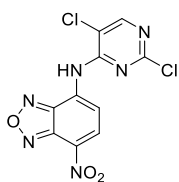


Chemical Formula: C₆H₄N₄O₃
Exact Mass: 180.0283

To a solution of 4-chloro-7-nitrobenzofurazan (1.0 g, 4.96 mmol) in MeOH (8 mL) was added ammonia (28% in H₂O). The mixture was stirred at room temperature for 24 h in a dark environment. The solvent was removed under reduced pressure. The residue was purified through silica gel column chromatography (eluent: cyclohexane/ethyl acetate=6/1~1/1). The titled compound was obtained as brown solid (530 mg, 59%).

¹H NMR (250 MHz, Methanol-*d*₄) δ 8.50 (d, *J* = 8.7 Hz, 1H), 6.40 (d, *J* = 8.7 Hz, 1H).

N-(2,5-Dichloropyrimidin-4-yl)-7-nitrobenzo[*c*][1,2,5]oxadiazol-4-amine (**140**)



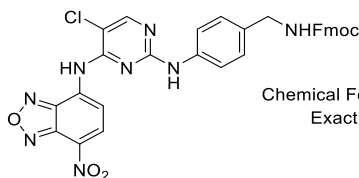
Chemical Formula: C₁₀H₄Cl₂N₆O₃
Exact Mass: 325.9722

To an ice-cooled solution of compound **139** (390 mg, 2.16 mmol) in distilled DMF was added NaH (130 mg, 60% in mineral oil, 3.24 mmol) in two portions. After 30 min, 2,4,5-trichloropyrimidine (247 μ L, 2.16 mmol) was added. After 1 h, the ice bath was removed and the mixture was heated to 90 °C and stirred overnight. Dilute the mixture with ethyl acetate, and washed with water and brine. The ethyl acetate phase was dried over MgSO₄ and concentrated *in vacuo*. The residue was purified by silica gel column chromatography (eluent: cyclohexane/ethyl acetate= 6/1~ 3/1) to give the title compound as yellow solid (193 mg, 27%).

¹H NMR (500 MHz, DMSO-*d*₆) δ 10.38 (s, 1H), 8.82 (d, *J* = 8.3, 1H), 8.72 (s, 1H), 7.99 (d, *J* = 8.4, 1H).

¹³C NMR (126 MHz, DMSO-*d*₆) δ 157.6, 156.5, 156.4, 146.1, 143.4, 134.6, 134.1, 131.2, 117.9, 116.1.

(9*H*-Fluoren-9-yl)methyl (4-((5-chloro-4-((7-nitrobenzo[*c*][1,2,5]oxadiazol-4-yl)amino)pyrimidin-2-yl)amino)benzyl)carbamate (**141**)



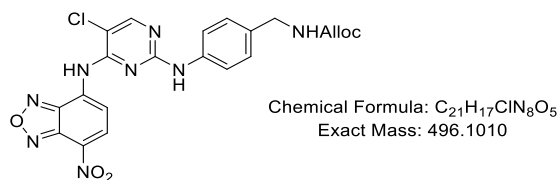
Chemical Formula: C₃₂H₂₃ClN₈O₅
Exact Mass: 634.1480

To a suspension of **140** (52 mg, 0.16 mmol) in 2-methoxyethanol (2 mL) was added **4** (55 mg, 0.16 mmol) and HCl (8 μ L, 4 M in 1,4-dioxane). The mixture was stirred at 110 °C for 20 h and then was concentrated *in vacuo*. The residue was triturated in DCM and

filtered to give the title compound as brown solid (35 mg, 35%).

^1H NMR (500 MHz, DMSO- d_6) δ 9.72 (s, 1H), 9.67 (s, 1H), 8.65 (d, J = 8.4 Hz, 1H), 8.48 (s, 1H), 8.25 (s, 1H), 7.88 (d, J = 7.6 Hz, 2H), 7.80 (t, J = 6.1 Hz, 1H), 7.70 (d, J = 7.5 Hz, 2H), 7.49 – 7.29 (m, 6H), 7.12 (d, J = 8.2 Hz, 2H), 4.35 (d, J = 6.9 Hz, 2H), 4.23 (t, J = 7.0 Hz, 1H), 4.13 (d, J = 6.1 Hz, 2H).

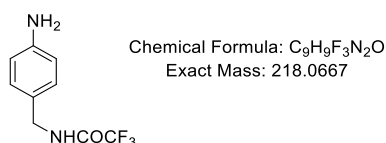
Allyl (4-((5-chloro-4-((7-nitrobenzo[c][1,2,5]oxadiazol-4-yl)amino)pyrimidin-2-yl)amino)benzyl)carbamate (**142**)



To a solution of **140** (95 mg, 0.29 mmol) in 2-methoxyethanol (3 mL) was added **6** (60 mg, 0.29 mmol) and HCl (15 μL , 4 M in 1,4-dioxane). The mixture was stirred at 110 $^\circ\text{C}$ for 20 h and then was concentrated *in vacuo*. The residue dissolved in ethyl acetate and washed with 1 M NaOH, water and brine. The organic phase was dried over MgSO₄ and purified by column chromatography (eluent: DCM/MeOH= 80/1~50/1) to give the title compound as orange solid (58 mg, 40%).

^1H NMR (250 MHz, Chloroform- d) δ 8.52 (s, 1H), 8.43 (s, 2H), 8.25 (s, 1H), 7.44 (d, J = 8.2 Hz, 2H), 7.30 (d, J = 8.1 Hz, 2H), 7.12 (s, 1H), 5.88 (ddd, J = 16.3, 10.8, 5.3 Hz, 1H), 5.30 – 5.14 (m, 2H), 5.07 (s, 1H), 4.58 (d, J = 5.7 Hz, 2H), 4.36 (d, J = 6.1 Hz, 2H).

N-(4-Aminobenzyl)-2,2,2-trifluoroacetamide (**143**)

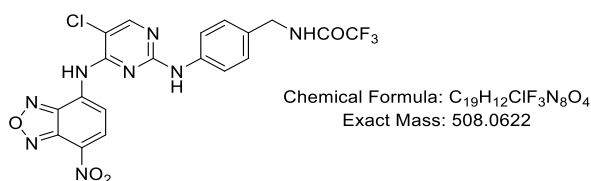


To an ice-cooled solution of 4-aminobenzylamine (200 μ L, 1.76 mmol) in MeOH (2 mL) was added dropwise methyl trifluoroacetate (178 μ L, 1.76 mmol). After 15 min, the ice bath was removed and the mixture was stirred at room temperature for a further 1 h. Then the solvent was removed under reduced pressure and the residue was purified through silica gel column chromatography (eluent: cyclohexane/ethyl acetate= 4/1~2/1) to obtain the title compound as off-white solid (335 mg, 87%).

^1H NMR (500 MHz, Chloroform-*d*) δ 7.07 (d, J = 7.9 Hz, 2H), 6.66 (d, J = 7.9 Hz, 2H), 6.53 (s, 1H), 4.39 (d, J = 5.4 Hz, 2H), 3.72 (s, 2H).

^{13}C NMR (126 MHz, CDCl_3) δ 146.7, 129.6, 125.6, 115.4, 43.8.

N-(4-((5-Chloro-4-((7-nitrobenzo[*c*][1,2,5]oxadiazol-4-yl)amino)pyrimidin-2-yl)amino)benzyl)-2,2,2-trifluoroacetamide (**144**)

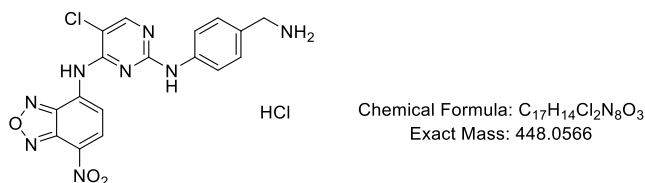


To a solution of **140** (100 mg, 0.306 mmol) in 2-methoxyethanol (3 mL) was added **143** (67 mg, 0.306 mmol) and HCl (77 μ L, 4 M in 1,4-dioxane). The mixture was stirred at 110 $^\circ\text{C}$ for 20 h and then was concentrated *in vacuo*. The residue was purified by column chromatography (eluent: DCM/MeOH= 80/1~50/1) to give the title compound as orange solid (115 mg, 74%).

^1H NMR (500 MHz, $\text{DMSO-}d_6$) δ 9.93 (t, J = 6.0 Hz, 1H), 9.73 (s, 1H), 8.64 (d, J = 8.4 Hz, 1H), 8.46 (s, 1H), 8.20 (s, 1H), 7.50 (d, J = 8.0 Hz, 2H), 7.16 (d, J = 8.1 Hz, 2H), 4.33 (d, J = 5.7 Hz, 2H).

^{13}C NMR (126 MHz, $\text{DMSO-}d_6$) δ 157.5, 156.6, 156.4, 156.1, 145.9, 143.4, 138.8, 134.9, 131.1, 128.5, 127.7, 119.6, 114.4, 106.4, 42.2.

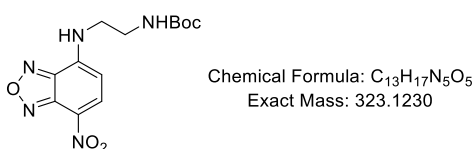
*N*²-(4-(Aminomethyl)phenyl)-5-chloro-*N*⁴-(7-nitrobenzo[*c*][1,2,5]oxadiazol-4-yl)pyrimidine-2,4-diamine (**145**)



A suspension of compound **144** (191 mg, 0.37 mmol) in a mixed solution of MeOH (10 mL) and HCl (4 M in 1,4-dioxane, 10 mL) was stirred at 60 °C for 20 h. After cooling to room temperature, the precipitate was filtered and washed with cold MeOH to give the title compound as yellow solid (144 mg, 86%).

¹H NMR (500 MHz, DMSO-*d*₆) δ 9.90 (s, 1H), 9.78 (s, 1H), 8.70 (d, *J* = 8.4 Hz, 1H), 8.50 (s, 1H), 8.27 (s, 3H, NH3), 7.57 (d, *J* = 8.1 Hz, 2H), 7.34 (d, *J* = 8.3 Hz, 2H), 3.94 (q, *J* = 5.6 Hz, 2H).

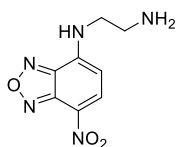
tert-Butyl (2-((7-nitrobenzo[*c*][1,2,5]oxadiazol-4-yl)amino)ethyl)carbamate (**146**)



To a stirred solution of compound **10** (615 mg, 3.84 mmol) in MeOH (20 mL) was added 4-chloro-7-nitrobenzofurazan (766 mg, 3.84 mmol) and DIPEA (220 μL, 3.84 mmol). The mixture was stirred at room temperature overnight before the concentration of solvent *in vacuo*. The residue was purified by silica gel column chromatography to obtain the title compound as a brown solid. (604 mg, 49%).

¹H NMR (500 MHz, Methanol-*d*₄) δ 8.47 (d, *J* = 8.8 Hz, 1H), 6.39 (d, *J* = 8.9 Hz, 1H), 3.62 (s, 2H), 3.40 (t, *J* = 6.1 Hz, 2H), 1.40 (s, 9H)

*N*¹-(7-Nitrobenzo[*c*][1,2,5]oxadiazol-4-yl)ethane-1,2-diamine (**147**)



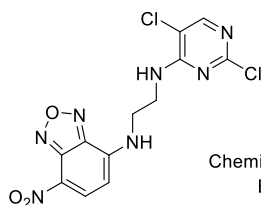
Chemical Formula: C₈H₉N₅O₃
Exact Mass: 223.0705

Compound **146** (604 mg, 1.87 mmol) was added to a mixture of DCM (1.5 mL) and trifluoroacetic acid (1.5 mL) and stirred for 30 min. The solvent was removed under reduced pressure to give the crude product, then diethyl ether was added and filtered to obtain titled compound as orange solid (578 mg, 92%).

¹H NMR (500 MHz, Methanol-*d*₄) δ 8.51 (d, *J* = 8.7 Hz, 1H), 6.45 (d, *J* = 8.7 Hz, 1H), 3.91 (t, *J* = 6.1 Hz, 2H), 3.38 (t, *J* = 6.2 Hz, 2H).

¹³C NMR (126 MHz, Methanol-*d*₄) δ 146.1, 146.0, 145.3, 138.0, 124.7, 100.6, 42.0, 39.1.

*N*¹-(2,5-Dichloropyrimidin-4-yl)-*N*²-(7-nitrobenzo[*c*][1,2,5]oxadiazol-4-yl)ethane-1,2-diamine (**148**)



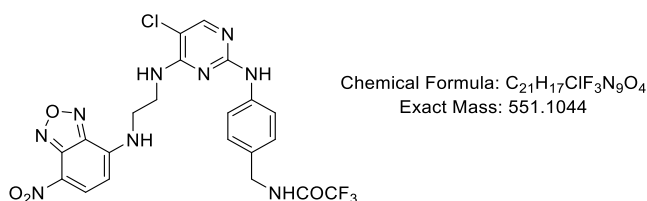
Chemical Formula: C₁₂H₉Cl₂N₇O₃
Exact Mass: 369.0144

To a solution of **147** (561 mg, 1.66 mmol) in MeOH (15 mL) was added 2,4,5-trichloropyrimidine (191 μL, 1.66 mmol) and DIPEA (580 μL, 3.32 mmol). The mixture was stirred at room temperature overnight, and then was filtered to give the title compound as orange solid (523 mg, 85%).

¹H NMR (500 MHz, DMSO-*d*₆) δ 9.39 (s, 1H), 8.51 (d, *J* = 8.8 Hz, 1H), 8.17 (s, 1H), 8.08 (s, 1H), 6.62 (d, *J* = 9.0 Hz, 1H), 3.69 (s, 4H).

¹³C NMR (126 MHz, DMSO-*d*₆) δ 158.9, 157.1, 153.8, 145.4, 144.5, 144.1, 137.6, 121.0, 113.1, 99.5, 42.1, 38.5.

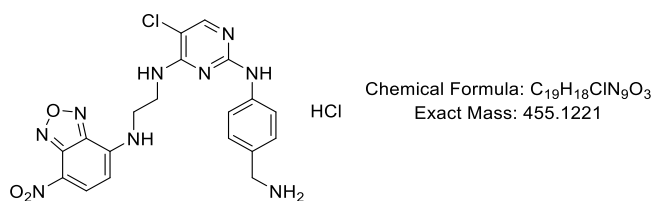
N-(4-((5-Chloro-4-((2-((7-nitrobenzo[*c*][1,2,5]oxadiazol-4-yl)amino)ethyl)amino)pyrimidin-2-yl)amino)benzyl)-2,2,2-trifluoroacetamide (**149**)



To a suspension of **148** (506 mg, 1.37 mmol) in *n*-BuOH (17 mL) was added **143** (298 mg, 1.37 mmol) and HCl (342 μ L, 4M in 1,4-dioxane). The mixture was stirred at 105 °C for 18 h. After cooling to room temperature the solvent was removed *in vacuo* and the resulted residue was washed with DCM and MeOH to give the title product as orange solid (603 mg, 79%). This compound was used directly for next step without further purification.

¹H NMR (500 MHz, DMSO-*d*₆) δ 10.20 (s, 1H), 9.94 (d, *J* = 6.2 Hz, 1H), 9.47 (s, 1H), 8.62 – 8.48 (m, 1H), 8.35 (d, *J* = 8.9 Hz, 1H), 8.20 (s, 1H), 7.43 (d, *J* = 8.0 Hz, 2H), 7.17 (d, *J* = 8.1 Hz, 2H), 6.41 (d, *J* = 8.9 Hz, 1H), 4.30 (d, *J* = 5.9 Hz, 2H), 3.81 (s, 7H).

*N*²-(4-(Aminomethyl)phenyl)-5-chloro-*N*⁴-(2-((7-nitrobenzo[*c*][1,2,5]oxadiazol-4-yl)amino)ethyl)pyrimidine-2,4-diamine hydrochloride (**150**)



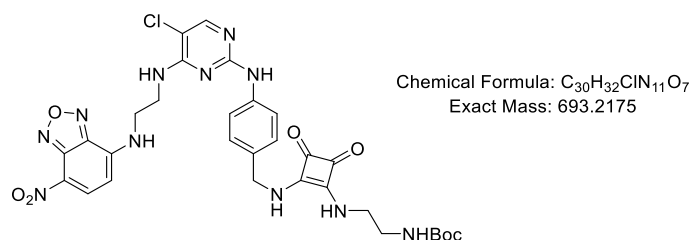
To a suspension of **149** (500 mg, 0.91 mmol) in MeOH (30 mL) was added solution of HCl in 1,4-dioxane (4 M, 30 mL). The suspension was stirred at 65 °C for 24 h in a sealed tube. The solvent was removed under reduced pressure. MeOH (5 mL) was added to the residue and filtered to obtain the title product as orange-brown solid (374 mg, 84%).

¹H NMR (500 MHz, DMSO-*d*₆) δ 10.72 (s, 1H), 9.51 (s, 1H), 8.88 (s, 1H), 8.48 (s, 3H),

8.31 (d, $J = 9.1$ Hz, 1H), 8.30 (s, 1H), 7.42 (d, $J = 8.1$ Hz, 2H), 7.36 (d, $J = 8.2$ Hz, 2H), 6.41 (d, $J = 9.0$ Hz, 1H), 3.92 – 3.71 (m, 6H).

^{13}C NMR (126 MHz, DMSO- d_6) δ 158.8, 151.4, 145.0, 144.3, 143.8, 142.2, 137.8, 137.2, 129.5, 129.1, 120.9, 119.9, 104.6, 99.4, 66.3, 42.4, 41.7.

tert-Butyl (2-((2-((4-((5-chloro-4-((2-((7-nitrobenzo[*c*][1,2,5]oxadiazol-4-yl)amino)ethyl)amino)pyrimidin-2-yl)amino)benzyl)amino)-3,4-dioxocyclobut-1-en-1-yl)amino)ethyl)carbamate (**151**)

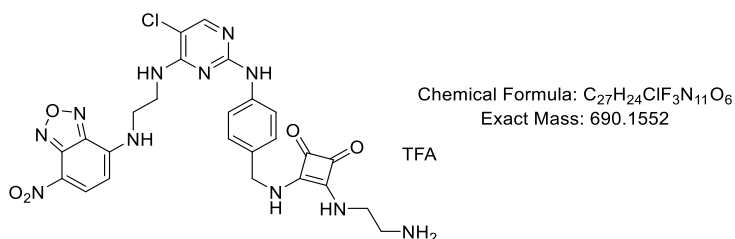


To a solution of **150** (338 mg, 0.686 mmol) in DMF (6mL) was added **94** (186 mg, 0.686 mmol) and DIPEA (240 μL , 1.372 mmol). The mixture was stirred at 83 $^\circ\text{C}$ overnight and then poured to ice water and filtered. The solid was purified through silica gel column chromatography (eluent: DCM/MeOH= 30/1 ~20/1) to give the title compound as orange solid (165mg, 35%).

^1H NMR (500 MHz, DMSO- d_6) δ 9.50 (s, 1H), 9.17 (s, 1H), 8.41 (d, $J = 8.9$ Hz, 1H), 7.96 (s, 1H), 7.63 (d, $J = 8.1$ Hz, 2H), 7.37 (d, $J = 5.9$ Hz, 1H), 7.18 (d, $J = 8.0$ Hz, 2H), 6.88 (d, $J = 5.9$ Hz, 1H), 6.43 (d, $J = 8.9$ Hz, 1H), 4.61 (d, $J = 6.3$ Hz, 2H), 3.84 – 3.65 (m, 4H), 3.51 (s, 2H), 3.09 (q, $J = 6.0$ Hz, 2H), 1.35 (s, 9H).

^{13}C NMR (126 MHz, DMSO- d_6) δ 182.6, 182.4, 168.0, 167.3, 157.8, 157.6, 155.7, 153.1, 145.2, 144.4, 144.0, 139.9, 137.8, 131.2, 127.8, 120.8, 118.7, 103.8, 99.4, 77.8, 46.5, 43.2, 42.8, 41.1, 40.1, 38.7, 28.2.

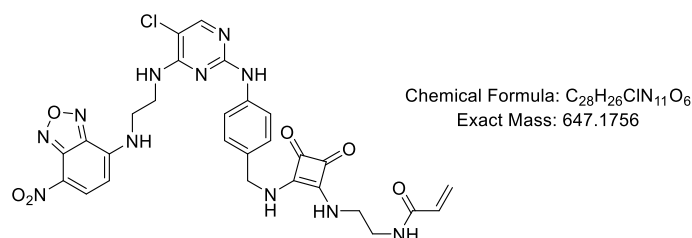
3-((2-aminoethyl)amino)-4-((4-((5-chloro-4-((2-((7-nitrobenzo[c][1,2,5]oxadiazol-4-yl)amino)ethyl)amino)pyrimidin-2-yl)amino)benzyl)amino)cyclobut-3-ene-1,2-dione trifluoroacetate salt (**152**)



Compound **151** (110 mg, 0.158 mmol) was added to the solution of TFA (1 mL) and DCM (1 mL) and stirred for 30 min at room temperature. The mixture was concentrated under reduced pressure. The residue was triturated with ethyl ether and was filtered to give the title compound as orange solid (140 mg, 95%). This compound was directly used for next step without further purification.

¹H NMR (500 MHz, Methanol-*d*₄) δ 8.14 (d, *J* = 8.8 Hz, 1H), 8.02 (s, 1H), 7.31 (s, 2H), 7.24 (s, 2H), 6.25 (d, *J* = 8.9 Hz, 1H), 4.74 (s, 2H), 3.97 (dt, *J* = 12.0, 5.7 Hz, 4H), 3.81 (s, 2H), 3.32 (d, *J* = 6.1 Hz, 2H).

N-(2-((2-((4-((5-Chloro-4-((2-((7-nitrobenzo[c][1,2,5]oxadiazol-4-yl)amino)ethyl)amino)pyrimidin-2-yl)amino)benzyl)amino)-3,4-dioxocyclobut-1-en-1-yl)amino)ethyl)acrylamide (**153**)



To a solution of **152** (100 mg, 0.107 mmol) in distilled DMF (1 mL), acryloyl chloride (14 μL, 0.16 mmol) and Et₃N (76 μL, 0.54 mmol) was added at 0°C. Then the mixture was

stirred at room temperature overnight and then poured into ice water. After filtration, the solid was purified by column chromatography (eluent: DCM/MeOH=30/1~20/1) to give the title compound as orange solid (40 mg, 55%).

^1H NMR (500 MHz, $\text{DMSO-}d_6$) δ 9.49 (s, 1H), 9.17 (s, 1H), 8.41 (d, $J = 8.7$ Hz, 1H), 8.31 – 8.20 (m, 1H), 7.96 (s, 1H), 7.64 (d, $J = 7.9$ Hz, 2H), 7.38 (s, 1H), 7.19 (d, $J = 7.9$ Hz, 2H), 6.43 (d, $J = 9.0$ Hz, 1H), 6.27 – 6.04 (m, 2H), 5.59 (d, $J = 10.2$ Hz, 1H), 4.62 (s, 2H), 3.90 – 3.77 (m, 2H), 3.73 (s, 2H), 3.58 (s, 2H).

^{13}C NMR (126 MHz, $\text{DMSO-}d_6$) δ 182.6, 182.4, 168.0, 167.4, 165.0, 157.8, 157.6, 153.1, 145.3, 144.4, 144.0, 139.9, 137.7, 131.5, 131.2, 127.8, 125.2, 120.8, 118.7, 103.8, 99.4, 69.8, 46.5, 42.9, 42.8, 40.0, 39.8, 39.7, 39.5, 39.3, 39.2, 39.0, 38.7.

References

- (1) Stewart, B. W., Wild, C. P. World Cancer Report 2014. *IARC Nonserial Publ.* **2014**, 630.
- (2) Bray, F.; Ferlay, J.; Soerjomataram, I.; Siegel, R. L.; Torre, L. A.; Jemal, A. Global cancer statistics 2018: GLOBOCAN estimates of incidence and mortality worldwide for 36 cancers in 185 countries <http://www.ncbi.nlm.nih.gov/pubmed/30207593>.
- (3) Cancer Tomorrow <https://gco.iarc.fr/tomorrow/home> (accessed Apr 9, 2019).
- (4) Spencer, C. M.; Faulds, D. Paclitaxel. *Drugs* **1994**, *48* (5), 794–847.
- (5) Longley, D. B.; Harkin, D. P.; Johnston, P. G. 5-Fluorouracil: Mechanisms of Action and Clinical Strategies. *Nat. Rev. Cancer* **2003**, *3* (5), 330–338.
- (6) Padma, V. V. An Overview of Targeted Cancer Therapy. *BioMedicine* **2015**, *5* (4), 19.
- (7) Deininger, M. W. N. Specific Targeted Therapy of Chronic Myelogenous Leukemia with Imatinib. *Pharmacol. Rev.* **2003**, *55* (3), 401–423.
- (8) Keir, M. E.; Butte, M. J.; Freeman, G. J.; Sharpe, A. H. PD-1 and Its Ligands in Tolerance and Immunity. *Annu. Rev. Immunol.* **2008**, *26* (1), 677–704.
- (9) Wang, C.; Thudium, K. B.; Han, M.; Wang, X.-T.; Huang, H.; Feingersh, D.; Garcia, C.; Wu, Y.; Kuhne, M.; Srinivasan, M.; *et al.* In Vitro Characterization of the Anti-PD-1 Antibody Nivolumab, BMS-936558, and In Vivo Toxicology in Non-Human Primates. *Cancer Immunol. Res.* **2014**, *2* (9), 846–856.
- (10) Miliotou, A. N.; Papadopoulou, L. C. CAR T-Cell Therapy: A New Era in Cancer Immunotherapy. *Curr. Pharm. Biotechnol.* **2018**, *19* (1), 5–18.
- (11) Manning, G.; Whyte, D. B.; Martinez, R.; Hunter, T.; Sudarsanam, S. The Protein Kinase Complement of the Human Genome. *Science (80-.)*. **2002**, *298* (5600), 1912–1934.
- (12) Johnson, L. N.; Lewis, R. J. Structural Basis for Control by Phosphorylation. *Chem. Rev.* **2001**, *101* (8), 2209–2242.

- (13) Hanks, S. K.; Hunter, T. Protein Kinases 6. The Eukaryotic Protein Kinase Superfamily: Kinase (Catalytic) Domain Structure and Classification. *FASEB J.* **1995**, *9* (8), 576–596.
- (14) Huse, M.; Kuriyan, J. The Conformational Plasticity of Protein Kinases. *Cell* **2002**, *109* (3), 275–282.
- (15) Hubbard, S. R.; Mohammadi, M.; Schlessinger, J. Autoregulatory Mechanisms in Protein-Tyrosine Kinases. *J. Biol. Chem.* **1998**, *273* (20), 11987–11990.
- (16) Hou, J.; Ju, J.; Zhang, Z.; Zhao, C.; Li, Z.; Zheng, J.; Sheng, T.; Zhang, H.; Hu, L.; Yu, X.; *et al.* Discovery of Potent Necroptosis Inhibitors Targeting RIPK1 Kinase Activity for the Treatment of Inflammatory Disorder and Cancer Metastasis. *Cell Death Dis.* **2019**, *10* (7), 493.
- (17) Chico, L. K.; Van Eldik, L. J.; Watterson, D. M. Targeting Protein Kinases in Central Nervous System Disorders. *Nat. Rev. Drug Discov.* **2009**, *8* (11), 892–909.
- (18) Kumar, R.; Singh, V. P.; Baker, K. M. Kinase Inhibitors for Cardiovascular Disease. *J. Mol. Cell. Cardiol.* **2007**, *42* (1), 1–11.
- (19) Malek, R.; Davis, S. N. Tyrosine Kinase Inhibitors under Investigation for the Treatment of Type II Diabetes. *Expert Opin. Investig. Drugs* **2016**, *25* (3), 287–296.
- (20) Roskoski, R. Properties of FDA-Approved Small Molecule Protein Kinase Inhibitors. *Pharmacol. Res.* **2019**, *144*, 19–50.
- (21) Wu, P.; Nielsen, T. E.; Clausen, M. H. FDA-Approved Small-Molecule Kinase Inhibitors. *Trends Pharmacol. Sci.* **2015**, *36* (7), 422–439.
- (22) Liu, Y.; Gray, N. S. Rational Design of Inhibitors That Bind to Inactive Kinase Conformations. *Nat. Chem. Biol.* **2006**, *2* (7), 358–364.
- (23) Tamaoki, T.; Nomoto, H.; Takahashi, I.; Kato, Y.; Morimoto, M.; Tomita, F. Staurosporine, a Potent Inhibitor of Phospholipid/Ca⁺⁺-dependent Protein Kinase. *Biochem. Biophys. Res. Commun.* **1986**, *135* (2), 397–402.
- (24) Karaman, M. W.; Herrgard, S.; Treiber, D. K.; Gallant, P.; Atteridge, C. E.; Campbell,

- B. T.; Chan, K. W.; Ciceri, P.; Davis, M. I.; Edeen, P. T.; *et al.* A Quantitative Analysis of Kinase Inhibitor Selectivity. *Nat. Biotechnol.* **2008**, *26* (1), 127–132.
- (25) Gazit, A.; Yaish, P.; Gilon, C.; Levitzki, A. Tyrphostins I: Synthesis and Biological Activity of Protein Tyrosine Kinase Inhibitors. *J. Med. Chem.* **1989**, *32* (10), 2344–2352.
- (26) Nurwidya, F.; Takahashi, F.; Takahashi, K. Gefitinib in the Treatment of Nonsmall Cell Lung Cancer with Activating Epidermal Growth Factor Receptor Mutation. *J. Nat. Sci. Biol. Med.* **2016**, *7* (2), 119–123.
- (27) Wakeling, A. E.; Guy, S. P.; Woodburn, J. R.; Ashton, S. E.; Curry, B. J.; Barker, A. J.; Gibson, K. H. ZD1839 (Iressa): An Orally Active Inhibitor of Epidermal Growth Factor Signaling with Potential for Cancer Therapy. *Cancer Res.* **2002**, *62* (20), 5749–5754.
- (28) Yun, C.-H.; Boggon, T. J.; Li, Y.; Woo, M. S.; Greulich, H.; Meyerson, M.; Eck, M. J. Structures of Lung Cancer-Derived EGFR Mutants and Inhibitor Complexes: Mechanism of Activation and Insights into Differential Inhibitor Sensitivity. *Cancer Cell* **2007**, *11* (3), 217–227.
- (29) Eyers, P. A.; Craxton, M.; Morricel, N.; Cohen, P.; Goedert, M. Conversion of SB 203580-Insensitive MAP Kinase Family Members to Drug-Sensitive Forms by a Single Amino-Acid Substitution. *Chem. Biol.* **1998**, *5* (6), 321–328.
- (30) Gammons, M. V.; Fedorov, O.; Ivison, D.; Du, C.; Clark, T.; Hopkins, C.; Hagiwara, M.; Dick, A. D.; Cox, R.; Harper, S. J.; *et al.* Topical Antiangiogenic SRPK1 Inhibitors Reduce Choroidal Neovascularization in Rodent Models of Exudative AMD. *Investig. Ophthalmology Vis. Sci.* **2013**, *54* (9), 6052.
- (31) Debreczeni, J. É.; Bullock, A. N.; Atilla, G. E.; Williams, D. S.; Bregman, H.; Knapp, S.; Meggers, E. Ruthenium Half-Sandwich Complexes Bound to Protein Kinase Pim-1. *Angew. Chemie Int. Ed.* **2006**, *45* (10), 1580–1585.
- (32) Karcher, S.; Laufer, S. Successful Structure-Based Design of Recent P38 MAP Kinase

- Inhibitors. *Curr. Top. Med. Chem.* **2009**, *9* (7), 655–676.
- (33) Zhang, C.; Kenski, D. M.; Paulson, J. L.; Bonshtien, A.; Sessa, G.; Cross, J. V.; Templeton, D. J.; Shokat, K. M. A Second-Site Suppressor Strategy for Chemical Genetic Analysis of Diverse Protein Kinases. *Nat. Methods* **2005**, *2* (6), 435–441.
- (34) Koeberle, S. C.; Romir, J.; Fischer, S.; Koeberle, A.; Schattel, V.; Albrecht, W.; Grütter, C.; Werz, O.; Rauh, D.; Stehle, T.; *et al.* Skepinone-L Is a Selective P38 Mitogen-Activated Protein Kinase Inhibitor. *Nat. Chem. Biol.* **2012**, *8* (2), 141–143.
- (35) Zhao, Z.; Wu, H.; Wang, L.; Liu, Y.; Knapp, S.; Liu, Q.; Gray, N. S. Exploration of Type II Binding Mode: A Privileged Approach for Kinase Inhibitor Focused Drug Discovery? *ACS Chem. Biol.* **2014**, *9* (6), 1230–1241.
- (36) Nagar, B.; Bornmann, W. G.; Pellicena, P.; Schindler, T.; Veach, D. R.; Miller, W. T.; Clarkson, B.; Kuriyan, J. Crystal Structures of the Kinase Domain of C-Abl in Complex with the Small Molecule Inhibitors PD173955 and Imatinib (STI-571). *Cancer Res.* **2002**, *62* (15), 4236–4243.
- (37) Carles, F.; Bourg, S.; Meyer, C.; Bonnet, P. PKIDB: A Curated, Annotated and Updated Database of Protein Kinase Inhibitors in Clinical Trials. *Molecules* **2018**, *23* (4), 908.
- (38) Wu, P.; Nielsen, T. E.; Clausen, M. H. FDA-Approved Small-Molecule Kinase Inhibitors. *Trends Pharmacol. Sci.* **2015**, *36* (7), 422–439.
- (39) Gavrin, L. K.; Saiah, E. Approaches to Discover Non-ATP Site Kinase Inhibitors. *Med. Chem. Commun.* **2013**, *4* (1), 41–51.
- (40) Wright, C. J. M.; McCormack, P. L. Trametinib: First Global Approval. *Drugs* **2013**, *73* (11), 1245–1254.
- (41) Takauki, Y.; Reina, K.; Nobuyuki, T.; Yoshihiro, S.; Sakai, T. Antitumor Activities of JTP-74057 (GSK1120212), a Novel MEK1/2 Inhibitor, on Colorectal Cancer Cell Lines in Vitro and in Vivo. *Int. J. Oncol.* **2011**, *39* (1), 23–31.
- (42) Ohren, J. F.; Chen, H.; Pavlovsky, A.; Whitehead, C.; Zhang, E.; Kuffa, P.; Yan, C.;

- McConnell, P.; Spessard, C.; Banotai, C.; *et al.* Structures of Human MAP Kinase Kinase 1 (MEK1) and MEK2 Describe Novel Noncompetitive Kinase Inhibition. *Nat. Struct. Mol. Biol.* **2004**, *11* (12), 1192–1197.
- (43) Gilmartin, A. G.; Bleam, M. R.; Groy, A.; Moss, K. G.; Minthorn, E. A.; Kulkarni, S. G.; Rominger, C. M.; Erskine, S.; Fisher, K. E.; Yang, J.; *et al.* GSK1120212 (JTP-74057) Is an Inhibitor of MEK Activity and Activation with Favorable Pharmacokinetic Properties for Sustained In Vivo Pathway Inhibition. *Clin. Cancer Res.* **2011**, *17* (5), 989–1000.
- (44) Adrián, F. J.; Ding, Q.; Sim, T.; Velentza, A.; Sloan, C.; Liu, Y.; Zhang, G.; Hur, W.; Ding, S.; Manley, P.; *et al.* Allosteric Inhibitors of Bcr-Abl-Dependent Cell Proliferation. *Nat. Chem. Biol.* **2006**, *2* (2), 95–102.
- (45) Zhang, J.; Adrián, F. J.; Jahnke, W.; Cowan-Jacob, S. W.; Li, A. G.; Iacob, R. E.; Sim, T.; Powers, J.; Dierks, C.; Sun, F.; *et al.* Targeting Bcr-Abl by Combining Allosteric with ATP-Binding-Site Inhibitors. *Nature* **2010**, *463* (7280), 501–506.
- (46) Park, B.; Pirmohamed, M.; Kitteringham, N. Idiosyncratic Drug Reactions: A Mechanistic Evaluation of Risk Factors. *Br. J. Clin. Pharmacol.* **1992**, *34* (5), 377–395.
- (47) Lonsdale, R.; Ward, R. A. Structure-Based Design of Targeted Covalent Inhibitors. *Chem. Soc. Rev.* **2018**, *47* (11), 3816–3830.
- (48) Bauer, R. A. Covalent Inhibitors in Drug Discovery: From Accidental Discoveries to Avoided Liabilities and Designed Therapies. *Drug Discov. Today* **2015**, *20* (9), 1061–1073.
- (49) Jones, A.; Zhang, X.; Lei, X. Covalent Probe Finds Carboxylic Acid. *Cell Chem. Biol.* **2017**, *24* (5), 537–539.
- (50) Platzer, G.; Okon, M.; McIntosh, L. P. PH-Dependent Random Coil ¹H, ¹³C, and ¹⁵N Chemical Shifts of the Ionizable Amino Acids: A Guide for Protein PKa Measurements. *J. Biomol. NMR* **2014**, *60* (2–3), 109–129.

- (51) Barf, T.; Kaptein, A. Irreversible Protein Kinase Inhibitors: Balancing the Benefits and Risks. *J. Med. Chem.* **2012**, *55* (14), 6243–6262.
- (52) Zhang, J.; Yang, P.; Gray, N. Targeting Cancer with Small Molecule Kinase Inhibitors. *Nat. Rev. Cancer* **2009**, *9* (1), 28–39.
- (53) Leproult, E.; Barluenga, S.; Moras, D.; Wurtz, J.-M.; Winssinger, N. Cysteine Mapping in Conformationally Distinct Kinase Nucleotide Binding Sites: Application to the Design of Selective Covalent Inhibitors. *J. Med. Chem.* **2011**, *54* (5), 1347–1355.
- (54) Solca, F.; Dahl, G.; Zoephel, A.; Bader, G.; Sanderson, M.; Klein, C.; Kraemer, O.; Himmelsbach, F.; Haaksma, E.; Adolf, G. R. Target Binding Properties and Cellular Activity of Afatinib (BIBW 2992), an Irreversible ErbB Family Blocker. *J. Pharmacol. Exp. Ther.* **2012**, *343* (2), 342–350.
- (55) Pettinger, J.; Jones, K.; Cheeseman, M. D. Lysine-Targeting Covalent Inhibitors. *Angew. Chemie Int. Ed.* **2017**, *56* (48), 15200–15209.
- (56) Isom, D. G.; Castaneda, C. A.; Cannon, B. R.; Garcia-Moreno E., B. Large Shifts in PKa Values of Lysine Residues Buried inside a Protein. *Proc. Natl. Acad. Sci.* **2011**, *108* (13), 5260–5265.
- (57) Pearson, R. G. Hard and Soft Acids and Bases. *J. Am. Chem. Soc.* **1963**, *85* (22), 3533–3539.
- (58) Migneault, I.; Dartiguenave, C.; Bertrand, M. J.; Waldron, K. C. Glutaraldehyde: Behavior in Aqueous Solution, Reaction with Crosslinking. *Biotechniques* **2004**, *37* (5), 790–802.
- (59) Dahal, U. P.; Gilbert, A. M.; Obach, R. S.; Flanagan, M. E.; Chen, J. M.; Garcia-Irizarry, C.; Starr, J. T.; Schuff, B.; Uccello, D. P.; Young, J. A. Intrinsic Reactivity Profile of Electrophilic Moieties to Guide Covalent Drug Design: N- α -Acetyl- L - Lysine as an Amine Nucleophile. *Medchemcomm* **2016**, *7* (5), 864–872.
- (60) Anscombe, E.; Meschini, E.; Mora-Vidal, R.; Martin, M. P.; Staunton, D.; Geitmann,

- M.; Danielson, U. H.; Stanley, W. A.; Wang, L. Z.; Reuillon, T.; *et al.* Identification and Characterization of an Irreversible Inhibitor of CDK2. *Chem. Biol.* **2015**, *22* (9), 1159–1164.
- (61) Schwans, J. P.; Sunden, F.; Gonzalez, A.; Tsai, Y.; Herschlag, D. Uncovering the Determinants of a Highly Perturbed Tyrosine PKa in the Active Site of Ketosteroid Isomerase. *Biochemistry* **2013**, *52* (44), 7840–7855.
- (62) Hett, E. C.; Xu, H.; Geoghegan, K. F.; Gopalsamy, A.; Kyne, R. E.; Menard, C. A.; Narayanan, A.; Parikh, M. D.; Liu, S.; Roberts, L.; *et al.* Rational Targeting of Active-Site Tyrosine Residues Using Sulfonyl Fluoride Probes. *ACS Chem. Biol.* **2015**, *10* (4), 1094–1098.
- (63) Hatcher, J. M.; Wu, G.; Zeng, C.; Zhu, J.; Meng, F.; Patel, S.; Wang, W.; Ficarro, S. B.; Leggett, A. L.; Powell, C. E.; *et al.* SRPKIN-1: A Covalent SRPK1/2 Inhibitor That Potently Converts VEGF from Pro-Angiogenic to Anti-Angiogenic Isoform. *Cell Chem. Biol.* **2018**, *25* (4), 460-470.e6.
- (64) Czerwinski, R. M.; Harris, T. K.; Massiah, M. A.; Mildvan, A. S.; Whitman, C. P. The Structural Basis for the Perturbed p K a of the Catalytic Base in 4-Oxalocrotonate Tautomerase: Kinetic and Structural Effects of Mutations of Phe-50 †. *Biochemistry* **2001**, *40* (7), 1984–1995.
- (65) Lei, J.; Zhou, Y.; Xie, D.; Zhang, Y. Mechanistic Insights into a Classic Wonder Drug—Aspirin. *J. Am. Chem. Soc.* **2015**, *137* (1), 70–73.
- (66) Fadeyi, O. O.; Hoth, L. R.; Choi, C.; Feng, X.; Gopalsamy, A.; Hett, E. C.; Kyne, R. E.; Robinson, R. P.; Jones, L. H. Covalent Enzyme Inhibition through Fluorosulfate Modification of a Noncatalytic Serine Residue. *ACS Chem. Biol.* **2017**, *12* (8), 2015–2020.
- (67) Serafimova, I. M.; Pufall, M. A.; Krishnan, S.; Duda, K.; Cohen, M. S.; Maglathlin, R. L.; McFarland, J. M.; Miller, R. M.; Frödin, M.; Taunton, J. Reversible Targeting of Noncatalytic Cysteines with Chemically Tuned Electrophiles. *Nat. Chem. Biol.*

- 2012**, 8 (5), 471–476.
- (68) Bradshaw, J. M.; McFarland, J. M.; Paavilainen, V. O.; Bisconte, A.; Tam, D.; Phan, V. T.; Romanov, S.; Finkle, D.; Shu, J.; Patel, V.; *et al.* Prolonged and Tunable Residence Time Using Reversible Covalent Kinase Inhibitors. *Nat. Chem. Biol.* **2015**, 11 (7), 525–531.
- (69) Shindo, N.; Fuchida, H.; Sato, M.; Watari, K.; Shibata, T.; Kuwata, K.; Miura, C.; Okamoto, K.; Hatsuyama, Y.; Tokunaga, K.; *et al.* Selective and Reversible Modification of Kinase Cysteines with Chlorofluoroacetamides. *Nat. Chem. Biol.* **2019**, 15 (3), 250–258.
- (70) Gehringer, M.; Laufer, S. A. Emerging and Re-Emerging Warheads for Targeted Covalent Inhibitors: Applications in Medicinal Chemistry and Chemical Biology. *J. Med. Chem.* **2019**, 62 (12), 5673–5724.
- (71) Hanks, S. K.; Calalb, M. B.; Harper, M. C.; Patel, S. K. Focal Adhesion Protein-Tyrosine Kinase Phosphorylated in Response to Cell Attachment to Fibronectin. *Proc. Natl. Acad. Sci. U. S. A.* **1992**, 89 (18), 8487–8491.
- (72) Avraham, S.; London, R.; Fu, Y.; Ota, S.; Hiregowdara, D.; Li, J.; Jiang, S.; Pasztor, L. M.; White, R. A.; Groopman, J. E.; *et al.* Identification and Characterization of a Novel Related Adhesion Focal Tyrosine Kinase (RAFTK) from Megakaryocytes and Brain. *J. Biol. Chem.* **1995**, 270 (46), 27742–27751.
- (73) Lee, B. Y.; Timpson, P.; Horvath, L. G.; Daly, R. J. FAK Signaling in Human Cancer as a Target for Therapeutics. *Pharmacol. Ther.* **2015**, 146, 132–149.
- (74) Chen, R.; Kim, O.; Li, M.; Xiong, X.; Guan, J. L.; Kung, H. J.; Chen, H.; Shimizu, Y.; Qiu, Y. Regulation of the PH-Domain-Containing Tyrosine Kinase Etk by Focal Adhesion Kinase through the FERM Domain. *Nat. Cell Biol.* **2001**, 3 (5), 439–444.
- (75) Lobo, M.; Zachary, I. Nuclear Localization and Apoptotic Regulation of an Amino-Terminal Domain Focal Adhesion Kinase Fragment in Endothelial Cells. *Biochem. Biophys. Res. Commun.* **2000**, 276 (3), 1068–1074.

- (76) Parsons, J. T. Focal Adhesion Kinase: The First Ten Years. *J. Cell Sci.* **2003**, *116* (8), 1409–1416.
- (77) Lietha, D.; Cai, X.; Ceccarelli, D. F. J.; Li, Y.; Schaller, M. D.; Eck, M. J. Structural Basis for the Autoinhibition of Focal Adhesion Kinase. *Cell* **2007**, *129* (6), 1177–1187.
- (78) Nowakowski, J.; Cronin, C. N.; McRee, D. E.; Knuth, M. W.; Nelson, C. G.; Pavletich, N. P.; Rogers, J.; Sang, B.-C.; Scheibe, D. N.; Swanson, R. V.; *et al.* Structures of the Cancer-Related Aurora-A, FAK, and EphA2 Protein Kinases from Nanovolume Crystallography. *Structure* **2002**, *10* (12), 1659–1667.
- (79) Schaller, M. D.; Hildebrand, J. D.; Shannon, J. D.; Fox, J. W.; Vines, R. R.; Parsons, J. T. Autophosphorylation of the Focal Adhesion Kinase, Pp125FAK, Directs SH2-Dependent Binding of Pp60src. *Mol. Cell. Biol.* **1994**, *14* (3), 1680–1688.
- (80) Frame, M. C.; Patel, H.; Serrels, B.; Lietha, D.; Eck, M. J. The FERM Domain: Organizing the Structure and Function of FAK. *Nat. Rev. Mol. Cell Biol.* **2010**, *11* (11), 802–814.
- (81) Sulzmaier, F. J.; Jean, C.; Schlaepfer, D. D. FAK in Cancer: Mechanistic Findings and Clinical Applications. *Nat. Rev. Cancer* **2014**, *14* (9), 598–610.
- (82) Golubovskaya, V. M. Targeting FAK in Human Cancer: From Finding to First Clinical Trials. *Front. Biosci. (Landmark Ed.)* **2014**, *19*, 687–706.
- (83) Tai, Y.-L.; Chen, L.-C.; Shen, T.-L. Emerging Roles of Focal Adhesion Kinase in Cancer. *Biomed Res. Int.* **2015**, *2015*, 690690.
- (84) Lark, A. L.; Livasy, C. A.; Dressler, L.; Moore, D. T.; Millikan, R. C.; Geradts, J.; Iacocca, M.; Cowan, D.; Little, D.; Craven, R. J.; *et al.* High Focal Adhesion Kinase Expression in Invasive Breast Carcinomas Is Associated with an Aggressive Phenotype. *Mod. Pathol.* **2005**, *18* (10), 1289–1294.
- (85) Lark, A. L.; Livasy, C. A.; Calvo, B.; Caskey, L.; Moore, D. T.; Yang, X.; Cance, W. G. Overexpression of Focal Adhesion Kinase in Primary Colorectal Carcinomas and Colorectal Liver Metastases: Immunohistochemistry and Real-Time PCR Analyses.

- Clin. Cancer Res.* **2003**, 9 (1), 215–222.
- (86) Kim, S. J.; Park, J. W.; Yoon, J. S.; Mok, J. O.; Kim, Y. J.; Park, H. K.; Kim, C. H.; Byun, D. W.; Lee, Y. J.; Jin, S. Y.; *et al.* Increased Expression of Focal Adhesion Kinase in Thyroid Cancer: Immunohistochemical Study. *J. Korean Med. Sci.* **2004**, 19 (5), 710–715.
- (87) Tremblay, L.; Hauck, W.; Aprikian, A. G.; Begin, L. R.; Chapdelaine, A.; Chevalier, S. Focal Adhesion Kinase (Pp125FAK) Expression, Activation and Association with Paxillin and P50CSK in Human Metastatic Prostate Carcinoma. *Int. J. cancer* **1996**, 68 (2), 164–171.
- (88) Carelli, S.; Zadra, G.; Vaira, V.; Falleni, M.; Bottiglieri, L.; Nosotti, M.; Di Giulio, A. M.; Gorio, A.; Bosari, S. Up-Regulation of Focal Adhesion Kinase in Non-Small Cell Lung Cancer. *Lung Cancer* **2006**, 53 (3), 263–271.
- (89) Su, J.-M.; Gui, L.; Zhou, Y.-P.; Zha, X.-L. Expression of Focal Adhesion Kinase and Alpha5 and Beta1 Integrins in Carcinomas and Its Clinical Significance. *World J. Gastroenterol.* **2002**, 8 (4), 613–618.
- (90) Judson, P. L.; He, X.; Cance, W. G.; Van Le, L. Overexpression of Focal Adhesion Kinase, a Protein Tyrosine Kinase, in Ovarian Carcinoma. *Cancer* **1999**, 86 (8), 1551–1556.
- (91) Gabarra-Niecko, V.; Schaller, M. D.; Dunty, J. M. FAK Regulates Biological Processes Important for the Pathogenesis of Cancer. *Cancer Metastasis Rev.* **2003**, 22 (4), 359–374.
- (92) Owens, L. V.; Xu, L.; Craven, R. J.; Dent, G. A.; Weiner, T. M.; Kornberg, L.; Liu, E. T.; Cance, W. G.; Kim, T. J.; Lu, C.; *et al.* Overexpression of the Focal Adhesion Kinase (P125FAK) in Invasive Human Tumors. *Cancer Res.* **1995**, 55 (13), 2752–2755.
- (93) Owens, L. V.; Xu, L.; Dent, G. A.; Yang, X.; Sturge, G. C.; Craven, R. J.; Cance, W. G. Focal Adhesion Kinase as a Marker of Invasive Potential in Differentiated Human

- Thyroid Cancer. *Ann. Surg. Oncol.* **1996**, *3* (1), 100–105.
- (94) Zagzag, D.; Friedlander, D. R.; Margolis, B.; Grumet, M.; Semenza, G. L.; Zhong, H.; Simons, J. W.; Holash, J.; Wiegand, S. J.; Yancopoulos, G. D. Molecular Events Implicated in Brain Tumor Angiogenesis and Invasion. *Pediatr. Neurosurg.* **2000**, *33* (1), 49–55.
- (95) Frisch, S. M.; Vuori, K.; Ruoslahti, E.; Chan-Hui, P. Y. Control of Adhesion-Dependent Cell Survival by Focal Adhesion Kinase. *J. Cell Biol.* **1996**, *134* (3), 793–799.
- (96) Golubovskaya, V. M.; Finch, R.; Cance, W. G. Direct Interaction of the N-Terminal Domain of Focal Adhesion Kinase with the N-Terminal Transactivation Domain of P53. *J. Biol. Chem.* **2005**, *280* (26), 25008–25021.
- (97) Lim, S.-T.; Chen, X. L.; Lim, Y.; Hanson, D. A.; Vo, T.-T.; Howerton, K.; Larocque, N.; Fisher, S. J.; Schlaepfer, D. D.; Ilic, D. Nuclear FAK Promotes Cell Proliferation and Survival through FERM-Enhanced P53 Degradation. *Mol. Cell* **2008**, *29* (1), 9–22.
- (98) Xu, L. H.; Owens, L. V.; Sturge, G. C.; Yang, X.; Liu, E. T.; Craven, R. J.; Cance, W. G. Attenuation of the Expression of the Focal Adhesion Kinase Induces Apoptosis in Tumor Cells. *Cell Growth Differ.* **1996**, *7* (4), 413–418.
- (99) Xu, L.-H.; Yang, X.; Bradham, C. A.; Brenner, D. A.; Baldwin, A. S.; Craven, R. J.; Cance, W. G. The Focal Adhesion Kinase Suppresses Transformation-Associated, Anchorage-Independent Apoptosis in Human Breast Cancer Cells. *J. Biol. Chem.* **2000**, *275* (39), 30597–30604.
- (100) Schlaepfer, D. D.; Mitra, S. K.; Ilic, D. Control of Motile and Invasive Cell Phenotypes by Focal Adhesion Kinase. *Biochim. Biophys. Acta - Mol. Cell Res.* **2004**, *1692* (2–3), 77–102.
- (101) Carragher, N. O.; Westhoff, M. A.; Fincham, V. J.; Schaller, M. D.; Frame, M. C. A Novel Role for FAK as a Protease-Targeting Adaptor Protein. *Curr. Biol.* **2003**, *13*

- (16), 1442–1450.
- (102) Franco, S. J.; Rodgers, M. A.; Perrin, B. J.; Han, J.; Bennin, D. A.; Critchley, D. R.; Huttenlocher, A. Calpain-Mediated Proteolysis of Talin Regulates Adhesion Dynamics. *Nat. Cell Biol.* **2004**, *6* (10), 977–983.
- (103) Guinamard, R.; Okigaki, M.; Schlessinger, J.; Ravetch, J. V. Absence of Marginal Zone B Cells in Pyk-2–Deficient Mice Defines Their Role in the Humoral Response. *Nat. Immunol.* **2000**, *1* (1), 31–36.
- (104) Mitra, S. K.; Mikolon, D.; Molina, J. E.; Hsia, D. A.; Hanson, D. A.; Chi, A.; Lim, S.-T.; Bernard-Trifilo, J. A.; Ilic, D.; Stupack, D. G.; *et al.* Intrinsic FAK Activity and Y925 Phosphorylation Facilitate an Angiogenic Switch in Tumors. *Oncogene* **2006**, *25* (44), 5969–5984.
- (105) Serrels, A.; Lund, T.; Serrels, B.; Byron, A.; McPherson, R. C.; von Kriegsheim, A.; Gómez-Cuadrado, L.; Canel, M.; Muir, M.; Ring, J. E.; *et al.* Nuclear FAK Controls Chemokine Transcription, Tregs, and Evasion of Anti-Tumor Immunity. *Cell* **2015**, *163* (1), 160–173.
- (106) Jiang, H.; Hegde, S.; Knolhoff, B. L.; Zhu, Y.; Herndon, J. M.; Meyer, M. A.; Nywening, T. M.; Hawkins, W. G.; Shapiro, I. M.; Weaver, D. T.; *et al.* Targeting Focal Adhesion Kinase Renders Pancreatic Cancers Responsive to Checkpoint Immunotherapy. *Nat. Med.* **2016**, *22* (8), 851–860.
- (107) Roberts, W. G.; Ung, E.; Whalen, P.; Cooper, B.; Hulford, C.; Autry, C.; Richter, D.; Emerson, E.; Lin, J.; Kath, J.; *et al.* Antitumor Activity and Pharmacology of a Selective Focal Adhesion Kinase Inhibitor, PF-562,271. *Cancer Res.* **2008**, *68* (6), 1935–1944.
- (108) Jones, S. F.; Siu, L. L.; Bendell, J. C.; Cleary, J. M.; Razak, A. R. A.; Infante, J. R.; Pandya, S. S.; Bedard, P. L.; Pierce, K. J.; Houk, B.; *et al.* A Phase I Study of VS-6063, a Second-Generation Focal Adhesion Kinase Inhibitor, in Patients with Advanced Solid Tumors. *Invest. New Drugs* **2015**, *33* (5), 1100–1107.

- (109) Ott, G. R.; Cheng, M.; Learn, K. S.; Wagner, J.; Gingrich, D. E.; Lisko, J. G.; Curry, M.; Mesaros, E. F.; Ghose, A. K.; Quail, M. R.; *et al.* Discovery of Clinical Candidate CEP-37440, a Selective Inhibitor of Focal Adhesion Kinase (FAK) and Anaplastic Lymphoma Kinase (ALK). *J. Med. Chem.* **2016**, *59* (16), 7478–7496.
- (110) Salem, I.; Alsalahi, M.; Chervoneva, I.; Aburto, L. D.; Addya, S.; Ott, G. R.; Ruggeri, B. A.; Cristofanilli, M.; Fernandez, S. V. The Effects of CEP-37440, an Inhibitor of Focal Adhesion Kinase, in Vitro and in Vivo on Inflammatory Breast Cancer Cells. *Breast cancer Res.* **2016**, *18* (1), 37.
- (111) Liu, T.-J.; LaFortune, T.; Honda, T.; Ohmori, O.; Hatakeyama, S.; Meyer, T.; Jackson, D.; de Groot, J.; Yung, W. K. A. Inhibition of Both Focal Adhesion Kinase and Insulin-like Growth Factor-I Receptor Kinase Suppresses Glioma Proliferation in Vitro and in Vivo. *Mol. Cancer Ther.* **2007**, *6* (4), 1357–1367.
- (112) Wang, L.; Ai, M.; Yu, J.; Jin, L.; Wang, C.; Liu, Z.; Shu, X.; Tang, Z.; Liu, K.; Luo, H.; *et al.* Structure-Based Modification of Carbonyl-Diphenylpyrimidines (Car-DPPYs) as a Novel Focal Adhesion Kinase (FAK) Inhibitor against Various Stubborn Cancer Cells. *Eur. J. Med. Chem.* **2019**, *172*, 154–162.
- (113) Qu, M.; Liu, Z.; Zhao, D.; Wang, C.; Zhang, J.; Tang, Z.; Liu, K.; Shu, X.; Yuan, H.; Ma, X. Design, Synthesis and Biological Evaluation of Sulfonamide-Substituted Diphenylpyrimidine Derivatives (Sul-DPPYs) as Potent Focal Adhesion Kinase (FAK) Inhibitors with Antitumor Activity. *Bioorganic Med. Chem.* **2017**, *25* (15), 3989–3996.
- (114) Liu, H.; Wu, B.; Ge, Y.; Huang, J.; Song, S.; Wang, C.; Yao, J.; Liu, K.; Li, Y.; Li, Y.; *et al.* Phosphamide-Containing Diphenylpyrimidine Analogues (PA-DPPYs) as Potent Focal Adhesion Kinase (FAK) Inhibitors with Enhanced Activity against Pancreatic Cancer Cell Lines. *Bioorg. Med. Chem.* **2017**, *25* (24), 6313–6321.
- (115) Infante, J. R.; Camidge, D. R.; Mileschkin, L. R.; Chen, E. X.; Hicks, R. J.; Rischin, D.; Fingert, H.; Pierce, K. J.; Xu, H.; Roberts, W. G.; *et al.* Safety, Pharmacokinetic, and Pharmacodynamic Phase I Dose-Escalation Trial of PF-00562271, an Inhibitor of Focal Adhesion Kinase, in Advanced Solid Tumors. *J. Clin. Oncol.* **2012**, *30* (13),

1527–1533.

- (116) Kang, Y.; Hu, W.; Ivan, C.; Dalton, H. J.; Miyake, T.; Pecot, C. V.; Zand, B.; Liu, T.; Huang, J.; Jennings, N. B.; *et al.* Role of Focal Adhesion Kinase in Regulating YB-1-Mediated Paclitaxel Resistance in Ovarian Cancer. *JNCI J. Natl. Cancer Inst.* **2013**, *105* (19), 1485–1495.
- (117) Lin, H.-M.; Lee, B. Y.; Castillo, L.; Spielman, C.; Grogan, J.; Yeung, N. K.; Kench, J. G.; Stricker, P. D.; Haynes, A.-M.; Centenera, M. M.; *et al.* Effect of FAK Inhibitor VS-6063 (Defactinib) on Docetaxel Efficacy in Prostate Cancer. *Prostate* **2018**, *78* (4), 308–317.
- (118) Cavazzoni, A.; La Monica, S.; Alfieri, R.; Ravelli, A.; Van Der Steen, N.; Sciarrillo, R.; Madeddu, D.; Lagrasta, C. A. M.; Quaini, F.; Bonelli, M.; *et al.* Enhanced Efficacy of AKT and FAK Kinase Combined Inhibition in Squamous Cell Lung Carcinomas with Stable Reduction in PTEN. *Oncotarget* **2017**, *8* (32), 53068–53083.
- (119) Shimizu, T.; Fukuoka, K.; Takeda, M.; Iwasa, T.; Yoshida, T.; Horobin, J.; Keegan, M.; Vaickus, L.; Chavan, A.; Padval, M.; *et al.* A First-in-Asian Phase 1 Study to Evaluate Safety, Pharmacokinetics and Clinical Activity of VS-6063, a Focal Adhesion Kinase (FAK) Inhibitor in Japanese Patients with Advanced Solid Tumors. *Cancer Chemother. Pharmacol.* **2016**, *77* (5), 997–1003.
- (120) Tanjoni, I.; Walsh, C.; Uryu, S.; Tomar, A.; Nam, J.-O.; Mielgo, A.; Lim, S.-T.; Liang, C.; Koenig, M.; Patel, N.; *et al.* PND-1186 FAK Inhibitor Selectively Promotes Tumor Cell Apoptosis in Three-Dimensional Environments. *Cancer Biol. Ther.* **2010**, *9* (10), 764–777.
- (121) Auger, K. R.; Smitheman, K. N.; Korenchuk, S.; McHugh, C.; Kruger, R.; Van Aller, G. S.; Smallwood, A.; Gontarek, R. R.; Faitg, T.; Johnson, N. The Focal Adhesion Kinase Inhibitor GSK2256098: A Potent and Selective Inhibitor for the Treatment of Cancer. *Eur. J. Cancer* **2012**, *48*, 118.
- (122) Zhang, J.; He, D.-H.; Zajac-Kaye, M.; Hochwald, S. N. A Small Molecule FAK Kinase

- Inhibitor, GSK2256098, Inhibits Growth and Survival of Pancreatic Ductal Adenocarcinoma Cells. *Cell Cycle* **2014**, *13* (19), 3143–3149.
- (123) Soria, J. C.; Gan, H. K.; Blagden, S. P.; Plummer, R.; Arkenau, H. T.; Ranson, M.; Evans, T. R. J.; Zalcman, G.; Bahleda, R.; Hollebecque, A.; *et al.* A Phase I, Pharmacokinetic and Pharmacodynamic Study of GSK2256098, a Focal Adhesion Kinase Inhibitor, in Patients with Advanced Solid Tumors. *Ann. Oncol.* **2016**, *27* (12), 2268–2274.
- (124) Dao, P.; Jarray, R.; Le Coq, J.; Lietha, D.; Loukaci, A.; Lepelletier, Y.; Hadj-Slimane, R.; Garbay, C.; Raynaud, F.; Chen, H. Synthesis of Novel Diarylamino-1,3,5-Triazine Derivatives as FAK Inhibitors with Anti-Angiogenic Activity. *Bioorganic Med. Chem. Lett.* **2013**, *23* (16), 4552–4556.
- (125) Sun, J.; Yang, Y.-S.; Li, W.; Zhang, Y.-B.; Wang, X.-L.; Tang, J.-F.; Zhu, H.-L. Synthesis, Biological Evaluation and Molecular Docking Studies of 1,3,4-Thiadiazole Derivatives Containing 1,4-Benzodioxan as Potential Antitumor Agents. *Bioorg. Med. Chem. Lett.* **2011**, *21* (20), 6116–6121.
- (126) Yang, X.-H.; Xiang, L.; Li, X.; Zhao, T.-T.; Zhang, H.; Zhou, W.-P.; Wang, X.-M.; Gong, H.-B.; Zhu, H.-L. Synthesis, Biological Evaluation, and Molecular Docking Studies of 1,3,4-Thiadiazol-2-Amide Derivatives as Novel Anticancer Agents. *Bioorg. Med. Chem.* **2012**, *20* (9), 2789–2795.
- (127) Zhang, L.-R.; Liu, Z.-J.; Zhang, H.; Sun, J.; Luo, Y.; Zhao, T.-T.; Gong, H.-B.; Zhu, H.-L. Synthesis, Biological Evaluation and Molecular Docking Studies of Novel 2-(1,3,4-Oxadiazol-2-Ylthio)-1-Phenylethanone Derivatives. *Bioorg. Med. Chem.* **2012**, *20* (11), 3615–3621.
- (128) Luo, Y.; Liu, Z.-J.; Chen, G.; Shi, J.; Li, J.-R.; Zhu, H.-L. 1,3,4-Oxadiazole Derivatives as Potential Antitumor Agents: Discovery, Optimization and Biological Activity Valuation. *Medchemcomm* **2016**, *7* (2), 263–271.
- (129) Zhang, Y.-B.; Liu, W.; Yang, Y.-S.; Wang, X.-L.; Zhu, H.-L.; Bai, L.-F.; Qiu, X.-Y.

- Synthesis, Molecular Modeling, and Biological Evaluation of 1,2,4-Triazole Derivatives Containing Pyridine as Potential Anti-Tumor Agents. *Med. Chem. Res.* **2013**, 22 (7), 3193–3203.
- (130) Duan, Y.-T.; Yao, Y.-F.; Huang, W.; Makawana, J. A.; Teraiya, S. B.; Thumar, N. J.; Tang, D.-J.; Tao, X.-X.; Wang, Z.-C.; Jiang, A.-Q.; *et al.* Synthesis, Biological Evaluation, and Molecular Docking Studies of Novel 2-Styryl-5-Nitroimidazole Derivatives Containing 1,4-Benzodioxan Moiety as FAK Inhibitors with Anticancer Activity. *Bioorg. Med. Chem.* **2014**, 22 (11), 2947–2954.
- (131) Choi, H. S.; Wang, Z.; Richmond, W.; He, X.; Yang, K.; Jiang, T.; Sim, T.; Karanewsky, D.; Gu, X. J.; Zhou, V.; *et al.* Design and Synthesis of 7H-Pyrrolo[2,3-d]Pyrimidines as Focal Adhesion Kinase Inhibitors. Part 1. *Bioorganic Med. Chem. Lett.* **2006**, 16 (8), 2173–2176.
- (132) Choi, H.-S.; Wang, Z.; Richmond, W.; He, X.; Yang, K.; Jiang, T.; Karanewsky, D.; Gu, X.; Zhou, V.; Liu, Y.; *et al.* Design and Synthesis of 7H-Pyrrolo[2,3-d]Pyrimidines as Focal Adhesion Kinase Inhibitors. Part 2. *Bioorg. Med. Chem. Lett.* **2006**, 16 (10), 2689–2692.
- (133) Zificsak, C. A.; Gingrich, D. E.; Breslin, H. J.; Dunn, D. D.; Milkiewicz, K. L.; Theroff, J. P.; Thieu, T. V.; Underiner, T. L.; Weinberg, L. R.; Aimone, L. D.; *et al.* Optimization of a Novel Kinase Inhibitor Scaffold for the Dual Inhibition of JAK2 and FAK Kinases. *Bioorganic Med. Chem. Lett.* **2012**, 22 (1), 133–137.
- (134) Heinrich, T.; Seenisamy, J.; Emmanuvel, L.; Kulkarni, S. S.; Bomke, J.; Rohdich, F.; Greiner, H.; Esdar, C.; Krier, M.; Grädler, U.; *et al.* Fragment-Based Discovery of New Highly Substituted 1 H -Pyrrolo[2,3- b]- and 3 H -Imidazolo[4,5- b]-Pyridines as Focal Adhesion Kinase Inhibitors. *J. Med. Chem.* **2013**, 56 (3), 1160–1170.
- (135) Wang, D.-D.; Chen, Y.; Chen, Z.-B.; Yan, F.-J.; Dai, X.-Y.; Ying, M.-D.; Cao, J.; Ma, J.; Luo, P.-H.; Han, Y.-X.; *et al.* CT-707, a Novel FAK Inhibitor, Synergizes with Cabozantinib to Suppress Hepatocellular Carcinoma by Blocking Cabozantinib-Induced FAK Activation. *Mol. Cancer Ther.* **2016**, 15 (12), 2916–2925.

- (136) Dao, P.; Smith, N.; Tomkiewicz-Raulet, C.; Yen-Pon, E.; Camacho-Artacho, M.; Lietha, D.; Herbeuval, J.; Coumoul, X.; Garbay, C.; Chen, H. Design, Synthesis, and Evaluation of Novel Imidazo[1,2- a][1,3,5]Triazines and Their Derivatives as Focal Adhesion Kinase Inhibitors with Antitumor Activity. *J. Med. Chem.* **2015**, *58* (1), 237–251.
- (137) Grädler, U.; Bomke, J.; Musil, D.; Dresing, V.; Lehmann, M.; Hölzemann, G.; Greiner, H.; Esdar, C.; Krier, M.; Heinrich, T. Fragment-Based Discovery of Focal Adhesion Kinase Inhibitors. *Bioorg. Med. Chem. Lett.* **2013**, *23* (19), 5401–5409.
- (138) Golubovskaya, V. M.; Nyberg, C.; Zheng, M.; Kweh, F.; Magis, A.; Ostrov, D.; Cance, W. G. A Small Molecule Inhibitor, 1,2,4,5-Benzenetetraamine Tetrahydrochloride, Targeting the Y397 Site of Focal Adhesion Kinase Decreases Tumor Growth. *J. Med. Chem.* **2008**, *51* (23), 7405–7416.
- (139) Tomita, N.; Hayashi, Y.; Suzuki, S.; Oomori, Y.; Aramaki, Y.; Matsushita, Y.; Iwatani, M.; Iwata, H.; Okabe, A.; Awazu, Y.; *et al.* Structure-Based Discovery of Cellular-Active Allosteric Inhibitors of FAK. *Bioorg. Med. Chem. Lett.* **2013**, *23* (6), 1779–1785.
- (140) Iwatani, M.; Iwata, H.; Okabe, A.; Skene, R. J.; Tomita, N.; Hayashi, Y.; Aramaki, Y.; Hosfield, D. J.; Hori, A.; Baba, A.; *et al.* Discovery and Characterization of Novel Allosteric FAK Inhibitors. *Eur. J. Med. Chem.* **2013**, *61*, 49–60.
- (141) Kurenova, E. V.; Hunt, D. L.; He, D.; Magis, A. T.; Ostrov, D. A.; Cance, W. G. Small Molecule Chloropyramine Hydrochloride (C4) Targets the Binding Site of Focal Adhesion Kinase and Vascular Endothelial Growth Factor Receptor 3 and Suppresses Breast Cancer Growth in Vivo. *J. Med. Chem.* **2009**, *52* (15), 4716–4724.
- (142) Gogate, P. N.; Ethirajan, M.; Kurenova, E. V.; Magis, A. T.; Pandey, R. K.; Cance, W. G. Design, Synthesis, and Biological Evaluation of Novel FAK Scaffold Inhibitors Targeting the FAK-VEGFR3 Protein-Protein Interaction. *Eur. J. Med. Chem.* **2014**, *80*, 154–166.

- (143) Dao, P.; Lietha, D.; Etheve-Quelquejeu, M.; Garbay, C.; Chen, H. Synthesis of Novel 1,2,4-Triazine Scaffold as FAK Inhibitors with Antitumor Activity. *Bioorg. Med. Chem. Lett.* **2017**, *27* (8), 1727–1730.
- (144) Yen-Pon, E. Fonctionnalisation de Pyrimidines:Développement de Nouveaux Inhibiteurs de La Kinase d'Adhésion Focale (FAK) à Visée Anti-Tumorale, 2016.
- (145) Yen-Pon, E.; Li, B.; Acebrón-Garcia-de-Eulate, M.; Tomkiewicz-Raulet, C.; Dawson, J.; Lietha, D.; Frame, M. C.; Coumoul, X.; Garbay, C.; Etheve-Quelquejeu, M.; *et al.* Structure-Based Design, Synthesis, and Characterization of the First Irreversible Inhibitor of Focal Adhesion Kinase. *ACS Chem. Biol.* **2018**, *13* (8), 2067–2073.
- (146) Marino, S. M.; Gladyshev, V. N. Cysteine Function Governs Its Conservation and Degeneration and Restricts Its Utilization on Protein Surfaces. *J. Mol. Biol.* **2010**, *404* (5), 902–916.
- (147) Van Linden, O. P. J.; Kooistra, A. J.; Leurs, R.; De Esch, I. J. P.; De Graaf, C. KLIFS: A Knowledge-Based Structural Database to Navigate Kinase-Ligand Interaction Space. *J. Med. Chem.* **2014**, *57* (2), 249–277.
- (148) Madeira, F.; Park, Y. M.; Lee, J.; Buso, N.; Gur, T.; Madhusoodanan, N.; Basutkar, P.; Tivey, A. R. N.; Potter, S. C.; Finn, R. D.; *et al.* The EMBL-EBI Search and Sequence Analysis Tools APIs in 2019. *Nucleic Acids Res.* **2019**, No. September.
- (149) Breslin, H. J.; Lane, B. M.; Ott, G. R.; Ghose, A. K.; Angeles, T. S.; Albom, M. S.; Cheng, M.; Wan, W.; Haltiwanger, R. C.; Wells-Knecht, K. J.; *et al.* Design, Synthesis, and Anaplastic Lymphoma Kinase (ALK) Inhibitory Activity for a Novel Series of 2,4,8,22-Tetraazatetracyclo[14.3.1.1^{3,7}.1^{9,13}]Docosa-1(20),3(22),4,6,9(21), 10,12,16, 18-Nonaene Macrocycles. *J. Med. Chem.* **2012**, *55* (1), 449–464.
- (150) Ward, R. A.; Anderton, M. J.; Ashton, S.; Bethel, P. A.; Box, M.; Butterworth, S.; Colclough, N.; Chorley, C. G.; Chuaqui, C.; Cross, D. A. E.; *et al.* Structure- and Reactivity-Based Development of Covalent Inhibitors of the Activating and Gatekeeper Mutant Forms of the Epidermal Growth Factor Receptor (EGFR). *J. Med.*

- Chem.* **2013**, *56* (17), 7025–7048.
- (151) Schomaker, J. M.; Delia, T. J. 2,4,6-Trichloropyrimidine. Reaction with Anilines. *J. Heterocycl. Chem.* **2000**, *37* (6), 1457–1462.
- (152) Large, J. M.; Clarke, M.; Williamson, D. M.; McDonald, E.; Collins, I. Synthesis of Trisubstituted Pyrimidines by Regioselective SNAr and Suzuki Reactions of Polyhalopyrimidines. *ChemInform* **2006**, *37* (31), 1–7.
- (153) Solberg, J.; Undheim, K.; Pettersson, L.; Öhman, L.-O.; Ruiz, J.; Colacio, E.; Mulichak, A. M.; Alming, T.; Erickson, M.; Grundevik, I.; *et al.* Regiochemistry in Pd-Catalysed Organotin Reactions with Halopyrimidines. *Acta Chem. Scand.* **1989**, *43*, 62–68.
- (154) Delia, T. J.; Nagarajan, A. 2,4,6-Trichloropyrimidine. Reaction with 4-Substituted Phenolate Ions. *J. Heterocycl. Chem.* **1998**, *35* (2), 269–273.
- (155) Huang, W.-S.; Liu, S.; Zou, D.; Thomas, M.; Wang, Y.; Zhou, T.; Romero, J.; Kohlmann, A.; Li, F.; Qi, J.; *et al.* Discovery of Brigatinib (AP26113), a Phosphine Oxide-Containing, Potent, Orally Active Inhibitor of Anaplastic Lymphoma Kinase. *J. Med. Chem.* **2016**, *59* (10), 4948–4964.
- (156) Lee, L.; Leroux, Y. R.; Hapiot, P.; Downard, A. J. Amine-Terminated Monolayers on Carbon: Preparation, Characterization, and Coupling Reactions. *Langmuir* **2015**, *31* (18), 5071–5077.
- (157) Preparation of Bipiperidinyll Derivatives as Inhibitors of CCR5 Receptors. WO2005042517, 2005.
- (158) Alexander, M. D.; McDonald, J. J.; Ni, Y.; Niu, D.; Petter, R. C.; Qiao, L.; Singh, J.; Wang, T.; Zhu, Z. MK2 Inhibitors and Uses Thereof. WO 2014/149164 A1, 2014.
- (159) Pelish, H. E.; Westwood, N. J.; Feng, Y.; Kirchhausen, T.; Shair, M. D. Use of Biomimetic Diversity-Oriented Synthesis to Discover Galanthamine-Like Molecules with Biological Properties beyond Those of the Natural Product. *J. Am. Chem. Soc.* **2001**, *123* (27), 6740–6741.

- (160) Ian Storer, R.; Aciro, C.; Jones, L. H. Squaramides: Physical Properties, Synthesis and Applications. *Chem. Soc. Rev.* **2011**, *40* (5), 2330.
- (161) Albers, H. M. H. G.; Hendrickx, L. J. D.; van Tol, R. J. P.; Hausmann, J.; Perrakis, A.; Ovaa, H. Structure-Based Design of Novel Boronic Acid-Based Inhibitors of Autotaxin. *J. Med. Chem.* **2011**, *54* (13), 4619–4626.
- (162) Firstenberg, M.; Shivananda, K. N.; Cohen, I.; Solomeshch, O.; Medvedev, V.; Tessler, N.; Eichen, Y. Harnessing “Click”-Type Chemistry for the Preparation of Novel Electronic Materials. *Adv. Funct. Mater.* **2011**, *21* (4), 634–643.
- (163) Abdel-Magid, A. F.; Carson, K. G.; Harris, B. D.; Maryanoff, C. A.; Shah, R. D. Reductive Amination of Aldehydes and Ketones with Sodium Triacetoxyborohydride. Studies on Direct and Indirect Reductive Amination Procedures 1. *J. Org. Chem.* **1996**, *61* (11), 3849–3862.
- (164) Bandyopadhyay, S.; Mukherjee, S.; Dey, A. Modular Synthesis, Spectroscopic Characterization and in Situ Functionalization Using “Click” Chemistry of Azide Terminated Amide Containing Self-Assembled Monolayers. *RSC Adv.* **2013**, *3* (38), 17174–17187.
- (165) Liang, L.; Astruc, D. The Copper(I)-Catalyzed Alkyne-Azide Cycloaddition (CuAAC) “Click” Reaction and Its Applications. An Overview. *Coord. Chem. Rev.* **2011**, *255* (23–24), 2933–2945.
- (166) Jia, Y.; Quinn, C.; Kwak, S.; Talanian, R. Current In Vitro Kinase Assay Technologies: The Quest for a Universal Format. *Curr. Drug Discov. Technol.* **2008**, *5* (1), 59–69.
- (167) Schwartz, P. A.; Kuzmic, P.; Solowiej, J.; Bergqvist, S.; Bolanos, B.; Almaden, C.; Nagata, A.; Ryan, K.; Feng, J.; Dalvie, D.; *et al.* Covalent EGFR Inhibitor Analysis Reveals Importance of Reversible Interactions to Potency and Mechanisms of Drug Resistance. *Proc. Natl. Acad. Sci.* **2014**, *111* (1), 173–178.
- (168) Cheng, R.; Guo, T.; Zhang-Negrerie, D.; Du, Y.; Zhao, K. One-Pot Synthesis of Quinazolinones from Anthranilamides and Aldehydes via p-Toluenesulfonic Acid

- Catalyzed Cyclocondensation and Phenylodine Diacetate Mediated Oxidative Dehydrogenation. *Synthesis (Stuttg)*. **2013**, 45 (21), 2998–3006.
- (169) Mazur, W. A.; He, Y.; Sorokin, V. Sulfurizing Reagents and Their Use for Oligonucleotides Synthesis. WO 2010/072831 A1, 2010.
- (170) Van Camp, J.; Xu, X.; Osuma, A. T.; Gregg, R.; Longenecker, K. L. Pyrrolopyrimidines as FAK and ALK Inhibitors for the Treatment of Cancer and Other Diseases. WO2012045195A1, 2012.
- (171) Hanson, P.; Hendrickx, R. A. A. J.; Smith, J. R. L. An Investigation by Means of Correlation Analysis into the Mechanisms of Oxidation of Aryl Methyl Sulfides and Sulfoxides by Dimethyldioxirane in Various Solvents. *Org. Biomol. Chem.* **2008**, 6 (4), 745–761.
- (172) Lévay, K.; Hegedűs, L. Selective Heterogeneous Catalytic Hydrogenation of Nitriles to Primary Amines. *Period. Polytech. Chem. Eng.* **2018**, 62 (4), 476–488.
- (173) Park, E. B.; Jeong, K. Chloride Transport Activities of Trans- and Cis-Amide-Linked Bisureas. *Chem. Commun.* **2015**, 51 (44), 9197–9200.
- (174) Qin, M.-Z.; Wang, L.; Yan, S.; Ma, J.-J.; Tian, Y.; Zhao, Y.-F.; Gong, P. Identification of Hydrazone Moiety-Bearing Aminopyrimidines as Potent Antitumor Agents with Selective Inhibition of Gefitinib-Resistant H1975 Cancer Cells. *Chinese Chem. Lett.* **2017**, 28 (5), 991–994.
- (175) Richter, D. T.; Kath, J. C.; Luzzio, M. J.; Keene, N.; Berliner, M. A.; Wessel, M. D. Selective Addition of Amines to 5-Trifluoromethyl-2,4-Dichloropyrimidine Induced by Lewis Acids. *Tetrahedron Lett.* **2013**, 54 (35), 4610–4612.
- (176) Pritchard, R. B.; Lough, C. E.; Currie, D. J.; Holmes, H. L. Equilibrium Reactions of n -Butanethiol with Some Conjugated Heteroenoid Compounds. *Can. J. Chem.* **1968**, 46 (5), 775–781.
- (177) Lee, C.-U.; Grossmann, T. N. Reversible Covalent Inhibition of a Protein Target. *Angew. Chemie Int. Ed.* **2012**, 51 (35), 8699–8700.

- (178) Proença, F.; Costa, M. A Simple and Eco-Friendly Approach for the Synthesis of 2-Imino and 2-Oxo-2H-Chromene-3-Carboxamides. *Green Chem.* **2008**, *10* (9), 995.
- (179) Basu, D.; Richters, A.; Rauh, D. Structure-Based Design and Synthesis of Covalent-Reversible Inhibitors to Overcome Drug Resistance in EGFR. *Bioorganic Med. Chem.* **2015**, *23* (12), 2767–2780.
- (180) Tomassi, S.; Lategahn, J.; Engel, J.; Keul, M.; Tumbrink, H. L.; Ketzer, J.; Mühlenberg, T.; Baumann, M.; Schultz-Fademrecht, C.; Bauer, S.; *et al.* Indazole-Based Covalent Inhibitors To Target Drug-Resistant Epidermal Growth Factor Receptor. *J. Med. Chem.* **2017**, *60* (6), 2361–2372.
- (181) Walter, A. O.; Sjin, R. T. T.; Haringsma, H. J.; Sun, J.; Ohashi, K.; Lee, K.; Dubrovskiy, A.; Labenski, M.; Wang, Z.; Zhu, Z.; *et al.* Discovery of a Mutant-Selective Covalent Inhibitor of EGFR That Overcomes T790M Mediated Resistance in NSCLC. *Cancer Discov.* **2013**, *3* (12), 1404–1415.
- (182) Krippendorff, B. F.; Neuhaus, R.; Lienau, P.; Reichel, A.; Huisinga, W. Mechanism-Based Inhibition: Deriving Ki and Kinact Directly from Time-Dependent Ic50 Values. *J. Biomol. Screen.* **2009**, *14* (8), 913–923.
- (183) Miyazaki, T.; Kato, H.; Nakajima, M.; Sohda, M.; Fukai, Y.; Masuda, N.; Manda, R.; Fukuchi, M.; Tsukada, K.; Kuwano, H. FAK Overexpression Is Correlated with Tumour Invasiveness and Lymph Node Metastasis in Oesophageal Squamous Cell Carcinoma. *Br. J. Cancer* **2003**, *89* (1), 140–145.
- (184) Watanabe, N.; Takaoka, M.; Sakurama, K.; Tomono, Y.; Hatakeyama, S.; Ohmori, O.; Motoki, T.; Shirakawa, Y.; Yamatsuji, T.; Haisa, M.; *et al.* Dual Tyrosine Kinase Inhibitor for Focal Adhesion Kinase and Insulin-like Growth Factor-I Receptor Exhibits Anticancer Effect in Esophageal Adenocarcinoma In Vitro and In Vivo. *Clin. Cancer Res.* **2008**, *14* (14), 4631–4639.
- (185) Gutenberg, A.; Brück, W.; Buchfelder, M.; Ludwig, H. C. Expression of Tyrosine Kinases FAK and Pyk2 in 331 Human Astrocytomas. *Acta Neuropathol.* **2004**, *108*

- (3), 224–230.
- (186) Rival, Y.; Grassy, G.; Michel, G. Synthesis and Antibacterial Activity of Some Imidazo[1,2-a]Pyrimidine Derivatives. *Chem. Pharm. Bull. (Tokyo)*. **1992**, *40* (5), 1170–1176.
- (187) Dao, P.; Garbay, C.; Chen, H. Regioselective Synthesis of Imidazo[1,2-a][1,3,5]Triazines and 3,4-Dihydroimidazo[1,2-a][1,3,5]Triazines from [1,3,5]Triazin-2,4-Diamines. *Tetrahedron* **2013**, *69* (19), 3867–3871.
- (188) Revankar, G. R.; Robins, R. K. Synthesis and Biological Activity of Some Nucleosides Resembling Guanosine: Imidazo[1,2-a]Pyrimidine Nucleosides. *Ann. N. Y. Acad. Sci.* **1975**, *255* (1), 166–176.
- (189) Lugari, M. T.; Maggiali, C. A.; Morini, G. High-Performance Liquid Chromatography of Phytotoxic Substances. *J. Chromatogr. A* **1984**, *315*, 384–388.
- (190) Laneri, S.; Sacchi, A.; Abignente, E. Research on Heterocyclic Compounds. XLII. The Vilsmeier Reaction in the Synthesis of Imidazo[1,2-a]Pyrimidine Derivatives. *J. Heterocycl. Chem.* **2000**, *37* (5), 1265–1267.
- (191) Han, Z.; Pinkner, J. S.; Ford, B.; Chorell, E.; Crowley, J. M.; Cusumano, C. K.; Campbell, S.; Henderson, J. P.; Hultgren, S. J.; Janetka, J. W. Lead Optimization Studies on FimH Antagonists: Discovery of Potent and Orally Bioavailable Ortho-Substituted Biphenyl Mannosides. *J. Med. Chem.* **2012**, *55* (8), 3945–3959.
- (192) Ma, Y.; Yung, L.-Y. L. Detection of Dissolved CO₂ Based on the Aggregation of Gold Nanoparticles. *Anal. Chem.* **2014**, *86* (5), 2429–2435.
- (193) Kosugi, M.; Kameyama, M.; Migita, T. Palladium-Catalyzed Aromatic Amination of Aryl Bromides with N,N-Diethylamino-Tributyltin. *Chem. Lett.* **1983**, *12* (6), 927–928.
- (194) Louie, J.; Hartwig, J. F. Palladium-Catalyzed Synthesis of Arylamines from Aryl Halides. Mechanistic Studies Lead to Coupling in the Absence of Tin Reagents. *Tetrahedron Lett.* **1995**, *36* (21), 3609–3612.

- (195) Guram, A. S.; Rennels, R. A.; Buchwald, S. L. A Simple Catalytic Method for the Conversion of Aryl Bromides to Arylamines. *Angew. Chemie Int. Ed. English* **1995**, *34* (12), 1348–1350.
- (196) Charles, M. D.; Schultz, P.; Buchwald, S. L. Efficient Pd-Catalyzed Amination of Heteroaryl Halides. *Org. Lett.* **2005**, *7* (18), 3965–3968.
- (197) Tierney, J. P.; Lidström, P. *Microwave Assisted Organic Synthesis*; Tierney, J. P., Lidström, P., Eds.; Blackwell Publishing Ltd.: Oxford, UK, 2005; Vol. 57.
- (198) Olofsson, K.; Larhed, M.; Hallberg, A. Highly Regioselective Palladium-Catalyzed β -Arylation of N,N -Dialkylallylamines. *J. Org. Chem.* **2000**, *65* (21), 7235–7239.
- (199) Mehta, V. P.; Van der Eycken, E. V. Microwave-Assisted C–C Bond Forming Cross-Coupling Reactions: An Overview. *Chem. Soc. Rev.* **2011**, *40* (10), 4925–4936.
- (200) Nilsson, P.; Olofsson, K.; Larhed, M. Microwave-Assisted and Metal-Catalyzed Coupling Reactions. *Top. Curr. Chem.* **2006**, *266* (June), 103–144.
- (201) Kaur, N. Review on the Synthesis of Six-Membered N,N -Heterocycles by Microwave Irradiation. *Synth. Commun.* **2015**, *45* (10), 1145–1182.
- (202) Li, Y.; Shen, M.; Zhang, Z.; Luo, J.; Pan, X.; Lu, X.; Long, H.; Wen, D.; Zhang, F.; Leng, F.; *et al.* Design, Synthesis, and Biological Evaluation of 3-(1 H -1,2,3-Triazol-1-Yl)Benzamide Derivatives as Potent Pan Bcr-Abl Inhibitors Including the Threonine 315 \rightarrow Isoleucine 315 Mutant. *J. Med. Chem.* **2012**, *55* (22), 10033–10046.
- (203) Elbert, B. L.; Farley, A. J. M.; Gorman, T. W.; Johnson, T. C.; Genicot, C.; Lallemand, B.; Pasau, P.; Flasz, J.; Castro, J. L.; MacCoss, M.; *et al.* C–H Cyanation of 6-Ring N-Containing Heteroaromatics. *Chem. - A Eur. J.* **2017**, *23* (59), 14733–14737.
- (204) Nara, S. J.; Jha, M.; Brinkhorst, J.; Zemanek, T. J.; Pratt, D. A. A Simple Cu-Catalyzed Coupling Approach to Substituted 3-Pyridinol and 5-Pyrimidinol Antioxidants. *J. Org. Chem.* **2008**, *73* (23), 9326–9333.
- (205) Okada, H.; Koyanagi, T.; Yamada, N.; Haga, T. Synthesis and Antitumor Activities of Novel Benzoylphenylurea Derivatives. *Chem. Pharm. Bull. (Tokyo)*. **1991**, *39* (9),

2308–2315.

- (206) Wong, K.-T.; Hung, T. S.; Lin, Y.; Wu, C.-C.; Lee, G.-H.; Peng, S.-M.; Chou, C. H.; Su, Y. O. Suzuki Coupling Approach for the Synthesis of Phenylene–Pyrimidine Alternating Oligomers for Blue Light-Emitting Material. *Org. Lett.* **2002**, *4* (4), 513–516.
- (207) Hanthorn, J. J.; Valgimigli, L.; Pratt, D. A. Preparation of Highly Reactive Pyridine- and Pyrimidine-Containing Diarylamine Antioxidants. *J. Org. Chem.* **2012**, *77* (16), 6908–6916.
- (208) Katz, J. D.; Haidle, A.; Childers, K. K.; Zabierek, A. A.; Jewell, J. P.; Hou, Y.; Altman, M. D.; Szewczak, A.; Chen, D.; Harsch, A.; *et al.* Structure Guided Design of a Series of Selective Pyrrolopyrimidinone MARK Inhibitors. *Bioorg. Med. Chem. Lett.* **2017**, *27* (1), 114–120.
- (209) Gao, M.; Yu, F.; Lv, C.; Choo, J.; Chen, L. Fluorescent Chemical Probes for Accurate Tumor Diagnosis and Targeting Therapy. *Chem. Soc. Rev.* **2017**, *46* (8), 2237–2271.
- (210) Nguyen, Q. T.; Olson, E. S.; Aguilera, T. A.; Jiang, T.; Scadeng, M.; Ellies, L. G.; Tsien, R. Y. Surgery with Molecular Fluorescence Imaging Using Activatable Cell-Penetrating Peptides Decreases Residual Cancer and Improves Survival. *Proc. Natl. Acad. Sci.* **2010**, *107* (9), 4317–4322.
- (211) Vetter, M. L.; Zhang, Z.; Liu, S.; Wang, J.; Cho, H.; Zhang, J.; Zhang, W.; Gray, N. S.; Yang, P. L. Fluorescent Visualization of Src by Using Dasatinib-BODIPY. *ChemBioChem* **2014**, *15* (9), 1317–1324.
- (212) Zhou, X.; Herbst-Robinson, K. J.; Zhang, J. Visualizing Dynamic Activities of Signaling Enzymes Using Genetically Encodable FRET-Based Biosensors. In *Methods in Enzymology*; Elsevier Inc., 2012; Vol. 504, pp 317–340.
- (213) Knight, Z. A.; Shokat, K. M. Features of Selective Kinase Inhibitors. *Chem. Biol.* **2005**, *12* (6), 621–637.
- (214) Kung, C.; Kenski, D. M.; Krukenberg, K.; Madhani, H. D.; Shokat, K. M. Selective

- Kinase Inhibition by Exploiting Differential Pathway Sensitivity. *Chem. Biol.* **2006**, *13* (4), 399–407.
- (215) Blair, J. A.; Rauh, D.; Kung, C.; Yun, C. H.; Fan, Q. W.; Rode, H.; Zhang, C.; Eck, M. J.; Weiss, W. A.; Shokat, K. M. Structure-Guided Development of Affinity Probes for Tyrosine Kinases Using Chemical Genetics. *Nat. Chem. Biol.* **2007**, *3* (4), 229–238.
- (216) Lim, S.-T. S. Nuclear FAK: A New Mode of Gene Regulation from Cellular Adhesions. *Mol. Cells* **2013**, *36* (1), 1–6.
- (217) Valeur, B. Molecular Fluorescence. In *digital Encyclopedia of Applied Physics*; Wiley-VCH Verlag GmbH & Co. KGaA: Weinheim, Germany, 2009; pp 477–531.
- (218) Ghosh, P. B.; Whitehouse, M. W. 7-Chloro-4-Nitrobenzo-2-Oxa-1,3-Diazole: A New Fluorogenic Reagent for Amino Acids and Other Amines. *Biochem. J.* **1968**, *108* (1), 155–156.
- (219) Lin, S.; Struve, W. S. Time-Resolved Fluorescence of Nitrobenzoxadiazole-Aminohexanoic Acid: Effect of Intermolecular Hydrogen-Bonding on Non-Radiative Decay. *Photochem. Photobiol.* **1991**, *54* (3), 361–365.
- (220) Hansen, A. H.; Sergeev, E.; Pandey, S. K.; Hudson, B. D.; Christiansen, E.; Milligan, G.; Ulven, T. Development and Characterization of a Fluorescent Tracer for the Free Fatty Acid Receptor 2 (FFA2/GPR43). *J. Med. Chem.* **2017**, *60* (13), 5638–5645.
- (221) Tietz, O.; Kaur, J.; Bhardwaj, A.; Wuest, F. R. Pyrimidine-Based Fluorescent COX-2 Inhibitors: Synthesis and Biological Evaluation. *Org. Biomol. Chem.* **2016**, *14* (30), 7250–7257.
- (222) Kileci-Ksoll, R.; Winklhofer, C.; Steglich, W. Synthesis of Schaefferals A and B, Unusual Phenylhydrazine Derivatives from Mushrooms of the Genus *Agaricus*. *Synthesis (Stuttg.)* **2010**, *2010* (13), 2287–2291.
- (223) King, S. B.; Ganem, B. Synthetic Studies on Mannostatin A and Its Derivatives: A New Family of Glycoprotein Processing Inhibitors. *J. Am. Chem. Soc.* **1994**, *116* (2), 562–570.

- (224) Hong, S.; Tian, S.; Metz, M. V.; Marks, T. J. C₂-Symmetric Bis(Oxazolinato)Lanthanide Catalysts for Enantioselective Intramolecular Hydroamination/Cyclization. *J. Am. Chem. Soc.* **2003**, *125* (48), 14768–14783.
- (225) Aboderin, A. A.; Semakula, R. E. K. Base-Promoted Cleavage of α -N-NBD-Peptides. *FEBS Lett.* **1973**, *34* (1), 90–94.
- (226) Saha, S. 4-Amino Derivatives of 7-Nitro-2,1,3-Benzoxadiazole: The Effect of the Amino Moiety on the Structure of Fluorophores. *Acta Crystallogr. Sect. C Cryst. Struct. Commun.* **2002**, *58* (3), 174–177.
- (227) Rostami, A.; Colin, A.; Li, X. Y.; Chudzinski, M. G.; Lough, A. J.; Taylor, M. S. N, N'-Diarylsquaramides: General, High-Yielding Synthesis and Applications in Colorimetric Anion Sensing. *J. Org. Chem.* **2010**, *75* (12), 3983–3992.
- (228) Grate, J. W.; Mo, K.-F.; Daily, M. D. Triazine-Based Sequence-Defined Polymers with Side-Chain Diversity and Backbone-Backbone Interaction Motifs. *Angew. Chemie Int. Ed.* **2016**, *55* (12), 3925–3930.
- (229) Park, E. B.; Jeong, K.-S. Chloride Transport Activities of Trans- and Cis-Amide-Linked Bisureas. *Chem. Commun.* **2015**, *51* (44), 9197–9200.

Structure-Based Design, Synthesis, and Characterization of the First Irreversible Inhibitor of Focal Adhesion Kinase

Expédite Yen-Pon,^{†,⊥} Bo Li,^{†,⊥} Marta Acebrón-García-de-Eulate,[‡] Céline Tomkiewicz-Raulet,[§] John Dawson,^{||} Daniel Lietha,[‡] Margaret C. Frame,^{||} Xavier Coumoul,[§] Christiane Garbay,[†] Mélanie Etheve-Quellejeu,[†] and Huixiong Chen^{*,†,⊥}

[†]Chemistry of RNA, Nucleosides, Peptides and Heterocycles, CNRS UMR8601, Université Paris Descartes, PRES Sorbonne Paris Cité, UFR Biomédicale, 45 rue des Saints-Pères, 75270 Paris Cedex 06, France

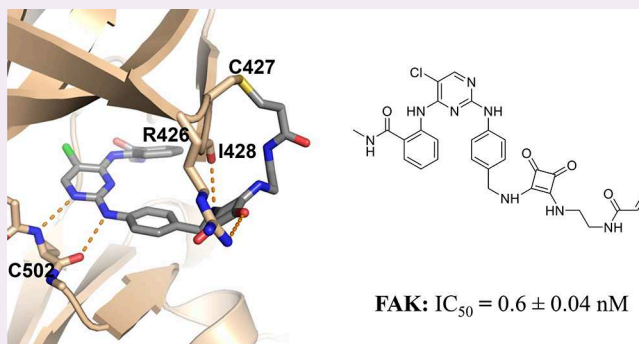
[‡]Cell Signalling and Adhesion Group, Structural Biology Programme, Spanish National Cancer Research Centre (CNIO), Calle Melchor Fernández Almagro 3, Madrid 28029, Spain

[§]Toxicologie, Pharmacologie et Signalisation Cellulaire, INSERM, UMR S 1124, Université Paris Descartes, PRES Sorbonne Paris Cité, UFR Biomédicale, 45 rue des Saints-Pères, 75270 Paris Cedex 06, France

^{||}Edinburgh Cancer Research UK Centre, Institute of Genetics and Molecular Medicine, University of Edinburgh, Edinburgh EH4 2XR, United Kingdom

Supporting Information

ABSTRACT: Focal Adhesion Kinase signaling pathway and its functions have been involved in the development and aggressiveness of tumor malignancy, it then presents a promising cancer therapeutic target. Several reversible FAK inhibitors have been developed and are being conducted in clinical trials. On the other hand, irreversible covalent inhibitors would bring many desirable pharmacological features including high potency and increased duration of action. Herein we report the structure-guided development of the first highly potent and irreversible inhibitor of the FAK kinase. This inhibitor showed a very potent decrease of autophosphorylation of FAK in squamous cell carcinoma. A cocrystal structure of the FAK kinase domain in complex with this compound revealed the inhibitor binding mode within the ATP binding site and confirmed the covalent linkage between the targeted Cys427 of the protein and the inhibitor.



Focal adhesion kinase (FAK) is a ubiquitously expressed nonreceptor protein tyrosine kinase and a scaffold protein localized to focal adhesions, which plays important roles in many biological processes including survival, proliferation, angiogenesis, adhesion, motility, metastasis, tumor micro-environment, epithelial to mesenchymal transition (EMT), as well as cancer stem cell renewal.^{1,2} FAK is also overexpressed in a variety of solid and non-solid tumors, which make it a promising therapeutic target.^{3,4} In recent years, numerous clinical trials have been developed with small FAK inhibitor molecules.^{5,6} The results of such inhibitors are interesting since the decrease of tumor growth and metastasis development was observed in some preclinical models and in cancer patients, even if some adverse events have been revealed.⁷ In order to enhance the efficacy of anti-FAK cancer treatments, the trials are conducted either individually or in combination. Recent advances in the evaluation of FAK inhibitors in preclinical and clinical models are very promising.^{7,8} Furthermore, FAK has recently been shown to be localized in the nucleus and could promote survival and cell proliferation by interacting directly

with p53.⁹ FAK inhibition could also trigger immune-mediated tumor regression through the control of regulatory T-cells (Treg) in the tumor environment.¹⁰

The development of covalent irreversible inhibitors to target kinases has recently garnered significant interest.^{11,12} From a therapeutic point of view, the main advantages of irreversible inhibitors are (i) an increase of the target residence time to obtain durable inhibition without maintaining continuous drug exposure and (ii) a better ability to avoid drug resistance by reducing the development of resistance mutations.¹³ Although there are only very few irreversible tyrosine kinase inhibitors used as therapeutic agents in the fields of oncology nowadays, the number of these new inhibitors is steadily increasing to enter clinical trials.

Received: March 16, 2018

Accepted: June 13, 2018

Published: June 13, 2018

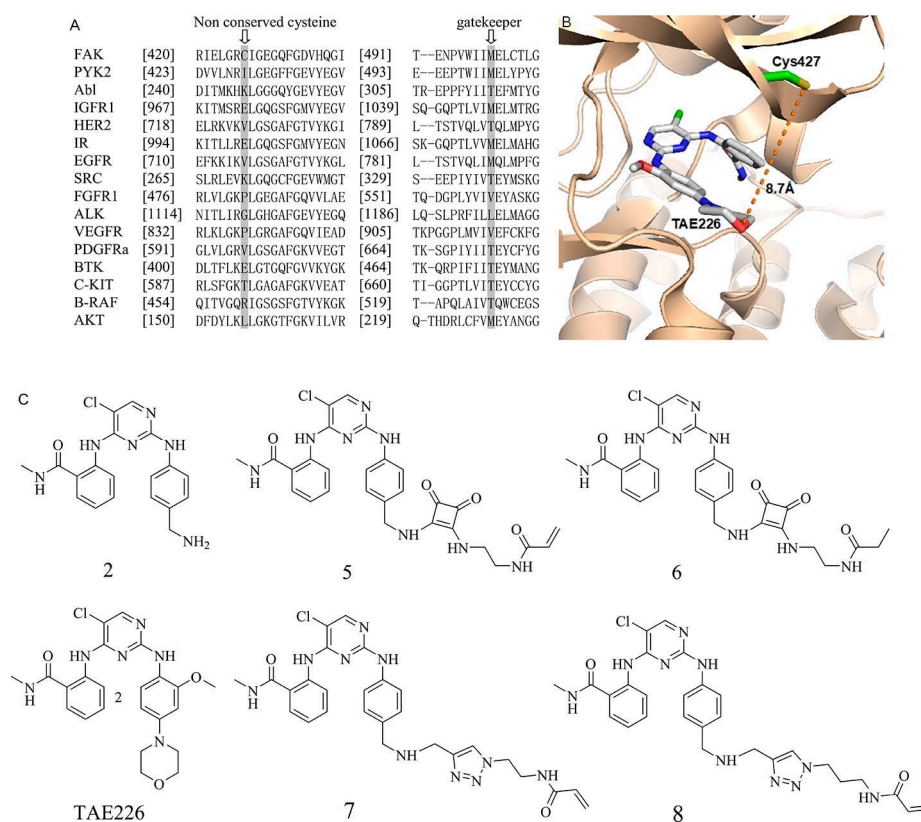


Figure 1. Design of a potent and electrophilic inhibitor of FAK guided by structural bioinformatics. (A) Partial sequence alignment of FAK with 15 other protein kinases. (B) Structural assessment of cysteine residue 427 for covalent binding to FAK. The structure shows the FAK kinase (tan ribbon) bound to TAE226 (white sticks; PDB ID: 2JKK). The Cys427 side chain is colored in green and its distance to TAE226 indicated. (C) Reversible and irreversible inhibitors of FAK.

RESULTS AND DISCUSSION

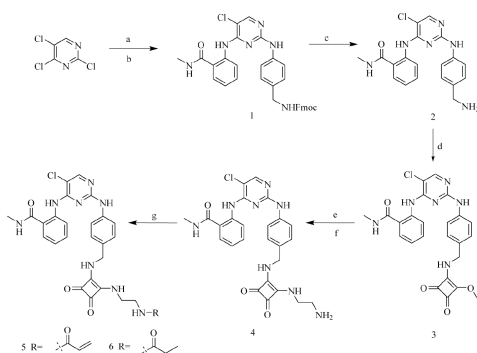
Design of Irreversible Covalent Inhibitors. In order to assess the feasibility of designing irreversible inhibitors of FAK, our strategy entailed identifying a suitable cysteine residue within or next to the ATP binding pocket. This approach would be amenable by using a kinome-wide sequence analysis in connection with 3D structure of the ATP site. In particular, we noticed that FAK contains a cysteine residue in the glycine-rich loop region closer to the ATP site, a feature which is not observed in most of other human kinases (Figure 1A). The distance between Cys427 and a reversible inhibitor, such as TAE226 (PDB ID: 2JKK)¹⁴ or PHM16 (PDB ID: 4BRX)¹⁵ in the ATP binding site is less than 10 Å (Figure 1B).

On the basis of the two-step process for kinase inhibition, we designed our inhibitors, which first bind reversibly to the enzyme, forming a noncovalent complex, and then form a covalent binding with the residue Cys427 of the enzyme to provide an irreversible complex (Figure S1, eq 1). Pyrimidine derivatives, especially 2,4-dianilino-pyrimidine derivatives, are one of the important scaffolds found in many compounds described by pharmaceutical companies and academic laboratories.^{6,16–18} These pyrimidine-containing inhibitors efficiently target the FAK scaffolding function and suppress tumor growth through inhibition of Akt signaling or activation of p53 signaling and its downstream targets.¹⁰ Our design strategy required the synthesis of 2,4-pyrimidine derivatives as a scaffold to maintain affinity similar to reversible inhibitors (compound 2, Figure 1C) and inclusion of a linker with Michael acceptor which could react with the nucleophilic

Cys427 residue. A number of diverse linkers were evaluated; we quickly focused upon two linkers, a squarate (3,4-bisaminocyclobutane-1,2-dione; 5 and 6) and a 1,2,3-triazole (7 and 8) motif, which are able to sustain a good orientation to target Cys427 in the glycine-rich loop region of the FAK kinase. Concerning the electrophile motif, an acrylate group was chosen to maintain reactivity (5, 7, and 8 in Figure 1C).

Synthesis of FAK Inhibitors. The synthetic route of new 2,4-pyrimidine compounds is outlined in Scheme 1 (for compounds 5 and 6) and Scheme S1 (for compounds 7 and 8). Starting from commercially available 2,4,5-trichloropyrimidine, the first chlorine atom in position 4 of 2,4,5-trichloropyrimidine is displaced by 2-amino-*N*-methylbenzamide in the presence of NaHCO₃ in EtOH at reflux to afford a monosubstituted intermediate in a yield of 93%. This was further substituted to compound 1 in the presence of the corresponding (9H-fluoren-9-yl)methyl(4-aminobenzyl)-carbamate and HCl in *n*-BuOH in a yield of 53%. The amino protecting Fmoc group of 1 was removed using piperidine to provide the key intermediate 2. Then, the electrophilic 1,4-addition reactions occurred between compound 1 and dimethyl squarate in the presence of DIPEA at RT to afford compound 3 in a yield of 81%. This was further condensed with *tert*-butyl (2-aminoethyl)carbamate in the presence of DIPEA, followed by the deprotection of the Boc group to give compound 4. Finally, acylation of the primary amine with acryloyl chloride or propionyl chloride gave the expected, targeted covalent inhibitor 5 and the corresponding reversible inhibitor 6, without the electrophilic warhead. Other

Scheme 1. Synthesis of FAK Targeted Covalent Inhibitor 5 and Reversible Inhibitor Matched-Pair 6^a



^aReagents and conditions: (a) 2-amino-*N*-methylbenzamide, NaHCO₃, EtOH, reflux; (b) (9H-fluoren-9-yl)methyl (4-aminobenzyl)carbamate, HCl, *n*-BuOH, 120 °C; (c) piperidine, DMF, RT; (d) dimethyl squarate, DIPEA, DMF, RT; (e) *tert*-butyl (2-aminoethyl)carbamate, DIPEA, DMF, 70 °C; (f) TFA, DCM, RT; (g) acryloyl chloride or propionyl chloride, NEt₃, DMF, RT.

potential irreversible inhibitors 7 and 8 bearing a 1,3,5-triazole linker were also synthesized in a similar manner (Scheme S1).

Biochemical Characterization of FAK Inhibitors. To establish whether our rationally designed targeted covalent inhibitors 5, 7, and 8 could form irreversible complexes, their inhibitory potency was first assessed using an ADP-Glo kinase assay. One previously reported inhibitor of FAK, TAE226, was used as a control. In this assay, TAE226 showed an IC₅₀ value of 5.8 nM against the kinase activity of FAK (Table 1), which was similar to previously reported data.¹⁹

Table 1. *In Vitro* Enzymatic Activities of Novel 2,4-Diarylamino-pyrimidines Compared with TAE226

No.	R ^a	IC ₅₀ (nM)
2	H	26 ± 2.2
5	Sq(CH ₂) ₂ NHCOCH=CH ₂	0.6 ± 0.04
6	Sq(CH ₂) ₂ NHCOCH ₂ CH ₃	4.7 ± 0.5
7	CH ₂ Tr(CH ₂) ₂ NH COCH=CH ₂	2.3 ± 0.3
8	CH ₂ Tr(CH ₂) ₃ NH COCH=CH ₂	1.2 ± 0.1
TAE226		5.8 ± 0.6

^aSq: squaramide group. Tr: 1,2,3-triazole group.

As expected, our selected 2,4-dianilino-pyrimidine scaffold (compound 2) showed potent inhibitory activity to FAK (IC₅₀ = 26 nM), as shown in Table 1. Interestingly, the introduction of different groups on the amine function of the benzylamino moiety (ring B) resulted in a very large increase in inhibitory potency on FAK kinase activity (compounds 5, 6, 7, and 8), showing specific contributions of these groups. Compounds bearing a 1,2,3-triazole group (7 and 8) gave an inhibitory potency of 2.3 and 1.2 nM, respectively, which are more potent than TAE226. Interestingly, compound 5 bearing a squarate group demonstrated the best inhibitory activity (IC₅₀ = 0.6 nM), which was largely better than that of the matched pair 6, without a reactive acryloyl group (IC₅₀ = 4.7 nM).

As irreversible inhibitors always increase inhibitory potency over time, we then investigated time-dependence inhibition of FAK kinase by the putative irreversible inhibitors 5, 7, and 8, as compared with the reversible matched pair 6. As shown in Figure 2, only compound 5 displayed an increase in its inhibitory potency over 2 h, which was consistent with the formation of a covalent bond. As expected, the reversible matched pair 6 displayed no time dependence. Unfortunately, the putative irreversible inhibitors of FAK 7 and 8 displayed no time dependence in this assay.

Since high intracellular ATP concentrations under physiological conditions influence the cellular potency of ATP-competitive inhibitors of protein kinases, non-ATP competitive inhibitors provide distinct advantages to conventional ATP-competitive binders. Thus, developing irreversible inhibitors is an attractive and alternative strategy to achieve the non-ATP competitive inhibition of kinase-mediated signaling. Therefore, we studied noncompetitive character versus ATP of the putative irreversible inhibitor 5, compared with the reversible matched pair 6. Indeed, as shown in Figure 3, inhibitor 5 showed the same inhibition at different concentrations of ATP. On the contrary, the inhibitory potency of the matched pair 6 on FAK kinase activity decreased with increasing concentration of ATP.

Crystal Structure of FAK Bound to Inhibitors. To confirm the formation of a covalent bond and to verify that the binding mode of the bis-anilino-pyrimidine part is similar to that of the reversible counterparts, we resolved the cocrystal structures of the FAK kinase domain successively with compounds 5 (PDB ID: 6GCX), 6 (PDB ID: 6GCW), and 7 (PDB ID: 6GCR). As shown in Figure 4, the mode of interaction of these compounds with the FAK kinase domain is very similar to that observed in complex with TAE226 or PHM16. Indeed, our inhibitors stabilize an unusual helical conformation of the DFG motif (D564-F565-G566) in which the phi torsion angle of Asp564 is rotated by 113°, compared to the active kinase domain. Compounds 5, 6, and 7 contain a common 5-chloro-2-anilino-4-(2-methylcarbamoyl)-anilino-pyrimidine scaffold, which binds well to the hinge region of the FAK kinase. Three hydrogen bonds are observed in the crystal structure of FAK bound to inhibitors. Among them, two are formed between the nitrogen in the pyrimidine and 2-aniline moieties with the backbone nitrogen and the carbonyl group of Cys502 in the kinase hinge (Figure 4A–C). Another one is formed between the CO of the carboxamide group of our inhibitor and the backbone nitrogen of Asp564 of the DFG motif. Some of hydrophobic interactions are observed between the carbon atoms of the 2-aniline ring and Ile428 and Gly505, but also between carbons in the pyrimidine ring and Ala452 and Leu553. As already observed in the crystallographic structure of a complex between the FAK kinase domain and TAE226, the chlorine atom on the pyrimidine ring is located in the ATP binding pocket, near the gatekeeper residue Met499 (Figure S2).

Interestingly, for 5, it is observed that two hydrogen bonds are formed between the side chain nitrogen of Arg426 and the carbonyl of the squarate, and the CO of Ile428 forms a hydrogen bond with the NH of the squaramide attached to the benzylamino moiety (Figure 5). On the contrary, the 1,2,3-triazole group cannot make this type of interaction (Figure 5), supporting that the binding of the squarate group to the FAK active site is crucial to guiding the electrophilic group of 5 for reaction with the nucleophilic thiol group of Cys427 (Figure

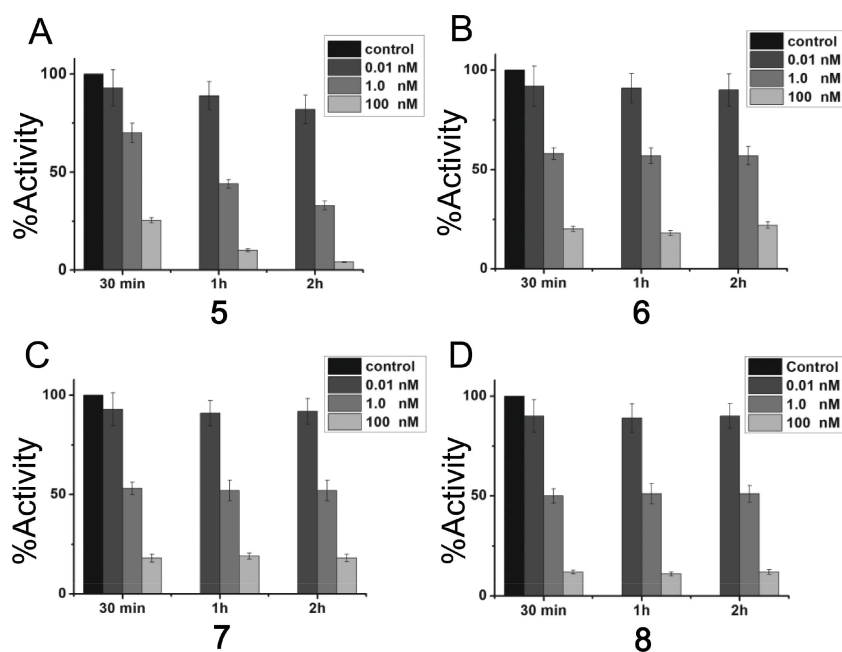


Figure 2. (A) Targeted covalent inhibitor **5** showing time-dependent inhibition of FAK kinase. (B–D) No time-dependent inhibition of FAK kinase with targeted reversible inhibitors **6**, **7**, **8**.

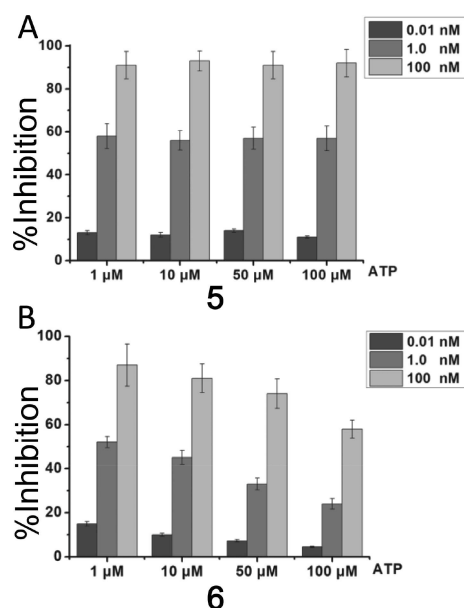


Figure 3. (A) Targeted covalent inhibitor **5** showing non-ATP dependent inhibition of FAK kinase, (B) ATP-dependent inhibition of FAK kinase with targeted reversible inhibitor **6**.

4A). Furthermore, only the cocrystal structure with **5** revealed a strong and continuous electron density between C427 and the electrophilic carbon in **5** (Figure 4D) and thus clearly confirmed a covalent bond formation.

Antiproliferation Activity of Compound **5 in SCC Cells.** Having established the potency and irreversibility of inhibitor **5** binding to the FAK active site *in vitro*, we investigated the inhibition of the full-length FAK kinase by **5** in squamous cell carcinoma (SCC) cells, which were induced in K14CreER FAK^{flox/flox} mice using a two stage chemical skin carcinogenesis assay as previously described.²⁰ In a previous study, we demonstrated that PF-562,271, a reversible inhibitor

of FAK kinase, was able to block the 3D proliferation of the SCC cells, cause squamous cell carcinoma regression, and inhibit tumor growth *in vivo*.²¹ The antiproliferation of the irreversible inhibitor **5** against SCC cells was first assessed using cell nuclei counts, and VS-4718, a highly potent reversible inhibitor of FAK which is under clinical development,²² was used as a control. Treatment of SCC FAK-WT cells with **5** resulted in a dose-dependent inhibition of proliferation with similar ED₅₀ ($1.73 \pm 0.1 \mu\text{M}$) to that of VS-4718 ($1.49 \pm 0.2 \mu\text{M}$) (Figure S3).

Covalent Inhibition of FAK by Compound **5 in SCC Cells.** We tested the inhibition of FAK autophosphorylation in the SCC cell line with the irreversible inhibitor **5**. As shown in Figure 6a, compound **5** blocked Tyr397 phosphorylation in a dose-dependent manner, and FAK autophosphorylation was significantly inhibited at low concentrations in these cancer cell lines, which is comparable to VS-4718. This is also consistent with its inhibitory activity against the FAK kinase, suggesting that this compound is able to effectively inhibit cellular FAK autophosphorylation and phosphorylation of kinase targets at low concentrations. Then, we examined the reversibility of the autophosphorylation of Tyr397 of FAK by performing washout experiments. Upon washout, VS-4718 lost its inhibition capacity against FAK, which is coherent with its reversible property. In contrast, **5** retained potent inhibition of FAK after washing out the inhibitor and demonstrated covalent binding (Figure 6d).

Kinase Selectivity Profile of Covalent Inhibitor **5.** In order to investigate the selectivity of the irreversible inhibitor **5**, we tested this compound *in vitro* against a panel of 10 kinases (EGFR, HER2/ERBB2, IGF1R, c-Kit, PDGFR, Pyk2, c-Src, IRR, and IR) determined by Eurofins Pharma Discovery Services, Poitiers, France to investigate its selectivity (Table S1, Supporting Information). A TR-FRET based kinase protocol was used with human recombinant protein in the presence of 1 μM of compound **5**. Interestingly, this compound showed only 21% inhibition on the IR (insulin receptor) kinase even at the

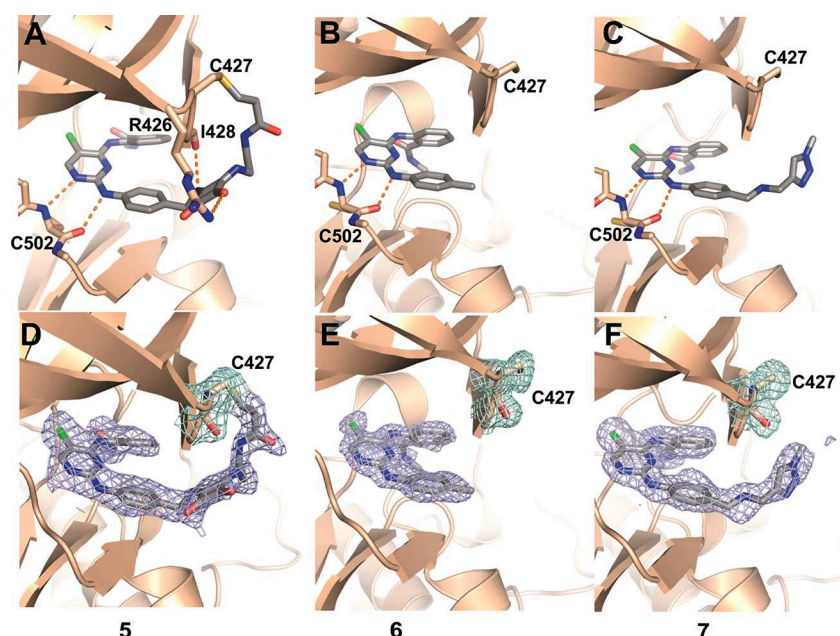


Figure 4. Crystal structures of the FAK kinase domain in complex with inhibitors **5** (PDB ID: 6GCX), **6** (PDB ID: 6GCW), and **7** (PDB ID: 6GCR). (A–C) The active sites of the FAK kinase domain bound to **5**, **6**, and **7** are shown. Inhibitors are shown in gray for ordered regions and white for disordered regions. Although the white regions are modeled, they are not supported by electron density as can be seen in panels A–C. Key hydrogen bonds between the compounds and the FAK kinase are shown as orange dashed lines. (D–F) $2F_o - F_c$ electron density countered at 1σ is shown for the compounds (blue mesh) and Cys427 (cyan mesh), which are shown in stick representation. The FAK kinase is shown as a ribbon in tan. Note that only compound **5** exhibits continuous density connecting to Cys427.

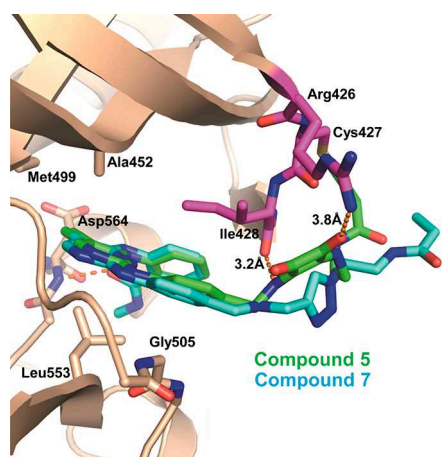


Figure 5. Superposition of the two structures of compounds **5** and **7** bound to FAK. The compounds **5** (green) and **7** (blue) and side chains in FAK interacting with the compound are shown in stick representation. Hydrogen bonds are shown as orange dashed lines.

high concentration of $1 \mu\text{M}$. This is in contrast to TAE226, which exhibited high potency toward IR ($\text{IC}_{50} = 26 \text{ nM}$).¹⁹ Even if TAE226 has displayed a potent antitumor effect both *in vitro* and *in vivo* in a large variety of cancers such as brain tumors,²³ esophageal cancer,²⁴ breast cancer,²⁵ ovarian cancer,²⁶ and gastrointestinal stroma tumor,²⁷ TAE226 never entered into clinic studies, because this compound inhibited the insulin receptor with a high potency and showed important side effects in animal studies.¹⁹

CONCLUSIONS

In summary, we described the first irreversible subnanomolar inhibitor of FAK containing a pyridimine scaffold and a

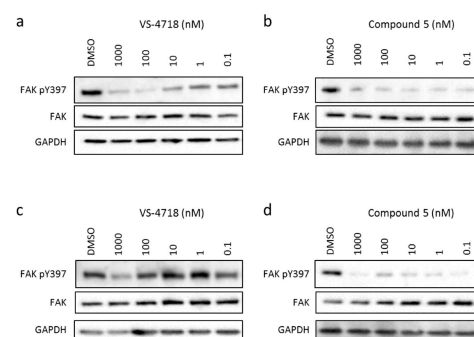


Figure 6. Inhibition of FAK autophosphorylation in SCC cells. (a,b) **5** and VS-4718 inhibited the autophosphorylation of FAK in a dose-dependent manner. (c,d) Washout experiments showed that the inhibition of FAK autophosphorylation could be reversed for the reversible inhibitor VS-4718, but not for the irreversible inhibitor **5**. The experiments were repeated three times and were consistent.

Michael acceptor as electrophile up to date through structure-based and medicinal chemistry optimization. The crystal structure of the FAK kinase domain in complex with this inhibitor was resolved to display the formation of a covalent bond. Beyond generating and characterizing the covalent FAK inhibitor, our approach can direct the design of new electrophilic inhibitors which target a noncatalytic cysteine in proteins. The irreversible inhibitor **5** showed a highly potent decrease of autophosphorylation of FAK in SCC cells, suggesting that this compound could efficiently block a key event of the intracellular FAK signaling pathway. It is worth noting that **5** exhibited an antiproliferative effect in SCC cells similar to that of VS-4718, which is currently under phase I studies. Moreover, this compound displayed low inhibition against the IR (insulin receptor) kinase, which might provide a new mode of action and overcome the side effects observed

with TAE226. Further studies into molecular mechanisms of this type of compound against cancer including antiproliferation of human cancer cells and the regulation of tumorigenesis and metastatic progression is underway in the laboratory to demonstrate the advantages for the development of novel cancer therapies.

METHODS

Chemistry. Methods for the synthesis of compounds, characterization, and spectra are described in detail in the [Supporting Information](#).

Enzyme Inhibition Studies. Inhibitory potency in an FAK enzymatic assay was determined using an ADP-Glo kinase assay. Briefly, 4 μL of assay mixture containing 0.5 μg of FAK substrate, 5 ng of FAK, 8 μM ATP, and 1 μL of compounds at desired concentrations in kinase reaction buffer (40 mM Tris, 20 mM MgCl_2 , 0.1 mg mL^{-1} BSA, 2 mM MnCl_2 , 2 μM DTT) was added into a 384-well plate. After incubation at 37 $^\circ\text{C}$ for 1 h, the kinase reaction was stopped by the addition of 5 μL of ADP-Glo Reagent to deplete the unconsumed ATP and leave only ADP. The plate was incubated at RT for 40 min and 10 μL of Kinase Detection Reagent added to convert ADP to ATP and introduce luciferase and luciferin to detect ATP. After incubation at RT for 15–20 min, the luminescence signal was detected with an Enspire plate reader. The IC_{50} value was determined for each compound, from a sigmoid dose–response curve using Graph-Pad Prism (GraphPad Software, San Diego, CA, USA).

Inhibition of FAK Autophosphorylation in SCC Cells. SCC FAK-WT cells were cultured in Glasgow Minimum Essential Medium (10% fetal calf serum, 2 mM L-glutamine, NEAA, sodium pyruvate, and MEM vitamins). Cells were seeded in six-well plates at 100 000 cells per well. Compounds were made up in DMSO to a 1000 \times final concentration and 24 h after cell seeding were added to the culture media resulting in a final DMSO concentration of 0.1%. Compounds were incubated on cells for 48 h before cell lysis. For washout experiments, cells were washed with PBS twice and fresh medium was added for 3 h.

For cell lysis, briefly, wells were washed in ice-cold PBS and drained and cells lysed in MD Anderson buffer (1% Triton \times 100, 50 mM Hepes at pH 7.4, 150 mM NaCl, 1.5 mM MgCl_2 , and 1 mM EGTA) supplemented with a protease and phosphatase tablet (Sigma-Aldrich). Cell lysates were clarified by centrifugation at 12 000g for 10 min and the protein concentration determined by Bradford assay (Thermo Fisher Scientific). Twenty micrograms of protein of each lysate was resolved using 4–15% polyacrylamide gels (Bio-Rad) and transferred to PVDF membranes, blocked, and probed with primary antibodies overnight. Blots were washed in TBS/0.1% Tween and incubated with antirabbit conjugated horseradish peroxidase. Blots were washed in TBS/0.1% Tween and visualized with BM Chemiluminescence Western Blotting Substrate (Sigma-Aldrich) on a Bio-Rad ChemiDoc imager. Blot densitometry was determined using Image Lab software (Bio-Rad).

Crystallization and Structure Determination. The kinase domain of the avian FAK protein (FAK411–686) was expressed and purified following a previously described assay.²⁸ The inhibitor–FAK complex was formed by incubation of the compound (final concentration 10 mM) with the protein (8 mg mL^{-1}) at 4 $^\circ\text{C}$ overnight. Crystals of the complex were grown, mixing an equal volume of the complex with the crystallization condition (100 mM Tris, pH 8.5, 100 mM Li_2SO_4 , 20–24% PEG4000, 10 mM TCEP). Crystals were cryoprotected by a quick soak in the following cryosolution: 100 mM Tris at pH 8.5, 100 mM Li_2SO_4 , 24% PEG4000, 10 mM TCEP, 35% ethylene glycol, and then flash-frozen. Diffraction data were collected at synchrotron facilities in beamline ID30-1 at ESRF (Grenoble, France; compounds 5, 7) or the XALOC beamline at ALBA (compound 6) and processed with XDS.²⁹ To provide an initial set of phases, the molecular replacement protocol in Phaser was used using the FAK kinase model from PDB 2JKK.³⁰ Refinement was carried out using the program Refmac, and manual rebuilding was performed with Coot.^{31,32} The Dundee PRODRG2

Server was used to create the initial model for inhibitors 5, 7, and 10.33. Final R-factors are 22.3/26.2 (Rwork/Rfree) for FAK/5, 19.5/22.3 for FAK/6, and 21.7/27.4 for FAK/7.

ASSOCIATED CONTENT

Supporting Information

The Supporting Information is available free of charge on the ACS Publications website at DOI: 10.1021/acschembio.8b00250.

Additional figures, experimental methods, and analyses (DOC)

Accession Codes

The structures of FAK domain bound to compounds 5, 6, and 7 have been deposited in the Protein Data Bank with PDB accession codes 6GCX, 6GCW, and 6GCR, respectively.

AUTHOR INFORMATION

Corresponding Author

*E-mail: huixiong.chen@parisdescartes.fr.

ORCID

Huixiong Chen: 0000-0001-7676-1584

Author Contributions

[†]These authors contributed equally.

Notes

The authors declare no competing financial interest.

ACKNOWLEDGMENTS

We thank the ESRF and ALBA synchrotron facilities for providing access to their facilities and the staff for their assistance in the data collection. D.L. was supported by the Spanish Ministry of Economy, Industry and Competitiveness (MEIC) Grant MEIC Project Retos BFU2016-77665-R cofunded by the European Regional Development Fund (ERDF) and the Worldwide Cancer Research (15-1177). B.L. thanks the China Scholarship Council (CSC) for financial support.

REFERENCES

- (1) Schober, M., and Fuchs, E. (2011) Tumor-initiating stem cells of squamous cell carcinomas and their control by TGF- β and integrin/focal adhesion kinase (FAK) signaling. *Proc. Natl. Acad. Sci. U. S. A.* 108, 10544–10549.
- (2) Serrels, A., Canel, M., Brunton, V. G., and Frame, M. C. (2011) Src/FAK-mediated regulation of E-cadherin as a mechanism for controlling collective cell movement: insights from in vivo imaging. *Cell Adh. Migr.* 5, 360–365.
- (3) Golubovskaya, V. M. (2014) Targeting FAK in human cancer: from finding to first clinical trials. *Front. Biosci., Landmark Ed.* 19, 687–706.
- (4) Golubovskaya, V. M. (2010) Focal adhesion kinase as a cancer therapy target. *Anti-Cancer Agents Med. Chem.* 10, 735–741.
- (5) Yoon, H., Dehart, J. P., Murphy, J. M., and Lim, S.-T. S. (2015) Understanding the roles of FAK in cancer: inhibitors, genetic models, and new insights. *J. Histochem. Cytochem.* 63, 114–128.
- (6) Shanthi, E., Krishna, M. H., Arunesh, G. M., Venkateswara Reddy, K., Sooriya Kumar, J., and Viswanadhan, V. N. (2014) Focal adhesion kinase inhibitors in the treatment of metastatic cancer: a patent review. *Expert Opin. Ther. Pat.* 24, 1077–1100.
- (7) Jones, S. F., Siu, L. L., Bendell, J. C., Cleary, J. M., Razak, A. R. A., Infante, J. R., Pandya, S. S., Bedard, P. L., Pierce, K. J., Houk, B., Roberts, W. G., Shreeve, S. M., and Shapiro, G. I. (2015) A phase I study of VS-6063, a second-generation focal adhesion kinase inhibitor, in patients with advanced solid tumors. *Invest. New Drugs* 33, 1100–1107.

- (8) Roy-Luzarraga, M., and Hodivala-Dilke, K. (2016) Molecular Pathways: Endothelial Cell FAK-A Target for Cancer Treatment. *Clin. Cancer Res.* 22, 3718–3724.
- (9) Lim, S. T., Miller, N. L., Chen, X. L., Tancioni, I., Walsh, C. T., Lawson, C., Uryu, S., Weis, S. M., Cheresch, D. A., and Schlaepfer, D. D. (2012) Nuclear-localized focal adhesion kinase regulates inflammatory VCAM-1 expression. *J. Cell Biol.* 197, 907–919.
- (10) Serrels, A., Lund, T., Serrels, B., Byron, A., McPherson, R. C., von Kriegsheim, A. V., Gómez-Cuadrado, L. G., Canel, M., Muir, M., Ring, J. E., Maniati, E., Sims, A. H., Pachter, J. A., Brunton, V. G., Gilbert, N., Anderton, S. M., Nibbs, R. J. B., and Frame, M. C. (2015) Nuclear FAK controls chemokine transcription, Tregs, and evasion of anti-tumor immunity. *Cell* 163, 160–173.
- (11) Sanderson, K. (2013) Irreversible kinase inhibitors gain traction. *Nat. Rev. Drug Discovery* 12, 649–651.
- (12) Singh, J., Petter, R. C., Baillie, T. A., and Whitty, A. (2011) The resurgence of covalent drugs. *Nat. Rev. Drug Discovery* 10, 307–317.
- (13) Barf, T., and Kaptein, A. (2012) Irreversible protein kinase inhibitors: balancing the benefits and risks. *J. Med. Chem.* 55, 6243–6262.
- (14) Lietha, D., and Eck, M. J. (2008) Crystal structures of the FAK kinase in complex with TAE226 and related bis-anilino pyrimidine inhibitors reveal a helical DFG conformation. *PLoS One* 3, e3800.
- (15) Dao, P., Jarray, R., Smith, N., Lepelletier, Y., Le Coq, J., Lietha, D., Hadj-Slimane, R., Herbeuval, J. P., Garbay, C., Raynaud, F., and Chen, H. (2014) Inhibition of both focal adhesion kinase and fibroblast growth factor receptor 2 pathways induces anti-tumor and anti-angiogenic activities. *Cancer Lett.* 348, 88–99.
- (16) Luzzio, M. J., and Kath, J. C. Pyrimidine derivatives for the treatment of abnormal cell growth. WO/2005/111024.
- (17) Imbach, P., Kawahara, E., Konishi, K., Matsuura, N., Miyake, T., Ohmori, O., Roesel, J., Teno, N., and Umemura, I. Pyrimidine derivatives. WO/2006/021454.
- (18) Sapountzis, I., Betzemeier, B., and Stadtmueller, H. 2,4-diaminopyrimidine derivatives as ptk2- inhibitors for the treatment of abnormal cell growth. WO/2010/055117.
- (19) Liu, T. J., LaFortune, T., Honda, T., Ohmori, O., Hatakeyama, S., Meyer, T., Jackson, D., de Groot, J., and Yung, W. K. A. (2007) Inhibition of both focal adhesion kinase and insulin-like growth factor-I receptor kinase suppresses glioma proliferation in vitro and in vivo. *Mol. Cancer Ther.* 6, 1357–1367.
- (20) McLean, G. W., Komiyama, N. H., Serrels, B., Asano, H., Reynolds, L., Conti, F., Hodivala-Dilke, K., Metzger, D., Chambon, P., Grant, S. G., and Frame, M. C. (2004) Specific deletion of focal adhesion kinase suppresses tumor formation and blocks malignant progression. *Genes Dev.* 18, 2998–3003.
- (21) Serrels, A., McLeod, K., Canel, M., Kinnaird, A., Graham, K., Frame, M. C., and Brunton, V. G. (2012) The role of focal adhesion kinase catalytic activity on the proliferation and migration of squamous cell carcinoma cells. *Int. J. Cancer* 131, 287–97.
- (22) Shapiro, I. M., Kolev, V. N., Vidal, C. M., Kadariya, Y., Ring, J. E., Wright, Q., Weaver, D. T., Menges, C., Padval, M., McClatchey, A. I., Xu, Q., Testa, J. R., and Pachter, J. A. (2014) Merlin deficiency predicts FAK inhibitor sensitivity: a synthetic lethal relationship. *Sci. Transl. Med.* 6, 237ra68.
- (23) Shi, Q., Hjelmeland, A. B., Keir, S. T., Song, L., Wickman, S., Jackson, D., Ohmori, O., Bigner, D. D., Friedman, H. S., and Rich, J. N. (2007) A novel low-molecular weight inhibitor of focal adhesion kinase, TAE226, inhibits glioma growth. *Mol. Carcinog.* 46, 488–496.
- (24) Watanabe, N., Takaoka, M., Sakurama, K., Tomono, Y., Hatakeyama, S., Ohmori, O., Motoki, T., Shirakawa, Y., Yamatsuji, T., Haisa, M., Matsuoka, J., Beer, D. G., Nagatsuka, H., Tanaka, N., and Naomoto, Y. (2008) Dual tyrosine kinase inhibitor for focal adhesion kinase and insulin-like growth factor-I receptor exhibits anticancer effect in esophageal adenocarcinoma in vitro and in vivo. *Clin. Cancer Res.* 14, 4631–4639.
- (25) Kurio, N., Shimo, T., Fukazawa, T., Takaoka, M., Okui, T., Hassan, N. M. M., Honami, T., Hatakeyama, S., Ikeda, M., Naomoto, Y., and Sasaki, A. (2011) Anti-tumor effect in human breast cancer by TAE226, a dual inhibitor for FAK and IGF-IR in vitro and in vivo. *Exp. Cell Res.* 317, 1134–1146.
- (26) Halder, J., Lin, Y. G., Merritt, W. M., Spannuth, W. A., Nick, A. M., Honda, T., Kamat, A. A., Han, L. Y., Kim, T. J., Lu, C., Tari, A. M., Bornmann, W., Fernandez, A., Lopez-Berestein, G., and Sood, A. K. (2007) Therapeutic efficacy of a novel focal adhesion kinase inhibitor TAE226 in ovarian carcinoma. *Cancer Res.* 67, 10976–10983.
- (27) Sakurama, K., Noma, K., Takaoka, M., Tomono, Y., Watanabe, N., Hatakeyama, S., Ohmori, O., Hirota, S., Motoki, T., Shirakawa, Y., Yamatsuji, T., Haisa, M., Matsuoka, J., Tanaka, N., and Naomoto, Y. (2009) Inhibition of focal adhesion kinase as a potential therapeutic strategy for imatinib-resistant gastrointestinal stromal tumor. *Mol. Cancer Ther.* 8, 127–134.
- (28) Dao, P., Jarray, R., Le Coq, J., Lietha, D., Loukaci, A., Lepelletier, Y., Hadj-Slimane, R., Garbay, C., Raynaud, F., and Chen, H. (2013) Synthesis of novel diarylamino-1,3,5-triazine derivatives as FAK inhibitors with anti-angiogenic activity. *Bioorg. Med. Chem. Lett.* 23, 4552–4556.
- (29) Kabsch, W. (2010) XDS. *Acta Crystallogr., Sect. D: Biol. Crystallogr.* 66, 125–132.
- (30) McCoy, A. J., Grosse-Kunstleve, R. W., Adams, P. D., Winn, M. D., Storoni, L. C., and Read, R. J. (2007) Phaser crystallographic software. *J. Appl. Crystallogr.* 40, 658–674.
- (31) Murshudov, G. N., Vagin, A. A., and Dodson, E. J. (1997) Refinement of macromolecular structures by the maximum-likelihood method. *Acta Crystallogr., Sect. D: Biol. Crystallogr.* 53, 240–255.
- (32) Emsley, P., and Cowtan, K. (2004) Coot: model-building tools for molecular graphics. *Acta Crystallogr., Sect. D: Biol. Crystallogr.* 60, 2126–2132.

Titre : Conception, synthèse et évaluation biologique de nouveaux inhibiteurs sélectifs de la kinase d'adhésion focale à activité anti-tumorale potentielle

Résumé :

La kinase d'adhésion focale (FAK) est une tyrosine kinase ubiquitaire surexprimée dans certaines cellules cancéreuses chez l'Homme. Son activation entraîne de nombreux processus biologiques tels que l'adhésion, la migration, l'invasion, la prolifération, la survie cellulaire et l'angiogenèse. FAK joue un rôle important dans la suppression de la réponse immunitaire et son inhibition a un effet synergique avec l'immunothérapie. FAK apparaît donc comme une cible de choix dans le cadre de thérapies ciblées dans la lutte contre le cancer. Le travail présenté au sein de cette thèse porte sur le développement d'inhibiteurs de FAK.

Dans une première partie, la conception d'inhibiteurs se liant de façon covalente avec un résidu cystéine de l'enzyme a été entreprise. Pour cela nous avons développé une voie de synthèse portant sur la modification d'un motif 2,4-diaminopyrimidine relié par un lien squaramide à un groupement électrophile. Des études biochimiques ont permis de mettre en évidence le caractère covalent de ce type d'inhibiteur. Afin d'augmenter la sélectivité pour la kinase, des modifications structurales au niveau du noyau pyrimidine et du motif électrophile ont été réalisées. Cette stratégie a permis d'obtenir 10 nouveaux inhibiteurs covalents dont l'un d'entre eux présentant une augmentation de la sélectivité pour FAK.

La modification de dérivés pyrimidines halo-substituées a ensuite été étudiée dans le cadre de la synthèse d'inhibiteurs de type II. Pour cela, la réaction d'amination de Buchwald-Hartwig a été optimisée, sous conditions micro-ondes permettant ainsi d'obtenir 29 exemples avec de bons rendements.

Finalement, la conception de composés fluorescents a permis d'accéder à de nouveaux outils d'étude pour la détection de FAK. Le motif fluorescent NBD a été introduit en position 4 du cycle pyrimidine via un groupement aminé ou un lien éthylène diamine. Par cette stratégie, 3 composés fluorescents ont été obtenus, dont l'un d'entre eux comporte un motif électrophile réactif.

Mots clés : cancer, FAK, inhibiteurs covalents, squaramide, amination de Buchwald-Hartwig, réaction micro-ondes, composés fluorescents.

Title: Design, synthesis and biological evaluation of novel selective inhibitors of focal adhesion kinase with potential anti-tumour activity

Abstract :

Focal adhesion kinase (FAK) is a ubiquitously over-expressed non-receptor tyrosine kinase in many human cancer cells. It has been proved that FAK is a key regulator in cell adhesion, motility, invasion, metastasis, survival and angiogenesis. Recently it has been found that FAK plays an important role in suppressing immune response and inhibition of FAK has a synergetic effect with immunotherapy. Hence, FAK kinase is a very promising target for the treatment of cancer. The work presented in this thesis is devoted to develop inhibitors of FAK.

In the first part, the conception of covalent inhibitors that contain an electrophile reacting with a specific cysteine was examined. A feasible synthetic route for the synthesis of 2,4-diaminopyrimidine scaffold covalent inhibitors was established and the biochemical characterisation proved covalent inhibitory feature of compound with a squaramide moiety as linker. In order to improve the kinase selectivity, structural modification on pyrimidine ring and electrophile was conducted to afford 10 new covalent inhibitors and one of them showed improved kinase selectivity.

Next, we turned our attention to the amination of 5-halo-2-substituted pyrimidine, which is a key step for the synthesis of type II inhibitor of FAK. We optimized the microwave-assisted Buchwald-Hartwig reaction and 29 examples were given in good to high yield.

In the final part, the fluorescent compound was designed as imaging tools for the detection of FAK. The fluorophore (NBD) was introduced to the 4 position of pyrimidine via an amino group or ethylenediamino linker. 3 fluorescent compounds including one covalent fluorescent compound were obtained.

Keywords: cancer, FAK, covalent inhibitor, squaramide, Buchwald-Hartwig amination, microwave reaction, fluorescent compounds.